



THE UNIVERSITY

of ADELAIDE

**Design and Mechanism Study of Electrocatalysts for Alkaline
Hydrogen Evolution**

Xuesi Wang

School of Chemical Engineering and Advanced Materials
Faculty of Engineering, Computer and Mathematical Science

A thesis submitted for the degree of Doctor of Philosophy

The University of Adelaide

June 2019

Table of Contents

Abstract	1
Declaration	3
Acknowledgments.....	4
Chapter 1 : Introduction.....	6
1.1 Significance of the project.....	6
1.2 Research objectives	6
1.3 Thesis outline	7
1.4 References.....	7
Chapter 2 : Literature Review.....	9
2.1 Introduction.....	9
2.2 Design Strategies of Electrocatalysts for Alkaline Hydrogen Evolution.....	10
2.3 Electronic and Structural Engineering of Carbon-Based Metal-Free Electrocatalysts for Water Splitting.....	47
Chapter 3 : Anomalous Hydrogen Evolution Behavior in High-pH Environment Induced by Locally Generated Hydronium Ions.....	58
3.1 Introduction.....	58
3.2 Anomalous Hydrogen Evolution Behavior in High-pH Environment Induced by Locally Generated Hydronium Ions	59
Chapter 4 : Breaking the Volcano-Plot Limits for Pt-based Electrocatalysts by Selective Tuning Adsorption of Multiple Intermediates.....	102
4.1 Introduction.....	102
4.2 Breaking the Volcano-Plot Limits for Pt-based Electrocatalysts by Selective Tuning Adsorption of Multiple Intermediates.....	103
Chapter 5 : Strain Effect in Bimetallic Electrocatalysts on the Hydrogen Evolution Reaction	139
5.1 Introduction.....	139

5.2	Strain Effect in Bimetallic Electrocatalysts on the Hydrogen Evolution Reaction	140
Chapter 6 : Conclusions and perspectives.....		165
6.1	Conclusions.....	165
6.2	Perspectives	166
Appendix I: Publications during PhD Candidature		168

Abstract

The hydrogen evolution reaction (HER) is one of the most important and fundamental electrochemical processes in sustainable photo/electrochemical energy generation technologies. However, even after decades of study, the HER mechanism in neutral/alkaline media is still unclear and the slow kinetics of the reaction remains an ongoing problem. Consequently, most of the alkaline HER catalysts, especially the highly cost-effective non-noble metal catalysts, are still inefficiently designed based on trial and error methods. This lack of knowledge surrounding the alkaline HER has not only affected the development of hydrogen-based catalysis, but also obstructed the proliferation of energy conversion technologies (e. g. fuel cell, sea water splitting etc.). Understanding the cause of the sluggish alkaline HER kinetics and developing efficient design protocols for highly active catalysts is now urgently required by both academia and industry. To this end, work contained in this thesis aims to contribute to meeting these needs.

The first two chapters of this thesis provide a systematic review on the current understanding and progress on alkaline HER catalysts. These chapters have introduced the latest opinions on the reaction mechanism of alkaline HER, concluded the design strategies of almost all the current catalytic materials for the reaction and give outlook on the future development of the field. The last three chapters of the thesis are specially focused on noble metal catalysts, which are the most representative candidates for the alkaline HER. Here, the thesis presents a series of Pt-based catalysts in two parts.

The first part of the thesis focuses on the unique alkaline HER mechanism on nanostructured electrocatalysts. So far, almost all studies on the alkaline HER mechanism are carried out using single/poly crystalline Pt as a model catalyst. However, it has been found that some of the mechanistic understandings drawn from the bulk model catalysts are inapplicable to highly active nanostructured catalysts in practice. Therefore, an alternative alkaline HER reaction mechanism for nanostructured catalysts was proposed based on the finding of a new reactive intermediate that has not been reported before on the model catalysts. In situ-Raman and a series of electrochemical characterizations were carried out to confirm that in a high-pH environment, a large amount of hydronium ions

(H_3O^+) are generated on the surface of nanostructured catalysts during the HER process. The H_3O^+ forms an acid-like environment on the surface of the catalysts which improve the overall activity by reducing the activation energy of the reaction. Such phenomenon distinct on nanostructured catalysts provides a comprehensive explanation to the observed differences in catalytic behavior between bulk and nanostructured catalysts.

In the second part of the thesis, the origin of the high activity on nanostructured catalysts are studied from the perspective of the material. Firstly, a catalyst design strategy is proposed to break the activity limitation or ‘volcano plot’. A volcano plot is a relationship between the catalytic performance of a series of catalysts and a certain descriptor, which in the current case is the hydrogen adsorption ability. By investigating a group of typical nanostructured catalysts, a volcano plot was built up for Pt-based bimetallic materials, and some unique dealloyed samples were found to go beyond the limitation of the volcano plot and represent much higher activity than theoretical predictions. Thermodynamic and kinetic characterizations indicate that the reason for the unusual performance of these samples is that dealloying can selectively optimize the H and OH binding energy on Pt sites, promoting the overall activity. Secondly, well-defined RuPt alloy and core-shell (Ru@Pt) nanoparticles were studied to demonstrate the contribution of the electronic and geometric effects of a nanostructured catalyst towards alkaline HER performance. The two groups of nanoparticles have similar electronic structures but differing surface strain. A comparison between the catalytic activity of the two materials indicated that the strain effect has a dominant role in determining the intrinsic alkaline HER activity of the catalyst. In particular, the compressive surface strain of Ru@Pt nanoparticles provided the catalyst with weakened hydrogen binding and improved interaction with hydroxyl species, leading to enhanced apparent activity.

Declaration

I declare that this is my original work that contains no material previously written or published, in whole or in part, by another person, or material which has been accepted for the award of any other degree or diploma in my name at any university or any other educational institution, except where due acknowledgment has been made in the thesis. Any contribution made to the co-authored works by others, with whom I have worked at The University of Adelaide or elsewhere, is clearly stated and acknowledged in the text. Also, I certify that no part of this work will be used in the future under my name for any purposes, without the prior approval of The University of Adelaide.

I grant the University Library the right to archive and to make available my thesis, in whole or part for loan and photocopying, subject to the provisions of the Copyright Act 1968.

I acknowledge that copyright of published works contained in this thesis resides with the copyright holders of those works, where copyright permissions have been obtained to reproduce published materials in this thesis.

I give permission for the electronic copy of my thesis to be made available online, via the University's digital research repository, the Library Search and also through web search engines, unless permission has been granted by the University to forbid access for a period of time.

Name of Candidate: Xuesi Wang

Signature:

Date: 4/July/2019

Acknowledgments

For the completion of this thesis, I'd like to express my gratitude to many people for their kind help and support during my Ph.D. study. Without them, I could hardly accomplish all the research in this thesis.

First and foremost, I'd like to thank my principal supervisor, Prof. Shizhang Qiao for his continuous guidance, valuable suggestions and deepest trust during my four years of research period. Moreover, he has provided me with the chance to cooperate with some of the world's top scientists and research institutes. It's a privilege to follow his leadership and work with him as well as other top young scientists in his group. I was, and I will always benefit from his diligent working attitude and his preciseness in science.

Also, I would like to give my sincere appreciation to my co-supervisor, Dr. Yao Zheng for his generous academic support all these years. Whenever I struggled with the difficulties on my research, Dr. Zheng would always provide a helping hand without hesitation. Words can't express my gratitude enough for his generous guidance.

A big thank you to my companions in my research group: Fangxi Xie, Chaochen Xu, Anthony Vasileff, Hunanyu Jin, Laiquan Li, Xin Liu, Xing Zhi, Bingquan Xia, Huan Li, Dr. Yan Jiao, Dr. Bo You and Dr. Cheng Tang for all the inspiring discussions, fascinating ideas and happy adventures we have shared in all these years.

Thanks to all my co-authors in my publications from other research institutes: Qun He, Dr. Yihan Zhu, Prof. Bin Zheng, Prof. Li Song, Dr. Shuangming Chen, Prof. Mietek Jaroniec, Prof. Wenchao Sheng, Dr. Zhichuan J. Xu for their professional assistance in my research.

I deeply appreciate the help from the school administrators Michelle Fitton and Sue Earle, workshop technician Jason Peak, Analytical Services Coordinator Dr. Qihong Hu, Microscopists Mr. Ken Neubauer, Dr. Animesh Basak and Dr. Ashley Slattery. Their excellent work contributes significantly to my research in this thesis.

I would also like to acknowledge The University of Adelaide and Australia Research Council (ARC) for financial support.

Finally, special thanks and a big bear hug to my parents and my boyfriend Guang for their years of unconditional love and emotional support to me. They are the only reason that I could keep going and meet all the challenges in my life.

Chapter 1 : Introduction

1.1 Significance of the project

Hydrogen-based energy conversion technologies (e. g. photo/electrocatalyzed water splitting, carbon dioxide and nitrogen reduction) provide solutions toward the generation of renewable energy sources that hopefully will replace fossil fuels in the future.¹⁻⁴ One of the core obstacles for these technologies to be further commercialized is the slow kinetics of the involved electrochemical processes in aqueous electrolytes.⁵⁻⁶ Being the most fundamental and most generally involved reaction in energy conversion process, alkaline HER is often used as a model catalysis to study the reaction mechanism of the hydrogen-based energy conversion reactions. However, even after decades of efforts, there's still no systematic explanation on the slow alkaline HER reaction kinetics.^{5, 7} Moreover, the limited mechanism studies of alkaline HER are usually carried out on single/polycrystal bulk metal, which is far from the nanostructured catalysts in practice.⁸⁻¹⁰ For alkaline HER, comprehensive mechanism understanding on nanostructured materials and corresponding catalyst-designing strategies are urgently needed for its further development in both science and industry.

1.2 Research objectives

The major goal of this thesis is to discover the reaction mechanism of alkaline HER on nanostructured catalysts and to find out the activity origin on highly active catalysts. The objectives of this thesis are as follow:

- ***To discover*** the reaction mechanism of alkaline HER on nanostructured catalysts based on a series of model Pt-based nanoparticles.
- ***To identify*** the origin of the anomalous hydrogen evolution behavior of the nanostructured catalysts in alkaline environments.
- ***To investigate*** the relationship between the HER activity and the intrinsic electronic structure of the nanostructured catalysts.
- ***To evaluate*** the influence of a variety of intermediates toward the alkaline HER activity.
- ***To design*** an applicable strategy to break the current activity limitation for most commonly used alkaline HER catalysts.

- *To optimize* the geometry of the Pt-based catalysts for better catalytic performance in alkaline environment.

1.3 Thesis outline

This thesis is partial outcomes of my PhD research presented in the form of journal publications. The chapters in this thesis are presented in the following sequence:

- *Chapter 1* introduces the general background and the significance of the project. It provides an outline and the research purpose of the current thesis.
- *Chapter 2* reviews the current development, mechanism understanding and the designing strategies of the electrocatalysts for HER.
- *Chapter 3* reports new reaction mechanism found for nanostructured catalysts in alkaline HER under high-pH environment.
- *Chapter 4* proposes and studies a new strategy for breaking the known adsorption-activity limitation for Pt-based nanostructured catalysts in alkaline HER.
- *Chapter 5* studies the strain effect on a RuPt-based bimetallic nanoparticle and its influence toward the intrinsic HER activity of the catalysts.
- *Chapter 6* provides the conclusions and perspectives for future work on design and improvement of the alkaline HER catalysts.

1.4 References

1. Zheng, Y.; Vasileff, A.; Zhou, X.; Jiao, Y.; Jaroniec, M.; Qiao, S.-Z. Understanding the roadmap for electrochemical reduction of CO₂ to multi-carbon oxygenates and hydrocarbons on copper-based catalysts. *J. Am. Chem. Soc.* **2019**, *141*, 7646-7659.
2. Tang, C.; Qiao, S.-Z. How to explore ambient electrocatalytic nitrogen reduction reliably and insightfully. *Chem. Soc. Rev.* **2019**, *48*, 3166-3180.
3. Singh, A. R.; Rohr, B. A.; Schwalbe, J. A.; Cargnello, M.; Chan, K.; Jaramillo, T. F.; Chorkendorff, I.; Nørskov, J. K. Electrochemical Ammonia Synthesis—The Selectivity Challenge. *ACS Catal.* **2016**, *7*, 706-709.
4. Stamenkovic, V. R.; Strmcnik, D.; Lopes, P. P.; Markovic, N. M. Energy and fuels from electrochemical interfaces. *Nat. Mater.* **2016**, *16*, 57-69.

5. Zheng, Y.; Jiao, Y.; Vasileff, A.; Qiao, S. Hydrogen Evolution Reaction in Alkaline Solution: From Theory, Single Crystal Models, to Practical Electrocatalysts. *Angew. Chem. Int. Ed. Engl.* **2018**, *57*, 7568-7579.
6. De Luna, P.; Hahn, C.; Higgins, D.; Jaffer, S. A.; Jaramillo, T. F.; Sargent, E. H. What would it take for renewably powered electrosynthesis to displace petrochemical processes? *Science* **2019**, *364*, eaav3506.
7. Davydova, E. S.; Mukerjee, S.; Jaouen, F.; Dekel, D. R. Electrocatalysts for Hydrogen Oxidation Reaction in Alkaline Electrolytes. *ACS Catal.* **2018**, *8*, 6665-6690.
8. Sheng, W.; Gasteiger, H. A.; Shao-Horn, Y. Hydrogen Oxidation and Evolution Reaction Kinetics on Platinum: Acid vs Alkaline Electrolytes. *J. Electrochem. Soc.* **2010**, *157*, B1529-B1536.
9. Sheng, W.; Myint, M.; Chen, J. G.; Yan, Y. Correlating the hydrogen evolution reaction activity in alkaline electrolytes with the hydrogen binding energy on monometallic surfaces. *Energ. Environ. Sci.* **2013**, *6*, 1509-1512.
10. Sheng, W.; Zhuang, Z.; Gao, M.; Zheng, J.; Chen, J. G.; Yan, Y. Correlating hydrogen oxidation and evolution activity on platinum at different pH with measured hydrogen binding energy. *Nat. Commun.* **2015**, *6*, 5848.

Chapter 2 : Literature Review

2.1 Introduction

This chapter can be divided into two parts.

In the first part, the reaction mechanism and catalyst designing strategies for alkaline HER is reviewed in general. With the fast-growing hydrogen economy, there's an increasing demand for technologies such as electrocatalytic water splitting in order to produce hydrogen-based energy carriers. For most of these technologies, the generation of hydrogen is taken place in alkaline or neutral media for safety and technique reasons. However, the HER kinetics in these media is usually 2-3 magnitudes slower than in acid environment. As the reaction mechanism of alkaline HER is still unclear, the origin of such slow kinetics is still a mystery. As a result, there's no systematic theoretical guide in catalyst designing for the reaction. So far, the development of catalysts for alkaline HER is still mostly based on a trial and error method.

To this end, this section of the review provides direct guidelines for alkaline HER from the perspective of mechanism study and material engineering. Both the classic ideas and the latest understanding of alkaline HER mechanism is represented in clear storylines according to the different theoretical viewpoints. Based on that, a series of catalyst designing strategies are listed closely aiming to make up for the kinetic drawbacks in alkaline HER catalysts. Detailed material engineering methods are given accordingly with typical examples in giving instructions on how to tailor the electronic and physical structure of the material to achieve best catalytic performance. These strategies are not only of guidance toward catalyst design for alkaline HER, but also for other catalysis involving multiple intermediates.

In the second part, a review is specifically given on catalysts in carbon-based metal-free materials. In the past few decades, carbon-based materials have attracted tremendous research interest because they are inexpensive and exhibit excellent performance as electrocatalysts for clean and sustainable energy conversion technologies. The excellent electrocatalytic activity of carbon was first discovered for the oxygen reduction reaction and was later extended to other reactions including water splitting and carbon dioxide

reduction. In principle, the performance of carbon-based catalysts is highly dependent on their electronic and physical properties. With the advances of theoretical calculations, advanced characterization techniques, and well-developed synthetic methods, researchers are now able to precisely engineer carbon nanomaterials to perform for specific reactions.

Here, using the fundamental water splitting reactions as a platform, we present commonly used strategies for engineering carbon for highly active electrocatalysis. Systematic analysis is given on how dopants, edge effects, and topological defects can be applied in tuning the electronic band of carbon materials. Next, further discussion is given on how the physical structure of carbon can be engineered to synergistically coordinate with the electronic structure in order to achieve the best electrocatalytic performance. We hope that these strategies will provide useful guidance for designing carbon-based metal-free materials for broader applications.

2.2 Design Strategies of Electrocatalysts for Alkaline Hydrogen Evolution

This chapter is included as it appears as a journal paper published by Xuesi Wang, Yao Zheng, Wenchao Sheng, Zhichuan J. Xu and Shi-Zhang Qiao: Designing Strategies for Alkaline Hydrogen Evolution Electrocatalysts, *invited review to be submitted to Materials Today*.

Statement of Authorship

Title of Paper	Designing Strategies for Alkaline Hydrogen Evolution Electrocatalysts
Publication Status	<input type="checkbox"/> Published <input type="checkbox"/> Accepted for Publication <input type="checkbox"/> Submitted for Publication <input checked="" type="checkbox"/> Unpublished and Unsubmitted work written in manuscript style
Publication Details	Wang, X. ; Zheng, Y. ; Sheng, W. ; Xu, Z. J. ; Qiao, S. -Z. Designing Strategies for Alkaline Hydrogen Evolution Electrocatalysts, to be submitted to Materials Today.

Principal Author

Name of Principal Author (Candidate)	Xuesi Wang		
Contribution to the Paper	This author organized and wrote the paper.		
Overall percentage (%)	80%		
Certification:	This paper reports on original research I conducted during the period of my Higher Degree by Research candidature and is not subject to any obligations or contractual agreements with a third party that would constrain its inclusion in this thesis. I am the primary author of this paper.		
Signature		Date	1 July 2019

Co-Author Contributions

By signing the Statement of Authorship, each author certifies that:

- i. the candidate's stated contribution to the publication is accurate (as detailed above);
- ii. permission is granted for the candidate to include the publication in the thesis; and
- iii. the sum of all co-author contributions is equal to 100% less the candidate's stated contribution.

Name of Co-Author	Yao Zheng		
Contribution to the Paper	This author contributed in providing funding and supervising the project.		
Signature		Date	1 July 2019

Name of Co-Author	Wenchao Sheng		
Contribution to the Paper	This author contributed in providing valuable suggestions to the paper.		
Signature		Date	1 July 2019

Name of Co-Author	Zhichuan J Xu		
Contribution to the Paper	This author contributed in providing valuable suggestions to the paper.		
Signature		Date	1 July 2019

Name of Co-Author	Shi-Zhang Qiao		
Contribution to the Paper	This author contributed in providing funding and supervising the project.		
Signature		Date	1 July 2019

Name of Co-Author			
Contribution to the Paper			
Signature		Date	

Please cut and paste additional co-author panels here as required.

Strategies for Design of Electrocatalysts for Hydrogen Evolution under Alkaline Conditions

Xuesi Wang^a, Yao Zheng^a, Wenchao Sheng^b, Zhichuan J. Xu^c, Mietek Jaroniec^d, Shi-Zhang Qiao^{a*}

^a Center for Materials in Energy and Catalysis, School of Chemical Engineering and Advanced Materials, The University of Adelaide, Adelaide, SA 5005, Australia.

^b State Key Laboratory of Pollution Control and Resource Reuse, College of Environmental Science and Engineering, Tongji University, 1239 Siping Road, Shanghai, 200092, P. R. China.

^c School of Material Science and Engineering, Nanyang Technological University, 50 Nanyang Avenue, Singapore, 639798, Singapore.

^d Department of Chemistry and Biochemistry, Kent State University, Kent, Ohio 44242, United States.

*Corresponding author: Qiao S.Z (s.qiao@adelaide.edu.au)

Abstract

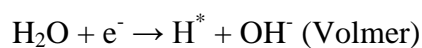
Electrocatalytic hydrogen evolution reaction (HER) in alkaline environments is one of the major energy conversion processes in water electrolysis technology. Very active and cost-effective catalysts are highly desirable for alkaline HER not only for its industrial value, but also for its fundamental importance in studying all electrocatalytic reactions occurring on cathode electrodes. However, to date, the reaction mechanism of alkaline HER is still under debate, which makes the design of catalysts largely a trial-and-error process. To address this issue, here we present strategies for the design of alkaline HER catalysts based on the current knowledge of the reaction mechanism by emphasizing the connection between the atomic-level materials engineering and reaction fundamentals. Particularly, we focus on the improvement of the inherent electronic structure of the materials to achieve desired interactions between the catalysts and reactive intermediates. By showing several successful examples of both theoretical and experimental design strategies, we aim to provide direct guidelines toward the design of catalysts for HER under alkaline conditions.

Keywords: Hydrogen evolution reaction; electrocatalysts; water dissociation; catalyst design; alkaline conditions.

Introduction

Producing clean energy through electro/photocatalytic methods has been one of the top priorities for the science community in recent decades. Renewable fuels, from simple hydrogen to complex energy carriers such as C2 molecules and ammonia, can be produced from water, carbon dioxide (CO₂) and nitrogen (N₂) through electrochemical or photochemical processes under mild conditions.¹⁻⁶ Among those, alkaline hydrogen evolution reaction (HER) plays a fundamental yet significant role for being the simplest cathode reaction in high pH environment. With only water dissociation and proton reduction processes, alkaline HER is critical in investigating the general role of water molecule in many reduction reactions.^{5,7} For example, an in-depth understanding of alkaline HER mechanism can build up strong foundation for the carbon dioxide reduction (CRR) and nitrogen reduction reaction (NRR), which always involve an initial water dissociation step (e.g. CO₂ + 6H₂O + 8e⁻ ↔ CH₄ + 8OH⁻; N₂ + 6H₂O + 6e⁻ ↔ 2NH₃ + 6OH⁻)(**Figure 1**).

Although an in-depth understanding has been achieved for acid HER, the reaction mechanism for alkaline HER is still a long-standing puzzle. The main argument remains the explanation to the origin of the sluggish alkaline HER kinetics, which is being 2-3 orders of magnitude slower than that in acid environments.^{8,9} It is a general consensus that the HER process in these two environments shares a similar reaction pathway, except that the hydrogen intermediates (H^{*}, * represent an adsorption site) in alkaline HER are generated through a water dissociation step. Thus, the overall reaction pathway of alkaline HER is as follows:



Despite several theories have been proposed, the cause of the widely observed pH dependence of the HER activity is still unclear. For example, on the benchmark Pt surface, Markovic et al. suggested that the additional energy barrier introduced by water dissociation determines the rate of alkaline HER,^{10,11} while the hydrogen binding energy (HBE) theory proposed by Sheng et al. states that the binding

energy between the catalyst and H^* intermediate dictates the reaction kinetics.^{12,13} Besides, other influential factors such as the potential of zero free charge (pzfc) and the efficiency of anion transfer through the electrochemical double layer region have also been reported.¹⁴⁻¹⁶ In general, all these theories focus on answering two key questions regarding the alkaline HER reaction mechanism: (i) what is the real cause of the slow kinetics; (ii) to what extent does water dissociation process influence the overall reaction kinetics in comparison to other factors (e.g., HBE and pzfc).

Due to the unclear reaction mechanism, the development of the alkaline HER catalysts is still relying mainly on trial-and-error experiences. Specifically, without identifying the weight of influence of the intermediates (i.e., H^* , OH^* and H_2O^*) involved in the reaction, the adsorption behavior of all these intermediates needs to be taken into account when designing a catalyst. By adjusting the electronic and physical structure of a material, it is desirable to build up a catalyst that has the lowest activation barrier and appropriate interaction ability with intermediates. Computational methods such as density functional theory (DFT) are often used to illuminate a quantitative relationship between the inherent characters of different materials and their HER performance (e.g., through a H adsorption ability - activity volcano plot).¹⁷⁻¹⁹ Although these results seem to fit the acid HER data perfectly, they are not such accurate for prediction of HER under alkaline environments. This is because in alkaline electrolytes, the HER reaction activity is most likely not only determined by one single rate-determining step (RDS) that can be evaluated by a sole intermediate. Besides, for alkaline HER, other factors such as reactive interface, electrochemical environment, and physical hybrid constructions of the catalyst, are more influential toward the reaction process comparing to that in an acid environment.²⁰⁻²⁵ The best way to study these critical factors is in-situ characterization (both spectroscopy and electrochemistry),²⁶⁻²⁸ which may provide more advanced guidance for design of catalysts.

In this review, we attempt to provide some recommendations for the design of highly active alkaline HER catalysts based on the newest theoretical and experimental achievements. First, we

briefly introduce the recent developments on the HER mechanism under alkaline conditions with special emphasis on the fundamentals of this process. Then, we discuss how this knowledge is linked to the principles of catalyst design by tailoring the electronic structure and/or creating active sites on the catalytic materials. We aim to (i) build up a clear connection between the mechanistic studies and the design of catalysts for alkaline HER; and (ii) directly present the catalyst design strategies based on the current knowledge. We hope that a comprehensive understanding of HER under alkaline conditions can provide more insights into other electrocatalytic reduction reactions like CRR and NRR under neutral conditions.

Origin of the slow kinetics of HER under alkaline conditions

Based on our best knowledge, one of the biggest mysteries about HER is the nature of its pH-dependent kinetics. As shown in **Figure 2 a-c**, it is very clear that the HER activity of a variety of Pt catalysts decreases continuously with increasing pH of electrolytes.^{11,12,29} For example, in an alkaline environment, the reaction activity can be two orders of magnitudes slower than that in acid media for Pt group metal catalysts. Such difference can be also reflected in kinetic and thermodynamic parameters for the majority of catalysts, including exchange current density (j_0), Tafel slope and reaction activation energy(ΔH).^{8,9} For more than a decade, some in-depth research has been done using model catalysts (Pt group single crystals) to find out a comprehensive explanation of this phenomenon.^{10-16,30} Based on all these works, the current studies are focusing on three most possible scenarios considered by: water dissociation theory, HBE theory, and interface water and/or anion transfer theory. So far, it is still hard to judge, which of these theories, if any, is close to the real mechanism of HER under alkaline conditions.

Water dissociation theory: what is the role of OH?

In acid environments, the abundant H^+ in electrolytes can create H^* -rich surface under an overpotential condition, while in alkaline/neutral environments, H^* can only be originated from water dissociation

process ($\text{H}_2\text{O} + \cdot \leftrightarrow \text{H}^{\cdot} + \text{OH}$). Therefore, it is very reasonable to conclude the energy barrier induced by extra water dissociation is the cause to the slow alkaline HER kinetics. Based on the systematic experiments performed for a series of Pt-based materials, Markovic et al. were the pioneers in explaining the effect of water dissociation on the HER kinetics under alkaline conditions.^{10,31} They suggested that during water dissociation process, adsorption of OH^{\cdot} competes with H^{\cdot} on one single active site, therefore weakening the generation of H_2 . By providing separate oxophilic sites that can host OH^{\cdot} for water dissociation, the generation of H^{\cdot} can be largely promoted, thus, improving the kinetics of Volmer step. For example, a well-defined Pt (111) catalyst with extra water dissociation sites (e.g., $\text{M}(\text{OH})_2$ clusters, $\text{M} = \text{Fe}, \text{Co}, \text{Ni}$) was constructed to demonstrate this concept (**Figure 2d**). It was proved that the aforementioned $\text{M}(\text{OH})_2$ sites can significantly improve the interaction between the catalyst and OH^{\cdot} , in turn, promote the water dissociation rate and overall HER activity. Based on this principle, it was later found that by creating dual sites for water dissociation using other oxophilic metals (such as Ru), one can further enhance HER activity under alkaline conditions.^{11,32-34} It was even reported that the activities of $\text{Pt}_{0.1}\text{Ru}_{0.9}$ in alkaline solutions and Pt in acid solutions are identical (**Figure 2e**).¹¹

However, although the ‘dual active sites’ strategy indeed improves the catalyst’s activity for alkaline HER, the enhancement origin raises some doubts. It was suggested that the outstanding alkaline HER kinetics of dual-site catalysts is not due to the so-called ‘dual active sites effect’, but likely due to the changed electronic structure of the material.^{35,36} Moreover, the original electronic structure of a metal can be altered when a second metal is introduced. With an optimized HBE, one catalyst’s overall HER performance can also be enhanced.^{37,38} This has been proved in the case of Ru@Pt nanoparticles, in which the oxophilic Ru sites are fully covered by Pt and cannot provide water dissociation sites.³⁹ Nevertheless, the Ru@Pt nanoparticles represent much better HER activity as compared to Pt or RuPt alloy.^{33,40} Besides, more recent studies suggest that adsorption of OH^{\cdot} does not participate in the Volmer step of alkaline HER, nor does it affect the HER activity.^{30,41} These doubts

have led to a more detailed consideration of catalyst-intermediate interactions in alkaline HER process beyond the initial water dissociation step.

Although it was suggested that adsorption of OH^* does not affect the activity of alkaline HER, the origin of slow HER kinetics is still believed to be related to the role of OH^- . Using in-situ X-ray absorption near edge structure (XANES) characterization, Jia et al. recently proposed that the transfer of OH^* is the RDS for alkaline HER, and this process can be promoted by the presence of adsorbed hydroxyl-water-alkali metal cation ($\text{OH}_{\text{ad}}\text{-(H}_2\text{O)}_x\text{-AM}^+$) in the double layer region.¹⁵ The $\text{OH}_{\text{ad}}\text{-(H}_2\text{O)}_x\text{-AM}^+$ adduct can help directly to remove OH from the electric double layer to the bulk solution right after water dissociation, therefore, promoting the overall HER activity (**Figure 2f**). Noticeably, unlike the water dissociation theory, where adsorption of OH^* is considered to be the key descriptor of the reaction,¹⁰ Jia et al. theoretical considerations emphasize the importance of transport process of OH^* through the double layer, i.e., the overall activity of a catalyst is not determined by the OH^* binding energy, but is largely dependent on the presence of metal cation (AM^+) and the structure of the electric double layer. By changing the AM^+ species in electrolytes (e.g., using Li^+ instead of K^+), the kinetics of OH_{ad} transfer can be altered and the overall HER activity can be increased. As the abundance of OH^- and AM^+ is pH-dependent, the HER kinetics is in turn closely controlled by the pH on the catalyst surface.

HBE theory: Is HBE a universal descriptor for HER?

Considering that the reaction pathway of HER is similar in alkaline and acid environments and is closely related to the catalyst-hydrogen interactions, many researchers believe that the HER activity is determined by the same factor in all pH environments: HBE of the catalyst.^{13,35,36} The first experimental evidence for this theory was provided by Yan et al.¹³ Using polycrystal Pt as a model catalyst, they proposed a systematic study on the dependence of HBE as a function of the electrolyte pH. As shown in the cyclic voltammetry (CV) of polycrystal Pt (**Figure 3a**), the peaks reflecting the under potential deposition of hydrogen (H_{upd}) can be assigned to Pt (110) and Pt (100), respectively.

The position of these peaks shows a pH-dependent shift. When the pH increased from 0.2 to 12.8, the H_{upd} peak shifts positively by 0.15 V, directly reflecting the pH-dependent HBE of Pt. Further, it is suggested that a stronger HBE leads to a higher activation barrier, which is responsible to the slow HER kinetics in high-pH environments. Similar phenomena were also found in nanostructured metal catalysts with good HER activity such as Pt, Ir, Pd and Rh (**Figure 3b**).¹² For these nanostructured catalysts, an obvious trend throughout all pH range is that a weaker H adsorption leads to larger exchange current density, and vice versa. This further suggests that HBE changes under various OH⁻ environments and determines the overall HER activity. Interestingly, HBE of a catalyst was shown to be an inherent property of a material and should be independent on the change of pH in local environments.^{8,9} To explain this contradiction, Yan. et al. hypothesized that the changed hydrogen/water adsorption energies result from different water dipole orientation under various OH⁻ concentrations of the electrolytes.¹² In other words, it is believed that the intermediates other than H^{*} (e.g., OH^{*} and H₂O^{*}) only influence the reaction by altering HBE of the catalyst. Although this hypothesis has not been confirmed experimentally, computational calculations showed that the orientation of water on Pt surface can indeed be changed under different pH conditions. Using molecular dynamics simulation, Goddard et al. simulated alkaline HER process under different conditions and concluded that the pH-dependent HER activity is due to the changes of water adsorption on the electrode.⁴² Specifically, under a higher pH value and a more negative applied potential, Pt (100) electrode becomes more hydrophobic as represented by the orientation distribution of water molecules close to the surface. As a result, the water adsorption decreases with increasing pH value, which in turn, increases the hydrogen bonding within the monolayer (**Figure 3c, d**). Based on this argument, they claimed that the weakened water adsorption is the dominant cause of the pH-dependent HBE.

Despite the successful theoretical computations, the HBE dependent theory seems to be not universal. For example, on Pt (111) surface, while the HER activity largely alters under different pH conditions, the position of H_{upd} peak does not change much.¹⁴ As a result, many researchers suggested

that the nature of H_{upd} is unlikely to be determined by adsorption of hydrogen alone.¹⁴⁻¹⁶ Therefore, the atomic-scale electrochemical interface structure on the catalyst surface was taken into account. For example, the changes in the electric double layer under different pH and its influence on the overall reaction have been considered. Koper et al. proposed a model indicating that the barrier of alkaline HER depends on the relationship between the electrode potential and pzfc.¹⁴ They found that the H_{upd} peak shifts in the same way as pzfc under changing pH conditions. Therefore, it is believed the changed pzfc alters the reorganization energy of the interfacial water to move H^+ or OH^- from the electrode surface to the electrolyte bulk. For HER in any water-based electrolyte, hydrogen adsorption has to proceed through the charge transfer within the interfacial double layer. The efficiency of such charge transfer is dependent on the charge separation between the electrode and the bulk electrolyte, which is determined by the position of pzfc. In an acid environment, the pzfc of Pt is close to the potential of hydrogen adsorption region. This means the reorganization energy is relatively small, while in an alkaline environment, such energy is much larger in comparison to that in acid environment. By introducing Ni hydroxide deposition on the Pt (111) surface, the pzfc can be shifted close to the potential of hydrogen adsorption region, therefore reducing the activation barrier for hydrogen adsorption and improving the overall activity. Importantly, this result provides a reasonable explanation to the so-called ‘dual-site’ alkaline HER electrocatalysts from the perspective of catalyst-hydrogen interactions.

Designing of the alkaline HER catalyst

As discussed before, it is still unsure whether water dissociation or hydrogen adsorption are the key factors in boosting the alkaline HER kinetics. As a result, many alkaline HER catalysts were designed following the guidelines for acid environments. Such methodology is based on the discovery of Nørskov et al.,^{18,19,43} which has been proved to be applicable for the reactions with a single type of reactive intermediates that is directly related to the RDS of the reaction, such as ORR and acid HER.

This designing strategy always starts from analysis of the electronic structure (e.g., position of D-band center) of a group of materials by DFT computations¹⁷⁻¹⁹ Afterwards, the adsorption ability toward key reactive intermediates (e.g., H^* for acid HER or OOH^* for ORR) can be estimated and be linked to the materials' inherent property.⁴⁴⁻⁴⁶ With this information, the so-called descriptor-based 'volcano plot' can be built up to directly represent the relationship between the calculated adsorption ability and the apparent activity of the catalysts.^{47,48} A candidate with the best activity is located at the top of the volcano plot.^{43,49,50}

However, it is still doubtful whether such strategy is applicable for alkaline HER. As both OH^- and H^+ ions participate in the reaction, it is important to evaluate the influence of both intermediates toward the catalytic activity and to design the balanced active sites correspondingly. From the perspective of catalyst design, all strategies for material engineering applied to catalysts should aim to achieve both or either of the two goals: optimizing the thermodynamics of the reaction by lowering water dissociation barrier; and/or enhancing the reaction kinetics by improving the catalyst-H interaction. In material engineering, several operational approaches can be used to achieve this goal, and they can be classified into a few categories, such as dual-site, surface strain and electronic structure engineering, which nowadays covers the design of the most successful alkaline HER catalysts (**Figure 4**). Note that good physical properties such as large active area and high conductivity can always benefit the activity of a catalyst. It is a regular routine that is applicable for all electrocatalysts despite of a specific reaction. Such strategies were explored in many excellent works and would not be emphasized in this review.^{26,51,52} Here, we only focus on the methods that can optimize catalysts' inherent properties by using chemical approaches.

Creating dual active sites

Although the specific role of OH^- is yet unknown in alkaline HER, it is clear that the interaction between the catalyst and OH^- is one of the key factors in controlling the catalytic activity. However, balancing the adsorption/desorption ability toward OH^* and H^* on one site is extremely hard due to the

poorly known scaling relationship between the binding energy of these two intermediates. In order to separately gain control over OH^* and H^* , one of the most accepted strategies is to create dual active sites that can individually feature distinct functions. Under this concept, Markovic et al. reported a series of catalysts by decorating bulk Pt with another metal or metal hydroxide sites.^{10,11,31,53,54} The general idea was to achieve a hybrid material with an appropriate HBE for HER by coupling a material on the top of the acid HER volcano plot, such as Pt, with an oxophilic metal that can provide good OH⁻ interaction sites for water dissociation process. A comparison of oxophilicity for several commonly used materials are shown in **Figure 5a**; a stronger oxophilicity indicates a stronger OH binding energy, *vice versa*.⁵⁵ Just like the case of HBE, the OH binding energy of a catalyst has to be neither too strong nor too weak in order to provide a proper catalyst-water interaction. Thus, a few candidates, such as Ni, Ru and Co, stand out for their appropriate oxophilicity. These materials are widely used in the design of catalysts with dual active sites and exhibit an outstanding performance.⁵⁶⁻⁶⁰

Based on the success of the alloys with dual sites, non-noble materials have been used to replace Pt as H^* interaction sites to construct more cost-effective catalysts. Just like Pt, MoS_2 and graphitic carbon nitride (g- C_3N_4) have all been proved to have perfect hydrogen adsorption ability in HER process. A good such example was reported by Yang et al., who used MoS_2 as H-active material and the layered double hydroxides (LDH) as OH-active sites for good HER performance (**Figure 5b**).⁶¹ The DFT calculations showed that the increased performance of MoS_2/LDH heterostructures is due to the lowered activation energy (**Figure 5c**), which is a result of the optimized water dissociation process. Just like Pt/ $\text{Ni}(\text{OH})_2$, the MoS_2/LDH provides distinct sites for H adsorption (on MoS_2) and water dissociation (on LDH). These sites act synergistically in promoting the overall alkaline HER process (**Figure 5d**). Similar as H-adsorption sites, OH-interaction sites can also be engineered or replaced with several materials. In another work, 2D MoN was used as OH^* adsorption site and coupled with C_3N_4 to boost alkaline HER.⁶² Using a salt-templated method, 2D MoN was fabricated and bonded to C_3N_4 through an electrostatic interaction (**Figure 6a**). Interestingly, such 2D MoN- C_3N_4 represents similar

HER activity in 1 M KOH and 0.5 M H₂SO₄ electrolytes (**Figure 6b**), which is very rare in the case of HER catalysts. Such trend indicates that the reaction barrier induced by water dissociation process does not affect the activity of 2D MoN-C₃N₄ due to the superior water dissociation ability of 2D MoN as confirmed by DFT computations (**Figure 6c**). By tuning the g-C₃N₄ to MoN ratio, the activity of the catalyst can be directly controlled as shown in the volcano plot, further indicating the importance of the balance between hydrogen adsorption (on C₃N₄ site) and water dissociation (on MoN site) abilities on a catalyst (**Figure 6d**). Similar dual-site catalysts with high alkaline HER activity such as Ni(OH)₂/MoS₂ and Ni (Fe, Co, Ru) doped MoS₂ were reported.^{56,61,63-68} In all cases, the successful designs are based on the idea of proper balancing water dissociation and hydrogen adsorption, which is proved to be an effective strategy for improving the activity of a catalyst for alkaline HER.

Controlling the electronic structure of the catalysts

For most of heterogeneous catalysts, the electronic structure is the sole factor that determines their inherent adsorption abilities toward all kinds of intermediates.^{17,22,26,44} Thus, interfering the electronic band of a catalyst is an effective way to control its catalytic performance. In particular, for alkaline HER, tuning the electronic structure of a catalyst mainly aims to improve its HBE, similar to the strategies in acid environments.

Metal catalysts: D-band engineering. For hydrogen, higher vacancy of the d-band of a metal catalyst indicates an upshift of d-band center in energy toward the Fermi level, which leads to a stronger adsorptive hydrogen bond, and *vice versa*.^{18,19,44} Alloying one metal with another is the most efficient way to engineer the d-band vacancy of a metal-based catalyst. As shown in **Figure 7a**, for most of metal catalysts, their HBE can be altered by alloying with a second metal, mostly as a result of the mass electron transfer between two different metal sites.^{37,46} In some cases, such massive electron transfer can also contribute to the electronic structure of the non-metallic sites, which work synergistically with metal alloy for the overall catalytic performance. One such example is a series of RuCo alloy encapsulated in N doped graphene layer.⁵⁹ Although Ru itself is already a very active metal

in catalyzing alkaline HER, the activity and stability of RuCoC alloy are even much better (**Figure 7b**). DFT calculations indicate that the good performance is closely related to the special electron structure of the carbon shell, in which the electron transfer from the metal to the carbon shell is largely changed due to the alloying of RuCo (**Figure 7c**). As a result, the C-H bond on the carbon surface is enhanced, lowering HBE of the catalyst, and improving the overall activity. Similar examples were also reported for other alloy catalysts.⁶⁹⁻⁷⁵ For example, Huang et al. reported a PtNi/NiS nanowire that exhibited a 5.58 times higher current density than Pt/C at -0.07 V vs. RHE.⁷⁶ Zheng. et al. reported a PtNi alloy in the form of hexagonally close-packed nano-multipods that showed a much better HER activity than Pt/C.⁷⁷

Noticeably, editing the electronic structure through alloying can also activate non-noble metal materials that normally have poor HER activities.^{71,72,74,78} Chen et al. reported a Cu-Ti bimetallic electrocatalyst that represents an outstanding alkaline HER activity.⁷² By adjusting Ti's concentration in the catalyst, the electronic structure of CuTi was altered, and HBE of the catalyst was optimized to a much more appropriate level, which placed this catalyst at the top of the volcano plot. As a result, although neither Cu or Ti is a good HER candidate, the Cu-Ti catalyst exhibited a tremendous activity.⁷² Similar situation was reported for MoNi₄ alloy.⁷⁹ Although Mo, Ni, and MoO₂ exhibit very sluggish alkaline HER kinetics, MoNi₄ alloy featured a significantly improved electronic structure and showed an outstanding water dissociation ability due to the reconstructed electronic structure of the alloy. These properties of MoNi₄ guaranteed its outstanding HER activity in alkaline environment.

Transition-metal based catalysts: Defect engineering and heteroatom doping. Thanks to the fast-developing synthesis techniques, earth abundant and cost-effective transition metal dichalcogenides, nitrides, chalcogenides, and phosphides with different morphologies have been widely developed in last decades.^{51,80-82} It was found that with proper electronic structure engineering, many transition metal based materials represent very good interaction with H.^{51,82} Among those, Mo-based catalysts such as MoS₂ and Mo₂C are the most popular ones due to their outstanding performance in acid

environments.^{51,83-85} However, in alkaline environments, the engineering of the transition metal based catalysts is more complicated as a result of the interfering of water dissociation process. Taking 2D MoS₂ and MoSe₂ as examples, it was found that their active sites for HER are different under acid and alkaline environments.^{84,86} While it is widely known that modifying the Mo edge sites and/or S/Se vacancies of these catalysts can be used to effectively promote their HER in acid, the same strategy does not work well in alkaline electrolytes. This is because these metal-terminated edge sites show strong OH adsorption ability in alkaline environment. With OH intermediates on the edge sites, the S(Se) -rich groups that are mostly present on the terrace of the catalyst are the dominant H^{*} active sites for alkaline HER.^{86,87}

The importance of S sites on the transition metal sulfides for alkaline HER was also proved by Markovic et al., who investigated the catalytic mechanism of metal sulfides on both bulk model catalyst (S island on Au (111)) and TMS_x (TM = Mo, Co, x = 4 - 6) nanomaterials.⁸⁸ It was found that the irreversibly adsorbed S (S_{ad}^{δ-}) on Au (111) acts as a promoter to alter the HER activity through the S_{ad}^{δ-} - cationⁿ⁺ - H₂O bonding (**Figure 8a**). Such connection can introduce hydrated cations to boost the water dissociation process, therefore promoting the alkaline HER process. This mechanism was then applied to design TMS_x catalysts, where S_{ad}^{δ-} - TMⁿ⁺ shows a similar behavior as S_{ad}^{δ-} - cationⁿ⁺. Further, the relationship between the activity and stability of the TMS_x catalysts was found to be governed by tunable substrate-adsorbate binding energy and the number of defects on the catalysts. The defect rich CoS_x blocks are highly active but not as stable as less active MoS_x material. It was found that by inducing Co doping into the original TMS_x, a new site for water dissociation can be generated and work synergistically with H-active S sites. By designing a CoMoS_x material, a catalyst with both enhanced stable building blocks, good water dissociation ability and high activity was created (**Figure 8c**). This balanced design was proved to be an efficient method for engineering transition-metal-based catalysts.

To change the electronic structure of 2D transition metals, the defect engineering is a highly efficient way.^{89,90} Taking 2D MoS₂ as an example, the defects can be naturally generated on the boundary of different phases; with a certain modification, even the boundary in the inert basal plane can be activated for alkaline HER.⁹¹ Further DFT study indicates that different kinds of boundaries can lead to the remarkable changes in the Gibbs free energy of H*, in which the 2H-1T heterophase boundary shows the best performance. Besides defect engineering, heteroatom doping is also a popular way for changing the electronic structure of 2D transition metals for acid HER applications,^{92,93} and can be adopted for the design catalysts for alkaline environment. For example, carbon doped MoS₂ (C-MoS₂, fabricated through the sulfurization of Mo₂C) presents high alkaline HER activity very close to that of Pt/C (**Figure 9a**).⁹⁴ The extraordinary activity is a result of the carbon doping, which changed the electronic structure of MoS₂. Instead of playing the role of a dual active site, the carbon in the catalyst induced empty 2p orbitals perpendicular to MoS₂ basal plane, which is favorable for water adsorption (**Figure 9b**). Consequently, the catalyst shows an increased water dissociation rate in alkaline environments and an improved overall activity. Noticeably, defect engineering and heteroatom doping are also effective strategies for carbon-based catalysts.^{22,27,49,50,95-102} For alkaline HER in particular, it has been proved that both defect engineering and heteroatom doping can be used to directly optimize the valence orbital energy for carbon sites, thus, improving the interaction between carbon and H* intermediates. However, the carbon-based materials usually show better performance when coupled with other catalysts instead of being the sole catalytic center in alkaline HER.^{56,103} Therefore, a detailed discussion of these materials is not the subject of this review.

Another commonly applied strategy for improving the inherent adsorption ability of the transition metals is to change the charge density of the catalytic surface. One of the most often used methods to achieve this goal is coupling transition metal based catalysts with another materials. Zou et al. reported a good example for controlling the charge transfer of Mo₂C-based HER catalyst.¹⁰⁴ By covering Mo₂C with nitrogen-rich carbon, the HER catalytic activity of the resultant material was boosted in all pH

environments (**Figure 9c**), which is the sole result of the optimized H adsorption ability of the catalyst. Different from the C doping case as mentioned before, it was revealed that the strong electron-withdrawing ability of N sites induced an electron transfer that draw electrons from Mo₂C to N via C sites. Such process activated the C atoms neighboring to N sites and created HER-active C sites that can work synergistically with Mo₂C (**Figure 9d**). As a result, the overall HER activity under all pH environments could be generally promoted. Similar strategies were also reported to other alkaline HER catalysts, and have been proved to be effective not only for adjusting the H adsorption ability of the catalysts, but also for optimizing the catalyst-water (OH) interaction.¹⁰⁵⁻¹⁰⁷ One typical example is MoP@C catalyst, which exhibited a remarkable HER activity in alkaline environment (**Figure 9e**).¹⁰⁷ The presence of carbon on the surface of MoP has resulted in the Mo-C bond in the catalyst, which largely altered the electronic structure of Mo. As a result, the improved Mo site has become appropriate for water dissociation, while the hydrogen recombination occurred on the neighboring P sites (**Figure 9f**). Such construction was shown to be an ideal platform for processing alkaline HER. Its simple design that can boost two processes in one attempt is the most efficient way for creating high-quality HER catalysts.

Adjusting surface geometry of the catalysts

Alkaline HER has been proved to be extremely sensitive to the surface structure of the catalysts.¹⁰⁸ As early as 1990s, Markovic et al. reported that HER/HOR on various Pt single crystals are very different, with increasing activity in the sequence of Pt(111) < Pt(100) < Pt(110) in alkaline environment.¹⁰⁹ Although DFT calculations clarified how various Pt crystal facets can alter the electronic structure and the H adsorption ability of the catalyst, the true surface-sensitive nature of the alkaline HER is still a puzzle. Until now, it is still unknown how H_{upd} and H_{opd} are separately influenced by the surface structure of the catalysts.⁸ In practice, one of the handiest ways to modify the surface structure of a catalyst is through the lattice strain engineering. It has been proved that a small change in the lattice strain can severely alter the interaction between the catalyst and intermediates. For example, 1 % lattice

strain on the Pt surface can result in a ~ 0.1 eV shift on its d-band center, which can make an obvious difference in Pt's HBE.^{44,110} In comparison to the catalyst-H interaction, the strain has more influence toward the interaction between the catalyst and O-bound intermediates (e. g., OH). It was found that for late transition metals such as Pt and Ru, the tensile lattice strain can cause a stronger interaction with O-based intermediates, and vice versa.^{111,112} Noticeably, such trend is opposite to early transition metals.¹¹³

Inducing the desired strain on the surface of a catalyst has always been challenging in material engineering. Typically, by lattice adjusting,¹¹⁴ fabricating certain core-shell structures¹¹⁵ and creating specially angled or defected morphologies,^{116,117} one can alter the surface strain of a variety of materials. For nanostructured catalysts in particular, the morphology modulation methods such as crystal shaping, dealloying and inducing lattice mismatch can also change the surface of a material into a more beneficially strained structure.¹¹⁸ These strategies have been used for improving the catalytic performance of the ORR catalysts, and were proved to be efficient for HER catalysts such as MoS₂ and WS₂ in acid environments.^{114,115,119-121} In recent years, many attempts have been made to extend this method into alkaline HER applications. One typical example of creating a highly active alkaline HER catalyst through a systematic processing of alloying induced strain engineering is the Pt₃Ni alloy reported by Stamenkovic et al.¹²² By constructing Pt₃Ni polyhedra, followed by removal of extra Ni and annealing the product in Ar atmosphere, Pt₃Ni nanoframes with Pt skin were constructed (**Figure 10a**). With Ni being covered by Pt, the outstanding alkaline HER catalytic performance of Pt₃Ni nanoframes cannot be originated from dual active sites for water dissociation. The high alkaline HER activity is solely the result of the optimized electronic structure of Pt. On one hand, the Pt₃Ni nanoframes provide a mixture of a variety of Pt crystal structures and crystal interfaces. On another, the core-shell structure of the Pt₃Ni nanoframes results in the compressive strain on the Pt surface. Together these properties shape the electronic band structure of the Pt₃Ni nanoframe catalyst, which results in an outstanding alkaline HER activity (**Figure 10b**).

Although strain engineering through alloying is always considered to be most effective in shifting the surface catalytic properties of noble metal materials, there are some concerns whether the improved catalytic performance is due to the electronic transfer between the two metals or a result of strain altering. To understand the sole influence of surface strain in HER, we studied the effect of the geometric and electronic effects separately for the core-shell structured RuPt catalysts (**Figure 10c**).⁴⁰ The core-shell bimetallic Ru@Pt represents a larger compressive strain (~ 3%) due to the lattice mismatch comparing to that in the RuPt alloy (**Figure 10d**). It was found that with the compressive strain, the catalyst showed the decreased H adsorption ability and enhanced catalyst-OH interaction, resulting in a largely increased activity (**Figure 10e**). Such strain-induced improvement in the HER activity is not limited to metal catalysts, but also was reported for transition metal oxides. A good example of such case material are the S-CoO sawtooth-rich nanorods with 3 % surface tensile strain.¹²³ As can be seen, for each little sawtooth structure, the strain component ϵ (associated with the expansion/contraction of the respective lattice vectors R1 and R2) shows a biaxial strain on the surface of the nanotooth (**Figure 10f**). Due to this tensile strain, a large number of O-vacancies was generated, which optimized the water dissociation barrier and the HBE of the catalyst. As a result, the tensile-strain of the S-CoO nanorods led to an impressive overall HER activity even comparable to the commercial noble metal catalysts (**Figure 10g**).

Conclusions and outlook

A large variety of highly active alkaline HER catalysts has been reported in the last decade due to the development of theoretical computation and material engineering technologies. These successful design strategies are aimed either to improve the interaction between the active sites and certain intermediates, or to lower the overall energy barrier of the reaction. Most of these methods are universal toward catalyst design for other energy conversion technologies. Aiming at a thorough understanding and total control of alkaline HER, we are still facing several challenges as below.

I. Fundamentally, the origin of the slow kinetics of alkaline HER is still unknown. From the experimental perspective, such mystery is likely to be solved by gaining better understanding toward the catalyst-intermediates interactions on the active sites during the reaction. This can only be achieved by employing more in-situ characterizations, such as TEM, X-ray and vibrational spectroscopies, etc, to monitor the course of reaction. The local environments (e.g., local pH, electric double layer), the dynamic transformation of the catalytic surface structure are all substantial factors in determining the alkaline HER mechanism and should be studied in the future.

II. The transfer of ions through the electric double layer/water layer is proved to be crucial during alkaline HER. However, in the catalyst design, currently there are no specific strategies aiming to optimize these aspects. As the structure of the electric double layer is closely related to the catalytic surface, it is important to gain a comprehensive understanding on the relationship between the material surface properties and the structure of electric double layer/water interface under electrocatalytic environments.

III. Beside focusing on the reaction mechanism on the traditional single crystal Pt model catalysts, more attention should be paid to systematically study the catalytic mechanism on the typical nanostructured catalysts that are more active and widely used in practice. With more complex surface structures, the reaction mechanism on nanostructured catalysts can be partially different from that on model single crystals. For typical nanostructured catalysts such as bimetallic alloys and transition metal-based compounds, finding the true activity origin on these highly complex surfaces is important for providing guideline toward design of new generation of catalysts.

IV. From the computation perspective, more feasible operando computation techniques are needed to better simulate the reaction process by taking the local environmental factors (e.g., influence of water, metal cations, and anions) into account. Ideally, the operando spectroscopy and computation could work synergistically in uncovering the nature of the alkaline HER. Noticeably, this point is also

one of the key issues regarding to other heterogeneous reduction reactions involving multiple intermediates such as CRR and NRR.

Acknowledgments

Y. Zheng and S. Z. Qiao acknowledge financial support from the Australian Research Council through Discovery and Linkage Project programs (DP160104866, DP170104464, LP160100927, DE160101163 and FL170100154).

References

1. Deng, J., *et al.*, *Joule* 2 (2018) 846.
2. Guo, C., *et al.*, *Energ. Environ. Sci.* 11 (2018) 45.
3. Kuhl, K. P., *et al.*, *J. Am. Chem. Soc.* 136 (2014) 14107.
4. Singh, A. R., *et al.*, *ACS Catal.* 7 (2016) 706.
5. Vasileff, A., *et al.*, *Chem* 4 (2018) 1809.
6. Dunwell, M., *et al.*, *ACS Catal.* 8 (2018) 8121.
7. Lum, Y., *et al.*, *J. Am. Chem. Soc.* 140 (2018) 9337.
8. Schmidt, T., *et al.*, *J. Electroanal. Chem.* 524 (2002) 252.
9. Marković, N., *et al.*, *J. Phys. Chem. B* 103 (1999) 8568.
10. Subbaraman, R., *et al.*, *Nat. Mater.* 11 (2012) 550.
11. Strmcnik, D., *et al.*, *Nat. Chem.* 5 (2013) 300.
12. Zheng, J., *et al.*, *Sci. Adv.* 2 (2016) e1501602.
13. Sheng, W., *et al.*, *Nat. Commun.* 6 (2015) 5848.
14. Ledezma-Yanez, I., *et al.*, *Nat. Energy* 2 (2017) 17031.
15. Liu, E., *et al.*, *J. Am. Chem. Soc.* 147 (2019) 3232.
16. Ramaswamy, N., *et al.*, *Nano Energy* 41 (2017) 765.
17. Nørskov, J. K., *et al.*, *Nat. Chem.* 1 (2009) 37.
18. Nørskov, J. K., *et al.*, *J. Electrochem. Soc.* 152 (2005) J23.
19. Skúlason, E., *et al.*, *J. Phys. Chem. C* 114 (2010) 18182.
20. Jin, H., *et al.*, *Chem. Rev.* 118 (2018) 6337.
21. Mahmood, N., *et al.*, *Adv. Sci.* 5 (2018) 1700464.
22. Wang, X., *et al.*, *Adv. Mater.* 31 (2018) 1803625.
23. Tang, C., *et al.*, *J. Energy Chem.* 26 (2017) 1077.

24. Stamenkovic, V. R., *et al.*, *Nat. Mater.* 16 (2016) 57.
25. Strmcnik, D., *et al.*, *Nano Energy* 29 (2016) 29.
26. Zheng, Y., *et al.*, *Adv. Mater.* 27 (2015) 5372.
27. Zhou, W., *et al.*, *Nano Energy* 28 (2016) 29.
28. Kang, Y., *et al.*, *Nano Today* 11 (2016) 587.
29. Zheng, J., *et al.*, *J. Electrochem. Soc.* 162 (2015) F1470.
30. Intikhab, S., *et al.*, *ACS Catal.* 7 (2017) 8314.
31. Subbaraman, R., *et al.*, *Science* 334 (2011)1256.
32. St. John, S., *et al.*, *J. Phys. Chem. C* 119 (2015) 13481.
33. Li, J., *et al.*, *Angew. Chem. Int. Ed. Engl.* 56 (2017) 15594.
34. Li, K., *et al.*, *Energ. Environ. Sci.* 11 (2018) 1232.
35. Wang, Y., *et al.*, *Energ. Environ. Sci.* 8 (2015) 177.
36. Durst, J., *et al.*, *Energy Environ. Sci.* 7 (2014) 2255.
37. Greeley, J., and Mavrikakis, M., *Nat. Mater.* 3 (2004) 810.
38. Xin, H., *et al.*, *Top. Catal.* 55 (2012) 376.
39. Elbert, K., *et al.*, *ACS Catal.* 5 (2015) 6764.
40. Wang, X., *et al.*, *ACS Energy Lett.* 3 (2018) 1198.
41. Rebollar, L., *et al.*, *J. Electrochem. Soc.* 165 (2018) J3209.
42. Cheng, T., *et al.*, *J. Am. Chem. Soc.* 140 (2018) 7787.
43. Kulkarni, A., *et al.*, *Chem. Rev.* 118 (2018) 2302.
44. Hammer, B., and Nørskov, J. K., Theoretical surface science and catalysis—calculations and concepts. In *Advances in Catalysis*, Elsevier (2000), Vol. 45, pp 71.
45. Ruban, A., *et al.*, *J. Mol. Catal. A: Chem.* 115 (1997) 421.
46. Stamenkovic, V. R., *et al.*, *Nat. Mater.* 6 (2007) 241.
47. Sheng, W., *et al.*, *Energ. Environ. Sci.* 6 (2013) 1509.
48. Laursen, A. B., *et al.*, *J. Chem. Educ.* 89 (2012) 1595.
49. Jiao, Y., *et al.*, *Nat. Energy* 1 (2016) 16130.
50. Zheng, Y., *et al.*, *ACS Nano* 8 (2014) 5290.
51. Gao, Q., *et al.*, *Adv. Mater.* 31 (2019) e1802880.
52. Jiao, Y., *et al.*, *Chem. Soc. Rev.* 44 (2015) 2060.
53. Zeng, Z., *et al.*, *Nat. Energy* 2 (2017) 17070.
54. Danilovic, N., *et al.*, *Angew. Chem.* 124 (2012) 12663.
55. Kepp, K. P., *Inorg. Chem.* 55 (2016) 9461.

56. Mahmood, J., *et al.*, *Nat. Nanotechnol.* 12 (2017) 441.
57. Yoon, D., *et al.*, *Small* 13 (2017) 1700052.
58. Yin, H., *et al.*, *Nat. Commun.* 6 (2015) 6430.
59. Su, J., *et al.*, *Nat. Commun.* 8 (2017) 14969.
60. Oh, A., *et al.*, *Nanoscale* 8 (2016) 16379.
61. Hu, J., *et al.*, *Joule* 1 (2017) 383.
62. Jin, H., *et al.*, *Nano Energy* 53 (2018) 690.
63. Liu, J., *et al.*, *Nanoscale* 9 (2017) 16616.
64. Zhang, B., *et al.*, *Nano Energy* 37 (2017) 74.
65. Zhang, J., *et al.*, *Energ. Environ. Sci.* 9 (2016) 2789.
66. Ma, Q., *et al.*, *Nano Energy* 41 (2017) 148.
67. Feng, J. X., *et al.*, *J. Am. Chem. Soc.* 140 (2018) 610.
68. Najafi, L., *et al.*, *ACS Nano* 13 (2019) 3162.
69. Wang, Z., *et al.*, *Nanoscale* 10 (2018) 12302.
70. Fang, M., *et al.*, *Nano Energy* 27 (2016) 247.
71. Li, Z., *et al.*, *ACS Catal.* 6 (2019) 5084.
72. Lu, Q., *et al.*, *Nat. Commun.* 6 (2015) 6567.
73. Lu, S., and Zhuang, Z., *J. Am. Chem. Soc.* 139 (2017) 5156.
74. Zhang, Q., *et al.*, *Small* 13 (2017) 1701648.
75. Jiang, P., *et al.*, *Adv. Mater.* 30 (2018) 1705324.
76. Wang, P., *et al.*, *Nat. Commun.* 8 (2017) 14580.
77. Cao, Z., *et al.*, *Nat. Commun.* 8 (2017) 15131.
78. Csernica, P. M., *et al.*, *ACS Catal.* 7 (2017) 3375.
79. Zhang, J., *et al.*, *Nat. Commun.* 8 (2017) 15437.
80. Chhowalla, M., *et al.*, *Nat. Chem.* 5 (2013) 263.
81. Yuan, C., *et al.*, *Angew. Chem. Int. Ed.* 53 (2014) 1488.
82. Chen, W.-F., *et al.*, *Chem. Commun.* 49 (2013) 8896.
83. Hinnemann, B., *et al.*, *J. Am. Chem. Soc.* 127 (2005) 5308.
84. Yan, Y., *et al.*, *ACS Catal.* 4 (2014) 1693.
85. Jaramillo, T. F., *et al.*, *Science* 317 (2007) 100.
86. Wiensch, J. D., *et al.*, *ACS Energy Lett.* 2 (2017) 2234.
87. Li, X., *et al.*, *J. Catal.* 137 (1992) 385.
88. Staszak-Jirkovsky, J., *et al.*, *Nat. Mater.* 15 (2016) 197.

89. Xie, J., *et al.*, *Adv. Mater.* 25 (2013) 5807.
90. Ye, G., *et al.*, *Nano Lett.* 16 (2016) 1097.
91. Zhu, J., *et al.*, *Nat. Commun.* 10 (2019) 1348.
92. Deng, J., *et al.*, *Energ. Environ. Sci.* 8 (2015) 1594.
93. Shi, Y., *et al.*, *J. Am. Chem. Soc.* 139 (2017) 15479.
94. Zang, Y., *et al.*, *Nat. Commun.* 10 (2019) 1217.
95. Yan, D., *et al.*, *Adv. Mater.* 29 (2017) 1606459.
96. Tang, C., *et al.*, *Adv. Mater.* 28 (2016) 6845.
97. Zheng, Y., *et al.*, *ACS Nano* 8 (2014) 5290.
98. Zhu, Y. P., *et al.*, *Acc. Chem. Res.* 50 (2017) 915.
99. Tang, C., and Zhang, Q., *Adv. Mater.* 29 (2017) 1604103.
100. Zheng, Y., *et al.*, *Angew. Chem. Int. Ed.* 54 (2015) 52.
101. Liu, X., and Dai, L., *Nat. Rev. Mater.* 1 (2016) 16064.
102. Jia, Y., *et al.*, *Adv. Mater.* 28 (2016) 9532.
103. Zheng, Y., *et al.*, *J. Am. Chem. Soc.* 138 (2016) 16174.
104. Liu, Y., *et al.*, *Angew. Chem. Int. Ed. Engl.* 54 (2015) 10752.
105. Chen, Y. Y., *et al.*, *ACS Nano* 10 (2016) 8851.
106. Wu, H. B., *et al.*, *Nat. Commun.* 6 (2015) 6512.
107. Li, G., *et al.*, *Adv. Energy Mater.* 8 (2018) 1801258.
108. Kitchin, J. R., *et al.*, *Phys. Rev. Lett.* 93 (2004) 156801.
109. Markovića, N. M., *et al.*, *J. Chem. Soc., Faraday Trans.* 92 (1996) 3719.
110. Deng, Q., *et al.*, *J. Catal.* 309 (2014) 351.
111. Mavrikakis, M., *et al.*, *Phys. Rev. Lett.* 81 (1998) 2819.
112. Hammer, B., and Nørskov, J., *Surf. Sci.* 343 (1995) 211.
113. Schnur, S., and Groß, A., *Phys. Rev. B* 81 (2010) 033402.
114. Wang, H., *et al.*, *Science* 354 (2016) 1031.
115. Strasser, P., *et al.*, *Nat. Chem.* 2 (2010) 454.
116. Luo, M., *et al.*, *Adv. Mater.* 30 (2018) 1705515.
117. Huang, H., *et al.*, *Angew. Chem. Int. Ed.* 56 (2017) 3594.
118. You, B., *et al.*, *Adv. Mater.* 31 (2019) 1807001.
119. Luo, M., and Guo, S., *Nat. Rev. Mater.* 2 (2017) 17059.
120. Li, H., *et al.*, *Nat. Mater.* 15 (2016) 364.
121. Voiry, D., *et al.*, *Nat. Mater.* 12 (2013) 850.

122. Chen, C., *et al.*, *Science* 343 (2014) 1339.
123. Ling, T., *et al.*, *Nat. Commun.* 8 (2017) 1509.

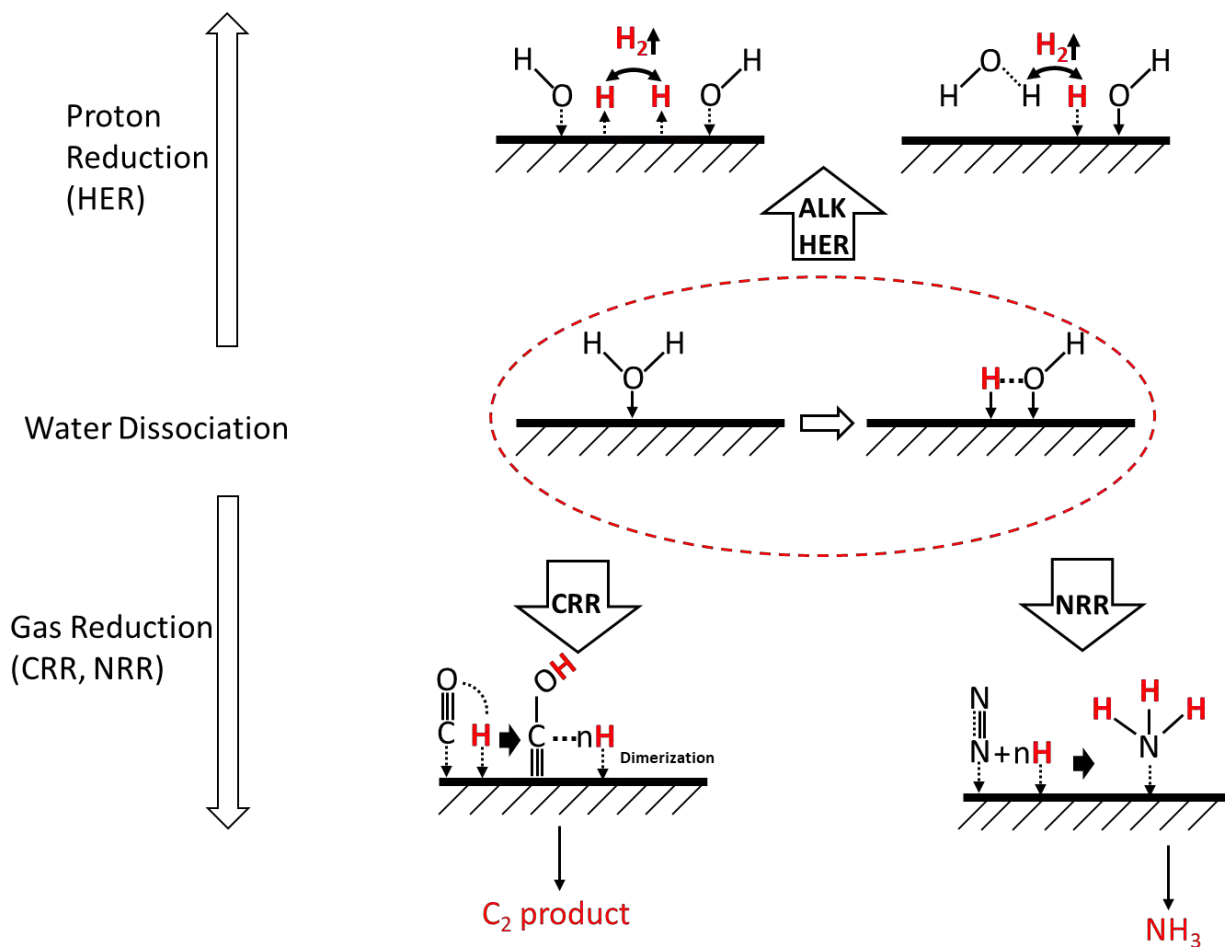


Figure 1 A scheme illustrating a comparison of water reduction, alkaline HER and two other widely studied heterogenous reduction reactions (CRR and NRR). For both CRR and NRR in natural/alkaline environments, water reduction and alkaline HER are two essential processes accompanying the gas reduction reactions. The red H shows the trace of the water dissociated hydrogen in different reactions.

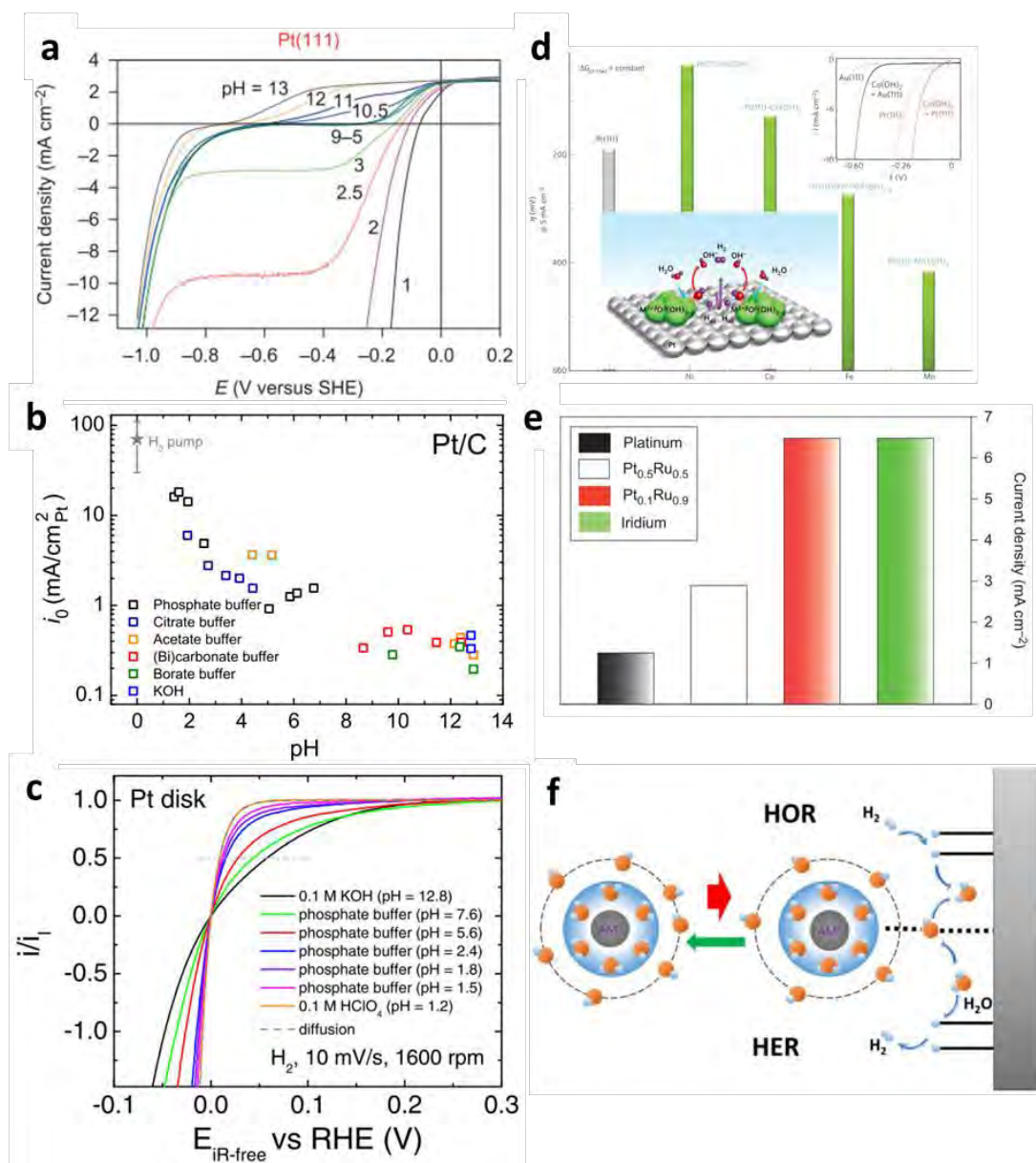


Figure 2 (a-c) The HER activity of several Pt-based materials in a variety of different environments. **(a)** Pt (111). Reproduced with permission.¹¹ Copyright 2013, Nature Publishing Group. **(b)** Pt/C. Reproduced with permission.¹² Copyright 2016, American Association for the Advancement of Science; **(c)** Pt disk. Reproduced with permission.²⁹ Copyright 2015, The Electrochemical Society. **(d)** Overpotential trend for HER of Pt (111) with a variety of 3d transition metal hydroxide sites. Inset: a schematic showing the reaction mechanism of alkaline HER on the catalysts. Reproduced with permission.¹⁰ Copyright 2012, Nature Publishing Group. **(e)** A comparison of current density at an overpotential of 0.05 V for several catalysts in 0.1 M KOH. Reproduced with permission.¹¹ Copyright 2013, Nature Publishing Group. **(f)** A scheme representing the mechanism of OH transfer in alkaline HER process. Reproduced with permission.¹⁵ Copyright 2019, The American Chemical Society.

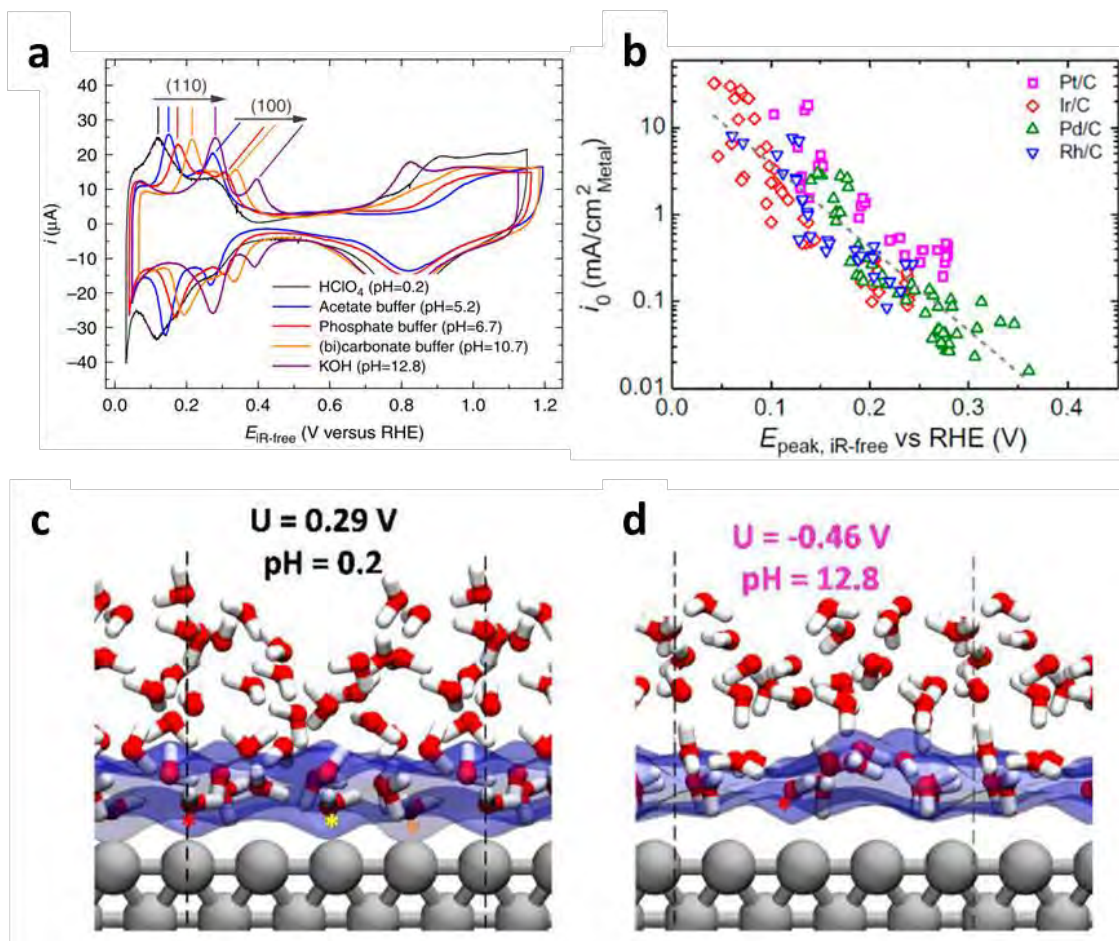


Figure 3 (a) A comparison of H_{upd} peak position for polycrystal Pt in a variety of electrolytes with different pH. Reproduced with permission.¹³ Copyright 2015, Nature Publishing Group. (b) A correlation between the exchange current density and H_{upd} peak position for a few Pt group metals. Reproduced with permission.¹² Copyright 2016, American Association for the Advancement of Science; (c-d) The snapshots of the simulation result showing details of the interfacial water orientation under different applied potential and pH. Reproduced with permission.⁴² Copyright 2018, The American Chemical Society.

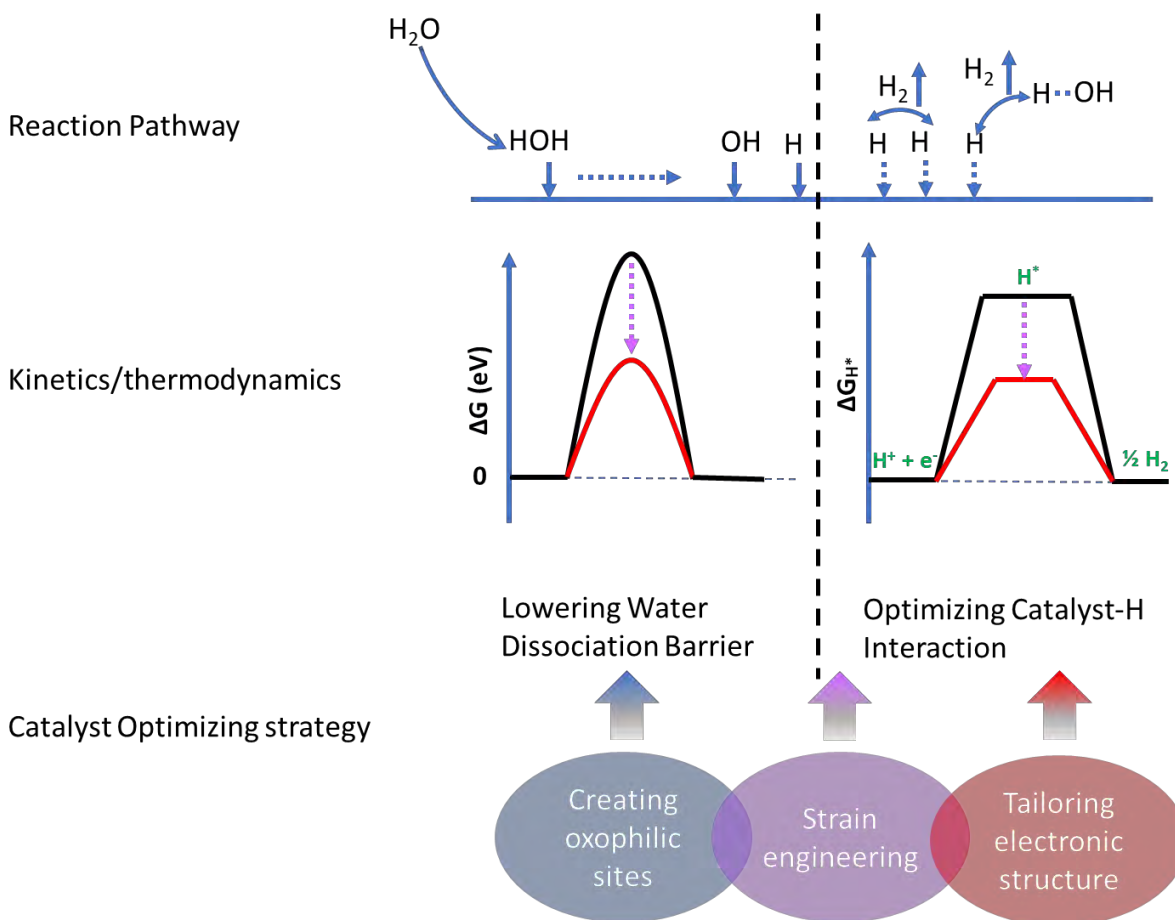


Figure 4 A scheme on the design strategies for alkaline HER based on the possible reaction mechanisms. The general idea is either to separately create water dissociation and hydrogen adsorption sites to achieve an ensemble effect, or to significantly optimize the hydrogen adsorption/desorption ability of the catalyst for a given reaction environment.

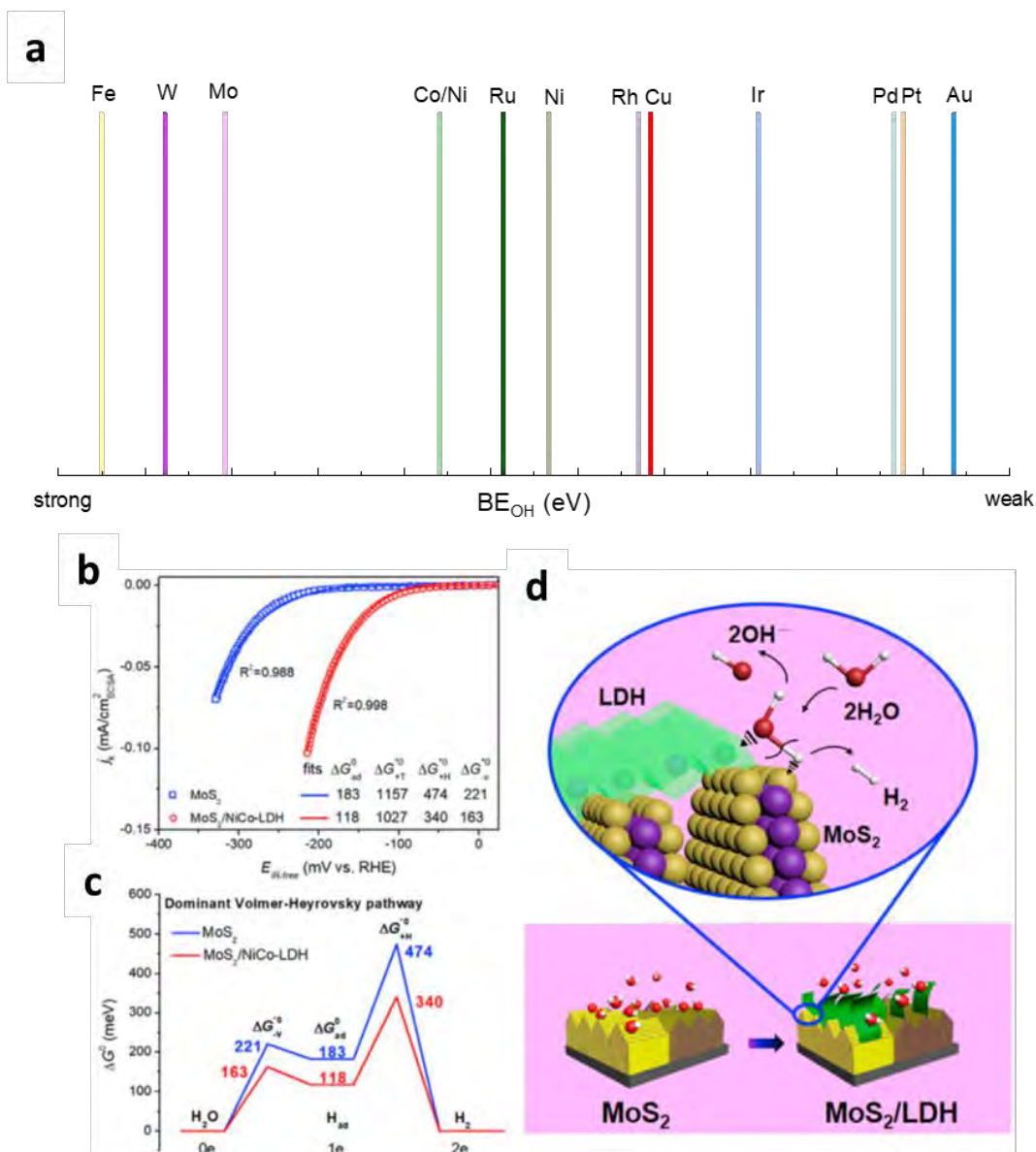


Figure 5 (a) A comparison of the oxophilicities of some metal materials that are commonly used as catalysts.⁵⁵ (b) A comparison between the HER activity of MoS₂ and MoS₂/NiCo-LDH in 1 M KOH with fitted standard activation free energies (meV). (c) Free energy diagram of the reaction pathway for MoS₂ and MoS₂/NiCo-LDH reproduced with permission. (d) A scheme of the alkaline HER reaction mechanism on the surface of the MoS₂/LDH catalyst.⁶¹ Copyright 2017, Elsevier.

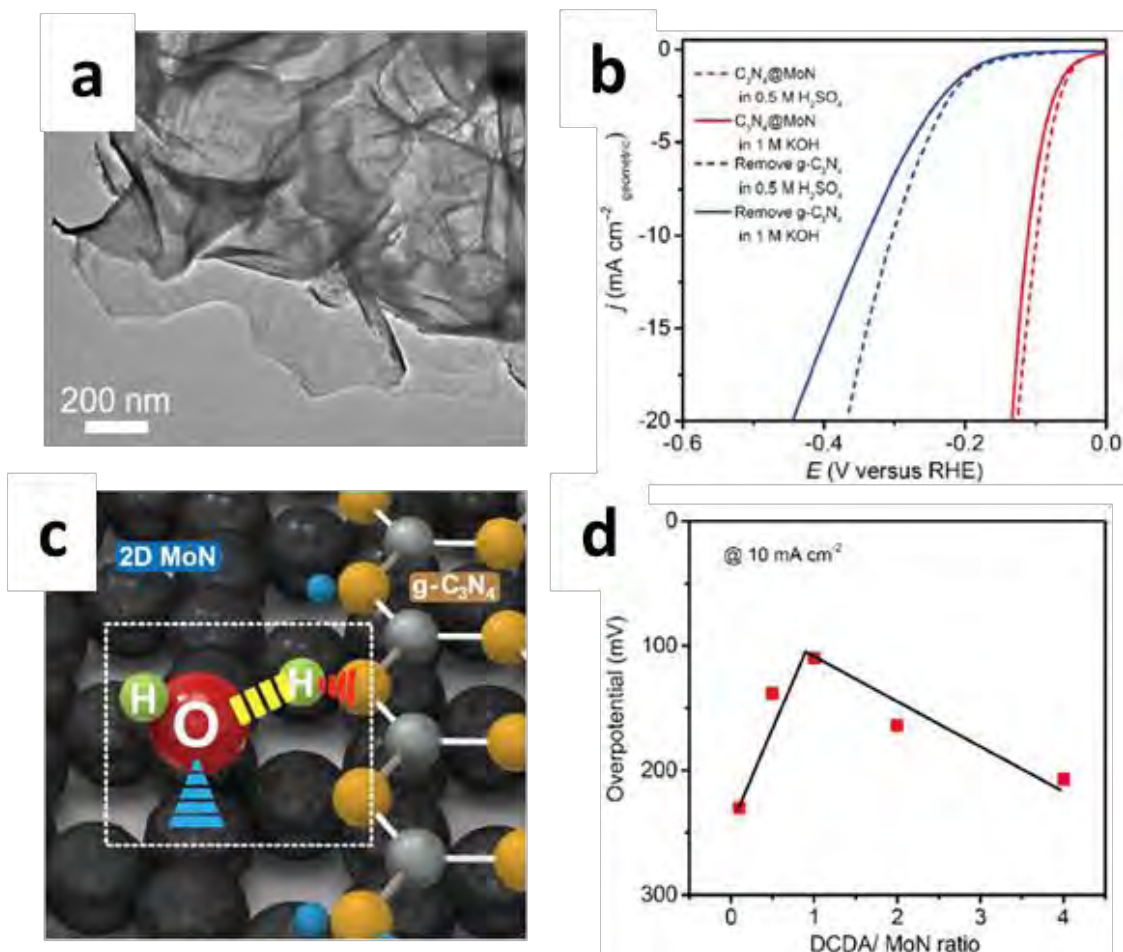


Figure 6 (a) TEM image of C₃N₄@MoN nanosheet. (b) A comparison of HER activity for C₃N₄@MoN before/after the removal of C₃N₄ in different electrolytes. (c) A scheme of water dissociation process on C₃N₄@MoN. (d) The relationship between a variety of DCDA (dicyandiamide as precursor for C₃N₄)/MoN ratios and the reaction overpotential at a current density of 10 mA cm⁻¹. Reproduced with permission.⁶² Copyright 2018, Elsevier.

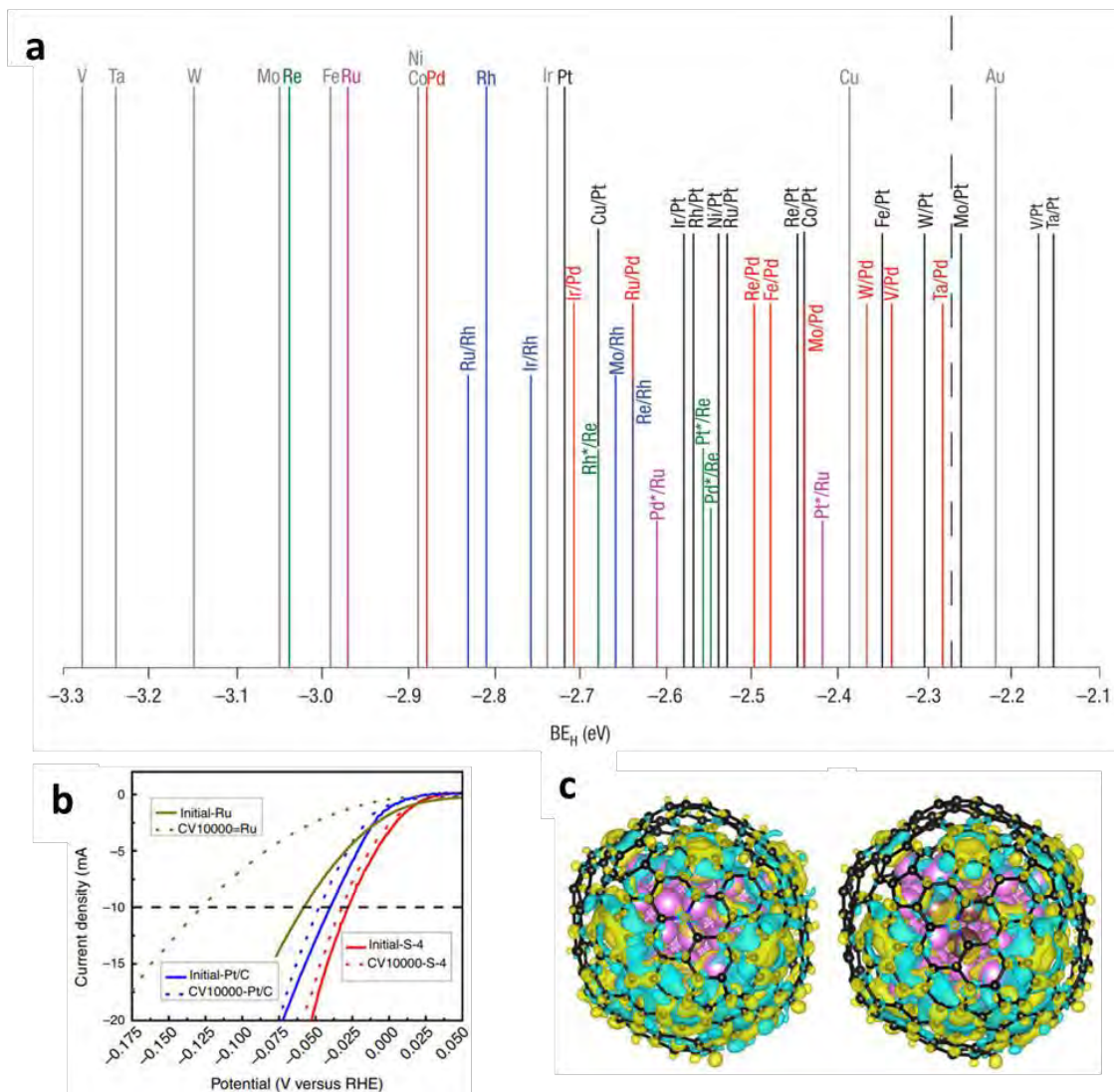


Figure 7 (a) A comparison of the HBE of some metal and alloy materials that are commonly used for the design of catalysts. Reproduced with permission.³⁷ Copyright 2004, Nature Publishing Group. (b) the HER activity of RuCo@NC hybrid in comparison to other candidates before/after 10000 round of CV cycles. (c) Calculated charge density differences on **left:** Co and **right:** Co₃Ru models. Yellow and cyan regions refer to corresponding increased/decreased charge distributions. Reproduced with permission.⁵⁹ Copyright 2016, Nature Publishing Group.

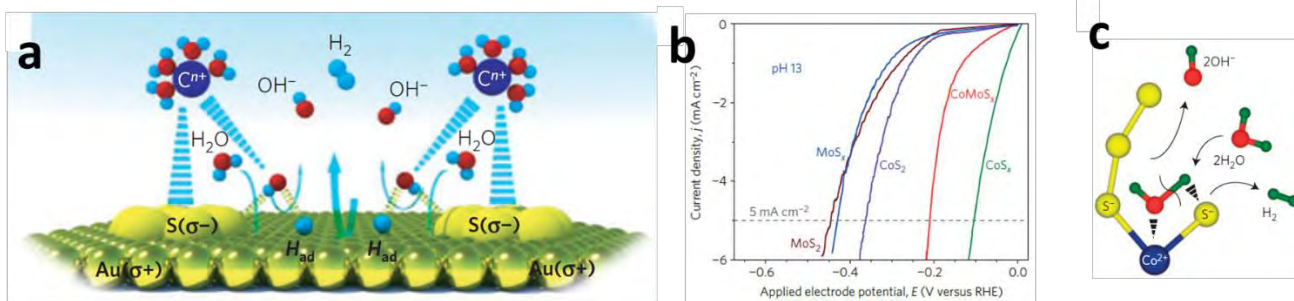


Figure 8 (a) A scheme of the HER mechanism on the surface of Au with $S_{ad}^{\delta-}$. (b) The alkaline HER activity of a series of Co/Mo sulfides. (c) Schematic illustration of the alkaline HER mechanism on $CoMoS_x$. Reproduced with permission.⁸⁸ Copyright 2015, Nature Publishing Group.

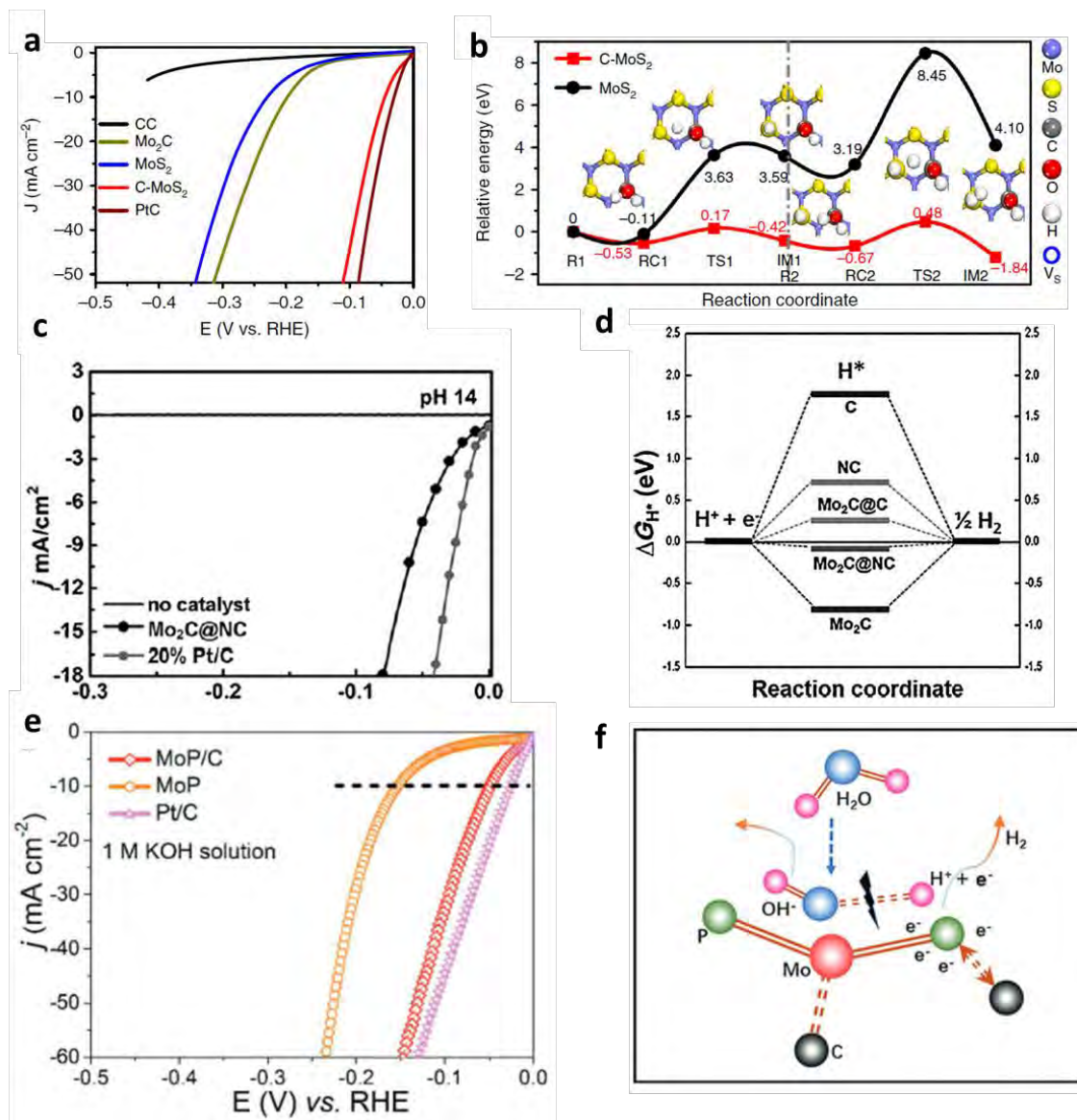


Figure 9 (a) The HER activity of C-MoS₂ in comparison to several similar catalysts and benchmark Pt/C in 1 M KOH. (b) The reactive energy diagram with the reaction coordinate representing the water dissociation process on the basal planes of MoS₂ and C-MoS₂, respectively. Reproduced with permission.⁹⁴ Copyright 2019, Nature Publishing Group. (c) HER activity of Mo₂C@NC in comparing to Pt/C. (d) the calculated free energy diagram of hydrogen adsorption for different structured Mo₂C-based catalysts. Reproduced with permission.¹⁰⁴ Copyright 2015, Wiley. (e) HER activity of MoP@C in comparison to that of Pt/C and MoP in 1 M KOH solution. (f) A scheme of HER mechanism on MoP@C. Copyright 2018, Wiley.

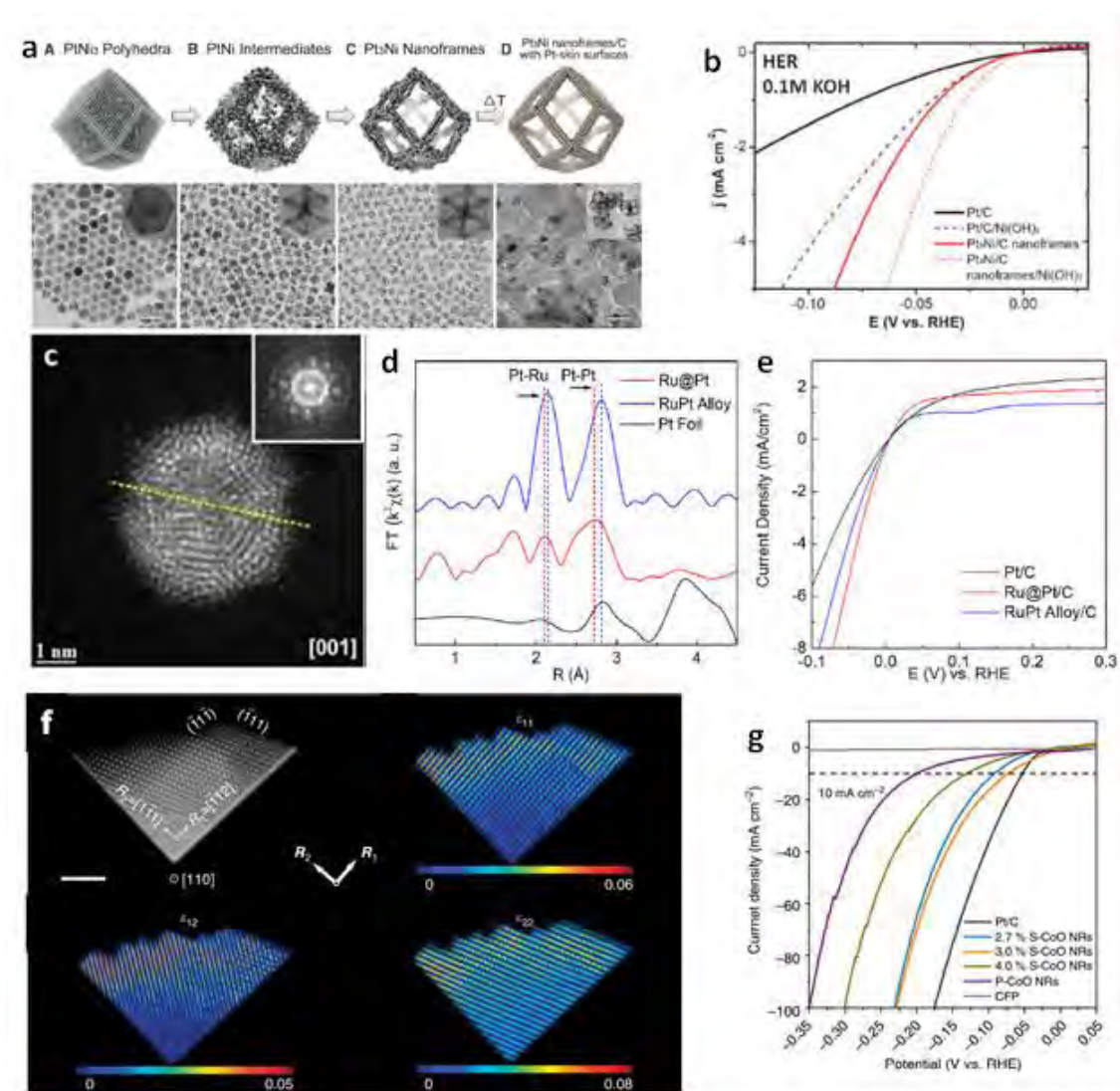


Figure 10 (a) A scheme and corresponding TEM images for the different stages in the formation process of Pt₃Ni nanoframes. (b) The HER activity of Pt₃Ni nanoframes in comparison to other benchmark catalysts in 0.1 M KOH. Reproduced with permission.¹²² Copyright 2014, American Association for the Advancement of Science. (c) Experimental TEM image of Ru@Pt nanoparticle. (d) EXAFS spectra of Ru@Pt in comparison to other catalysts. (e) HER activity of Ru@Pt/C in comparison to Pt/C and RuPt alloy/C in 0.1 M KOH. Reproduced with permission.⁴⁰ Copyright 2018, American Chemical Society. (f) Contour plots of the strain component ϵ_{xy} relative to the reference values on the nano sawtooth. R1 and R2 are lattice vectors referencing for the strain analysis. (g) HER activity of the S-CoO nanorods in comparison to some other catalysts in 1 M KOH. Reproduced with permission.¹²³ Copyright 2017, Nature Publishing Group.

2.3 Electronic and Structural Engineering of Carbon-Based Metal-Free Electrocatalysts for Water Splitting

This chapter is included as it appears as a journal paper published by Xuesi Wang, Anthony Vasileff, Yan Jiao, Yao Zheng, Shi-Zhang Qiao: Electronic and Structural Engineering of Carbon-Based Metal-Free Electrocatalysts for Water Splitting, *Advanced Materials*, 2018, 31, 1803625.

Statement of Authorship

Title of Paper	Electronic and Structural Engineering of Carbon - Based Metal - Free Electrocatalysts for Water Splitting.
Publication Status	<input checked="" type="checkbox"/> Published <input type="checkbox"/> Accepted for Publication <input type="checkbox"/> Submitted for Publication <input type="checkbox"/> Unpublished and Unsubmitted work written in manuscript style
Publication Details	Wang, X.; Vasileff, A.; Jiao, Y.; Zheng, Y.; Qiao, S. Z. Electronic and Structural Engineering of Carbon-Based Metal-Free Electrocatalysts for Water Splitting. Adv. Mater. 2018, 1803625.

Principal Author

Name of Principal Author (Candidate)	Xuesi Wang		
Contribution to the Paper	This author organized and wrote the paper.		
Overall percentage (%)	90%		
Certification:	This paper reports on original research I conducted during the period of my Higher Degree by Research candidature and is not subject to any obligations or contractual agreements with a third party that would constrain its inclusion in this thesis. I am the primary author of this paper.		
Signature		Date	11 June 2019

Co-Author Contributions

By signing the Statement of Authorship, each author certifies that:

- i. the candidate's stated contribution to the publication is accurate (as detailed above);
- ii. permission is granted for the candidate to include the publication in the thesis; and
- iii. the sum of all co-author contributions is equal to 100% less the candidate's stated contribution.

Name of Co-Author	Anthony Vasileff		
Contribution to the Paper	This author contributed in editing the paper.		
Signature		Date	11 June 2019

Name of Co-Author	Yao Zheng		
Contribution to the Paper	This author contributed in providing funding and supervising the project.		
Signature		Date	11 June 2019

Name of Co-Author	Shi-Zhang Qiao		
Contribution to the Paper	This author contributed in providing funding and supervising the project.		
Signature		Date	11 June 2019

Please cut and paste additional co-author panels here as required.

Name of Co-Author	Yan Jiao		
Contribution to the Paper	This author contributed in providing valuable suggestions to this work.		
Signature		Date	11 June 2019

Please cut and paste additional co-author panels here as required.

Electronic and Structural Engineering of Carbon-Based Metal-Free Electrocatalysts for Water Splitting

Xuesi Wang, Anthony Vasileff, Yan Jiao, Yao Zheng,* and Shi-Zhang Qiao*

Since first being reported as possible electrocatalysts to substitute platinum for the oxygen reduction reaction (ORR), carbon-based metal-free nanomaterials have been considered a class of promising low-cost materials for clean and sustainable energy-conversion reactions. However, beyond the ORR, the development of carbon-based catalysts for other electrocatalytic reactions is still limited. More importantly, the intrinsic activity of most carbon-based metal-free catalysts is inadequate compared to their metal-based counterparts. To address this challenge, more design strategies are needed in order to improve the overall performance of carbon-based materials. Herein, using water splitting as an example, some state-of-the-art strategies in promoting carbon-based nanomaterials are summarized, including graphene, carbon nanotubes, and graphitic-carbon nitride, as highly active electrocatalysts for hydrogen evolution and oxygen evolution reactions. It is shown that by rationally tuning the electronic and/or physical structure of the carbon nanomaterials, adsorption of reaction intermediates is optimized, consequently improving the apparent electrocatalytic performance. These strategies may facilitate the development in this area and lead to the discovery of advanced carbon-based nanomaterials for various applications in energy-conversion processes.

1. Introduction


The hydrogen evolution/oxidation reactions (HER/HOR) and oxygen reduction/evolution reactions (ORR/OER) are the fundamental electrochemical processes in fuel cells and water electrolyzers. Both devices play critical roles in the development of renewable energy conversion and storage technologies. In order for these electrocatalytic processes to achieve high efficiency while being commercially viable, carbon-based metal-free materials are being developed as cost-effective alternatives to traditional noble-metal catalysts. Carbon materials, from traditional amorphous carbon to the more recent carbon nanotubes (CNTs) and porous nanocarbons, are popular because of their low cost, excellent electrical and thermal conductivity, large surface area, and mechanical/chemical strength throughout a wide

potential window. These properties are all advantageous for designing high performance electrocatalysts. Another unique feature of these carbon materials is that they can exist with various morphologies and have highly tunable electronic structures.^[1,2] This makes them the ideal platform for the design of catalysts at the atomic level. To date, many carbon-based materials with different architectures have been engineered into highly active electrocatalysts for the ORR and many other reactions. These materials include low-dimensional nanostructures like CNTs, graphene, and graphitic-carbon nitride (g-C₃N₄) to hybrids and functional carbon composites.^[3–5] The motivation behind these efforts is to replace precious metal electrocatalysts with low-cost alternatives for energy conversion applications. This is especially sought after for water splitting where the performance of conventional precious metals is yet to be surpassed.

In an electrocatalytic process, a catalyst's activity is mainly determined by its adsorption/desorption ability toward the key reaction intermediates involved in the reaction. Therefore, the intrinsic adsorption energy for these reaction intermediates on a range of catalysts can be correlated to a specific activity descriptor (e.g., exchange current density) in the shape of a volcano plot.^[6,7] Furthermore, adsorption behavior is fundamentally determined by the electronic properties of the catalyst, which can be analyzed using density functional theory (DFT) calculations. Accordingly, one could pursue highly active electrocatalysts by first engineering the electronic structure (e.g., *p*-band for carbons) of the material, and then optimizing its physical structure to maximize catalytic performance.^[8] Engineering of electronic structures can be achieved by introducing a secondary element or fabricating specific defect structures in the pristine carbon framework. Such approaches can create active sites by either inducing electron- or spin-redistribution in the sp² conjugated carbon matrix. The generated active sites can then be scaled up through nanostructure engineering techniques. Thus, the overall apparent performance of a catalyst can be synergistically increased by both enhanced intrinsic activity and improved physical properties (e.g., conductivity or surface area).

In this research news, we summarize current strategies used for the electronic and structure design of carbon-based electrocatalysts for water splitting applications. Due to its simplicity

X. Wang, A. Vasileff, Dr. Y. Jiao, Dr. Y. Zheng, Prof. S.-Z. Qiao
School of Chemical Engineering
The University of Adelaide
Adelaide, SA 5005, Australia
E-mail: yao.zheng01@adelaide.edu.au; s.qiao@adelaide.edu.au

 The ORCID identification number(s) for the author(s) of this article can be found under <https://doi.org/10.1002/adma.201803625>.

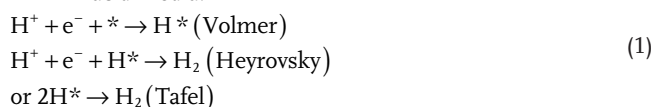
DOI: 10.1002/adma.201803625

as well as its economic importance, water splitting is an ideal platform for investigating carbon-based electrocatalysts for the clean energy development. The focus of this research news is i) approaches used to engineer the electronic structure of carbon materials, ii) the relationship between electronic structure and electrocatalytic activity on carbon materials, and iii) ways to maximize the overall electrocatalytic activity by simultaneously engineering the physical structure and chemical composition of carbon-based electrocatalysts.

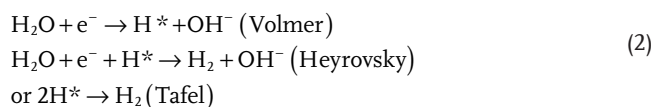
2. Engineering the Electronic Structure of Carbon-Based Materials

Usually, electronic engineering is achieved by disrupting the uniform carbon matrix, either by heteroatom doping, generating active edge sites, or by creating topologic defects. However, each strategy has a different impact on specific reaction intermediates in different reactions. For overall water splitting, both the HER and OER processes are involved. The reaction intermediates involved in these processes are outlined in the following reaction pathways (* represents an active site on the catalyst):

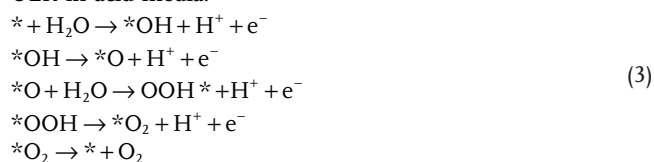
HER in acid media:



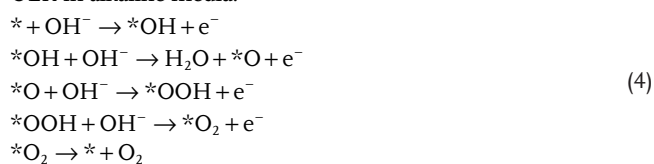
HER in alkaline media:



OER in acid media:



OER in alkaline media:



For the HER, H adsorption ability is the most important factor to consider when designing electrocatalysts, while for the OER, the ability to adsorb OH* from solution and to generate adsorbed OOH* are key to high activity.^[9] Unlike metal catalysts, an understanding of the effects of specific electronic states toward reaction intermediate energetics on carbon materials is still inconclusive.

2.1. Electronic Structure Engineering by Doping

Doping carbon with various heteroatoms (such as N, O, P, S, F, or B) is one of the most commonly used methods for

tuning its electronic structure.^[3,10–19] The effect of doping can be controlled by changing the configuration, location, and species of the dopants. Dual- and triple-doping has even shown to enhance the activity of carbon toward higher reaction efficiencies.^[12,14,20,21] To date, a great variety of experimental approaches for heteroatom doping have been developed, ranging from traditional hydrothermal treatments and pyrolysis to advanced chemical vapor deposition.^[12,22,23] In general, doping is a simple yet effective method in terms of both the fabrication process and parameter control.

The valence band orbital is often applied to explain the efforts of different dopants to the adsorption/desorption ability of the active sites in the carbon matrix (Figure 1a).^[24,25] In this regard, a linear relationship can be built between the density of states of the active site and its adsorption/desorption free energy (ΔG) to an intermediate (Figure 1b).^[26] As illustrated in Figure 1c, dopant atoms can act as electron donors or electron acceptors when anchored into a carbon matrix; doping the carbon matrix with electron donors such as P and S can introduce electron depletion on adjacent carbon atoms, and vice versa.^[17] This charge transfer can lead to optimized valence orbital energy for active carbon sites, consequently improving intrinsic activity.

With guidance from DFT, one can construct active sites on carbon-based electrocatalysts with deliberate design to maximize the benefit of doping. For example, for the HER in acidic solutions, the contribution of different doping species toward the overall reaction activity of graphene has been evaluated by DFT calculations and experimental measurements, and is represented in a volcano-shaped plot (Figure 1d).^[24] It is clear that the heteroatom-doped graphene materials all show lower activity compared to MoS₂ and Pt/C benchmarks, mainly due to their relatively weaker H* adsorption abilities. Accordingly, two different heteroatoms with a large difference in charge density (usually one electron donor and one electron acceptor) were introduced into the matrix to engineer the valence band of carbon. DFT calculations showed that dual-doping could significantly upshift the valence bands of the active carbon sites, thus improve the interaction with adsorbed H (Figure 1e).^[12,17,24,27]

A similar dual-doping approach has also shown to be effective for fabricating carbon-based electrocatalysts for the OER. For example, N, P co-doped carbon nanofiber achieved superior activity compared to benchmark IrO₂ due to its optimized reaction intermediate adsorption energies (Figure 1f,g).^[28] Significantly, many dual-doped and tri-doped carbon materials have multifunctional active sites for the HER, OER, and ORR simultaneously.^[20,29–32] From the above, it is clear that heteroatom doping is of universal significance toward tuning the adsorption energetics of carbon-based materials for different reactions.

2.2. Electronic Structure Engineering by Edge Site and Topological Defect Exposure

Edge sites and topological defects are inherent in carbon-based nanomaterials and are formed during the physical and/or chemical fabrication process.^[1,2] The former usually includes dangling groups and vacancies at the edge of the carbon matrix, while the latter contains intrinsic topologic vacancies

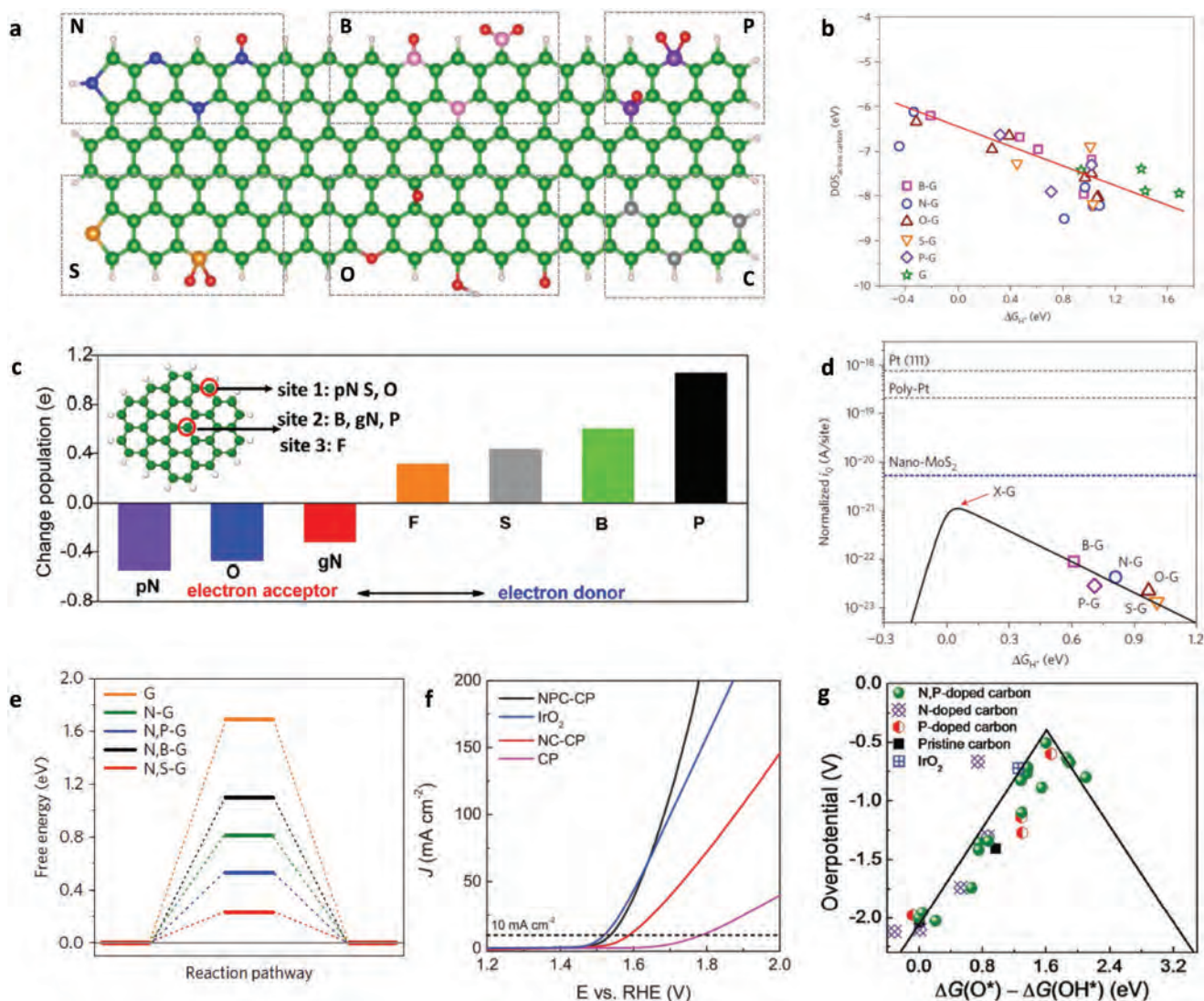


Figure 1. Engineering electronic structure of carbon material through doping. a) Model of various heteroatom doping on a carbon matrix. b) Relationship between the adsorption energy of H and the highest peak position of density of states of the active carbon. c) Natural bond orbital population analysis of different nonmetallic doping atoms. Inset indicates the locations of the corresponding doping sites. d) Volcano plot between normalized theoretical exchanged current per active site and free energy change of hydrogen adsorption for the graphene matrix with different dopants. e) Free energy diagram for the graphene matrix with different single- and codopants. a,b,d,e) Reproduced with permission.^[25] Copyright 2016, Nature Publishing Group. c) Reproduced with permission.^[17] Copyright 2014, American Chemical Society. f) OER polarization curves for N and P co-doped carbon in 1 M KOH. g) Volcano plot of the overpotential versus the difference between the adsorption energy of O and OH for carbon with different doping sites. f,g) Reproduced with permission.^[28] Copyright 2016, Wiley-VCH.

and deformations at both bulk domains and edges. Although it has been long known that both features modify the electronic structure of a material, it was not until recently that these sites were deliberately manipulated during material fabrication.^[33] In carbon-based electrocatalysis, edge sites and topological defects usually play two important roles: i) providing anchoring points for other active species such as a metal or heteroatoms and ii) acting as active sites directly.

The function of edge sites in electrocatalysis was first found and studied for the ORR.^[34] Edge sites generally contain many functional groups, which can significantly improve the hydrophilicity of the carbon and enhance adsorption of heteroatoms and molecules. In fact, dopant and edge effects are inseparable

in electrocatalysts when the promoting mechanism is taken into account. Moreover, it is generally believed that the activity origin of materials rich with edge sites is that dopants are more active when anchored on an edge compared to the basal plane.^[35] For example, in the DFT calculation for the ORR/OER on N-doped graphene nanoribbons performed by Xia et al. (Figure 2a), it was identified that the most active sites are the carbon atoms near the nitrogen doping on the armchair edge of graphene (Figure 2a,b). Additionally, the location of N dopants also plays an important role in the overall activity of the material. As demonstrated in Figure 2c, the OER has a smaller overpotential when N is doped in some specific edge sites. For near-edge N-doped armchair nanoribbons, a minimum theoretical OER

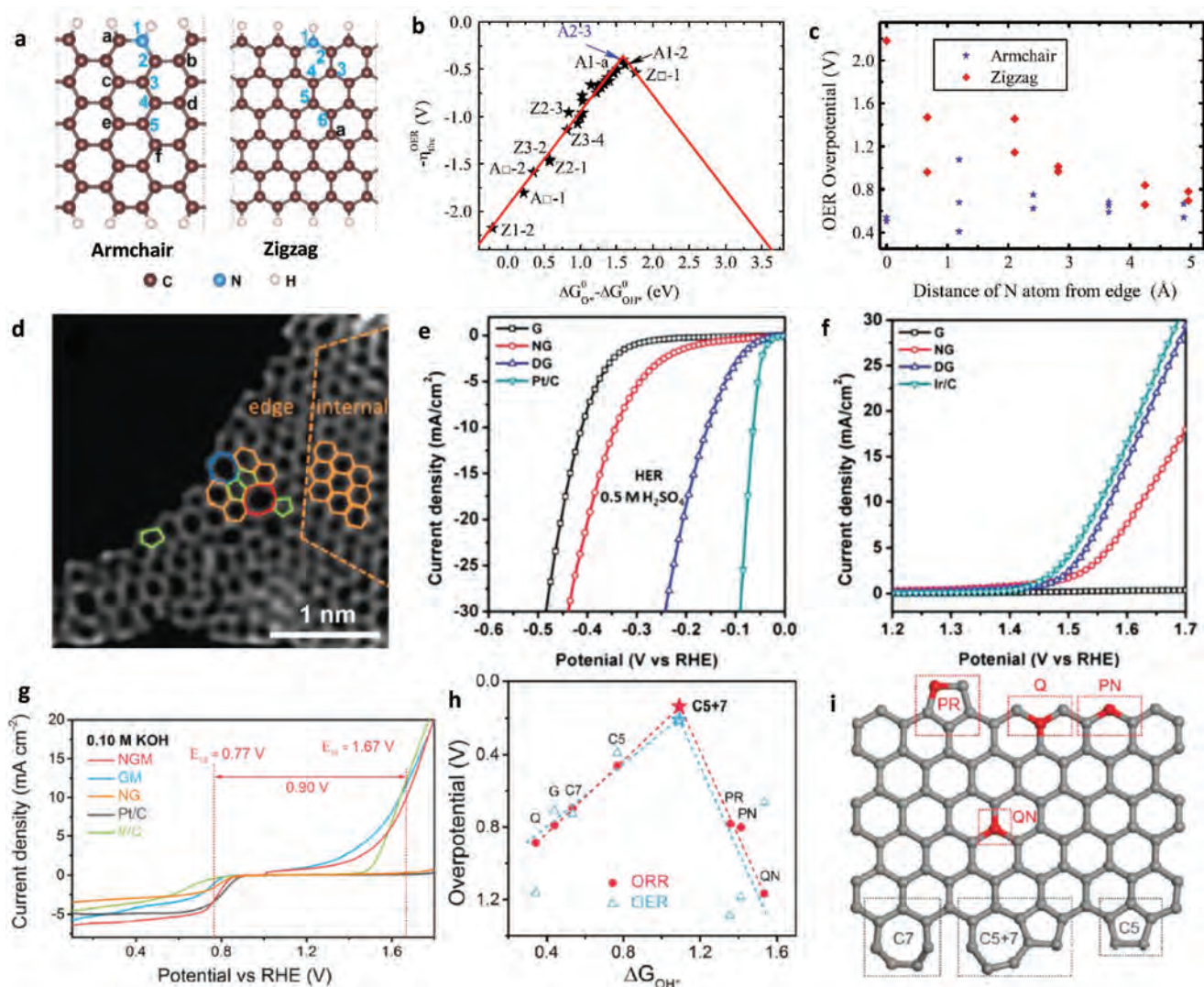


Figure 2. Engineering electronic structure of carbon material through edge sites and topological defects. a) Scheme of N-doped graphene nanoribbons with armchair and zigzag edges. b) Volcano plot of the OER overpotential versus the difference between the adsorption energy of O and OH on different graphene armchair and zigzag sites. c) OER overpotential versus the distance of N from edge for different sites. a–c) Reproduced with permission.^[35] Copyright 2014, Elsevier. d–f) HAADF-STEM image and corresponding polarization curves of defected graphene and N-doped graphene for the OER and HER. d–f) Reproduced with permission.^[38] Copyright 2016, Wiley-VCH. g) ORR and OER polarization curves of defective graphene. h, i) The volcano plot of the OER overpotential on different sites and corresponding models. g–i) Reproduced with permission.^[41] Copyright 2016, Wiley-VCH.

overpotential of 0.405 V can be achieved, which is comparable to noble-metal electrocatalysts.^[35] Later experimental works show that the effect of edge-doping can be extended to other heteroatoms.^[36,37] For example, a combination of experiments and DFT calculations showed that O doping at edge sites and at defective sites generated the most active sites for the OER.^[37]

Although edge sites can provide highly active centers for electrocatalysis, they are not the only contributor toward the activity of a material. Topological defects also play an important role in reaction activity, as they participate in determining the electronic structure of carbon-based materials. Topological defects are unavoidable in carbon-based materials, and are generated either during the fabrication process or formed naturally due to crystalline disorder. For carbon with a hexagonal matrix such as graphene, these defects can exist as nonhexagonal units in

the form of a random point mismatch or patterned defects etc. (Figure 2d).^[38] DFT calculations showed that these topological defects can significantly alter the charge density of neighboring carbon atoms.^[39] For the ORR, line-defects on graphene are more efficient for promoting the reaction by optimizing energy barriers to the four-electron transfer reaction pathway compared to other defect models. Although calculations for the HER and OER were not included, it is reasonable to predict that the structure and position of defects in carbon-based materials also play important roles.

Such predictions have been proven more recently by both experimental evidence and DFT calculations.^[40] Yao et al. prepared a dopant-free defective graphene (DG) as model to emphasize the role of defects in tuning the electrocatalytic activities of carbon materials.^[38] By removing the N dopants in an N-doped graphene (NG), they fabricated a DG with various

defect units (pentagons, heptagons, and octagons). Compared to NG, the DG exhibited much higher activities for the ORR, OER, and HER due to the various kinds of defect sites (Figure 2d–f). DFT calculations indicated that when a certain defect (e.g., pentagon, 585, or 7557) was introduced to the graphene framework, the edge atoms around the defect reconstruct the electronic structure of active carbon atoms, and therefore change their adsorption energetics. In oxygen related reactions, all the active sites are the carbon atom adjacent the defective edge (Figure 2f). However, these sites do not fit for promoting HER activity due to their overly strong hydrogen binding energy. Instead, the conjunction carbons at the defects are responsible for providing more suitable hydrogen binding energy (Figure 2e).

Wei et al. also confirmed that the diverse structures in topological defects could play different roles in electrocatalytic processes.^[41] They fabricated a graphene sheet with N doping and in-plane defects, which exhibited superior ORR activity than Pt/C and comparable OER activity to Ir/C in alkaline media (Figure 2g). To identify the active center for each reaction, the possible active sites on the N-doped defective graphene were categorized by the different N species (Q: quaternary N on the edge, QN: quaternary N in the bulk, PN: Pyridinic N, and PR: pyrrolic N) and topological defect sites (C7, C5+7, and C5), as indicated in Figure 2i. DFT calculations concluded that for the OER, topological defects with a C5+7 structure provides the most appropriate adsorption energy for OH species, resulting in the smallest overpotential (Figure 2h). Interestingly, although not being the best interacting sites for OH intermediates, the C5 and C7 sites are preferable for O and OOH adsorption, respectively. As the process of adding an OH to adsorbed O* to form an OOH* is the rate-determining step in the OER, the interaction between the surface and O/OOH species is also important for overall OER performance. As a result, optimized adsorption toward different intermediates combined leads to enhanced OER activity. Although many methods have been proposed for optimizing electronic structures and creating active sites, it is still a challenge in carbon materials to experimentally confirm the catalytically active sites. This is largely because of the difficulty in fabricating carbon materials with uniform active site type which match the models proposed by DFT calculation.

3. Engineering the Physical Structure of Carbon-Based Materials

Sufficient apparent activity of carbon materials is generally not obtained with well-designed active sites alone. To reach a high overall performance, the quantity of the active sites as well as other material properties also need to be taken into account. For example, hierarchical nanostructures are often applied for carbon-based materials to increase surface area, improve charge transfer rate, and expose more active sites.

3.1. Activity Promoted by Synergistic Effects

The synergistic effects that are apparent in carbon-metal hybrid materials has long been exploited for high performing

electrocatalysts.^[42–46] In such systems, carbon is usually used as a host material to support the metallic catalysts, provide better conductivity, and offer greater surface area.^[47,48] Moreover, the interaction between carbon and metallic materials are often so strong that it can change the electronic properties of the whole hybrid. Thereby new active sites with enhanced adsorption ability are created. In terms of metal-free systems, such synergistic effects can also be exploited by carefully manipulating the interaction between different types of carbon-based materials.^[49]

One typical example is g-C₃N₄-based electrocatalysts. As a semiconductor, g-C₃N₄ has always been an inert electrocatalyst due to its poor conductivity and inappropriate adsorption of H- and O-relevant intermediates.^[50] However, when coupled with other carbon materials, the catalytic performance of g-C₃N₄ can be significantly increased. Interestingly, although g-C₃N₄ is considered unsuitable for the HER due to its overly strong H* adsorption, several g-C₃N₄-carbon hybrids have exhibited extraordinary HER activity.^[23,51,52] For example, when g-C₃N₄ was coupled with NG to form a double layered structure, the HER activity of the hybrid material was greatly increased and comparable to that of MoS₂ (Figure 3a,b).^[51] Experimental evidence and DFT calculations both revealed that the improvement in activity originated from improved ability to adsorb and reduce protons from solution, which was induced by the intrinsic chemical and electronic coupling between carbon and g-C₃N₄ (Figure 3d). In another case, a g-C₃N₄-graphene mesh-on-mesh hybrid structure was synthesized using a simple template-free method.^[53] The unique layered porous structure offered fast charge and mass transport and also provided significant surface area for hydrogen adsorption. As a result, the overall activity of the material in acidic solution was extremely high compared to other nonmetallic electrocatalysts. This structurally induced synergistic effect was also been demonstrated for the OER. By assembling g-C₃N₄ with CNTs into a 3D porous structure, a composite with high N content and large surface area was obtained (Figure 3e).^[54] This composite exhibited outstanding OER activity (even outperforming benchmark IrO₂) which was attributed to the significantly improved conductivity of the material and the large number of exposed active sites (Figure 3f).

3.2. Application Supported by Mechanical Properties

The physical structures of carbon-based materials can serve purposes other than contributing to the reaction activity. A good example is their stability in harsh electrolytes and oxidizing environments. These properties allow electrocatalysts to be more adaptable to extreme reaction conditions, making them more applicable for practical devices.

Seeking suitable electrocatalysts for the OER in acidic solutions has always been a challenge due to the harsh oxidizing environments present (even for the noble metals). Surprisingly, it was found that multiwalled carbon nanotubes (MWCNTs) had unexpected activity and stability as OER electrocatalysts in acidic media.^[55] The oxidation process during the reaction activated the MWCNTs in the initial stages, and then became stable under the highly oxidizing environment. The unique

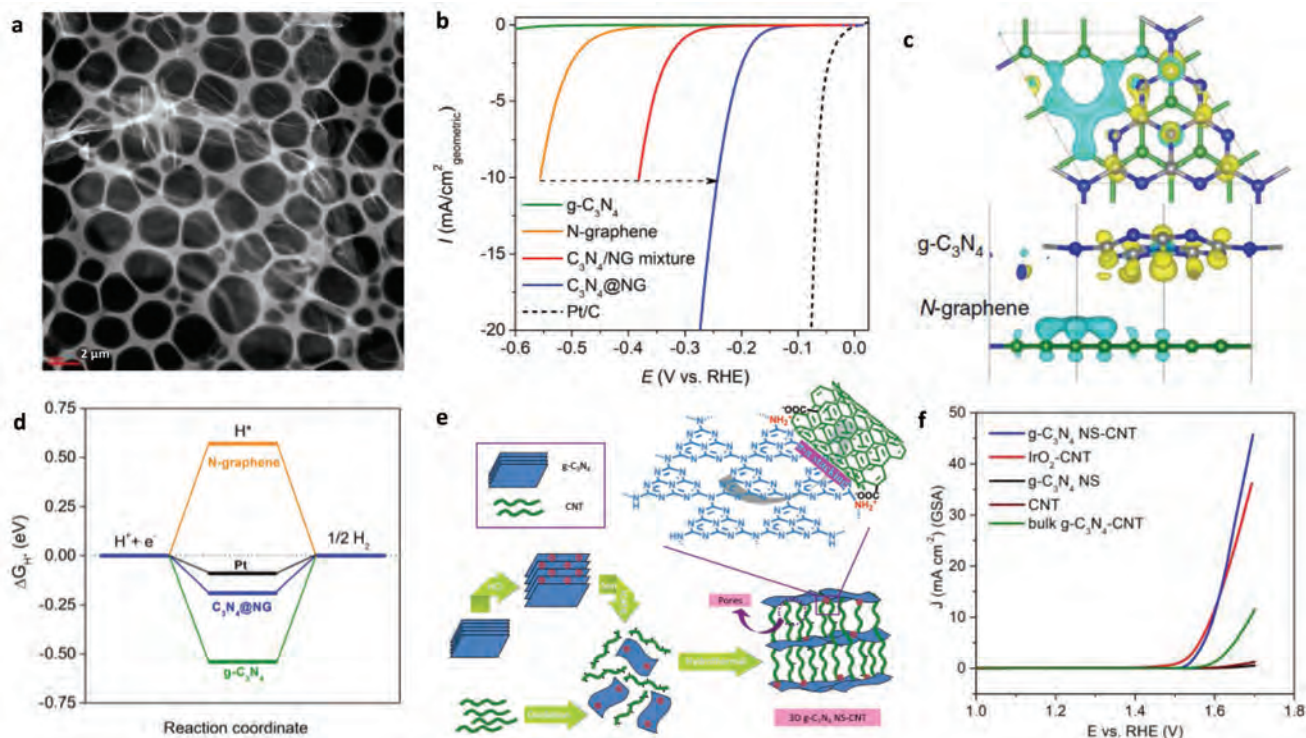


Figure 3. Engineering physical structure of carbon-based materials. a,b) TEM image of C_3N_4/NG hybrid and its HER performance. c,d) A scheme of the structure of C_3N_4/NG and its calculated free-energy diagram for the HER. a–d) Reproduced with permission.^[51] Copyright 2014, Nature Publishing Group. e,f) A scheme of the structure and fabrication procedure for C_3N_4-CNT 3D composites and OER performance. e,f) Reproduced with permission.^[54] Copyright 2014, Wiley-VCH.

stability of the MWCNTs makes them viable candidates for the development of OER electrocatalysts in acidic solutions.

Other than enhanced stability in extreme environments, properly constructing the physical architecture of nanocarbons can induce other beneficial properties, such as flexibility and durability into the material.^[52,56] For example, carbon paper and carbon cloth are often used as soft current collectors for carbon-based electrocatalysts. These substrates are easily treated and have excellent conductivity, hence, they are often used for in situ construction of electroactive nanocarbon structures.^[28,57] Moreover, by using filter techniques, $g-C_3N_4$, NG, and CNTs can be directly made into highly flexible self-assembled layered films or membranes.^[52,54] In these cases, the as-fabricated electrocatalysts exhibited high stability induced by their structural integrity and high activity. These self-supported carbon electrocatalysts have the potential to be directly applied as electrodes in energy conversion devices such as metal–air batteries.^[58–60]

4. Conclusions and Perspectives

In recent decades, interest in carbon-based metal-free electrocatalysts has grown significantly due to their unique chemical and physical properties. Among all accomplishments achieved in theoretical and experimental electrocatalysis, research on electrocatalytic water splitting is still of the highest priority due to its fundamental role in the field. Thanks to the

development of nanotechnologies, a series of strategies such as heteroatom doping, edge-site generation, and topological defect engineering, are now able to create specific active sites in carbon-based materials with optimized adsorption abilities toward reactive intermediates. Further, with the assistance of DFT calculations, theory-led design of carbon materials is much more accessible and convenient. When these strategies are coupled with structural engineering of nanocarbons, significantly improved catalyst activity and stability are possible.

However, despite the achievements made so far, the development of metal-free carbon electrocatalysts is still far behind that of their metal counterparts. Two major challenges, namely improving activity and stability, need to be addressed before carbon-based metal-free electrocatalysts can compete with the current state-of-the-art. In terms of activity, both DFT calculations and experimental evidence clearly indicate that the activity of carbon electrocatalysts is still below that of metal electrocatalysts in most cases. Although the OER activity of some carbon-based electrocatalysts is now comparable to noble-metal materials, their HER activity is still far from their metal-based counterparts. To solve this problem, further study of the fundamental principles is needed to gain full knowledge of the origin of activity enhancement. Only through this can we find a way to break the inherent linear scaling relationships that limit the activity of carbon electrocatalysts. Consequently, the current activity limit of carbon-based electrocatalysts could be surpassed, and possibly even reach that of metal catalysts. More advanced surface engineering strategies, such as precise

defect engineering and dimer doping, are expected to produce nanocarbons with more uniform physical structures and precisely controlled surface properties. This is also critical for model construction in DFT studies and to gain better control over the adsorption/desorption ability toward targeted intermediates. Regarding stability improvement, advanced engineering and synthesis methods are expected to produce carbon materials with higher mechanical and chemical stability to resist the harsh environments during electrocatalytic processes. Also, as more active nanocarbon catalysts are being developed for the OER, it is expected that lower potentials and hence less oxidizing environments will be required for this process.

As shown by many experimental and DFT studies, the methods of electronic and physical structure engineering summarized here are of general applicability. These strategies are expected to be extended to other catalytic processes for the design of more candidate catalysts. By providing a brief review on the current knowledge of engineering nanocarbons, we hope this general guidance could be of assistance in other energy conversion fields such as the CO₂ reduction reaction and nitrogen reduction reaction.

Acknowledgements

The authors gratefully acknowledge financial support from the Australian Research Council through Discovery and Linkage Project programs (DP160104866, DP170104464, LP160100927, DE160101163, and FL170100154).

Conflict of Interest

The authors declare no conflict of interest.

Keywords

carbon engineering, hydrogen evolution reactions, metal-free electrocatalysts, oxygen evolution reactions, water splitting

Received: June 7, 2018

Revised: July 20, 2018

Published online: October 1, 2018

- [1] D. S. Su, S. Perathoner, G. Centi, *Chem. Rev.* **2013**, *113*, 5782.
 [2] M. J. Allen, V. C. Tung, R. B. Kaner, *Chem. Rev.* **2009**, *110*, 132.
 [3] L. Qu, Y. Liu, J.-B. Baek, L. Dai, *ACS Nano* **2010**, *4*, 1321.
 [4] Y. Li, W. Zhou, H. Wang, L. Xie, Y. Liang, F. Wei, J.-C. Idrobo, S. J. Pennycook, H. Dai, *Nat. Nanotechnol.* **2012**, *7*, 394.
 [5] K. Gong, F. Du, Z. Xia, M. Durstock, L. Dai, *Science* **2009**, *323*, 760.
 [6] E. Skúlason, V. Tripkovic, M. E. Björketun, S. d. Gudmundsdóttir, G. Karlberg, J. Rossmeisl, T. Bligaard, H. Jónsson, J. K. Nørskov, *J. Phys. Chem. C* **2010**, *114*, 18182.
 [7] J. K. Nørskov, T. Bligaard, A. Logadottir, J. R. Kitchin, J. G. Chen, S. Pandalov, U. Stimming, *J. Electrochem. Soc.* **2005**, *152*, J23.
 [8] Y. Zheng, Y. Jiao, S. Z. Qiao, *Adv. Mater.* **2015**, *27*, 5372.
 [9] Y. Jiao, Y. Zheng, M. Jaroniec, S. Z. Qiao, *Chem. Soc. Rev.* **2015**, *44*, 2060.
 [10] X. Huang, Y. Zhao, Z. Ao, G. Wang, *Sci. Rep.* **2014**, *4*, 7557.
 [11] W. Cui, Q. Liu, N. Cheng, A. M. Asiri, X. Sun, *Chem. Commun.* **2014**, *50*, 9340.
 [12] Y. Ito, W. Cong, T. Fujita, Z. Tang, M. Chen, *Angew. Chem., Int. Ed.* **2015**, *54*, 2131.
 [13] Y. Zhao, R. Nakamura, K. Kamiya, S. Nakanishi, K. Hashimoto, *Nat. Commun.* **2013**, *4*, 2390.
 [14] R. Li, Z. Wei, X. Gou, *ACS Catal.* **2015**, *5*, 4133.
 [15] G. L. Tian, Q. Zhang, B. Zhang, Y. G. Jin, J. Q. Huang, D. S. Su, F. Wei, *Adv. Funct. Mater.* **2014**, *24*, 5956.
 [16] Y. Cheng, Y. Tian, X. Fan, J. Liu, C. Yan, *Electrochim. Acta* **2014**, *143*, 291.
 [17] Y. Zheng, Y. Jiao, L. H. Li, T. Xing, Y. Chen, M. Jaroniec, S. Z. Qiao, *ACS Nano* **2014**, *8*, 5290.
 [18] Z. Zhang, T. Cao, S. Liu, X. Duan, L. M. Liu, S. Wang, Y. Liu, *Part. Part. Syst. Charact.* **2017**, *34*, 1600207.
 [19] Z. Yi, Z. Zhang, S. Wang, G. Shi, *J. Mater. Chem. A* **2017**, *5*, 519.
 [20] K. Qu, Y. Zheng, Y. Jiao, X. Zhang, S. Dai, S.-Z. Qiao, *Adv. Energy Mater.* **2017**, *7*, 1602068.
 [21] K. Qu, Y. Zheng, X. Zhang, K. Davey, S. Dai, S. Z. Qiao, *ACS Nano* **2017**, *11*, 7293.
 [22] J. Zhang, Z. Zhao, Z. Xia, L. Dai, *Nat. Nanotechnol.* **2015**, *10*, 444.
 [23] Y. Zhao, F. Zhao, X. Wang, C. Xu, Z. Zhang, G. Shi, L. Qu, *Angew. Chem., Int. Ed.* **2014**, *53*, 13934.
 [24] Y. Jiao, Y. Zheng, K. Davey, S.-Z. Qiao, *Nat. Energy* **2016**, *1*, 16130.
 [25] Y. Jiao, Y. Zheng, M. Jaroniec, S. Z. Qiao, *J. Am. Chem. Soc.* **2014**, *136*, 4394.
 [26] Y. Zheng, Y. Jiao, M. Jaroniec, S. Z. Qiao, *Angew. Chem., Int. Ed.* **2015**, *54*, 52.
 [27] D. Yan, S. Dou, L. Tao, Z. Liu, Z. Liu, J. Huo, S. Wang, *J. Mater. Chem. A* **2016**, *4*, 13726.
 [28] Y. P. Zhu, Y. Jing, A. Vasileff, T. Heine, S. Z. Qiao, *Adv. Energy Mater.* **2017**, *7*, 1602928.
 [29] J. Zhang, L. Qu, G. Shi, J. Liu, J. Chen, L. Dai, *Angew. Chem., Int. Ed.* **2016**, *55*, 2230.
 [30] T. Sun, Q. Wu, Y. Jiang, Z. Zhang, L. Du, L. Yang, X. Wang, Z. Hu, *Chem. - Eur. J.* **2016**, *22*, 10326.
 [31] J. Zhang, L. Dai, *Angew. Chem., Int. Ed.* **2016**, *128*, 13490.
 [32] C. Hu, L. Dai, *Adv. Mater.* **2017**, *29*, 1604942.
 [33] L. D. Carr, M. T. Lusk, *Nat. Nanotechnol.* **2010**, *5*, 316.
 [34] P. J. Britto, K. S. Santhanam, A. Rubio, J. A. Alonso, P. M. Ajayan, *Adv. Mater.* **1999**, *11*, 154.
 [35] M. Li, L. Zhang, Q. Xu, J. Niu, Z. Xia, *J. Catal.* **2014**, *314*, 66.
 [36] Z. Xiao, X. Huang, L. Xu, D. Yan, J. Huo, S. Wang, *Chem. Commun.* **2016**, *52*, 13008.
 [37] Z. Liu, Z. Zhao, Y. Wang, S. Dou, D. Yan, D. Liu, Z. Xia, S. Wang, *Adv. Mater.* **2017**, *29*, 1606207.
 [38] Y. Jia, L. Zhang, A. Du, G. Gao, J. Chen, X. Yan, C. L. Brown, X. Yao, *Adv. Mater.* **2016**, *28*, 9532.
 [39] L. Zhang, Q. Xu, J. Niu, Z. Xia, *Phys. Chem. Chem. Phys.* **2015**, *17*, 16733.
 [40] Z. Zhang, Z. Yi, J. Wang, X. Tian, P. Xu, G. Shi, S. Wang, *J. Mater. Chem. A* **2017**, *5*, 17064.
 [41] C. Tang, H. F. Wang, X. Chen, B. Q. Li, T. Z. Hou, B. Zhang, Q. Zhang, M. M. Titirici, F. Wei, *Adv. Mater.* **2016**, *28*, 6845.
 [42] Y. Liang, Y. Li, H. Wang, H. Dai, *J. Am. Chem. Soc.* **2013**, *135*, 2013.
 [43] H. Wang, H. Dai, *Chem. Soc. Rev.* **2013**, *42*, 3088.
 [44] R. Zhou, S. Z. Qiao, *Chem. Mater.* **2014**, *26*, 5868.
 [45] J. Liang, R. F. Zhou, X. M. Chen, Y. H. Tang, S. Z. Qiao, *Adv. Mater.* **2014**, *26*, 6074.
 [46] J. Duan, S. Chen, S. Dai, S. Z. Qiao, *Adv. Funct. Mater.* **2014**, *24*, 2072.
 [47] M. Gong, Y. Li, H. Wang, Y. Liang, J. Z. Wu, J. Zhou, J. Wang, T. Regier, F. Wei, H. Dai, *J. Am. Chem. Soc.* **2013**, *135*, 8452.
 [48] A. Vasileff, S. Chen, S. Z. Qiao, *Nanoscale Horiz.* **2016**, *1*, 41.

- [49] Y. P. Zhu, C. Guo, Y. Zheng, S. Z. Qiao, *Acc. Chem. Res.* **2017**, *50*, 915.
- [50] Y. Zheng, J. Liu, J. Liang, M. Jaroniec, S. Z. Qiao, *Energy Environ. Sci.* **2012**, *5*, 6717.
- [51] Y. Zheng, Y. Jiao, Y. Zhu, L. H. Li, Y. Han, Y. Chen, A. Du, M. Jaroniec, S. Z. Qiao, *Nat. Commun.* **2014**, *5*, 3783.
- [52] J. Duan, S. Chen, M. Jaroniec, S. Z. Qiao, *ACS Nano* **2015**, *9*, 931.
- [53] Q. Han, Z. Cheng, J. Gao, Y. Zhao, Z. Zhang, L. Dai, L. Qu, *Adv. Funct. Mater.* **2017**, *27*, 1606352.
- [54] T. Y. Ma, S. Dai, M. Jaroniec, S. Z. Qiao, *Angew. Chem., Int. Ed.* **2014**, *53*, 7281.
- [55] Y. Yi, J. Tornow, E. Willinger, M. G. Willinger, C. Ranjan, R. Schlögl, *ChemElectroChem* **2015**, *2*, 1929.
- [56] S. Chen, J. Duan, M. Jaroniec, S. Z. Qiao, *Adv. Mater.* **2014**, *26*, 2925.
- [57] T. Y. Ma, J. Ran, S. Dai, M. Jaroniec, S. Z. Qiao, *Angew. Chem., Int. Ed.* **2015**, *54*, 4646.
- [58] Q. Liu, Y. Wang, L. Dai, J. Yao, *Adv. Mater.* **2016**, *28*, 3000.
- [59] S. Chen, J. Duan, Y. Zheng, X. Chen, X. W. Du, M. Jaroniec, S.-Z. Qiao, *Energy Storage Mater.* **2015**, *1*, 17.
- [60] J. Han, X. Guo, Y. Ito, P. Liu, D. Hojo, T. Aida, A. Hirata, T. Fujita, T. Adschiri, H. Zhou, M. Chen, *Adv. Energy Mater.* **2016**, *6*, 1501870.

Chapter 3 : Anomalous Hydrogen Evolution Behavior in High-pH Environment Induced by Locally Generated Hydronium Ions

3.1 Introduction

The current understanding on electrocatalytic reactions are mostly from the mechanic studies based on bulk metal materials. Nevertheless, it is nanostructured electrocatalysts that have attracted more interests in practice due to their high efficiency and cost-effectiveness in heterogenous reactions. However, some of the reaction mechanisms accounted from bulk materials are inapplicable to nanocatalysts due to the unique behavior of the reactive intermediates induced by the nanostructured catalytic surface. As a result, nanocatalysts designed from current mechanic studies sometimes represent unpredictable catalytic performance, especially for homogenous reduction reactions such as carbon dioxide and nitrogen reduction.

Here using electrocatalytic hydrogen evolution reaction (HER) as an example, we conducted in-situ study to probe the interaction between the intermediates and the catalyst on a series of nanostructured electrocatalysts. By identifying the local reactive intermediates on the catalysts, a new reaction mechanism that uncovers the intermediate-catalyst interaction on nanostructured surface was found. This new mechanism not only explained the origin of the widely reported anomalous HER activity in high-pH electrolytes, but also brings new guidance toward catalyst designing for other electrocatalytic reduction reactions in aqueous environment. The highlights of this work include:

- The widely reported, yet unexplained anomalous HER activity of nanostructured electrocatalysts in high-pH electrolytes is first being analyzed.
- A new intermediate (in-situ generated H_3O^+) is detected for the first time on nanostructured electrocatalysts using in-situ Raman characterizations during the electrocatalytic HER process in high-pH environment.
- Using a series of electrochemical thermal and kinetic analysis, we investigated the origin of the in-situ generated H_3O^+ . Further, we uncovered the significant influence of H_3O^+

intermediates in reducing the reaction energy barrier, changing the rate-determining step of HER, and improving the overall HER activity.

- Based on the above-mentioned evidence, we proposed a new HER reaction mechanisms on nanostructured catalytic surface under high-pH environment.

3.2 Anomalous Hydrogen Evolution Behavior in High-pH Environment Induced by Locally Generated Hydronium Ions

This chapter is included as it appears as a journal paper published by Xuesi Wang, Chaochen Xu, Mietek Jaroniec, Yao Zheng and Shi-Zhang Qiao: Anomalous Hydrogen Evolution Behavior in High-pH Environment Induced by Locally Generated Hydronium Ions,

Statement of Authorship

Title of Paper	Anomalous Hydrogen Evolution Behavior in High-pH Environment Induced by Locally Generated Hydronium Ions
Publication Status	<input type="checkbox"/> Published <input type="checkbox"/> Accepted for Publication <input checked="" type="checkbox"/> Submitted for Publication <input type="checkbox"/> Unpublished and Unsubmitted work written in manuscript style
Publication Details	Wang, X. ; Xu, C. ; Jaroniec, M. ; Zheng, Y. ; and Qiao, S. -Z. Anomalous Hydrogen Evolution Behavior in High-pH Environment Induced by Locally Generated Hydronium Ions. Nature Communacations, under revision

Principal Author

Name of Principal Author (Candidate)	Xuesi Wang		
Contribution to the Paper	This author did all the electrochemical experiments and wrote the paper.		
Overall percentage (%)	80%		
Certification:	This paper reports on original research I conducted during the period of my Higher Degree by Research candidature and is not subject to any obligations or contractual agreements with a third party that would constrain its inclusion in this thesis. I am the primary author of this paper.		
Signature		Date	1 July 2019

Co-Author Contributions


By signing the Statement of Authorship, each author certifies that:

- i. the candidate's stated contribution to the publication is accurate (as detailed above);
- ii. permission is granted for the candidate to include the publication in the thesis; and
- iii. the sum of all co-author contributions is equal to 100% less the candidate's stated contribution.

Name of Co-Author	Chaochen Xu		
Contribution to the Paper	This author contributed in carrying out in-situ Raman characterizations in this paper.		
Signature		Date	1 July 2019

Name of Co-Author	Mietek Jaroniec		
Contribution to the Paper	This author contributed in paper editing.		
Signature	Digitally signed by Mietek Jaroniec DN: cn=Mietek Jaroniec, o, ou=Kent State, email=jaroniec@kent.edu, c=US Date: 2019.06.11 09:35:04 -0400	Date	1 July 2019

Name of Co-Author	Yao Zheng		
Contribution to the Paper	This author contributed in providing funding and supervising the project.		
Signature		Date	1 July 2019

Name of Co-Author	Shi-Zhang Qiao		
Contribution to the Paper	This author contributed in providing funding and supervising the project.		
Signature		Date	1 July 2019

Please cut and paste additional co-author panels here as required.

Anomalous Hydrogen Evolution Behavior in High-pH Environment Induced by Locally Generated Hydronium Ions

Xuesi Wang^{a‡}, Chaochen Xu^{a‡}, Mietek Jaroniec^b, Yao Zheng^{a*} and Shi-Zhang Qiao^{a*}

^a School of Chemical Engineering, The University of Adelaide, Adelaide SA 5005, Australia

^b Department of Chemistry and Biochemistry, Kent State University, Kent, Ohio 44242, United States

E-mail: s.qiao@adelaide.edu.au; yao.zheng01@adelaide.edu.au

Abstract

Most fundamental studies of electrocatalysis are based on the experimental/simulation results obtained for bulk model materials. Some of these mechanistic understandings are inapplicable for more active nanostructured electrocatalysts. Herein, considering the simplest and typical electrocatalytic process, hydrogen evolution reaction, an alternative reaction mechanism is proposed for nanomaterials based on the identification of a new intermediate, which differs from those commonly known for the bulk counterparts. In-situ Raman spectroscopy and electrochemical thermal/kinetic measurements were conducted on a series of nanomaterials under different conditions. In high-pH electrolytes with negligible hydronium (H_3O^+) concentration in bulk phase, massive H_3O^+ intermediates are found generating on the catalytic surface during water dissociation and hydrogen adsorption processes. These H_3O^+ intermediates create a unique “acid-like” local reaction environment on nanostructured catalytic surface and cut the energy barrier of the overall reaction. Such phenomena on nanostructured electrocatalysts explain their widely observed anomalously high activity under high-pH conditions.

Introduction

Heterogeneous electrocatalytic reduction reactions, e.g., water, nitrogen, and carbon dioxide reduction, are attracting more attention due to their importance for production of hydrogen, carbon monoxide/methane and ammonia through simple electrochemical hydrogenation processes.¹⁻⁷ To carry out these reactions under mild and cost-effective conditions, water-based alkaline solutions are usually used as the hydrogen source. During these reactions, water is not only a solvent but is usually dissociated into H* and OH* species (* represents an active site on the catalyst), which further interact with other reactive intermediates through proton-coupled electron transfer to generate the final products.^{2,4,8-12} As a result, it is important to reveal the local environments about the reactant, reaction intermediates and catalyst surfaces. So far, the understanding of this complicated issue in electrocatalysis is mostly achieved based on the experimental and simulation studies for uniform single-/poly-crystal models.¹³⁻²² These fundamental studies were always carried out for alkaline hydrogen evolution reaction (HER) as a simple model that involves both water dissociation and proton reduction processes. Most results showed that alkaline HER activity of a single-/poly-crystal material is dependent on the pH value of the electrolyte, i.e., the HER kinetics gradually decreases with increasing pH.^{15,18,23} This may be due to pH-dependent H adsorption energy and/or water dissociation energy barrier.^{15,24-26} More importantly, such mechanism suggests a sluggish HER kinetics on bulk materials in high-pH environments (e.g., 1 M KOH), largely limiting their practical applications in the aforementioned reduction reactions.

On the other hand, due to the high specific surface area and a variety of active sites, nanomaterials are more efficient and cost-effective as heterogeneous electrocatalysts. Thus, the design of more active nanostructured electrocatalysts is now the key research concept.²⁷ However, when the reaction mechanism is taken into account, the well-known principles established for the bulk materials are sometimes inapplicable for nanostructured electrocatalysts.²⁰ One of the well-known facts is that

the HER activity of many nanostructured electrocatalysts is much better in high-pH (0.1 to 1 M KOH, pH = 13-13.5) electrolytes than in less alkalic environments (0.01 M KOH to neutral buffer, pH = 12-7.1).²⁸⁻³³ This is opposite to the HER activity trend observed for single-/poly-crystal metals (e.g. activity decreases with raising pH). This different behavior of nanostructured and bulk electrocatalysts indicates not only different HER mechanism on these catalysts, but more importantly, suggests that the water dissociation and proton adsorption/reduction on the surface of nanostructured electrocatalysts are more complicated than those on bulk metals. However, very little research has been conducted toward distinguishing the difference in the reaction mechanisms on the bulk and nanostructured electrocatalysts. As a result, the design principle of nanostructured electrocatalysts for reduction reactions in aqueous electrolytes is still mainly based on the ‘inappropriate’ knowledge of the bulk materials.

Herein, we report a new insight into HER process on the surface of nanostructured electrocatalysts different from that for the well-understood bulk materials, specifically at high-pH electrolytes that contain a negligible amount of hydronium ions (H_3O^+) in the bulk aqueous solutions. This study shows that H_3O^+ ions are in-situ generated on the nanostructured Pt-based catalyst’s surface during the HER process, inducing an acidic local surface environment. As a result, these catalysts exhibit an anomalous acid-like HER activity at high-pH electrolytes, e.g., high activity with acid-like Tafel slope of $\sim 30 \text{ mV dec}^{-1}$ and low activation energy. Formation of the favorable H_3O^+ layer is most likely due to the high-rate water dissociation process that results in a large amount of free H_3O^+ within the electric double layer of nanostructured electrodes, confirmed by in-situ Raman spectroscopy and electrochemical thermal and kinetic analysis. This alternative mechanism as compared to that on the bulk materials sheds a new light toward the design of electrocatalytic nanomaterials by taking the effect of local intermediates in aqueous electrolytes into account.

Results

HER Kinetics

In correspondence to the mechanical studies carried out on bulk Pt and its alloys, we use the standard Pt/C and a series of Pt-based bimetallic nanomaterials as models to reveal the nature of water dissociation and proton reduction on nanostructured electrocatalysts.³⁴ Characterization of these materials (including transmission electron microscopy images and X-ray powder diffraction patterns) provided in Supporting Information (**Supplementary Figure 1, 2**) shows that the differences in their structural properties are tiny. **Figure 1a** shows the HER polarization curves recorded for Pt/C (20 wt % metal) in electrolytes from neutral buffer (pH = 7.1) to 1 M KOH (pH = 13.5). It can be seen that the apparent activity of Pt/C is significantly higher under high OH⁻ concentration ([OH⁻]) in comparison to that under less alkaline environment. Note that the low activity in 2 M solution may be due to the slower kinetics of OH⁻ transfer in such highly alkaline environment than the rate of water dissociation. Additionally, Pt/C's activity in 1 M KOH is much higher than those in other conditions, which trend is very different from the previous results obtained for bulk Pt electrode (**Figure 1b**).^{15,25,35} Further, the rate-determining step (RDS) of HER is also various in different alkaline electrolytes, which is evidenced in the Tafel plots shown in **Figure 1c, d**. Tafel slopes in different electrolytes are compared in similar range (~50 mV negative than the equilibrium potential) to avoid the influence from the high overpotential polarization and formed bubbles. The Tafel slope for Pt/C is ~180 mV dec⁻¹ in buffer and 0.01 M KOH solutions, indicating that in these environments RDS for HER is water dissociation process. However, the Tafel slope drops to 94 mV dec⁻¹ when [OH⁻] increases to 0.1 M while in 1 M KOH solution, the Tafel slope for HER on Pt/C is around 30 mV dec⁻¹ (~40 mV·dec⁻¹ in 2 M KOH solution). For these reactions with a Tafel slope under 120 mV·dec⁻¹, the RDS of the reaction is either proton recombination (Volmer-Tafel) step or electrochemical desorption (Volmer-Heyrovsky) step, similar to the RDS of Pt/C in acid environments. Both reaction pathways indicate that there is a sufficient amount of hydronium ions on the electrode surface for HER process. Otherwise, water

dissociation should be the RDS of the reaction, yielding a Tafel slope larger than $120 \text{ mV}\cdot\text{dec}^{-1}$. Such phenomena are also observed in LiOH-based electrolytes (**Supplementary Figure**

3), indicating the small Tafel slope in high-pH environment is not induced by a specific cation but generally exists in different types of alkaline solutions. Additionally, these results can be observed on other Pt-based nanomaterials as well (**Supplementary Figure 4-6**), further confirming that the nanostructured electrocatalysts have an acid-like RDS for HER in high-pH environments.

HER activity trends

As the HER activity is closely dependent on the H adsorption ability of the materials, we investigated the change of H adsorption for a series of Pt-based nanomaterials under different $[\text{OH}^-]$ conditions. Here, the experimentally obtained d-band vacancies (calculated through the ex-situ X-ray absorption near edge structure spectra, XANES, shown in **Supplementary Figure 7**) are used to represent the H adsorption ability of the catalysts; the larger vacancy of the Pt's d-band, the stronger Pt-H bond, and *vice versa*.^{36,37} Afterwards, by quantitatively evaluating the H adsorption ability of a group of different Pt-based nanomaterials, we obtained a relationship between the H adsorption ability and the material's activity.³⁴ As can be seen in **Figure 2a**, the activities of all these catalysts in different electrolytes follow the order: $1 \text{ M KOH} > 0.1 \text{ M KOH} \gg \text{neutral buffer} > 0.01 \text{ M KOH}$. This confirms that the nanostructured electrocatalysts studied exhibit anomalously high HER activities in high-pH solutions. More importantly, it can be seen that a volcano-type relationship exists between the H adsorption ability and the activity of the materials in 1 M (only the left side of the volcano plot was achieved for the catalysts tested in 1M solution) and 0.1 M KOH electrolytes. Such volcano relationship is not observed in 0.01 M KOH and neutral buffer electrolytes (**Supplementary Figure 8**). It is well known that in an acid environment, the HER activity of a catalyst is solely depending on its hydrogen adsorption ability that has a very close relationship with catalyst's electronic structure (e.g., d-band vacancy).³⁸⁻⁴⁰ However, in an alkaline environment, the HER activity of a catalyst is more dependent

on other factors (e.g., water dissociation rate) but not only on the hydrogen adsorption ability. Normally, for the bulk metal surfaces the relationship between hydrogen adsorption ability and catalysts' HER activities does not match the volcano shape in alkaline environments well.⁴¹ Thus, the observed volcano relationship between the H adsorption ability of the catalysts and their activities in high-pH electrolyte indicates the HER behavior of the nanostructured electrocatalysts under such conditions is more like that in the acid environment.

In-situ Raman characterization

We used in-situ Raman spectra to detect the adsorbates on the catalysts in different alkaline environments and support our above assumption.⁴² The samples used in Raman testing were freshly prepared and Nafion was not used in the ink (5 mg/mL catalyst-water solution without any binder) to avoid the presence of an additional acid-spectator. To rule out the influence from the bulk solution, the reference spectra (with no potential applied) were taken for each group of samples, on which no peaks of electrochemically adsorbed intermediates can be observed. As shown in **Figure 3a** and **Supplementary Figure 9**, a series of peaks such as Pt-H ($\sim 2100\text{ cm}^{-1}$),⁴³ H₂O ($\sim 1600\text{ cm}^{-1}$) and H₃O⁺ ($\sim 1750\text{ cm}^{-1}$) is observed on the spectra of nanostructured Pt/C surfaces at high-pH electrolyte. The positions of these peaks are consistent with theoretical values and/or reported data.⁴³⁻⁴⁵ However, such features are absent on the spectra of bulk Pt samples (**Figure 3b**) and Pt/C in 0.01 M solution (**Figure 3a**). Specifically, as can be seen from **Supplementary Figure 9**, the H intermediates are already adsorbed on the Pt/C catalyst before the onset potential (0 V) of HER and soon get desorbed when a negative potential is applied. Meanwhile, the original G-band peak of the materials ($\sim 1590\text{ cm}^{-1}$) also becomes broader with increasing potential as compared to the reference curve due to the a large amount of adsorbed water (**Figure 3a**).⁴⁴ Interestingly, the Pt-H₃O⁺ interaction peak appears and becomes stronger with increasing overpotential (**Figure 3a**). Noted that the concentration of H₃O⁺ species in the bulk of all tested alkaline electrolytes is extremely low (10^{-13} M). Thus, the H₃O⁺ species detected by

Raman spectra on the surface of catalysts have to be in-situ generated during the HER process. So far, the interaction between Pt and H_3O^+ was only reported on the bulk Pt in acid environments and was not observed on the bulk Pt in any alkaline solutions.^{44,46} With such strong H_3O^+ signal detected here, one can assume that an acid-like environment with rich H_3O^+ species is created on the catalyst surface in a high-pH environment. Such formation of H_3O^+ during HER process in 0.1 M KOH solution is not only observed on Pt/C, but also on other nanomaterials. As highly active nanostructured HER electrocatalysts, PtNi/C and dealloyed PtCo/C were also examined in different alkaline environments. For both materials, Pt- H_3O^+ features can be detected at around -0.1 V in 0.1 M KOH electrolytes (**Supplementary Figure 10**). Moreover, the existence of H_3O^+ was further confirmed by deuterium substitution experiment with both LiOH and KOH electrolytes. As can be seen in **Figure 3c**, the corresponding D_3O^+ ($\sim 2720\text{ cm}^{-1}$) and $\text{HD}_2\text{O}^+/\text{H}_2\text{DO}^+$ ($\sim 2850\text{ cm}^{-1}$) signals can be observed on the spectra of nanostructured Pt/C in 0.1 M solution.⁴⁵ In comparison, such signals are not observed on the spectra of bulk Pt and any other nanostructured electrocatalysts when the reaction takes place in 0.01 M KOH solution in either H_2O or D_2O environment (**Supplementary Figure 11-13**). This indicates that the Pt- H_3O^+ interaction is distinctive for high-pH environments.

Interaction between electrocatalyst and intermediates

We propose the formation of H_3O^+ is closely related to the generation of H^* and water dissociation process in the reaction. It is well known that water dissociation can be facilitated by good interaction between OH intermediates and the catalytic surface. Additionally, such interaction can be monitored using carbon monoxide (CO) stripping tests.⁴⁷⁻⁵⁰ Qualitatively, a lower CO oxidation potential suggests stronger interaction between the catalyst and the OH^* , indicating better water dissociation proceeds. As shown in **Figure 4a**, Pt/C and other nanostructured electrocatalysts show much stronger interactions (lower oxidation potential) with OH^- with increasing $[\text{OH}^-]$, indicating the water dissociation process is improved in high-pH electrolytes on these nanomaterials.

Afterwards, the interaction between the catalyst and H^* is studied. The previous studies conducted for bulk polycrystal Pt show that desorption of H is more difficult with growing pH in alkaline environment.^{17,18,25} Such strongly adsorbed H is believed to be unbeneficial toward water reduction.^{17,18,25} To compare these results with the current case, we recorded the cyclic voltammograms (CVs) for Pt/C and bulk Pt under different $[OH^-]$ environments. For bulk materials, the underpotentially detected H (H_{upd}) peak can only be clearly observed in 0.01 M and 0.1 M KOH, with the H_{upd} potential becoming more positive with increasing $[OH^-]$ (**Figure 4b**). When $[OH^-]$ is higher than 0.1 M, only a weak H_{upd} peak can be detected. This may be caused by a large amount of OH^- blocking some of the H adsorption sites on the bulk Pt surface. In general, the peak associated with H adsorption on the bulk Pt appears at higher potentials and shifts with increasing pH. Conversely, for Pt/C, the H_{upd} peak is shifting to the lower potentials with increasing pH, indicating the H adsorption weakens (**Figure 4c**). At this stage, it is clear that Pt/C shows the improved water dissociation ability and weakened H adsorption ability with increasing $[OH^-]$. We suggest that such changes can lead to the generation of the large amount of H_3O^+ during the HER process; the detailed formation mechanism will be explained later.

Activation energy

The activation energy (E_a) values for Pt/C and a series of Pt-based nanostructured electrocatalysts were calculated to reveal how the in-situ generated H_3O^+ changes the overall kinetics of the reaction in different alkaline environments. The values of E_a were calculated according to the Arrhenius equation from the HER polarization curves under different temperatures (**Figure 5a** and **Supplementary Figure14, 15**).⁵¹ **Figure 5b** shows the E_a values for Pt/C, PtNi/C and dealloyed PtCo/C under three different alkaline environments. It is clear that the values of E_a are obviously smaller at 1 M/0.1 M KOH as compared to those at 0.01 M KOH. This demonstrates that the in-situ generated H_3O^+

intermediates lowered the energy barrier for the overall reaction, most likely by providing an acid-like environment that significantly optimizes the proton reduction process and changes RDS of the reaction.

Origin of H_3O^+

Based on the in in-situ Raman spectra and electrochemical thermal/kinetic analysis, an alternative water reduction mechanism is revealed for the nanostructured Pt-based electrocatalysts. In all alkaline electrolytes, water dissociation is always the most important step toward producing hydrogen source needed for HER process. Under high $[\text{OH}^-]$, large amounts of OH^- are available in the electrolyte and can be easily adsorbed to the catalyst, strongly promotes the water dissociation process. As a result, large amounts of H^* are produced and the majority of the H active sites are soon covered with strongly bonded H_{upd} . Note that under negative potential, water molecules are connected to each other.⁵² As water dissociation continues, more and more H ions are still bonded to nearby water molecules but not the catalyst's surface, which is being occupied by H_{upd} species. Thus, a large amount of free H_3O^+ ions is generated within the double layer, resulting an acid-like local environment. With more electrons being transferred on the surface, H_{upd} turns to H_{opd} (overpotential deposited hydrogen) and the later combines each other to form H_2 gas (following the Tafel mechanism evidenced by a Tafel slope of $\sim 30 \text{ mV}\cdot\text{dec}^{-1}$), leaving an empty site. At the same time, H_3O^+ is reduced to H^* on that site to form the cycle (**Figure 6a**).

On the other hand, another dissociation product, OH intermediates, does not dissociated as OH^- within the double layer. According to the report by Jia et al,⁵³, OH intermediates will directly form a hydroxyl-water-alkali metal cation adduct (in our case, $\text{OH}^*-(\text{H}_2\text{O})_n-\text{K}^+$), which can be directly desorbed through the double layer into the bulk solution. As a result, the local concentration of OH^- does not increase and the generated $\text{OH}^*-(\text{H}_2\text{O})_n-\text{K}^+$ does not react with hydronium species. In the current study, this assumption has also been confirmed by in-situ Raman spectra. As shown in **Supplementary Figure. 16**, under different overpotentials, the OH stretching mode (Raman shift

3200-3600 cm^{-1}) does not change much, indicating a stable status of $[\text{OH}^-]$ on the catalytic surface during the reaction (**Figure 6a**).

However, the same process cannot take place in less alkaline solutions due to the low $[\text{OH}^-]$ in the environment to facilitate the key water dissociation process and to supply H intermediates. In this case, Volmer step ($\text{H}_2\text{O} + \text{e}^- \rightarrow \text{H}^* + \text{OH}^-$) becomes the RDS of the overall reaction as indicated by Tafel slope of $166 \text{ mV} \cdot \text{dec}^{-1}$. High overpotential is needed for the catalysts to interact with water to start water dissociation under such low $[\text{OH}^-]$ environment, resulting in a high activation energy for the overall reaction. Moreover, the low concentration of metal cation also causes a slow removal of OH intermediates from the double layer. As a result, the generation of H^* is sluggish, which results in the low overall HER activity (**Figure 6b**).

Noticeably, this H_3O^+ induced water reduction mechanism seems to be unique to nanostructured electrocatalysts. This is most likely due to the complex surface structure of nanomaterials allowing the existence of a variety of different active sites to facilitate water adsorption/dissociation without interfering with the H-catalyst interactions. Since these two key processes can proceed at the same time, a facile generation of H_3O^+ is guaranteed. However, for uniform bulk materials with a single kind of active sites, the competition for active sites between the water dissociation and hydrogen adsorption reduces the water dissociation efficiency significantly, and consequently, affects the generation of hydrogen species (**Figure 6c**).^{24,50} As a result, the water reduction on nanostructured electrocatalysts can be promoted with increasing $[\text{OH}^-]$, while hydrogen production is reduced on the bulk catalysts.

Discussion

In summary, we studied a series of Pt-based nanostructured electrocatalysts to reveal the unique water dissociation and proton reduction mechanism on nanomaterials. A unique H_3O^+ intermediate layer that creates an acidic environment on the catalyst's surface was first identified under high $[\text{OH}^-]$ conditions. This H_3O^+ intermediate layer was found to be responsible for an anomalous acid-like HER activity of

nanostructured electrocatalysts in alkaline electrolytes. More electrochemical analysis and in-situ Raman characterizations have indicated that these H_3O^+ are generated by high-rate water dissociation process that promotes desorption of H^* on the surface of electrocatalysts. This unique reaction mechanism on nanomaterials may provide an important guidance for the design/selection of catalysts/electrolytes for the nanomaterial-catalyzed reactions in an aqueous environment, including carbon dioxide reduction, nitrogen reduction and other electrocatalytic reduction reactions.

Methods

Fabrication of Electrocatalysts

Commercialized Pt/C (20 wt.%), PtM/C (20 wt.%, M = Fe, Co, Ni) were purchased from FuelCellStore without further treatment. The acid-treated PtM/C samples were fabricated by mixing 10 mg of PtM/C with 30 mL of HClO_4 solution (0.1 M) and stirring overnight. The products were then washed several times and freeze-dried. The annealed PtM/C samples were fabricated by annealing 10 mg of PtM/C at 900 °C for 5 hours in H_2/Ar ($\text{H}_2 = 5 \text{ vol.}\%$) atmosphere. All the catalysts are metal nanoparticles (size: ~ 5 nm) supported on carbon black.

In-situ Raman Characterization

The in-situ Raman spectra were recorded by HORIBA Scientific Raman Spectroscopy (laser wavelength = 532 nm) using a screen-printed electrode from Pine Research Instrumentation. The electrolytes were prepared with extra care to avoid contaminations from other ions and glassware. The tests were carried out using a screen-printed chip electrode from Pine Research Instrumentation. 10 μL of the ink gel was added to the printed electrode before dried in room temperature. For the test with bulk materials, a Pt-printed chip electrode with bulk Pt surface from Pine Research Instrumentation was used.

Electrochemical Testing Setup

All the electrochemical data were recorded by a CHI 760E bipotentiostat (CH Instruments, INC.). The powdered electrocatalysts were first dispersed in 0.05 wt.% Nafion aqueous solution to form a 2.0 mg/mL homogeneous ink gel. The working electrode was prepared by adding 20 μ L of the ink gel onto the glassy carbon rotating disk electrode (RDE, surface area of the glassy carbon = 0.196 cm², Pine Research Instrumentation) and dried at room temperature. The reference electrode was an Ag/AgCl wire in 4 M KCl solution. The counter electrode was a pure gold wire. All the potentials in this work were referenced to the reversible hydrogen electrode (RHE) using pure hydrogen calibration and all polarization curves were iR corrected. All the polarization data were represented after calibration with respect to the electrochemical active surface area (ECSA). During the experiments, a flow of argon was maintained over all the cyclic voltammograms tests, while a flow of H₂ was purged to ensure an H₂-oversaturated electrolyte environment during recording all the polarization curves. The electrolytes used were KOH solution with different concentrations (0.01, 0.1 and 1 M) and phosphate buffer solution (1 M). During all the tests, the working electrode was rotated at 1600 rpm. A water jacket cell from Pine Research Instrumentation was used for all the tests to achieve controllable temperature.

Data Availability

The data that support the findings of this study are available from the corresponding author upon request. The source data underlying Figures 1a-d, 2a, 3a-c, 4a-c and 5a, b and Supplementary Figures 1-16 are provided as a Source Data file.

References

- 1 Deng, J., Iñiguez, J. A. & Liu, C. Electrocatalytic nitrogen reduction at low temperature. *Joule* **2**, 846-856 (2018).
- 2 Yang, X. *et al.* Mechanistic Insights into Electrochemical Nitrogen Reduction Reaction on Vanadium Nitride Nanoparticles. *J. Am. Chem. Soc.* **140**, 13387-13391 (2018).

- 3 Guo, C., Ran, J., Vasileff, A. & Qiao, S.-Z. Rational design of electrocatalysts and photo (electro) catalysts for nitrogen reduction to ammonia (NH₃) under ambient conditions. *Energ. Environ. Sci.* **11**, 45-56 (2018).
- 4 Vasileff, A., Xu, C., Jiao, Y., Zheng, Y. & Qiao, S.-Z. Surface and Interface Engineering in Copper-Based Bimetallic Materials for Selective CO₂ Electroreduction. *Chem* **4**, 1809-1831 (2018).
- 5 Jiao, Y., Zheng, Y., Chen, P., Jaroniec, M. & Qiao, S.-Z. Molecular scaffolding strategy with synergistic active centers to facilitate electrocatalytic CO₂ reduction to hydrocarbon/alcohol. *J. Am. Chem. Soc.* **139**, 18093-18100 (2017).
- 6 Kuhl, K. P. *et al.* Electrocatalytic conversion of carbon dioxide to methane and methanol on transition metal surfaces. *J. Am. Chem. Soc.* **136**, 14107-14113 (2014).
- 7 Sun, X. *et al.* Molybdenum–bismuth bimetallic chalcogenide nanosheets for highly efficient electrocatalytic reduction of carbon dioxide to methanol. *Angew. Chem. Int. Ed.* **55**, 6771-6775 (2016).
- 8 Wang, L. *et al.* Electrochemical Carbon Monoxide Reduction on Polycrystalline Copper: Effects of Potential, Pressure, and pH on Selectivity toward Multicarbon and Oxygenated Products. *ACS Catal.* **8**, 7445-7454 (2018).
- 9 Dunwell, M., Luc, W., Yan, Y., Jiao, F. & Xu, B. Understanding surface-mediated electrochemical reactions: CO₂ reduction and beyond. *ACS Catal.* **8**, 8121-8129 (2018).
- 10 Singh, A. R. *et al.* Electrochemical Ammonia Synthesis—The Selectivity Challenge. *ACS Catal.* **7**, 706-709 (2016).
- 11 Zhuang, T.-T. *et al.* Copper nanocavities confine intermediates for efficient electrosynthesis of C₃ alcohol fuels from carbon monoxide. *Nat. Catal.* **1**, 946-951 (2018).
- 12 Zheng, Y. *et al.* Understanding the roadmap for electrochemical reduction of CO₂ to multi-carbon oxygenates and hydrocarbons on copper-based catalysts. *J. Am. Chem. Soc.* **141**, 7646-7659 (2019).
- 13 Xiao, H., Cheng, T. & Goddard III, W. A. Atomistic mechanisms underlying selectivities in C₁ and C₂ products from electrochemical reduction of CO on Cu (111). *J. Am. Chem. Soc.* **139**, 130-136 (2016).

- 14 Ito, M. Structures of water at electrified interfaces: Microscopic understanding of electrode potential in electric double layers on electrode surfaces. *Surf. Sci. Rep.* **63**, 329-389 (2008).
- 15 Strmcnik, D. *et al.* Improving the hydrogen oxidation reaction rate by promotion of hydroxyl adsorption. *Nat. Chem.* **5**, 300-306 (2013).
- 16 Nakamura, M., Kobayashi, T. & Hoshi, N. Structural dependence of intermediate species for the hydrogen evolution reaction on single crystal electrodes of Pt. *Surf. Sci.* **605**, 1462-1465 (2011).
- 17 Zheng, J., Sheng, W., Zhuang, Z., Xu, B. & Yan, Y. Universal dependence of hydrogen oxidation and evolution reaction activity of platinum-group metals on pH and hydrogen binding energy. *Sci. Adv.* **2**, e1501602 (2016).
- 18 Sheng, W., Myint, M., Chen, J. G. & Yan, Y. Correlating the hydrogen evolution reaction activity in alkaline electrolytes with the hydrogen binding energy on monometallic surfaces. *Energ. Environ. Sci.* **6**, 1509-1512 (2013).
- 19 Cheng, T., Wang, L., Merinov, B. V. & Goddard, W. A. Explanation of Dramatic pH-Dependence of Hydrogen Binding on Noble Metal Electrode: Greatly Weakened Water Adsorption at High pH. *J. Am. Chem. Soc.* **140**, 7787-7790 (2018).
- 20 Zheng, Y., Jiao, Y., Vasileff, A. & Qiao, S. Hydrogen Evolution Reaction in Alkaline Solution: From Theory, Single Crystal Models, to Practical Electrocatalysts. *Angew. Chem. Int. Ed.* **57**, 7568-7579 (2017).
- 21 Davydova, E. S., Mukerjee, S., Jaouen, F. & Dekel, D. R. Electrocatalysts for Hydrogen Oxidation Reaction in Alkaline Electrolytes. *ACS Catal.* **8**, 6665-6690 (2018).
- 22 Intikhab, S., Snyder, J. D. & Tang, M. H. Adsorbed Hydroxide Does Not Participate in the Volmer Step of Alkaline Hydrogen Electrocatalysis. *ACS Catal.* **7**, 8314-8319 (2017).
- 23 Ledezma-Yanez, I. *et al.* Interfacial water reorganization as a pH-dependent descriptor of the hydrogen evolution rate on platinum electrodes. *Nat. Energy* **2**, 17031 (2017).
- 24 Subbaraman, R. *et al.* Enhancing hydrogen evolution activity in water splitting by tailoring Li(+)-Ni(OH)₂-Pt interfaces. *Science* **334**, 1256-1260, (2011).
- 25 Sheng, W. *et al.* Correlating hydrogen oxidation and evolution activity on platinum at different pH with measured hydrogen binding energy. *Nat. Commun.* **6**, 5848 (2015).

- 26 Stamenkovic, V. R., Strmcnik, D., Lopes, P. P. & Markovic, N. M. Energy and fuels from electrochemical interfaces. *Nat. Mater.* **16**, 57-69 (2016).
- 27 Jiao, Y., Zheng, Y., Jaroniec, M. & Qiao, S. Z. Design of electrocatalysts for oxygen-and hydrogen-involving energy conversion reactions. *Chem. Soc. Rev.* **44**, 2060-2086 (2015).
- 28 Liu, J., Zhu, D., Ling, T., Vasileff, A. & Qiao, S.-Z. S-NiFe₂O₄ ultra-small nanoparticle built nanosheets for efficient water splitting in alkaline and neutral pH. *Nano Energy* **40**, 264-273 (2017).
- 29 Zhang, R. *et al.* Ternary NiCo₂P_x Nanowires as pH-Universal Electrocatalysts for Highly Efficient Hydrogen Evolution Reaction. *Adv. Mater.* **29**, 1605502 (2017).
- 30 Zheng, Y. *et al.* High electrocatalytic hydrogen evolution activity of an anomalous ruthenium catalyst. *J. Am. Chem. Soc.* **138**, 16174-16181 (2016).
- 31 Liu, T. *et al.* Self-Standing CoP Nanosheets Array: A Three-Dimensional Bifunctional Catalyst Electrode for Overall Water Splitting in both Neutral and Alkaline Media. *ChemElectroChem* **4**, 1840-1845 (2017).
- 32 Huang, Z.-F. *et al.* Hollow cobalt-based bimetallic sulfide polyhedra for efficient all-pH-value electrochemical and photocatalytic hydrogen evolution. *J. Am. Chem. Soc.* **138**, 1359-1365 (2016).
- 33 Liu, T. *et al.* Mn doping of CoP nanosheets array: an efficient electrocatalyst for hydrogen evolution reaction with enhanced activity at all pH values. *ACS Catal.* **7**, 98-102 (2016).
- 34 Wang, X. *et al.* Breaking the Volcano-Plot Limits for Pt-based Electrocatalysts by Selective Tuning Adsorption of Multiple Intermediates. *J. Mater. Chem. A* **7**, 13635-13640 (2019).
- 35 Bagotzky, V. & Osetrova, N. Investigations of hydrogen ionization on platinum with the help of micro-electrodes. *J. Electroanal. Chem.* **43**, 233-249 (1973).
- 36 Mukerjee, S., Srinivasan, S., Soriaga, M. P. & McBreen, J. Role of structural and electronic properties of Pt and Pt alloys on electrocatalysis of oxygen reduction An in situ XANES and EXAFS investigation. *J. Electrochem. Soc.* **142**, 1409-1422 (1995).
- 37 Ramaswamy, N. *et al.* Hydrogen oxidation reaction in alkaline media: Relationship between electrocatalysis and electrochemical double-layer structure. *Nano Energy* **41**, 765-771 (2017).

- 38 Greeley, J., Norskov, J. K., Kibler, L. A., El-Aziz, A. M. & Kolb, D. M. Hydrogen evolution over bimetallic systems: understanding the trends. *Chemphyschem* **7**, 1032-1035 (2006).
- 39 Kulkarni, A., Siahrostami, S., Patel, A. & Norskov, J. K. Understanding Catalytic Activity Trends in the Oxygen Reduction Reaction. *Chem. Rev.* **118**, 2302-2312 (2018).
- 40 Nørskov, J. K. *et al.* Trends in the Exchange Current for Hydrogen Evolution. *J. Electrochem. Soc.* **152**, J23-J26 (2005).
- 41 Danilovic, N., Subbaraman, R., Strmcnik, D., Stamenkovic, V. & Markovic, N. Electrocatalysis of the HER in acid and alkaline media. *J. Serb. Chem. Soc.* **78**, 2007-2015 (2013).
- 42 Deng, Y. & Yeo, B. S. Characterization of electrocatalytic water splitting and CO₂ reduction reactions using in situ/operando Raman spectroscopy. *ACS Catal.* **7**, 7873-7889 (2017).
- 43 Jiang, Y.-X. *et al.* Characterization of surface water on Au core Pt-group metal shell nanoparticles coated electrodes by surface-enhanced Raman spectroscopy. *Chem. Commun.*, 4608-4610 (2007).
- 44 Ren, B. *et al.* Surface Raman spectra of pyridine and hydrogen on bare platinum and nickel electrodes. *J. Electroanal. Chem.* **415**, 175-178 (1996).
- 45 Colvin, M. E., Raine, G. P., Schaefer III, H. F. & Dupuis, M. Infrared intensities of H₃O⁺, H₂DO⁺, HD₂O⁺, and D₃O⁺. *J. Chem. Phys.* **79**, 1551-1552 (1983).
- 46 Osawa, M., Tsushima, M., Mogami, H., Samjeske, G. & Yamakata, A. Structure of water at the electrified platinum– water interface: A study by surface-enhanced infrared absorption spectroscopy. *J. Phys. Chem. C* **112**, 4248-4256 (2008).
- 47 Gasteiger, H. A., Markovic, N., Ross, P. N. & Cairns, E. J. Carbon monoxide electrooxidation on well-characterized platinum-ruthenium alloys. *J. Phys. Chem.* **98**, 617-625 (1994).
- 48 Ochal, P. *et al.* CO stripping as an electrochemical tool for characterization of Ru@Pt core-shell catalysts. *J. Electroanal. Chem.* **655**, 140-146 (2011).
- 49 Rudi, S., Cui, C., Gan, L. & Strasser, P. Comparative Study of the Electrocatalytically Active Surface Areas (ECSAs) of Pt Alloy Nanoparticles Evaluated by Hupd and CO-stripping voltammetry. *Electrocatalysis* **5**, 408-418 (2014).
- 50 Subbaraman, R. *et al.* Trends in activity for the water electrolyser reactions on 3d M(Ni,Co,Fe,Mn) hydr(oxy)oxide catalysts. *Nat. Mater.* **11**, 550-557 (2012).

- 51 Marković, N., Grgur, B. & Ross, P. N. Temperature-dependent hydrogen electrochemistry on platinum low-index single-crystal surfaces in acid solutions. *J. Phys. Chem. B* **101**, 5405-5413 (1997).
- 52 Li, C. Y. *et al.* In situ probing electrified interfacial water structures at atomically flat surfaces. *Nat Mater*, doi:10.1038/s41563-019-0356-x (2019).
- 53 Liu, E. *et al.* Unifying the Hydrogen Evolution and Oxidation Reactions Kinetics in Base by Identifying the Catalytic Roles of Hydroxyl-Water-Cation. *J. Am. Chem. Soc.* **141**, 3232-3239 (2019).

Acknowledgements

We acknowledge financial support from the Australian Research Council through Discovery and Linkage Project programs (DP160104866, DP170104464, LP160100927, DE160101163 and FL170100154). We also gratefully acknowledge the Australian Synchrotron for X-ray absorption spectroscopy characterizations for providing the XANES data.

Author contributions

X. Wang and C. Xu contributed equally. The electrochemical experiments were done by X. Wang; The Raman characterizations were done by C. Xu. The manuscript was written through the contributions of all authors. All authors have given approval to the final version of the manuscript.

Competing interests

The authors declare no competing interests.

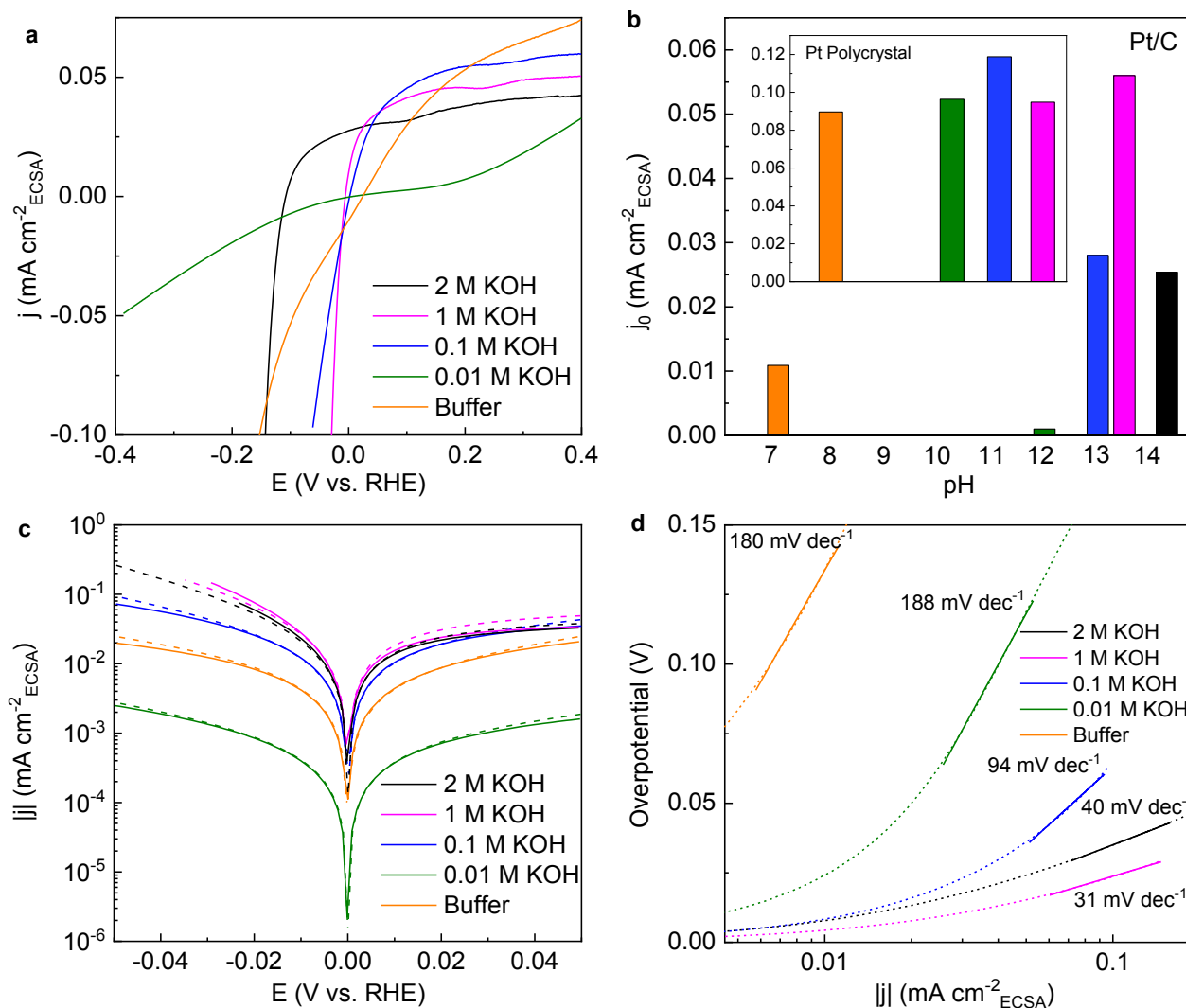


Figure 1 HER activity comparison under different alkaline environments. **a** The HER polarization curves of Pt/C under different conditions. **b** The activity trend for Pt/C and polycrystal Pt (inset) under different conditions. The data for polycrystal Pt were taken from reference.³⁵ **c** Tafel plots and the corresponding Butler-Volmer fitting results for Pt/C under different conditions. **d** The Tafel slope for Pt/C under different conditions.

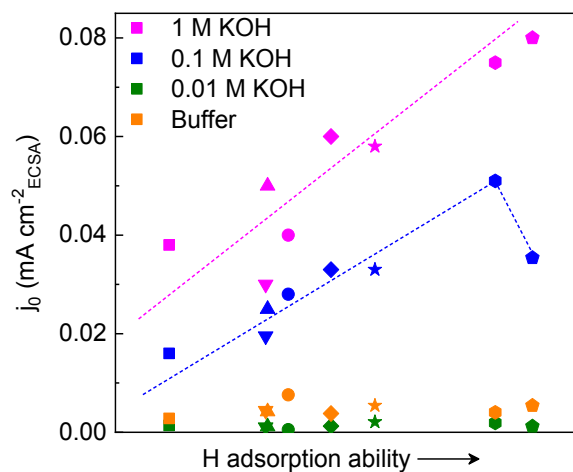


Figure 2 The experimentally acquired relationship between the H adsorption ability and the activity (j_0) for a series of Pt-based materials using different electrolytes. The symbols in the figure are ●: Pt/C ■: PtFe/C ▲: PtCo@Pt/C ▼: PtCo/C ◆: PtNi/C ★: PtFe@Pt/C ♠: dealloyed PtNi/C ●: PtNi@Pt/C The H adsorption ability of the electrocatalysts is represented according to the d-band vacancies of each material.

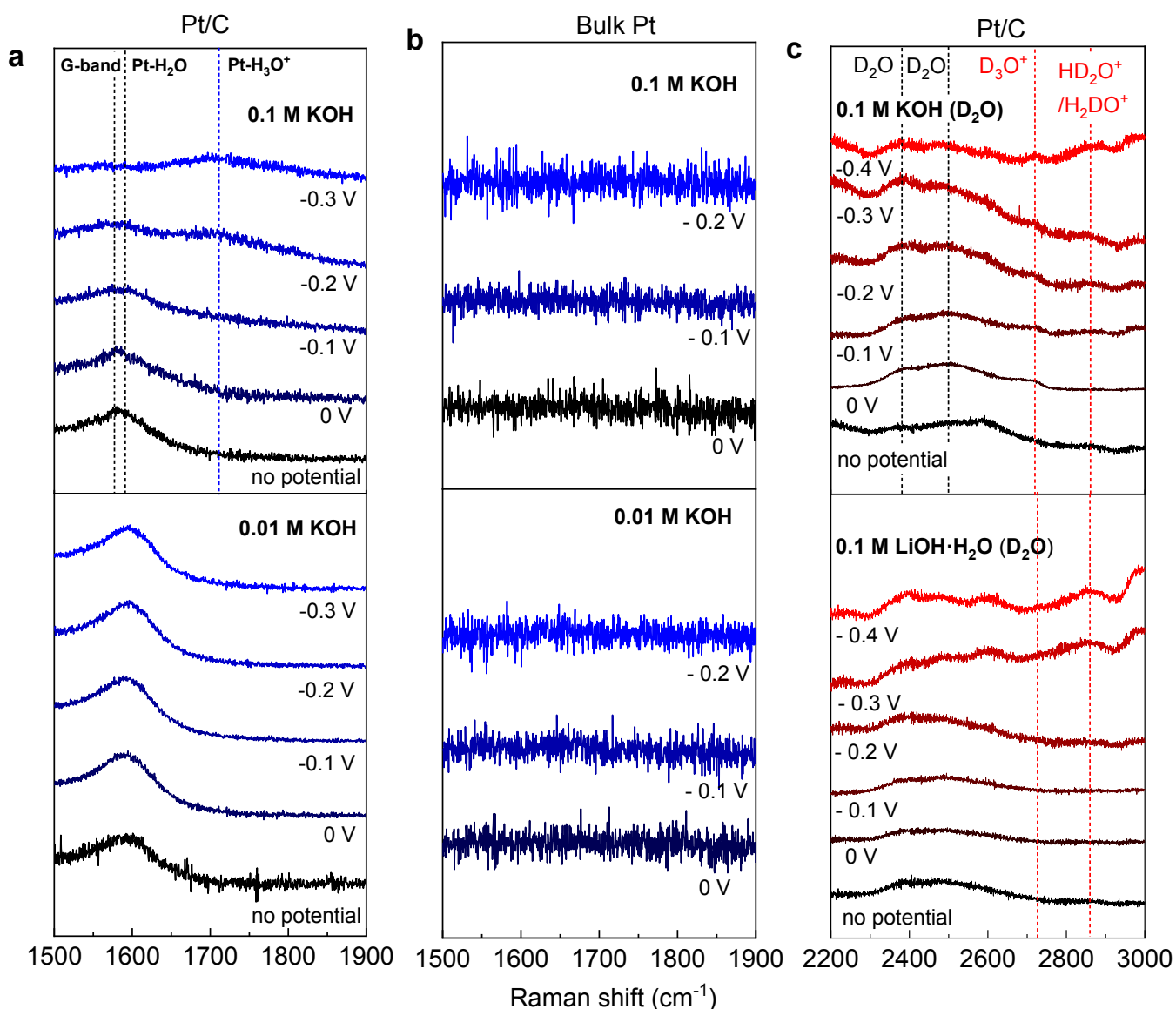


Figure 3 Raman spectra of Pt/C and bulk Pt at various conditions. The Raman spectra for: **a** Pt/C and **b** bulk Pt in water-based alkaline environments. **c** Pt/C in deuterium water-based alkaline environments. The marked overpotential is in comparing to the on-set potential of HER (e.g. -0.1 V is 0.1 V more negative to onset potential). The Raman signals on the surface of the catalyst are identified as: g-band of carbon: $\sim 1580 \text{ cm}^{-1}$; H₂O: $\sim 1600 \text{ cm}^{-1}$; H₃O⁺: $\sim 1750 \text{ cm}^{-1}$; D₃O⁺: $\sim 2720 \text{ cm}^{-1}$; HD₂O/H₂DO⁺: $\sim 2850 \text{ cm}^{-1}$; D₂O: $\sim 2380 \text{ cm}^{-1}$, $\sim 2500 \text{ cm}^{-1}$.⁴³⁻⁴⁵

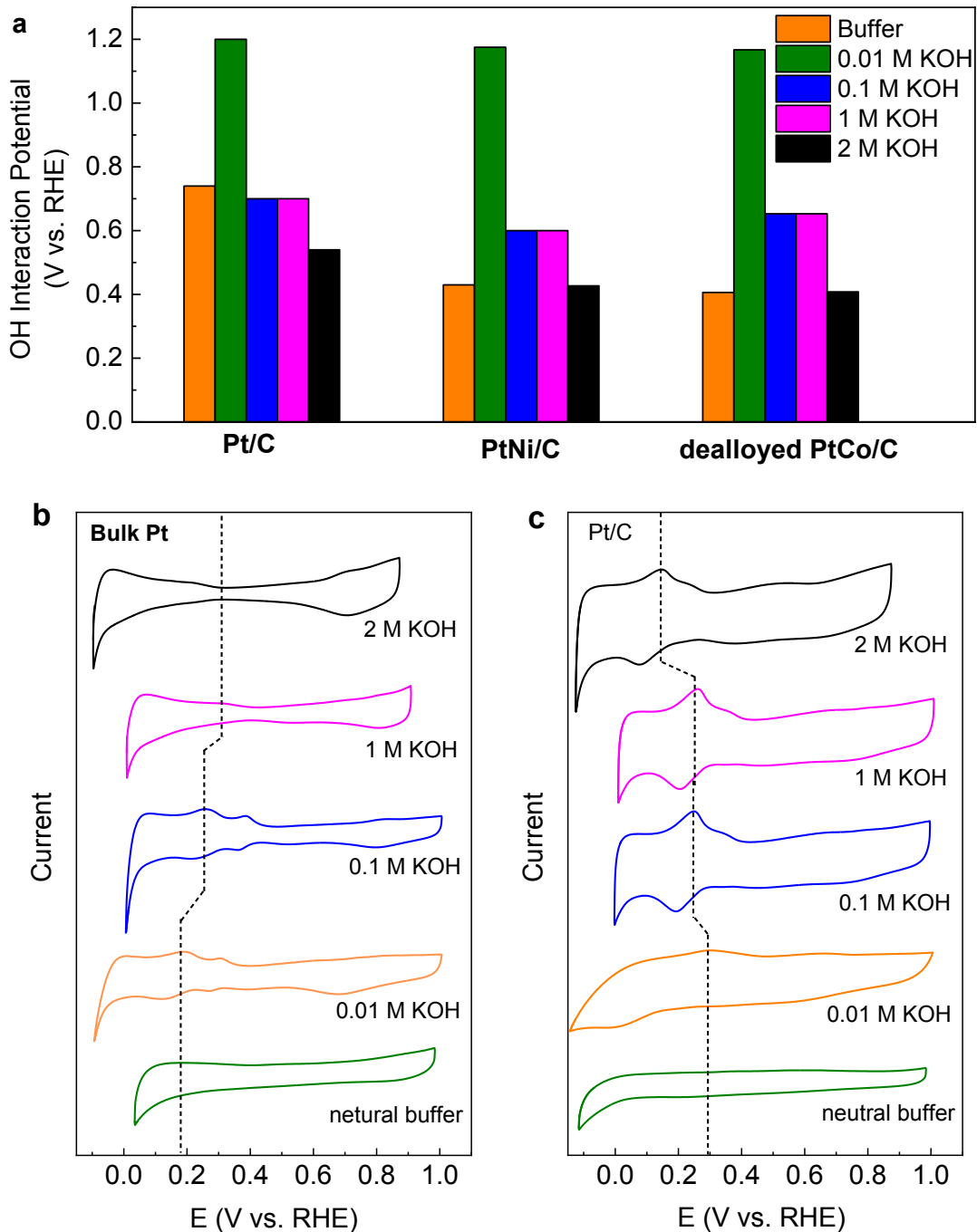


Figure 4 The trends of H and OH interactions with different catalysts. **a** OH interaction potentials obtained for three catalysts in different electrolytes. Data obtained from CO stripping measurements. **b-c** CVs of bulk Pt and Pt/C in different electrolytes. The dotted line indicates the shifting trend of the H_{upd} peak.

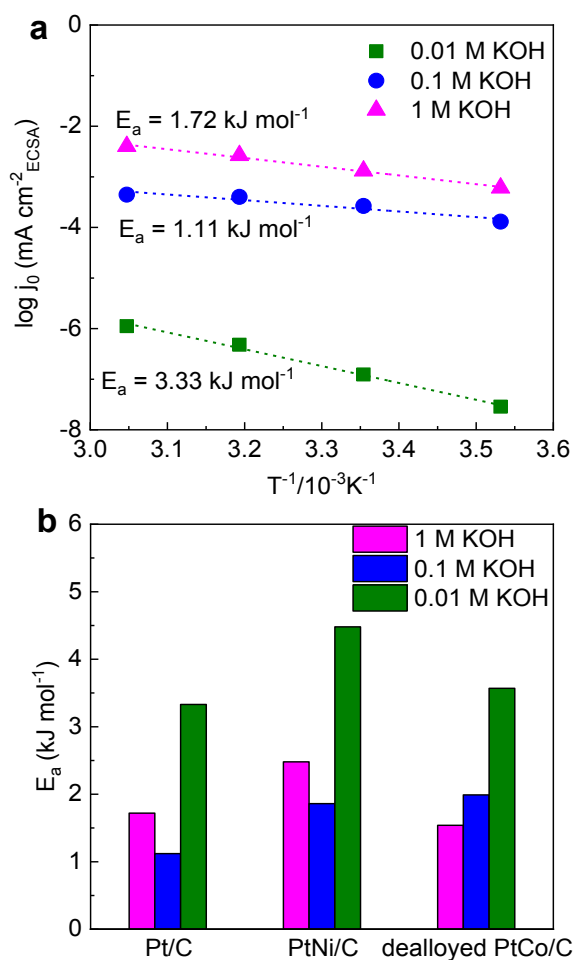


Figure 5 HER energy barrier for various nanostructured electrocatalysts. **a** The relationship between the temperature and the catalytic activity of Pt/C under certain temperature range (10 °C to 55 °C). **b** A comparison of the activation energy (E_a) for a series of different Pt-based nanostructured electrocatalysts in different alkaline environments.

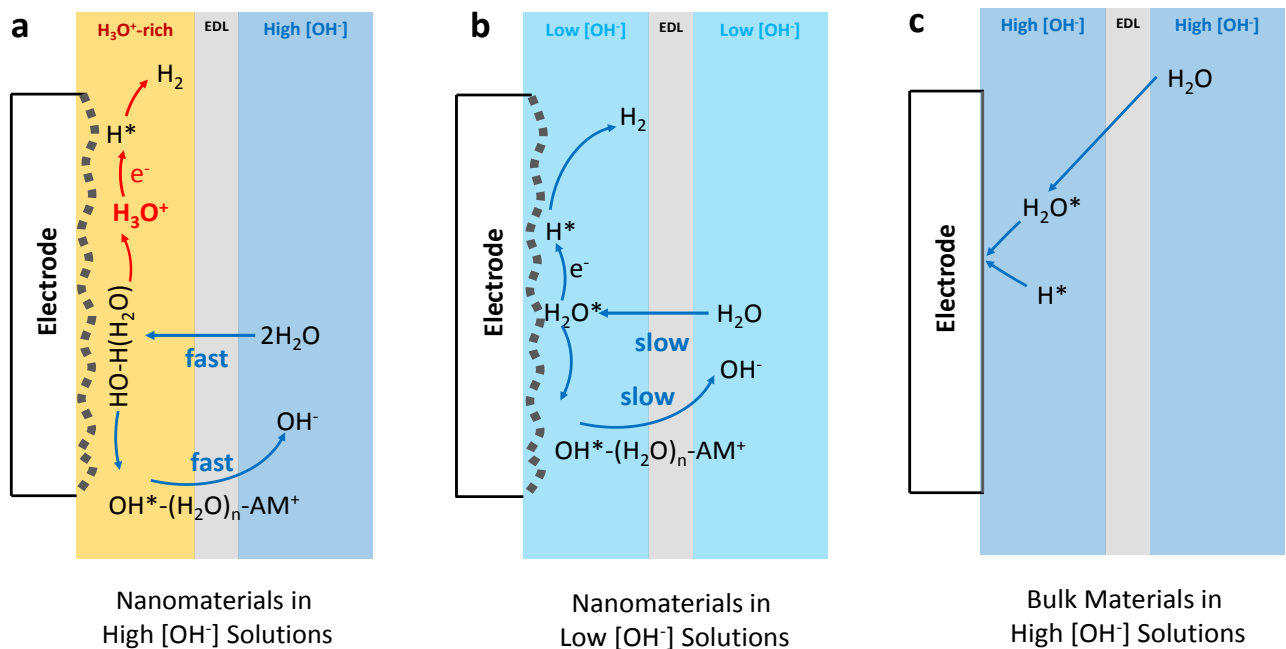


Figure 6 Schematic illustration of the water reduction mechanism on the nanostructured electrocatalysts. **a** Surface intermediates on the nanostructured electrocatalysts in solutions with high $[\text{OH}^-]$; **b** Surface intermediates on the nanostructured electrocatalysts in solutions with low $[\text{OH}^-]$. **c** Water reduction mechanism on the bulk electrocatalysts in high-pH environments. EDL represents the electric double layer.

Supplementary Information

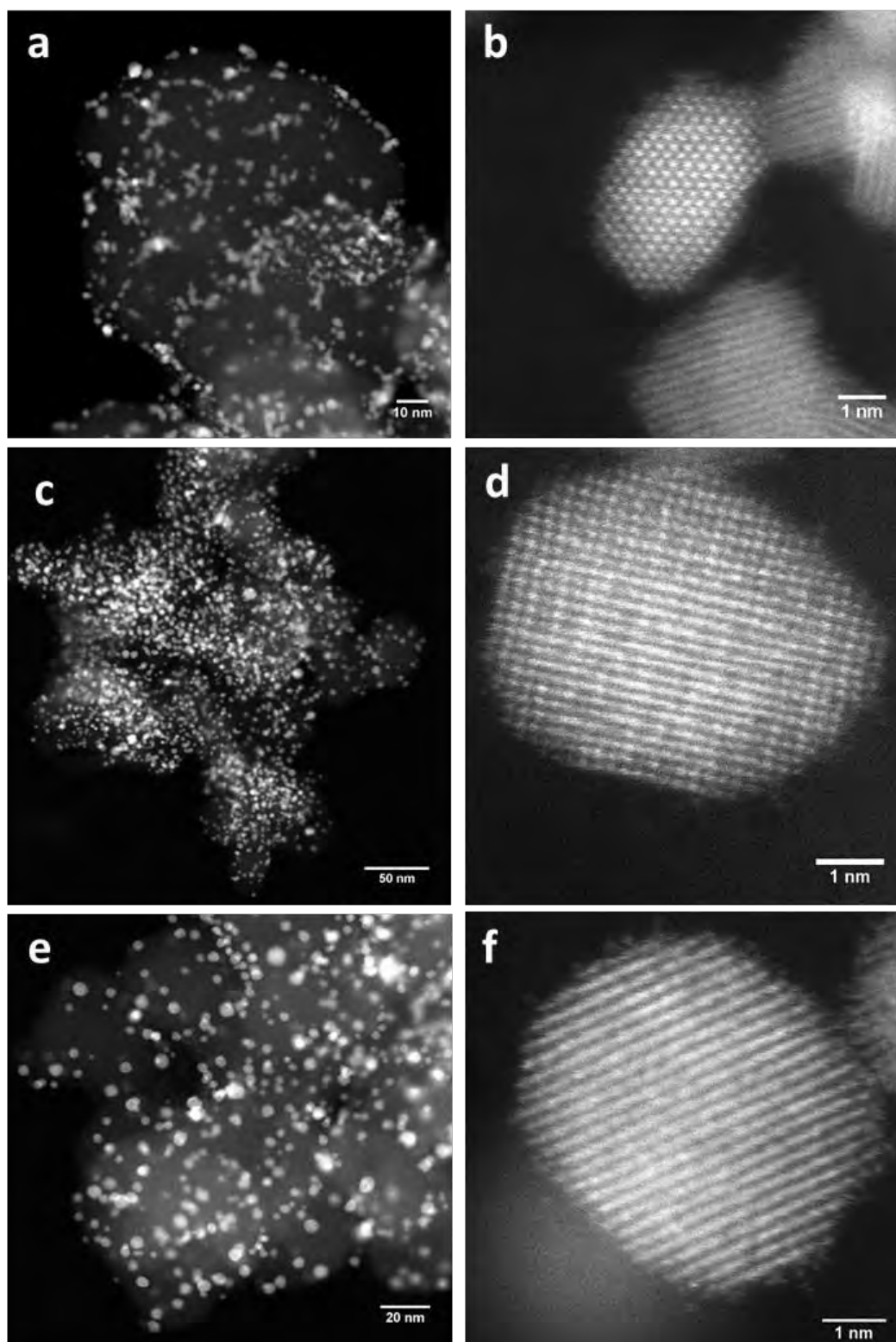
Anomalous Hydrogen Evolution Behavior in High-pH Environment Induced by Locally Generated Hydronium Ions

Xuesi Wang^{a‡}, Chaochen Xu^{a‡}, Mietek Jaroniec^b, Yao Zheng^{a*} and Shi-Zhang Qiao^{a*}

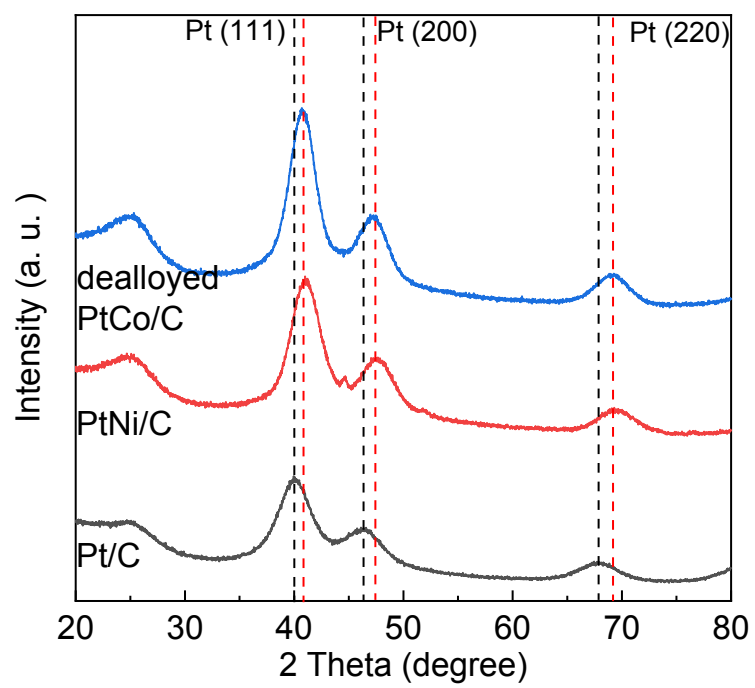
^a School of Chemical Engineering, The University of Adelaide, Adelaide SA 5005, Australia

^b Department of Chemistry and Biochemistry, Kent State University, Kent, Ohio 44242, United States

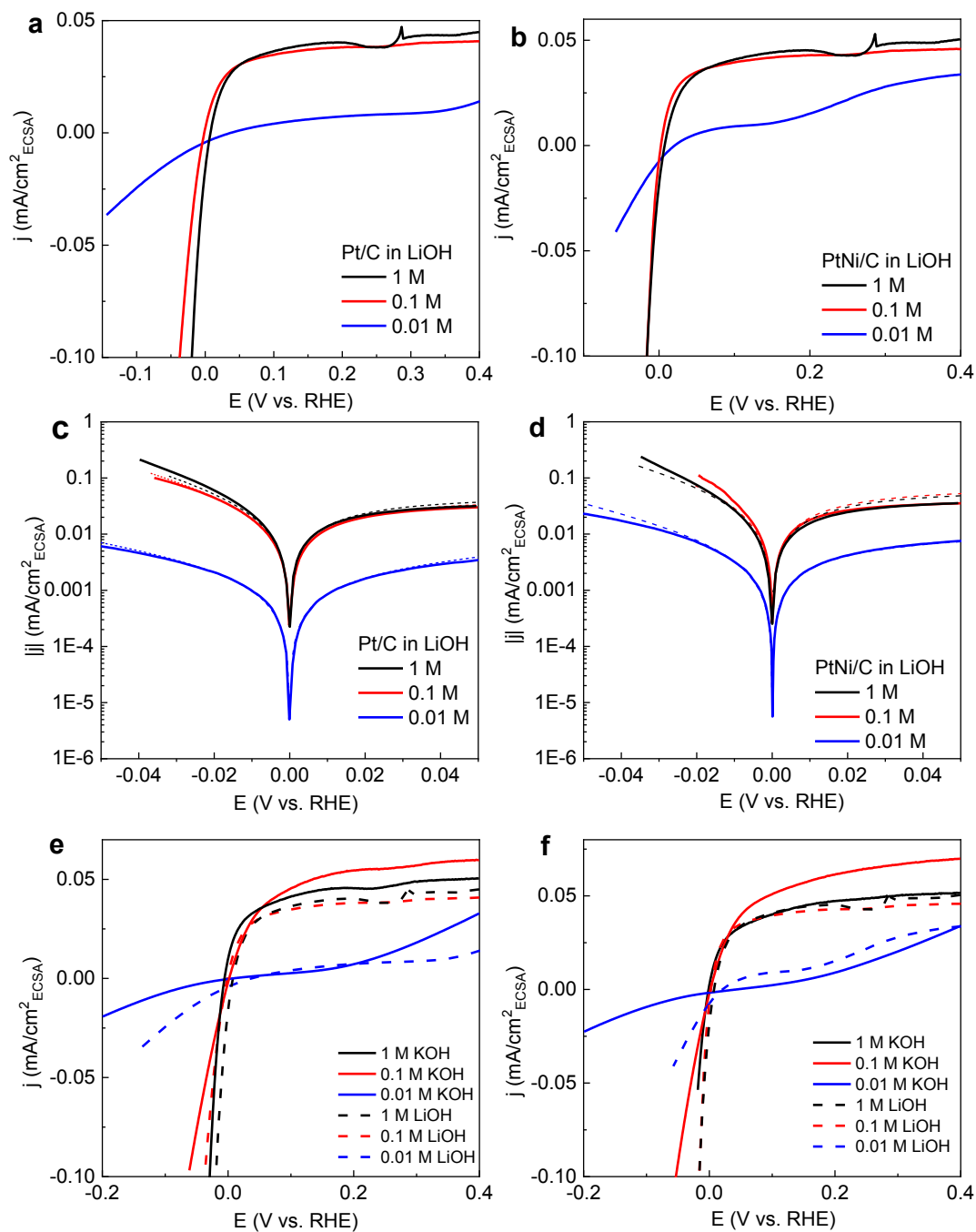
E-mail: s.qiao@adelaide.edu.au; yao.zheng01@adelaide.edu.au



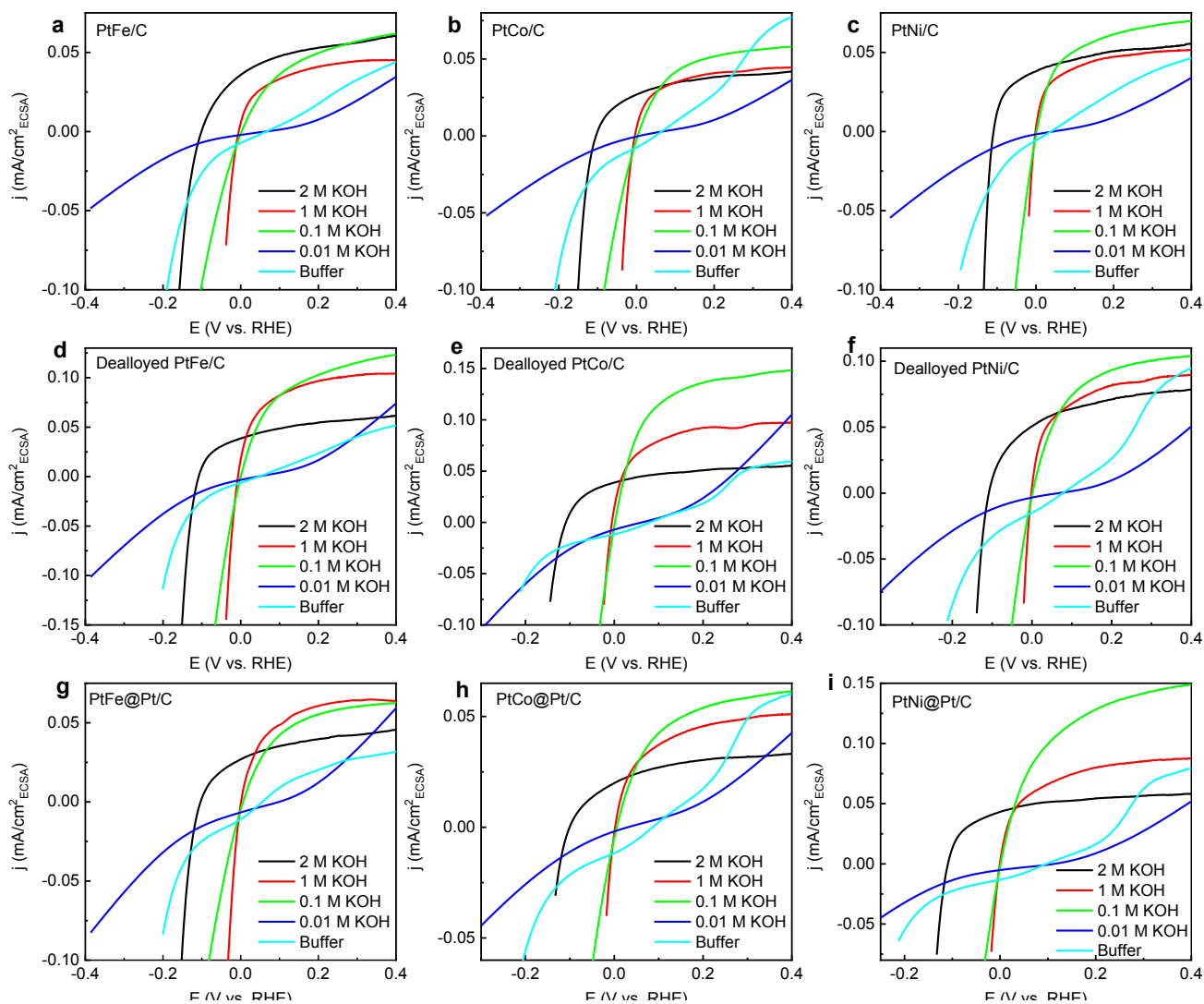
Supplementary Figure 1 The high-angle annular dark-field scanning transmission electron microscopy (HAADF-STEM) images of the samples. HAADF-STEM images of **a, b** Pt/C; **c, d** PtNi/C; **e, f** dealloyed PtCo/C nanosized electrocatalysts.



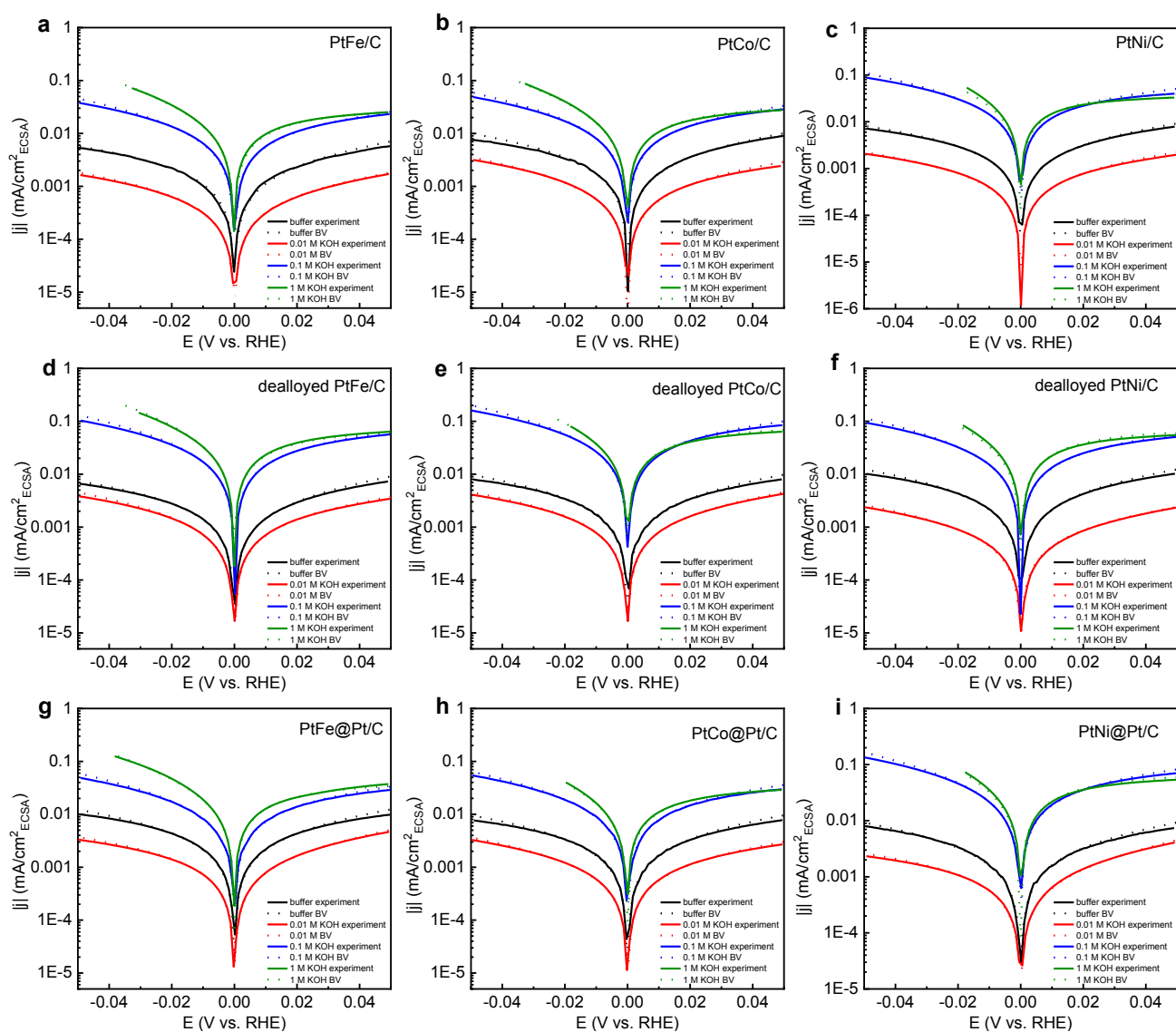
Supplementary Figure 2 XRD spectra of Pt/C, PtNi/C and dealloyed PtCo/C catalysts.



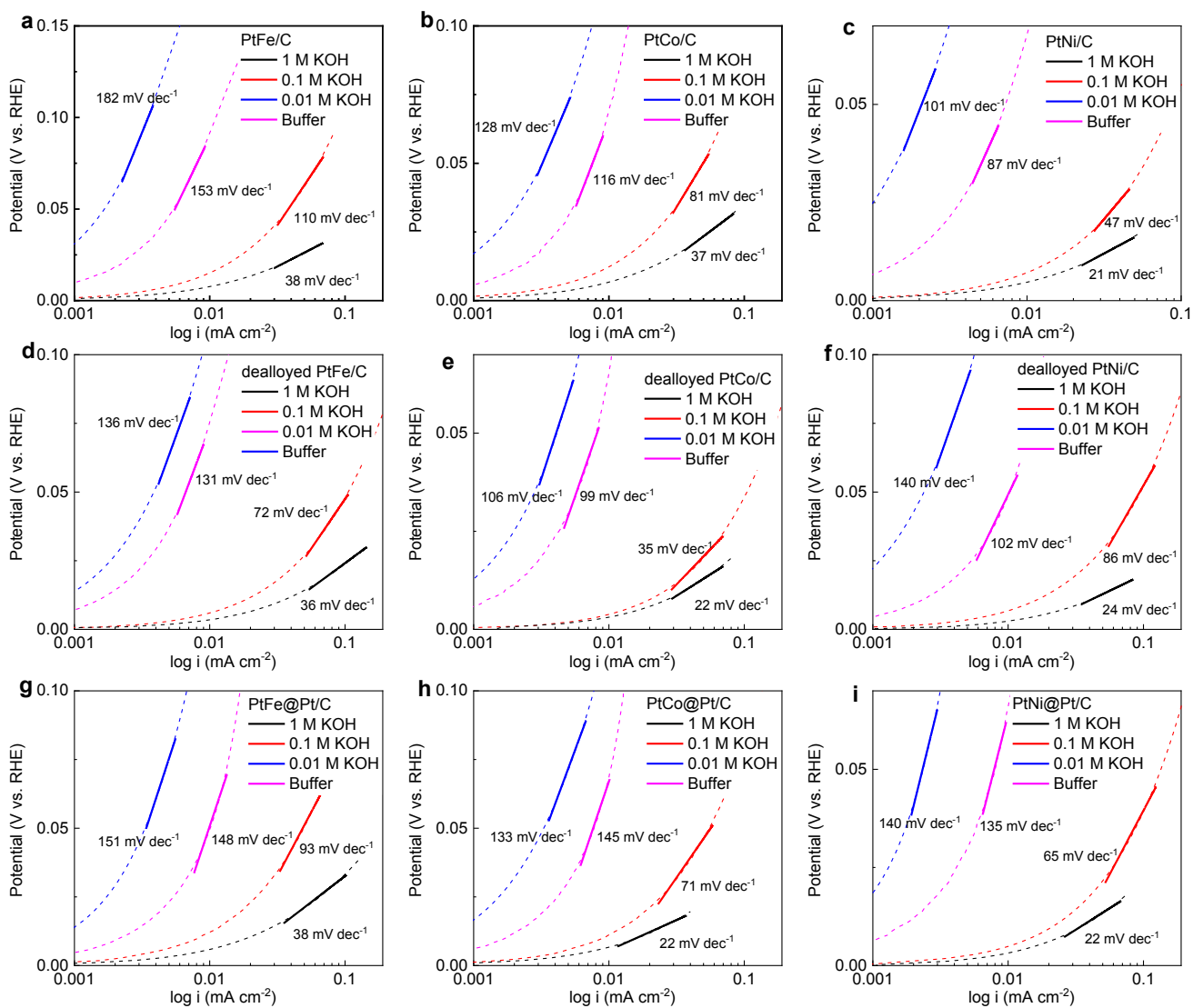
Supplementary Figure 3 The HER activity of the electrocatalysts. **a-b** The HER polarization curves measured for **a** Pt/C; **b** PtNi/C under different LiOH electrolytes. **c-d** The corresponding Butler-Volmer fitting results for **c** Pt/C; **d** PtNi/C under different conditions. **e-f** A comparison of the polarization curves measured for **e** Pt/C; **f** PtNi/C in two different electrolytes for a series of concentrations.



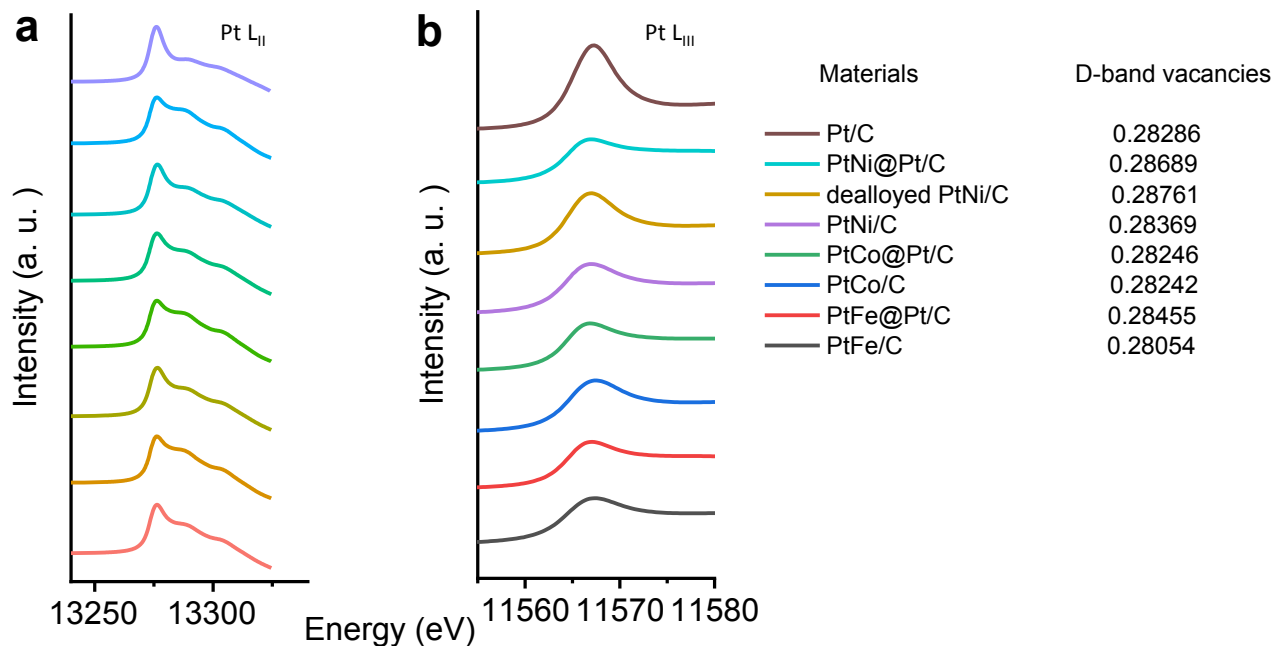
Supplementary Figure 4 The HER/HOR polarization curves obtained for a series of Pt-based nanosized electrocatalysts in different alkaline environments. The electrocatalysts are: **a** PtFe/C; **b** PtCo/C; **c** PtNi/C; **d** dealloyed PtFe/C; **e** dealloyed PtCo/C; **f** dealloyed PtNi/C; **g** PtFe@Pt/C; **h** PtCo@Pt/C; **i** PtNi@Pt/C.



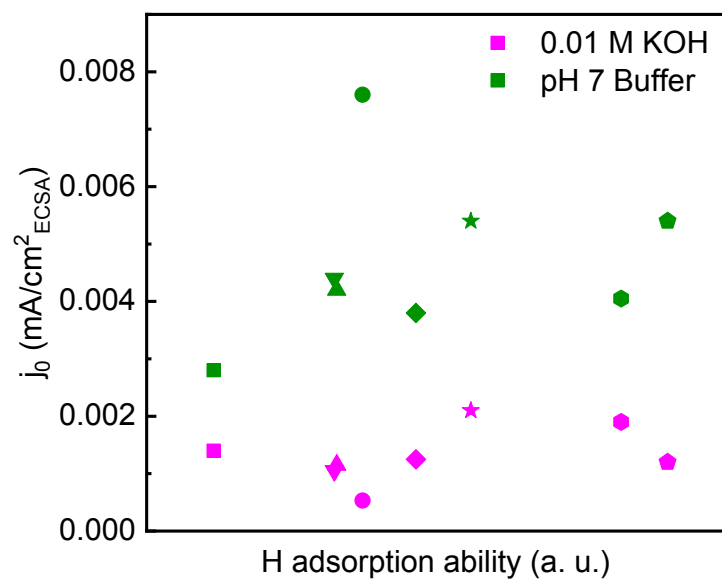
Supplementary Figure 5 The experimental Tafel plots and the corresponding Butler-Volmer fitting data (BV) for a series of Pt-based nanostructured electrocatalysts in different alkaline solutions. The electrocatalysts are: **a** PtFe/C; **b** PtCo/C; **c** PtNi/C; **d** dealloyed PtFe/C; **e** dealloyed PtCo/C; **f** dealloyed PtNi/C; **g** PtFe@Pt/C; **h** PtCo@Pt/C; **i** PtNi@Pt/C.



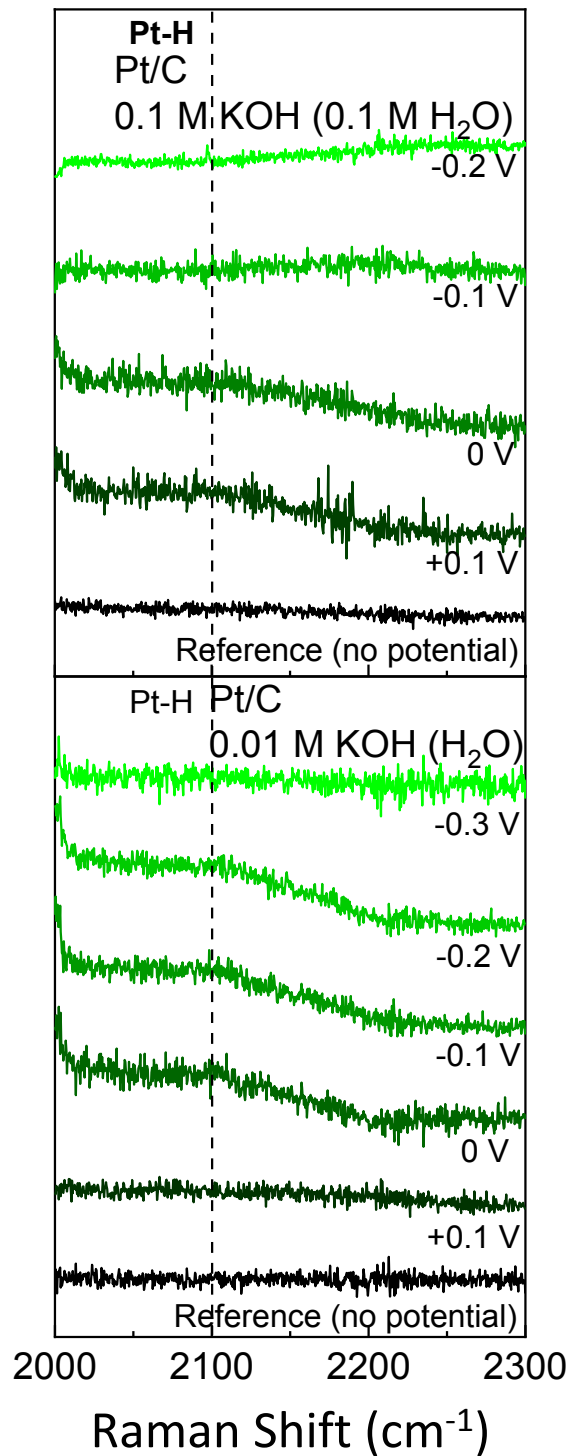
Supplementary Figure 6 Tafel slopes for a series of Pt-based nanostructured electrocatalysts in different alkaline solutions. The electrocatalysts are: **a** PtFe/C; **b** PtCo/C; **c** PtNi/C; **d** dealloyed PtFe/C; **e** dealloyed PtCo/C; **f** dealloyed PtNi/C; **g** PtFe@Pt/C; **h** PtCo@Pt/C; **i** PtNi@Pt/C.



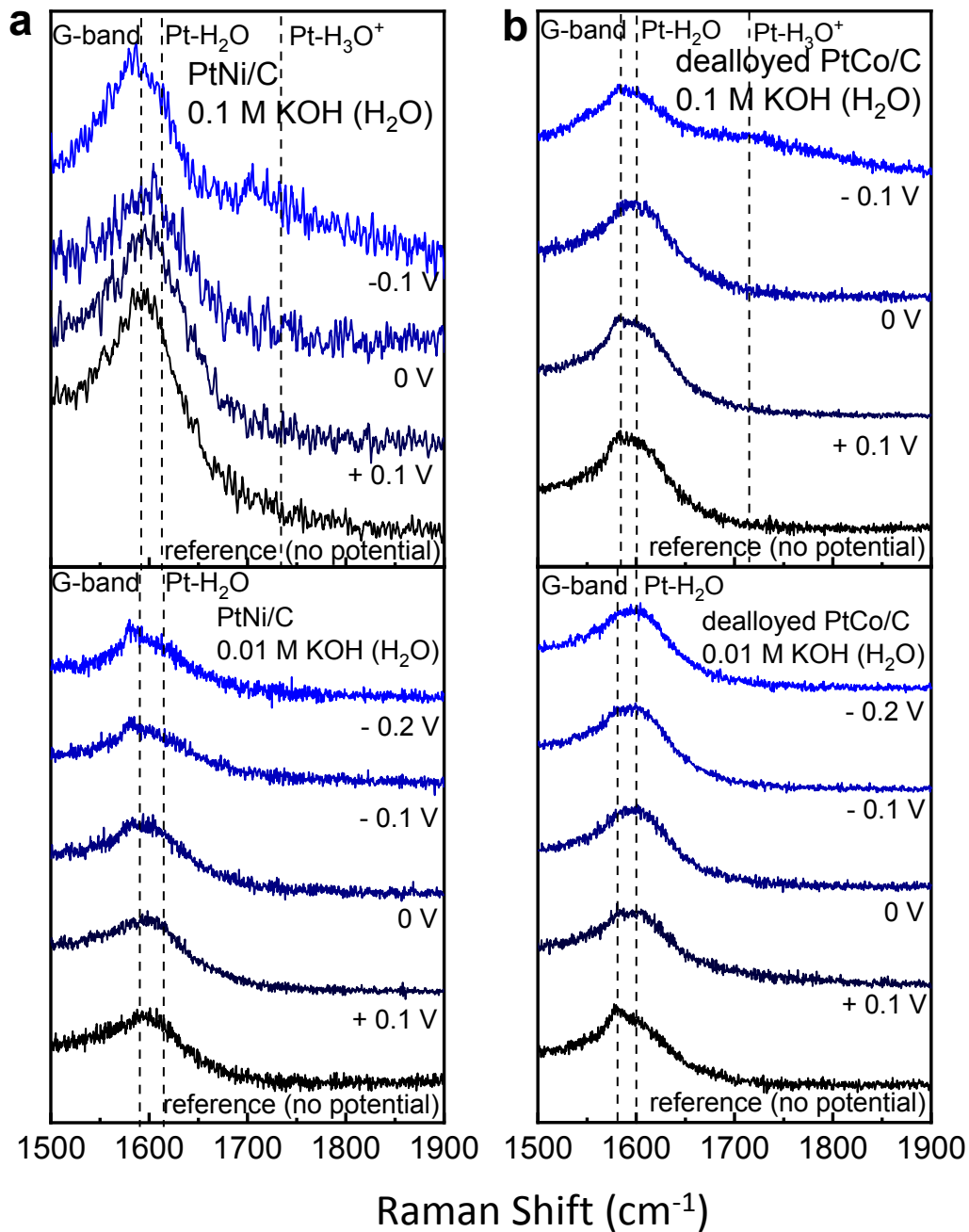
Supplementary Figure 7 The XANES spectra for a series of Pt-based nanosized electrocatalysts. The d-band vacancies were calculated based on the XANES data. **a** Pt L_{II} edge. **b** Pt L_{III} edge.



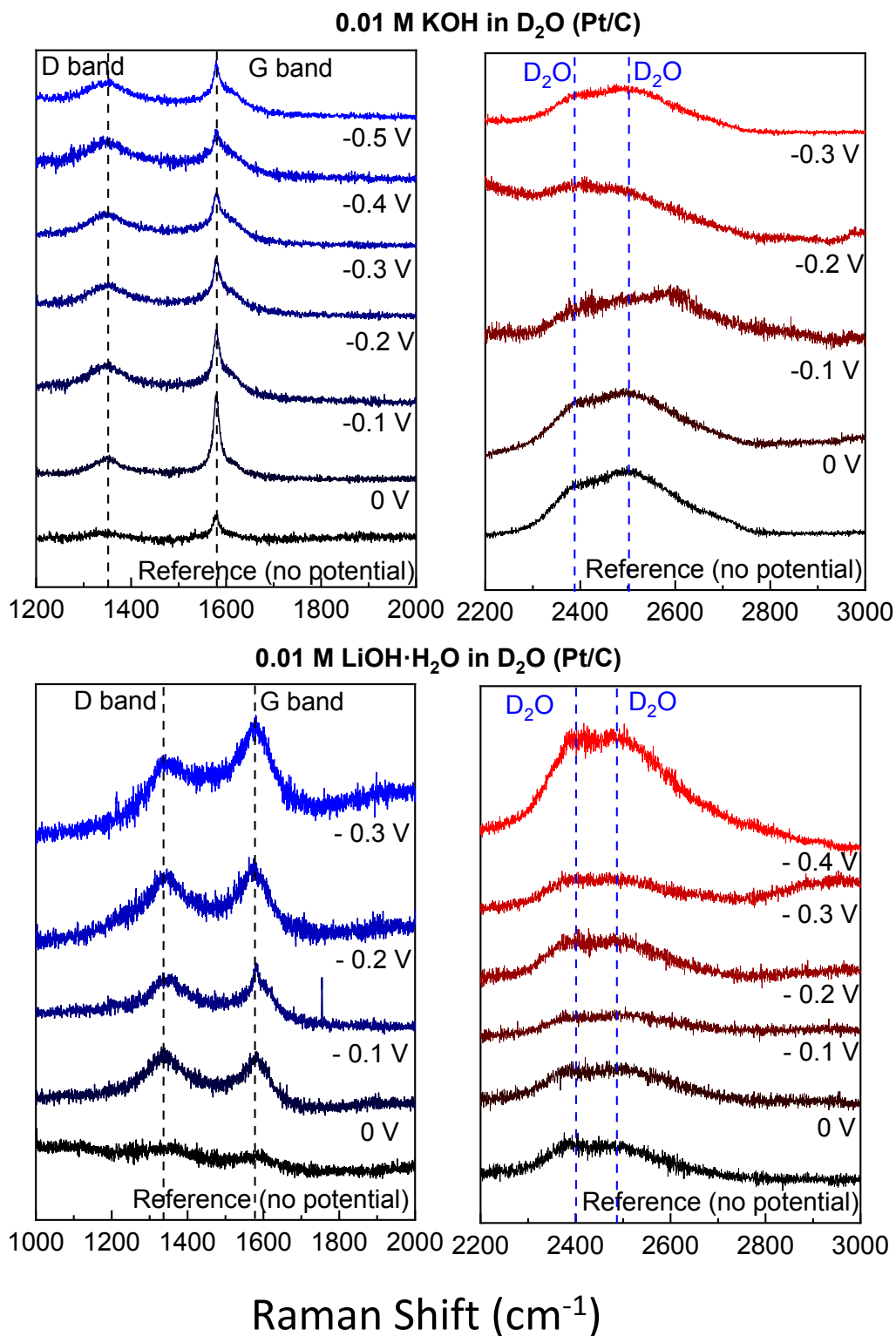
Supplementary Figure 8 The experimentally acquired relationship between the H adsorption ability and the activity (j_0) for a series of Pt based materials using different electrolytes. The H adsorption ability of the electrocatalysts is represented according to the d-band vacancies of each material.



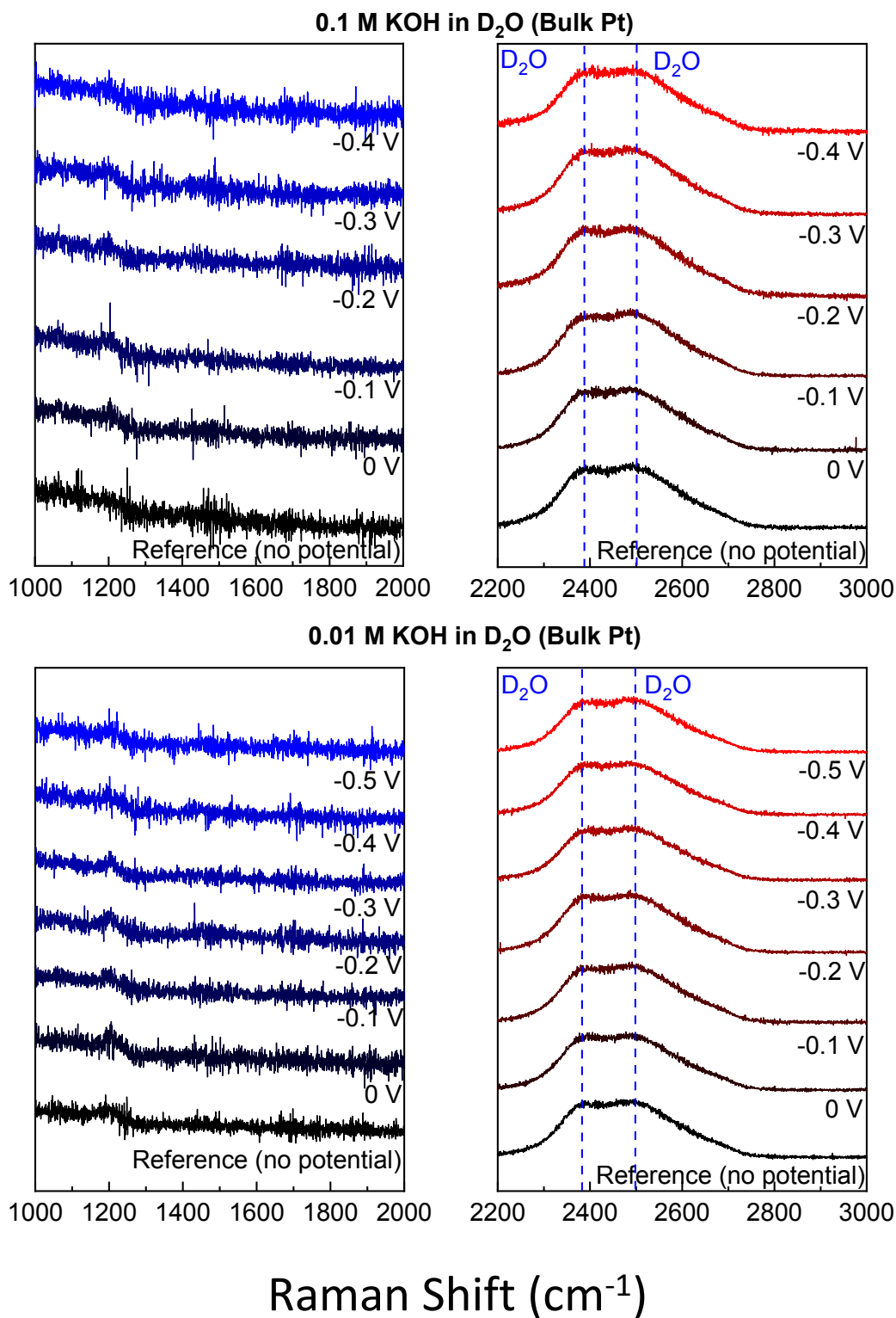
Supplementary Figure 9 Raman signal of Pt/C in different alkaline environments. Raman spectra of Pt/C in 0.1 M (above) and 0.01 M (below) KOH (H₂O) solutions at the Raman shift range of 2000-2300 cm^{-1} .



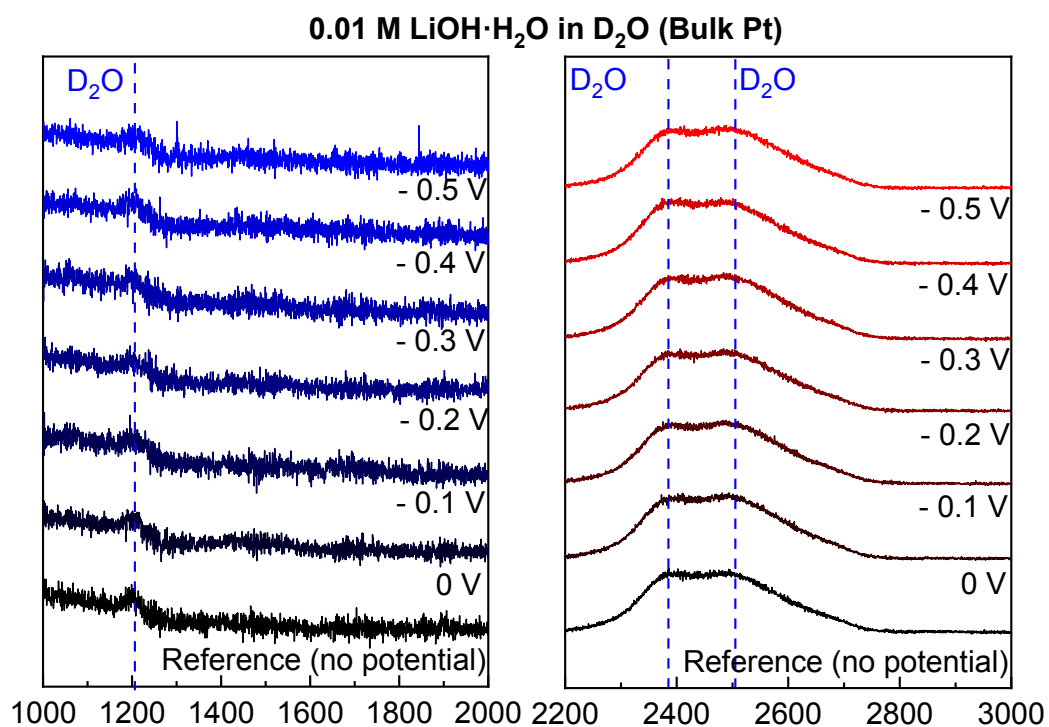
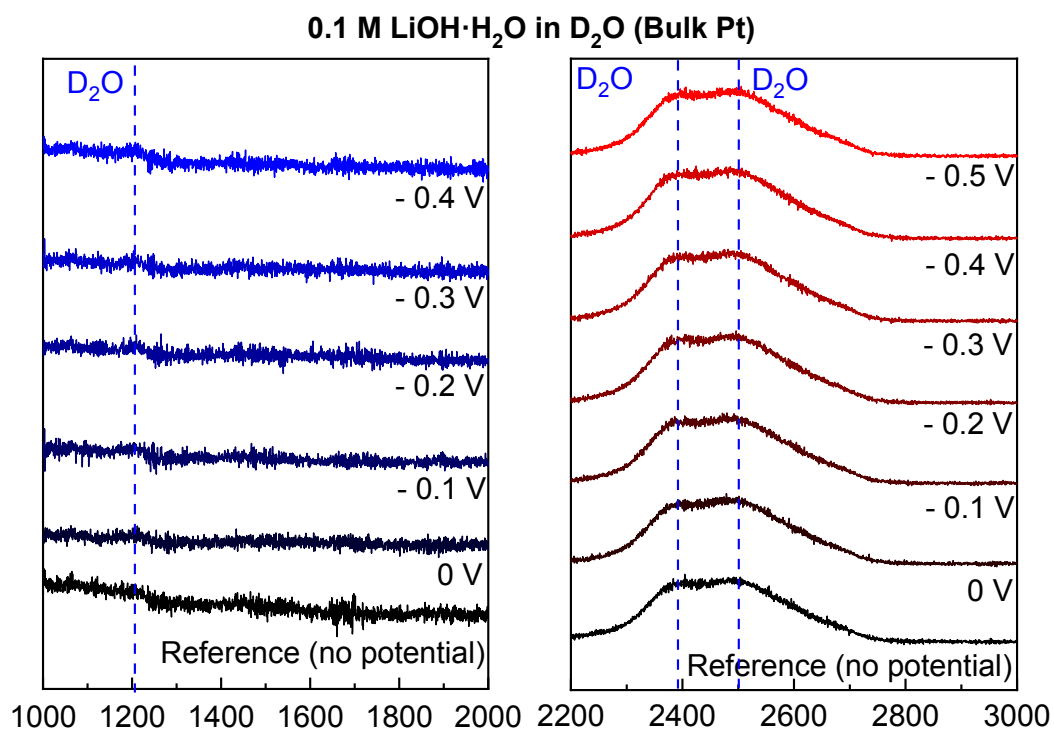
Supplementary Figure 10 Raman signal of different electrocatalysts. Raman spectra of: **a** PtNi/C in 0.1 M (above) and 0.01 M (below) KOH (H₂O), respectively. **b** dealloyed PtCo/C in 0.1 M (above) and 0.01 M (below) KOH, respectively.



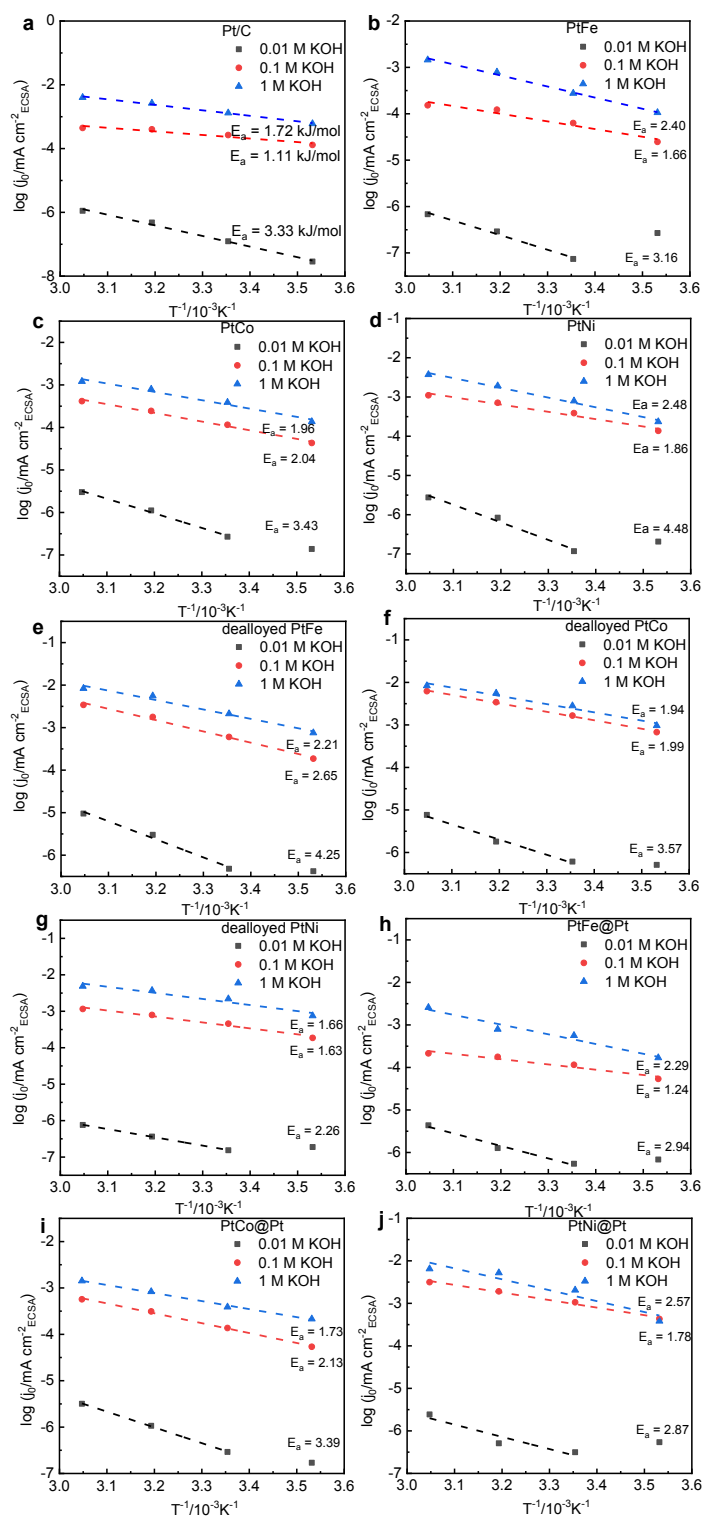
Supplementary Figure 11 Raman spectra of Pt/C in different environments. The electrolytes are 0.01 M KOH (top panels) and 0.01 M LiOH·H₂O (bottom panels) in D₂O solutions, respectively.



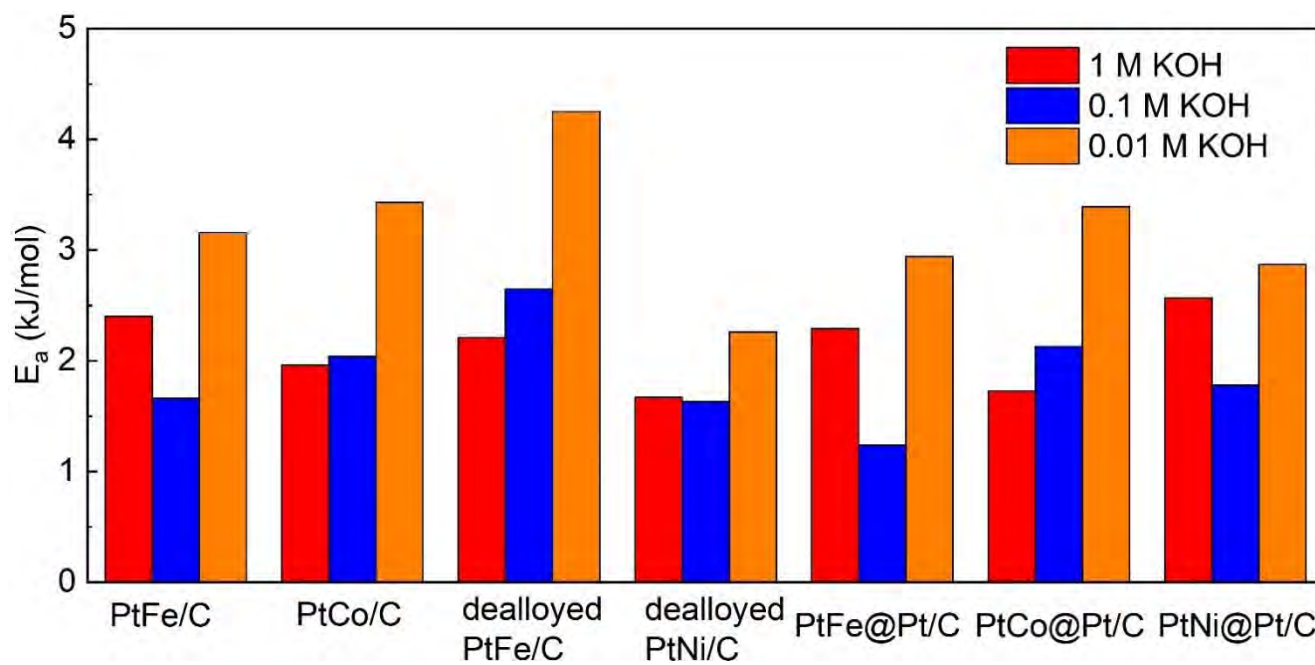
Supplementary Figure 12 Raman spectra of bulk Pt in different environments. The electrolytes are 0.1 M (top panels) and 0.01 M (bottom panels) KOH in D₂O solutions, respectively.



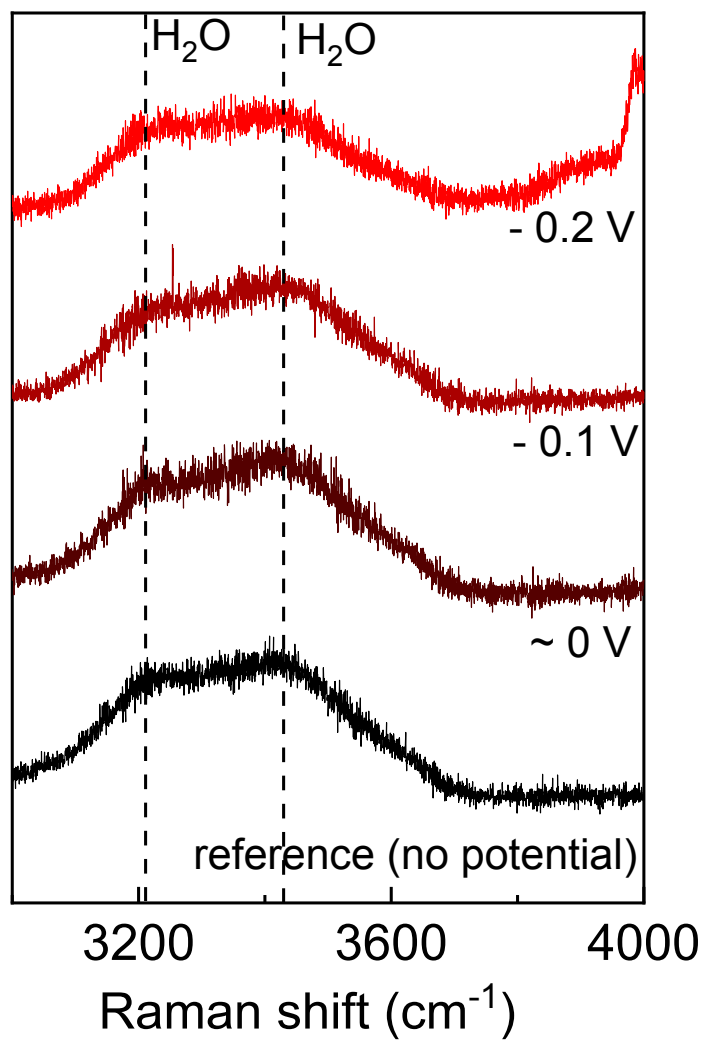
Supplementary Figure 13 Raman spectra of Pt/C in different environments. The electrolytes are 0.1 M (top panels) and 0.01 M (bottom panels) LiOH·H₂O in D₂O solutions, respectively.



Supplementary Figure 14 The activation energy calculated using the relationship between j_0 and temperature in different alkaline environments for a series of Pt-based electrocatalysts. The electrocatalysts are: **a** PtFe/C; **b** PtCo/C; **c** PtNi/C; **d** dealloyed PtFe/C; **e** dealloyed PtCo/C; **f** dealloyed PtNi/C; **g** PtFe@Pt/C; **h** PtCo@Pt/C; **i** PtNi@Pt/C.



Supplementary Figure 15 A comparison of E_a for a series of different Pt-based nanosized electrocatalysts in different alkaline environments.



Supplementary Figure 16 Raman spectra of dealloyed PtCo/C in 0.1 M KOH aqueous solution.

Chapter 4 : Breaking the Volcano-Plot Limits for Pt-based Electrocatalysts by Selective Tuning Adsorption of Multiple Intermediates

4.1 Introduction

In heterogeneous electrocatalysis, the activities of a series of electrocatalysts are closely related to the materials' adsorption affinity toward key reactive intermediates. This relationship is usually represented as a volcano-shaped plot, in which the top of the volcano is the theoretically highest activity achieved by this series of electrocatalysts. Such upper limit of activity is hard to break due to the inherent strong scaling relationship between binding energies among different reactive intermediates. More importantly, this relationship limits the development of new electrocatalysts that could be more active than the conventional benchmarks. Here, using hydrogen evolution reaction (HER) as a model reaction, we propose a simple but feasible strategy that can be used to break the activity limits imposed by volcano plot. For the first time, we proved that by selective tuning the adsorption affinity of electrocatalysts the scaling relationship between the binding energies of *H and *OH in alkaline HER process can be broken, leading to the specific electrocatalysts with activities beyond the limits imposed by volcano plot. The highlights of this work include:

- For the first time, experimental HER volcano plots under different alkaline reaction environments for a series of Pt alloys are reported;
- A new general strategy for breaking the limits imposed by volcano plot is proposed for HER under alkaline conditions;
- Using the aforementioned strategy, the intrinsic activity of newly developed electrocatalysts is twice higher than that of conventional Pt/C benchmark;
- It is proved that the poorly known scaling relationship between the binding energies of *H and *OH can be broken. As a result, the activity of electrocatalysts can be significantly improved.

4.2 Breaking the Volcano-Plot Limits for Pt-based Electrocatalysts by Selective Tuning Adsorption of Multiple Intermediates

This chapter is included as it appears as a journal paper published by Xuesi Wang, Qun He, Li Song, Mietek Jaroniec, Yao Zheng and Shi-Zhang Qiao: Breaking the Volcano-Plot Limits for Pt-based Electrocatalysts by Selective Tuning Adsorption of Multiple Intermediates, *Journal of Material Chemistry A*, **2019**, 7, 13645-13640

Statement of Authorship

Title of Paper	Breaking the volcano-plot limits for Pt-based electrocatalysts by selective tuning adsorption of multiple intermediates
Publication Status	<input checked="" type="checkbox"/> Published <input type="checkbox"/> Accepted for Publication <input type="checkbox"/> Submitted for Publication <input type="checkbox"/> Unpublished and Unsubmitted work written in manuscript style
Publication Details	Wang, X.; He, Q.; Song, L.; Jaroniec, M.; Zheng, Y.; Qiao, S. Breaking the Volcano-Plot Limits for Pt-based Electrocatalysts by Selective Tuning Adsorption of Multiple Intermediates. J. Mater. Chem. A 2019, 7, 13635-13640.

Principal Author

Name of Principal Author (Candidate)	Xuesi Wang		
Contribution to the Paper	This author did all the experiments and wrote the paper.		
Overall percentage (%)	90%		
Certification:	This paper reports on original research I conducted during the period of my Higher Degree by Research candidature and is not subject to any obligations or contractual agreements with a third party that would constrain its inclusion in this thesis. I am the primary author of this paper.		
Signature		Date	1 July 2019

Co-Author Contributions

By signing the Statement of Authorship, each author certifies that:

- the candidate's stated contribution to the publication is accurate (as detailed above);
- permission is granted for the candidate to include the publication in the thesis; and
- the sum of all co-author contributions is equal to 100% less the candidate's stated contribution.

Name of Co-Author	Qun He		
Contribution to the Paper	This author analysed all the XAS data in the paper.		
Signature		Date	1 July 2019

Name of Co-Author	Li Song		
Contribution to the Paper	This author contributed in data analysing.		
Signature		Date	1 July 2019

Name of Co-Author	Mietek Jaroniec		
Contribution to the Paper	This author contributed in paper editing. Digitally signed by Mietek Jaroniec DN: cn=Mietek Jaroniec, o, ou=Kent State, email=jaroniec@kent.edu, c=US Date: 2019.06.11 09:33:36 -04'00'		
Signature		Date	1 July 2019

Name of Co-Author	Yao Zheng		
Contribution to the Paper	This author contributed in providing funding and supervising the project.		
Signature		Date	1 July 2019

Name of Co-Author	Shi-Zhang Qiao		
Contribution to the Paper	This author contributed in providing funding and supervising the project.		
Signature		Date	1 July 2019

Please cut and paste additional co-author panels here as required.

Cite this: *J. Mater. Chem. A*, 2019, 7,
13635

Breaking the volcano-plot limits for Pt-based electrocatalysts by selective tuning adsorption of multiple intermediates†

Xuesi Wang,^a Qun He,^{‡b} Li Song,^b Mietek Jaroniec,^c Yao Zheng^{*a}
and Shi-Zhang Qiao^{*a}

The development of heterogeneous electrocatalysts with enhanced activity as compared to conventional benchmarks is a highly important but challenging task. One of the main reasons is that the performance of current catalysts is limited by a 'volcano plot', which defines the relationship between the activities of a family of catalysts and a series of specific descriptors (e.g., adsorption ability of reaction intermediate(s)). Here, using the alkaline hydrogen evolution reaction as an example, we propose a strategy to break such activity limits. By building up volcano plots for a group of Pt alloys, we found that some "unique" samples did not follow the trend and possessed higher activities beyond the volcano top. Our thermodynamic and kinetic measurements revealed that dealloying can break the poorly known scaling relationship between the binding energies of *H and *OH, and thus, selectively optimize the adsorption properties toward *H and *OH reaction intermediates on Pt surfaces and boost the overall activity. This provides a new insight into the aforementioned activity limits, which can be avoided by regulating the adsorption behaviors of two or more intermediates.

Received 14th March 2019
Accepted 8th May 2019

DOI: 10.1039/c9ta02801c

rsc.li/materials-a

Introduction

The development of new electrocatalysts with enhanced activity has been one of the priorities in materials science for renewable energy.¹ Although various new catalysts have been reported for energy-related electrocatalytic reactions such as the hydrogen evolution reaction (HER), oxygen reduction reaction (ORR), oxygen evolution reaction (OER), *etc.*, their activities did not show significant improvement as compared with those of conventional benchmarks.^{2–9} Through merging theoretical computations and experimental measurements, one is able to establish the activity trend of a group of catalysts with similar properties in a form of the so-called 'volcano plot'.^{10–17} This plot links the activity of a solid catalyst with its thermodynamic adsorption ability toward one or more reactive intermediates.^{14,18–23} More importantly, this volcano-plot-activity relationship has been widely accepted as a powerful guide for the development of new electrocatalysts for a wide range of

electrolysis processes by evaluating their activity and predicting the potential maximum activity (the volcano top).^{2,11,14,19} As the top of a volcano plot always shows the best activity for this family of catalysts, it also sets the activity boundary for the development of related materials.

However, the limits of the volcano plot are hard to break because of the complexity of electrocatalytic processes. In principle, the adsorption affinity of an electrocatalyst toward the reactive intermediate of the rate-determining step (RDS) is always used to determine its activity. However, for most practical reactions, multiple intermediates can influence RDS. In such cases, the adsorption affinity of a catalyst toward different intermediates can significantly affect its overall performance.^{8,24–27} The well-studied typical example is the ORR, where the adsorption energies of catalysts toward *OH, *O and *OOH intermediates are essential for the activity of catalysts. For example, on the Pt surface, a strong binding of *OOH and/or weak binding of *OH can lead to higher activity. However, since both species are attached to the catalysts' surface through O atoms, a linear scaling relationship can be found between the adsorption affinity of *OOH and *OH, which means that the adsorption energy of these intermediates varies in the same way (increase or decrease simultaneously). This leads to the result that the performance of catalysts is strictly limited by the volcano plot. Consequently, the activity of any newly developed catalyst may be very close to the activity at the volcano top, but impossible to go beyond that.¹⁴

^aSchool of Chemical Engineering, The University of Adelaide, Adelaide SA 5005, Australia. E-mail: yao.zheng01@adelaide.edu.au; s.qiao@adelaide.edu.au

^bNational Synchrotron Radiation Laboratory, University of Science and Technology of China, Hefei 230029, China

^cDepartment of Chemistry and Biochemistry, Kent State University, Kent, Ohio 44242, USA

† Electronic supplementary information (ESI) available. See DOI: 10.1039/c9ta02801c

‡ These authors contributed equally.

As indicated above, unless the scaling relationship between the adsorption energies of multiple adsorbates is broken, *e.g.*, one increases while the other one decreases or is unchanged, the volcano relationship still sets the boundary for the development of new catalysts. Such a rule applies to all heterogeneous electrocatalysts. In general, the simplest and most representative reaction to describe this complicated relationship is the HER in alkaline solutions, where the reaction is believed to be strongly determined by the interaction between the electrocatalyst and two adsorbates: $*\text{H}$ and $*\text{OH}$.^{28–34} Specifically, while the H adsorption affinity of a material was proved to be the key criterion to the HER activity and determines the shape of the volcano plot,^{28,31,35} the material's interaction with OH is also crucial for the overall activity.^{27,36–40} To this end, alkaline HER catalysts with optimized OH adsorption sites have been widely designed, such as PtRu and PtNi alloys, and have been proved to be highly active.^{17,41} However, due to the scaling relationship between adsorbed $*\text{H}$ and $*\text{OH}$, the activities of these alloys are still within the limits of the volcano relationship, although their H adsorption affinity is altered by changes in their composition, as evidenced by a shift in the volcano plot.^{20,23,42,43}

Herein, we propose a new strategy to break the limits of the volcano relationship between the adsorption energy and the activity of catalysts for the alkaline HER. First, a volcano-shaped plot determined by the electronic structures (*i.e.*, d-band vacancies) and the apparent HER activities of three different classes of Pt-based materials is constructed. Interestingly, two materials namely dealloyed PtCo and dealloyed PtFe showed unique performance by breaking the limits of the volcano plot. Furthermore, the kinetic analysis indicated that these two materials feature lower activation barriers for water dissociation as compared to their counterparts, which could be traced back to the Pt sites with higher coordination of O species. With these OH-active Pt sites, the dealloyed samples have appropriate interaction with OH species without an obvious effect on the H adsorption energy. Thus, the dealloyed samples are able to represent very high overall HER activity.

Results and discussion

Ten Pt based nanoparticles were prepared to build up the relationship between the H adsorption energy and the electrocatalytic activity. Pt (20 wt% metal on carbon) and three PtM/C (20 wt% metal on carbon, M = Fe, Co, Ni, Pt : M = 1 : 1) samples were used to fabricate bimetallic nanoparticles with different compositions and structures. Starting with PtM, dealloyed PtM samples were obtained by acid leaching and bimetallic samples with Pt skin were prepared by annealing (see the ESI†). The high-angle-annular-dark-field scanning transmission electron microscopy (HAADF-STEM) images of the PtCo series of samples are shown in Fig. 1. The original PtCo alloy consists of 4–7 nm nanoparticles with Pt and Co homogeneously configured into a uniform 1 : 1 metal component (Fig. 1a). As compared to the PtM alloys, the post-processing mainly changed the surface structure of the materials as schematically demonstrated in the inset of Fig. 1. Specifically, the acid-treated

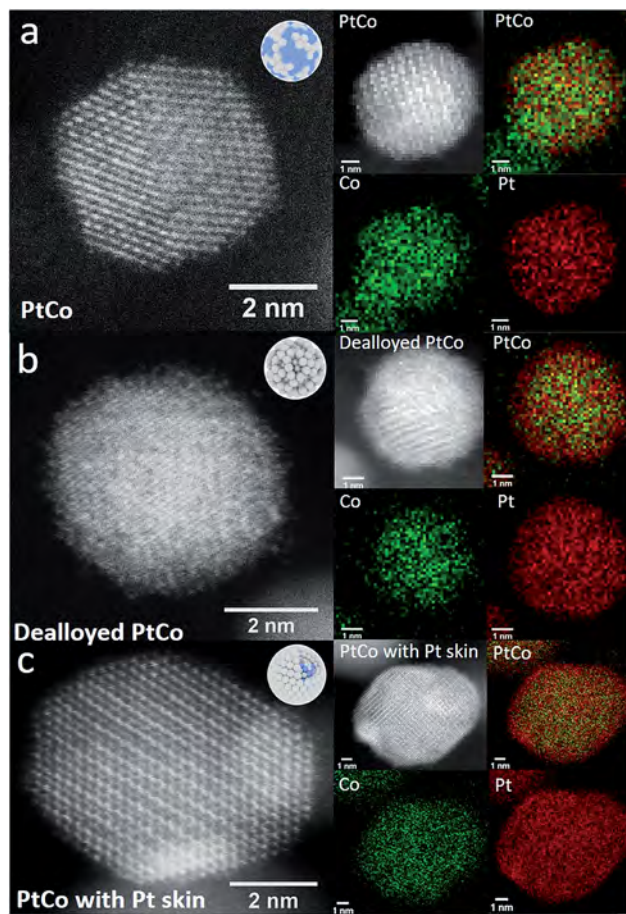


Fig. 1 (a–c) Left column: HAADF-STEM images of several randomly chosen particles. Right column: EDS mapping images of the different bimetallic nanomaterials. Green mapping is for Co while red is for Pt. (a) PtCo alloy sample, (b) dealloyed PtCo sample, and (c) PtCo with Pt skin. Insets show models for the corresponding samples.

dealloyed samples present a defect-rich Pt surface with a trace amount of M metal left (1.56 wt_{metal}% Fe for dealloyed PtFe, 6.4 wt_{metal}% Co for PtCo and 5.7 wt_{metal}% Ni for PtNi according to inductively coupled plasma mass spectra), while the annealed samples show a 2–3 atom thick layer of Pt skin on the surface (Fig. 1b and c). Such surface variability is also clearly visible in the energy dispersive X-ray spectroscopy (EDS) mapping images showing that the dealloyed PtCo has a thick Pt-rich shell decorated by a trace amount of Co element and both Pt and Co are located in the core, while the annealed PtCo has a very thin layer of Pt skin with high compressive strain on the surface of the original PtCo alloy. Similar structural variability can also be observed for the other PtM samples (Fig. S1 and S2†). Such structural differences are also represented in X-ray diffraction (XRD) spectra (Fig. S3†), where peaks of Pt shift toward higher degrees for all the annealed materials compared to dealloyed samples, indicating great differences in the lattice strain between the two kinds of materials. These structural differences not only affect the surface properties of the different bimetallic materials but also influence their electronic bands.

The changes in the electronic structure of these Pt-based bimetallic materials are quantitatively evidenced by X-ray absorption near edge structure (XANES) spectroscopy (Fig. 2). On the Pt L_{III} -edge, a blue shift of the white line (WL) can be observed for all dealloyed PtM samples as compared with the original PtM alloys, indicating a change in the electronic state of Pt sites (Fig. 2a inset, Fig. S4a and b[†]). Such a change in the electronic structure is especially obvious for dealloyed PtCo, where the WL is shifted by 0.6 eV. To quantitatively evaluate this electronic structure diversity, the XANES spectra of the Pt L_{II} -edge were also taken for all the samples (Fig. 2b, S4c and d[†]). Based on both spectra, the Pt's d-band vacancies can be confirmed for all the samples, which has been proved to be closely related to the H adsorption affinity of the Pt surface (e.g., larger d-band vacancy leads to a stronger adsorptive H bond).^{18,23,25,43–47} Therefore, based on the d-band vacancies in the bimetallic materials, their H adsorption affinity can also be quantitatively determined (Fig. 2c and Table S1[†]).

The apparent HER activities of the freshly made samples were recorded in different alkaline solutions and the polarization curves were normalized by the electrocatalytically active surface area (ECSA) to show the intrinsic activity of each active site (see the ESI, Fig. S5–S7 and Table S2[†]).⁴⁸ Typically, in 0.1 M KOH media, the activity of the samples increases in the order of PtM < Pt \leq PtM with Pt skin < dealloyed PtM (Fig. 3a and b). Furthermore, the dealloyed Fe and Co samples clearly feature faster kinetics than the other bimetallic samples according to the Tafel plots fitted by using classic Butler–Volmer equations (Fig. 3c and d). Such a HER activity trend has also been verified in 0.01 M KOH and 1 M KOH solutions (Fig. S8 and S9[†]). As shown in Fig. 3e and f, by normalizing the exchange current density (j_0) of the samples with that of pure Pt, one can see that the dealloyed PtFe (Co) retains its superiority with increasing

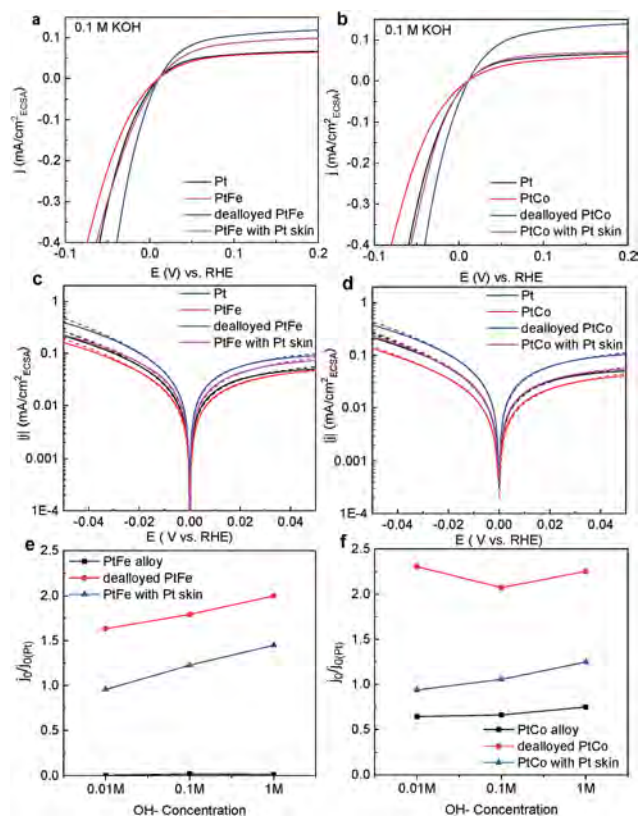


Fig. 3 HER polarization curves of (a) a series of PtFe samples and (b) a series of PtCo samples in 0.1 M KOH solution with (c and d) their corresponding Tafel plots. The dotted lines indicate Butler–Volmer fitting results. (e and f) A comparison of the j_0 specific value for a series of PtFe samples and a series of PtCo samples in different solutions.

OH[−] concentration. Interestingly, many reports show that the introduced M metal sites in the PtM alloys can provide better OH adsorption sites and thus promote water dissociation capacity in alkaline HER processes.^{29,30,36} However, this study shows that when OH[−] concentration increases the dealloyed materials with a smaller number of surface transition metal sites have higher activities than the PtM alloys. This unusual phenomenon indicates that other factors may promote the critical water dissociation process, which was not reported before.

To represent the relationship between the adsorption affinities of the materials and their HER activities, the volcano plot for all the samples was constructed, where d-band vacancies were used to scale the H adsorption affinity and j_0 values were used to represent the apparent HER activity (Fig. 4a and b). It is obvious that the majority of tested materials follow the volcano trend, indicating that H adsorption is still the dominating descriptor for the HER activity, even in strong alkaline media. The activity of PtNi with thin Pt skin is located at the top of the volcano plot (0.1 M KOH), indicating that its best HER performance is due to the appropriate adsorption affinity toward the H intermediate.⁴⁹ Obviously, the dealloyed PtFe (Co) does not follow the activity trend scaled by H adsorption affinity and even shows higher activity than PtNi with Pt skin. Similar

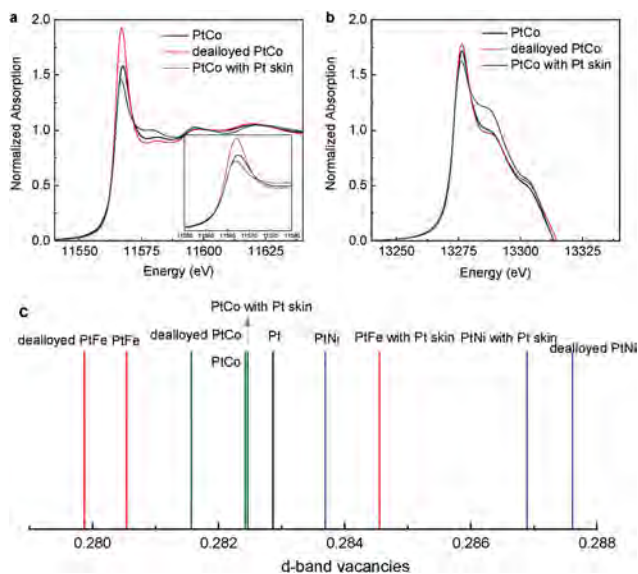


Fig. 2 XANES spectra of the (a) Pt L_{III} -edge and (b) Pt L_{II} -edge of a series of PtCo samples. Detailed WL shifting spectra are shown in the inset of panel (a). (c) The distribution of d-band vacancies in different Pt-based samples calculated by using the XANES spectra.

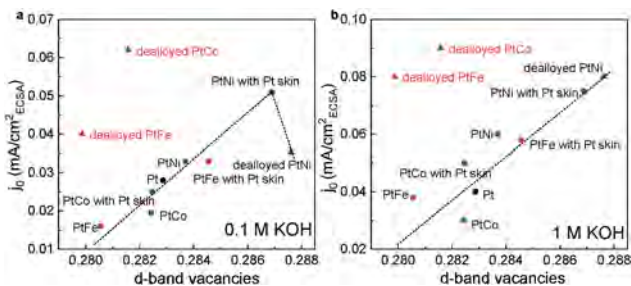


Fig. 4 (a and b) The experimentally acquired relationship between the d-band vacancies and j_0 for a series of Pt based materials in (a) 0.1 M KOH and (b) 1 M KOH solutions. The activities of dealloyed PtCo(Fe) samples (labelled in red) are beyond the limits of volcano plots.

phenomena in volcano relationships have also been observed in 1 M (Fig. 4b) and 0.5 M (Fig. S10 and S11[†]) KOH environments. Considering that the H adsorption affinity does not show the most appropriate location on the volcano plot, other factors besides H adsorption on these two samples should be taken into account.

It is known that the H intermediates in the alkaline HER originate from the water dissociation process, and therefore, we proposed that the barrier of water dissociation, which can also be considered as the energy barrier for the overall HER, may play a dominant role in determining the apparent activities of dealloyed PtFe (Co) samples. A series of kinetic analyses were carried out to calculate the activation energy (E_a) of the HER on each sample, which can provide a quantitative evaluation toward the HER energy barrier. Here, using the Co groups of bimetallic materials as examples, the values of E_a were calculated according to the Arrhenius equation from the HER

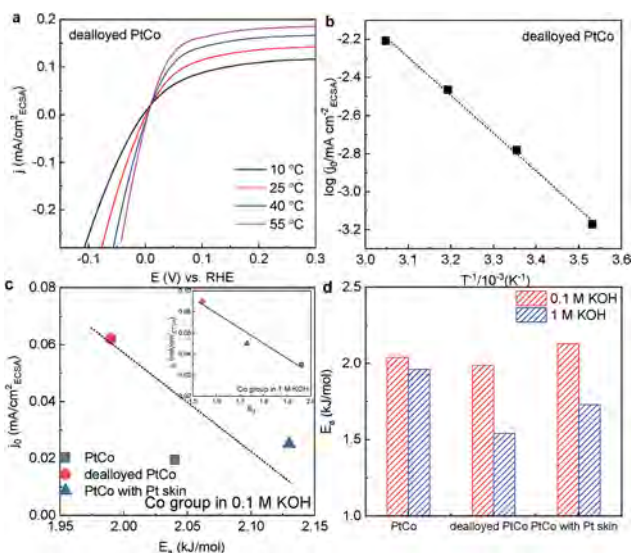


Fig. 5 (a) The HER polarization curves of the dealloyed PtCo sample at different temperatures in 0.1 M KOH solutions. (b) The relationship between j_0 and temperature for dealloyed PtCo in 0.1 M KOH. (c) The relationship between E_a and j_0 in 0.1 M KOH and 1 M KOH solutions (inset). (d) E_a values under different conditions for a series of PtCo materials.

polarization curves (Fig. 5a and b, S12–S17[†]).⁵⁰ Based on the linear trend between E_a and j_0 values, one can see that the energy barrier of the alkaline HER indeed plays an important role in promoting the overall activity of a catalyst (Fig. 5c and inset). For example, the lower energy barrier of the dealloyed PtCo indeed leads to its higher activity as compared to the counterpart. Additionally, as the concentration of OH increased from 0.1 to 1 M, the E_a of the dealloyed PtCo dropped from 1.99 kJ mol⁻¹ to 1.54 kJ mol⁻¹, much more than that in the case of the counterpart (Fig. 5d). This indicates that the interaction between the dealloyed PtCo surface and OH species in the electrolyte may be the key in determining the energy barrier of the HER.

To validate the importance of OH interaction with the dealloyed PtCo surface toward breaking the volcano plot limits, a series of cyclic voltammograms (CVs) were recorded (Fig. 6a). Although the H adsorption signals (the peaks at ~0.25 V in the red zone) do not change for different PtCo samples, the OH desorption/adsorption signals (the peaks at 0.7–0.85 V in the green zone) are obviously different. More specifically, the OH adsorption peak on the dealloyed PtCo sample is shifted to higher potentials as compared to the other Co-containing samples, indicating that this OH adsorption peak does not originate from Co sites but from Pt sites. A similar outcome can also be observed on the PtFe samples (Fig. S18[†]). This finding is also confirmed by the carbon monoxide (CO) stripping voltammogram, where the CO oxidation potential is used to evaluate the OH adsorption affinity of the material. As shown in

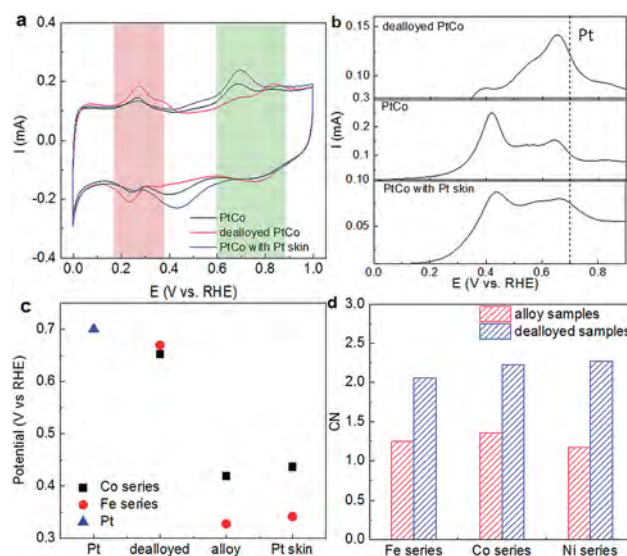


Fig. 6 (a) CVs of a series of PtCo materials in 0.1 M KOH solution. The H adsorption/desorption zone is marked by a pink rectangle and the OH adsorption/desorption zone is marked by a green rectangle. (b) CO stripping of PtCo materials in 0.1 M KOH solution. The dotted line marks the position of Pt's CO stripping peak. A high CO oxidation potential indicates low OH adsorption ability of the material and vice versa. An appropriate OH adsorption ability (neither too strong nor too weak) is most promotive toward good catalytic performance. (c) The CO adsorption distribution on PtFe and PtCo materials. (d) A comparison of CN for alloy and dealloyed samples.

Fig. 6b and S18a,† the PtM alloy samples and the samples with Pt skin show strong CO oxidation peaks in the lower potential zones, which could be attributed to the OH interaction with 'M' metal sites. The dealloyed samples feature only a single Pt–OH interaction peak in a relatively higher potential zone. By comparing the OH adsorption affinity of different samples with that of the Pt/C standard, all alloyed and dealloyed samples show different OH adsorption affinities of Pt sites (Fig. 6c). Thus, it is clear that the intrinsic OH adsorption of Pt has been changed. Interestingly, contrary to the commonsense, it seems that improving OH adsorption by introducing a second metal as a water dissociation site cannot directly lead to higher HER activity nor a lower energy barrier. Instead, changing the OH adsorption affinity of Pt itself affects directly the material's activity. A detailed analysis of Fig. 6a–c shows that the dealloying process improves OH interaction with Pt without noticeable influence on the H adsorption affinity of the materials studied. This indicates that the scaling relationship between the binding energy of *H and *OH can be broken, and it is possible to individually tune the H and OH adsorption affinities of a catalyst. In the current case, changing the OH adsorption affinity of materials may be related to the higher Pt–O coordination number (CN) of the dealloyed samples, which has been proved by extended X-ray absorption fine structure (EXAFS) spectroscopy (Fig. 6d, S19–S21 and Table S3†). Namely, after the dealloying process, the Pt sites are more active toward O species, which is likely to be the reason for the favorable Pt–OH interaction. Noticeably, although the interaction between the catalysts and OH* has played a critical role in determining the performance of a material, it can't be used as a direct parameter to evaluate the overall activity of the catalysts (Fig. S22†). For the majority of catalysts, the hydrogen adsorption ability is still the most important factor in determining the HER activity in highly concentrated alkaline environments. The interaction between OH intermediates and catalysts may significantly alter the activity of materials but is not as a determining factor. To get the ultimate activity of the catalysts, the influence of both intermediates (H and OH) are needed to be taken into consideration.

Conclusions

In this work, based on the example of the HER in alkaline solutions, we demonstrated that the strategy of creating highly active electrocatalysts could result in breaking the limits imposed by the volcano-shape plot. Using this strategy, we can create Pt sites with higher interaction affinity toward OH species, while their H adsorption affinity is not changed. As a result, these samples possess a very low energy barrier for water dissociation and present high overall activity beyond the limits imposed by the volcano plot. Instead of the commonsense that the oxophilic metal sites in bimetallic materials are beneficial to the overall HER activity, we proved that the enhanced HER kinetics on the dealloyed Pt materials is more likely due to the improved OH interaction with Pt itself. Therefore, we found an alternative method to create new Pt sites with modulated adsorption properties for two critical reaction

intermediates. Such a strategy proved that the possible *H and *OH scaling relationship can be broken, and consequently, the selective control of adsorption of each intermediate can be used to boost the overall activity of an electrocatalyst beyond the volcano plot limits. The above strategy offers an inspiration to break the activity limits for other electrocatalytic reactions, such as the carbon dioxide reduction reaction, whose activities are limited by the adsorption of two or more competitive intermediates.

Conflicts of interest

There are no conflicts to declare.

Acknowledgements

We gratefully acknowledge the Australian Synchrotron for X-ray absorption spectroscopy characterization for providing the XANES data. Y. Zheng and S. Z. Qiao acknowledge financial support from the Australian Research Council through Discovery and Linkage Project programs (DP160104866, DP170104464, LP160100927, DE160101163 and FL170100154).

References

- 1 M. K. Debe, *Nature*, 2012, **486**, 43–51.
- 2 Y. Jiao, Y. Zheng, M. Jaroniec and S. Z. Qiao, *Chem. Soc. Rev.*, 2015, **44**, 2060–2086.
- 3 X. Liu and L. Dai, *Nat. Rev. Mater.*, 2016, **1**, 16064.
- 4 B. Hinnemann, P. G. Moses, J. Bonde, K. P. Jørgensen, J. H. Nielsen, S. Horch, I. Chorkendorff and J. K. Nørskov, *J. Am. Chem. Soc.*, 2005, **127**, 5308–5309.
- 5 H. Jin, C. Guo, X. Liu, J. Liu, A. Vasileff, Y. Jiao, Y. Zheng and S.-Z. Qiao, *Chem. Rev.*, 2018, **118**, 6337–6408.
- 6 L. Dai, Y. Xue, L. Qu, H.-J. Choi and J.-B. Baek, *Chem. Rev.*, 2015, **115**, 4823–4892.
- 7 P. Xiao, W. Chen and X. Wang, *Adv. Energy Mater.*, 2015, **5**, 1500985.
- 8 A. Vasileff, C. Xu, Y. Jiao, Y. Zheng and S.-Z. Qiao, *Chem*, 2018, **4**, 1809–1831.
- 9 M. S. Burke, L. J. Enman, A. S. Batchellor, S. Zou and S. W. Boettcher, *Chem. Mater.*, 2015, **27**, 7549–7558.
- 10 M. Shao, Q. Chang, J.-P. Dodelet and R. Chenitz, *Chem. Rev.*, 2016, **116**, 3594–3657.
- 11 S. Anantharaj, S. R. Ede, K. Sakthikumar, K. Karthick, S. Mishra and S. Kundu, *ACS Catal.*, 2016, **6**, 8069–8097.
- 12 X. Zou and Y. Zhang, *Chem. Soc. Rev.*, 2015, **44**, 5148–5180.
- 13 M. Tahir, L. Pan, F. Idrees, X. Zhang, L. Wang, J.-J. Zou and Z. L. Wang, *Nano Energy*, 2017, **37**, 136–157.
- 14 A. Kulkarni, S. Siahrostami, A. Patel and J. K. Nørskov, *Chem. Rev.*, 2018, **118**, 2302–2312.
- 15 E. S. Davydova, S. Mukerjee, F. Jaouen and D. R. Dekel, *ACS Catal.*, 2018, **8**, 6665–6690.
- 16 M. Luo, Y. Yang, Y. Sun, Y. Qin, C. Li, Y. Li, M. Li, S. Zhang, D. Su and S. Guo, *Mater. Today*, 2018, **23**, 45–56.

- 17 C. Chen, Y. Kang, Z. Huo, Z. Zhu, W. Huang, H. L. Xin, J. D. Snyder, D. Li, J. A. Herron and M. Mavrikakis, *Science*, 2014, **343**, 1339–1343.
- 18 J. K. Nørskov, T. Bligaard, A. Logadottir, J. R. Kitchin, J. G. Chen, S. Pandelov and U. Stimming, *J. Electrochem. Soc.*, 2005, **152**, J23–J26.
- 19 Y. Zheng, Y. Jiao and S. Z. Qiao, *Adv. Mater.*, 2015, **27**, 5372–5378.
- 20 J. R. Kitchin, J. K. Nørskov, M. A. Barteau and J. G. Chen, *Phys. Rev. Lett.*, 2004, **93**, 156801.
- 21 J. K. Nørskov, T. Bligaard, J. Rossmeisl and C. H. Christensen, *Nat. Chem.*, 2009, **1**, 37.
- 22 M. Luo and S. Guo, *Nat. Rev. Mater.*, 2017, **2**, 17059.
- 23 J. Greeley, J. K. Nørskov, L. A. Kibler, A. M. El-Aziz and D. M. Kolb, *ChemPhysChem*, 2006, **7**, 1032–1035.
- 24 Y. Yang, M. Luo, W. Zhang, Y. Sun, X. Chen and S. Guo, *Chem*, 2018, **9**, 2054–2083.
- 25 N. Ramaswamy, S. Ghoshal, M. K. Bates, Q. Jia, J. Li and S. Mukerjee, *Nano Energy*, 2017, **41**, 765–771.
- 26 I. Ledezma-Yanez, W. D. Z. Wallace, P. Sebastián-Pascual, V. Climent, J. M. Feliu and M. T. M. Koper, *Nat. Energy*, 2017, **2**, 17031.
- 27 T. Cheng, L. Wang, B. V. Merinov and W. A. Goddard, *J. Am. Chem. Soc.*, 2018, **140**, 7787–7790.
- 28 W. Sheng, M. Myint, J. G. Chen and Y. Yan, *Energy Environ. Sci.*, 2013, **6**, 1509–1512.
- 29 R. Subbaraman, D. Tripkovic, K. C. Chang, D. Strmcnik, A. P. Paulikas, P. Hirunsit, M. Chan, J. Greeley, V. Stamenkovic and N. M. Markovic, *Nat. Mater.*, 2012, **11**, 550–557.
- 30 D. Strmcnik, M. Uchimura, C. Wang, R. Subbaraman, N. Danilovic, D. van der Vliet, A. P. Paulikas, V. R. Stamenkovic and N. M. Markovic, *Nat. Chem.*, 2013, **5**, 300–306.
- 31 W. Sheng, Z. Zhuang, M. Gao, J. Zheng, J. G. Chen and Y. Yan, *Nat. Commun.*, 2015, **6**, 5848.
- 32 D. Strmcnik, P. P. Lopes, B. Genorio, V. R. Stamenkovic and N. M. Markovic, *Nano Energy*, 2016, **29**, 29–36.
- 33 L. Rebollar, S. Intikhab, J. D. Snyder and M. H. Tang, *J. Electrochem. Soc.*, 2018, **165**, J3209–J3221.
- 34 X. Tian, P. Zhao and W. Sheng, *Adv. Mater.*, 2019, DOI: 10.1002/adma.201808066.
- 35 J. Zheng, W. Sheng, Z. Zhuang, B. Xu and Y. Yan, *Sci. Adv.*, 2016, **2**, e1501602.
- 36 R. Subbaraman, D. Tripkovic, D. Strmcnik, K. C. Chang, M. Uchimura, A. P. Paulikas, V. Stamenkovic and N. M. Markovic, *Science*, 2011, **334**, 1256–1260.
- 37 V. R. Stamenkovic, D. Strmcnik, P. P. Lopes and N. M. Markovic, *Nat. Mater.*, 2016, **16**, 57–69.
- 38 Y. Zheng, Y. Jiao, Y. Zhu, L. H. Li, Y. Han, Y. Chen, M. Jaroniec and S.-Z. Qiao, *J. Am. Chem. Soc.*, 2016, **138**, 16174–16181.
- 39 J. Durst, A. Siebel, C. Simon, F. Hasché, J. Herranz and H. A. Gasteiger, *Energy Environ. Sci.*, 2014, **7**, 2255–2260.
- 40 E. Liu, J. Li, L. Jiao, H. T. T. Doan, Z. Liu, Z. Zhao, Y. Huang, K. M. Abraham, S. Mukerjee and Q. Jia, *J. Am. Chem. Soc.*, 2019, **141**, 3232–3239.
- 41 X. Wang, Y. Zhu, A. Vasileff, Y. Jiao, S. Chen, L. Song, B. Zheng, Y. Zheng and S.-Z. Qiao, *ACS Energy Lett.*, 2018, **3**, 1198–1204.
- 42 Y. Wang, G. Wang, G. Li, B. Huang, J. Pan, Q. Liu, J. Han, L. Xiao, J. Lu and L. Zhuang, *Energy Environ. Sci.*, 2015, **8**, 177–181.
- 43 T. Bligaard and J. K. Nørskov, *Electrochim. Acta*, 2007, **52**, 5512–5516.
- 44 S. Mukerjee, S. Srinivasan, M. P. Soriaga and J. McBreen, *J. Electrochem. Soc.*, 1995, **142**, 1409–1422.
- 45 Y. Zheng, Y. Jiao, A. Vasileff and S. Qiao, *Angew. Chem., Int. Ed. Engl.*, 2017, **57**, 7568–7579.
- 46 J. Greeley and M. Mavrikakis, *Nat. Mater.*, 2004, **3**, 810–815.
- 47 S. J. Yoo, H. Y. Park, T. Y. Jeon, I. S. Park, Y. H. Cho and Y. E. Sung, *Angew. Chem.*, 2008, **120**, 9447–9450.
- 48 S. Rudi, C. Cui, L. Gan and P. Strasser, *Electrocatalysis*, 2014, **5**, 408–418.
- 49 S. Lu and Z. Zhuang, *J. Am. Chem. Soc.*, 2017, **139**, 5156–5163.
- 50 N. Marković, B. Grgur and P. N. Ross, *J. Phys. Chem. B*, 1997, **101**, 5405–5413.

Supporting Information

Breaking the Volcano-Plot Limits for Pt-based Electrocatalysts by Selective Tuning Adsorption of Multiple Intermediates

Xuesi Wang,^{a‡} Qun He,^{b‡} Li Song,^b Mietek Jaroniec,^c Yao Zheng^{a,*} and Shi-Zhang Qiao^{a,*}

^a School of Chemical Engineering, The University of Adelaide, Adelaide SA 5005, Australia

^b National Synchrotron Radiation Laboratory, University of Science and Technology of China, Hefei
230029, China

^c Department of Chemistry and Biochemistry, Kent State University, Kent, Ohio 44242, United States

E-mail: s.qiao@adelaide.edu.au; yao.zheng01@adelaide.edu

Experimental Section

Chemicals and materials. Commercialized Pt/C (20 wt.%), PtM/C (20 wt.%, M = Fe, Co, Ni) were purchased from FuelCellStore without further treatment. All the other chemicals used in the experiments were purchased from Sigma-Aldrich Co. LLC.

Fabrication of electrocatalysts. The acid-treated PtM/C samples were fabricated by mixing 10 mg of PtM/C with 30 mL of HClO₄ solution (0.1 M) followed by overnight stirring. The products were then washed several times with deionized water and freeze-dried. The annealed PtM/C samples were fabricated by annealing 10 mg of PtM/C under 900 °C for 5 hours in H₂/Ar (H₂=5 vol.%) atmosphere.

Characterization of materials. Scanning transmission electron microscopy (STEM) images were collected on a Titan G2 80-200 Field-Emission-Gun electron microscope. The Pt L₃ edge X-ray adsorption fine structure (XAFS) spectra of various Pt-based alloys were recorded in transmission mode (Si 111) under mode 2 (8.5 - 18.5 keV) at the Australian Synchrotron. The data were normalized and analyzed using Athena and Artemis. The composition of the dealloyed samples are measured by an Agilent 7900x inductively coupled plasma mass spectrometer (ICP-MS).

The d-band vacancies calculation. The d-band vacancies of Pt in all the alloys and Pt/C samples were calculated using the following equation:

$$(h_j)_{total, sample} = (1 + f_d)(h_j)_{total, reference}$$

where h_j refers to the total number of unoccupied d-states for Pt. The h_j for standard Pt foil reference has been evaluated to be 0.3, and f_d is:

$$f_d = (\Delta A_3 + 1.11\Delta A_2)/(A_{3r} + 1.11A_{2r})$$

where ΔA is:

$$\Delta A = A_s - A_r$$

The term A represents the areas under XANES adsorption edge. The number refers to the L₂ or L₃ absorption edge, 'r' refers to reference material, and 's' refers to the sample.

Electrochemical testing setup. All the electrochemical data were recorded on a CHI 760E bipotentiostat (CH Instruments, INC.). The powdered electrocatalysts were dispersed in distilled water containing 0.05 wt.% of Nafion to form a 2.0 mg/mL homogeneous ink gel. The working electrode was prepared by adding 20 μ L of the ink gel onto the glassy carbon rotating disk electrode (RDE, surface area of the glassy carbon = 0.196 cm², Pine Research Instrumentation) and dried at room temperature. The reference electrode was an Ag/AgCl in 4 M KCl solution. The counter electrode was a pure gold wire. All the potentials were referenced to reversible hydrogen electrode (RHE) by using pure hydrogen calibration and all polarization curves were iR corrected. A flow of Argon was maintained over all the cyclic voltammograms (CVs) tests, while a flow of H₂ was purged during obtaining all the polarization curves. During all the tests, the working electrode was rotated at 1600 rpm. A special cell with water jacket from Pine Research Instrumentation was used for all the tests to achieve controllable temperature.

Exchange current density. The kinetic current densities are worked out through the equation:

$$\frac{1}{j} = \frac{1}{j_k} + \frac{1}{j_d} \#$$

where j , j_k and j_d are the measured current, kinetic current and diffusion limit current, respectively. The HER current is commonly considered not limited by H⁺ transport, therefore, the diffusion current is not counted into the calculation. The j_0 of HER was obtained by fitting j_k into the Butler-Volmer equation:

$$j_k = j_0 \left[\exp\left(\frac{\alpha F \eta}{RT}\right) - \exp\left(\frac{(\alpha - 1) F \eta}{RT}\right) \right] \#$$

where α is the transfer coefficient, η is the overpotential, F is Faraday's constant, R is the universal gas constant and T is the thermodynamic temperature.

ECSA calculation. The ECSA could be calculated using the function below:

$$ECSA \left(\frac{m^2}{g, metal} \right) = \frac{Q_{CO}}{M_{metal} \times Q_{CO}^{theo}}$$

In the equation, Q_{CO} is the CO stripping charge, M_{metal} is the mass loading of the metal on the working electrode. Q_{CO}^{theo} is the theoretical value of Q_{CO} , which is $420 \mu C/cm^2$ for a two-electron transfer of one CO molecule to a CO_2 per electrocatalyst atom. The as calculated ECSA of Pt is $92 m^2/g_{metal}$, within the reported range of Pt ECSA. The detailed ECSAs of Pt/C and other Pt based samples are as Table S2.

Before CO stripping, a few cycles of CVs was run for each sample to clear the electrochemical surface. The CO stripping process was conducted in 0.1 M KOH using RDE. CO adsorption was under potential control at 0.06 V/RHE, followed by two cycles of CVs at 0.05 V/s to determine CO-based ECSA.

The activation energy (E_a) measurement and calculation. The E_a of the samples are acquired through the natural logarithm of Arrhenius' equation.

$$\ln(k) = \frac{-E_a}{R} \left(\frac{1}{T} \right) + \ln(A)$$

Where k is the rate constant, T is the absolute temperature in kelvin, R is the universal gas constant, A is the pre-exponential factor and E_a is the activation energy. In this work, we considering k as the j_0 of each reaction, and a relationship between j_0 and the temperature of the reaction can be established. The HER polarization curves of each sample were measured under 4 different temperatures (10 °C, 25 °C, 40 °C, 55 °C) in a water jacket cell with H_2 purging. The corresponding j_0 was then acquired by fitting j_k into the Butler-Volmer equation. As a result, a linear relationship could be built between $1/T$ and $\ln j_0$. The slope of the plot is considered as $-E_a/R$, from where E_a could be easily calculated. The similar process had been used to acquire the E_a of all the other samples in different solutions.

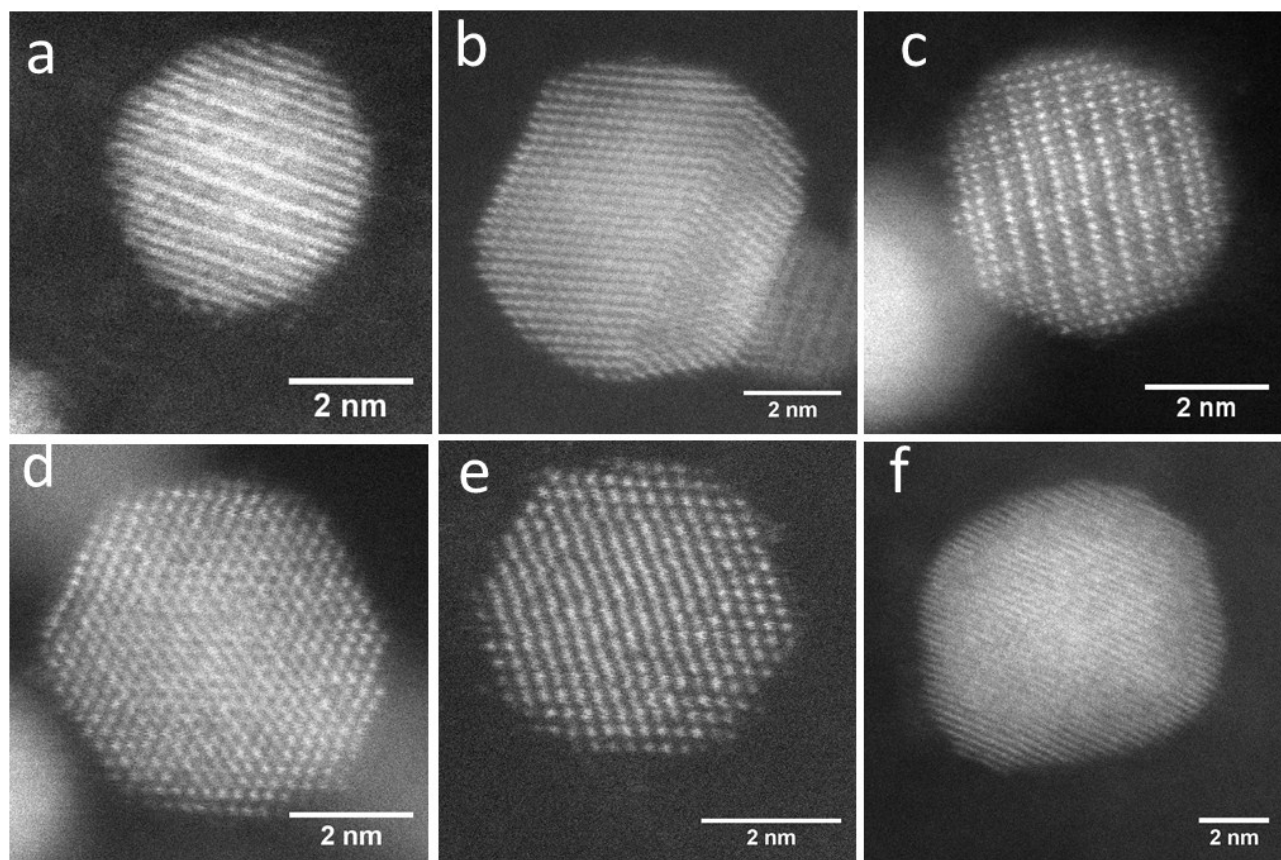


Fig. S1 HAADF-STEM images of (a) PtFe alloy nanoparticle (b) dealloyed PtFe nanoparticle (c) Fe nanoparticle with Pt skin. (d) PtNi alloy nanoparticle (e) dealloyed PtNi nanoparticle (f) PtNi nanoparticle with Pt skin.

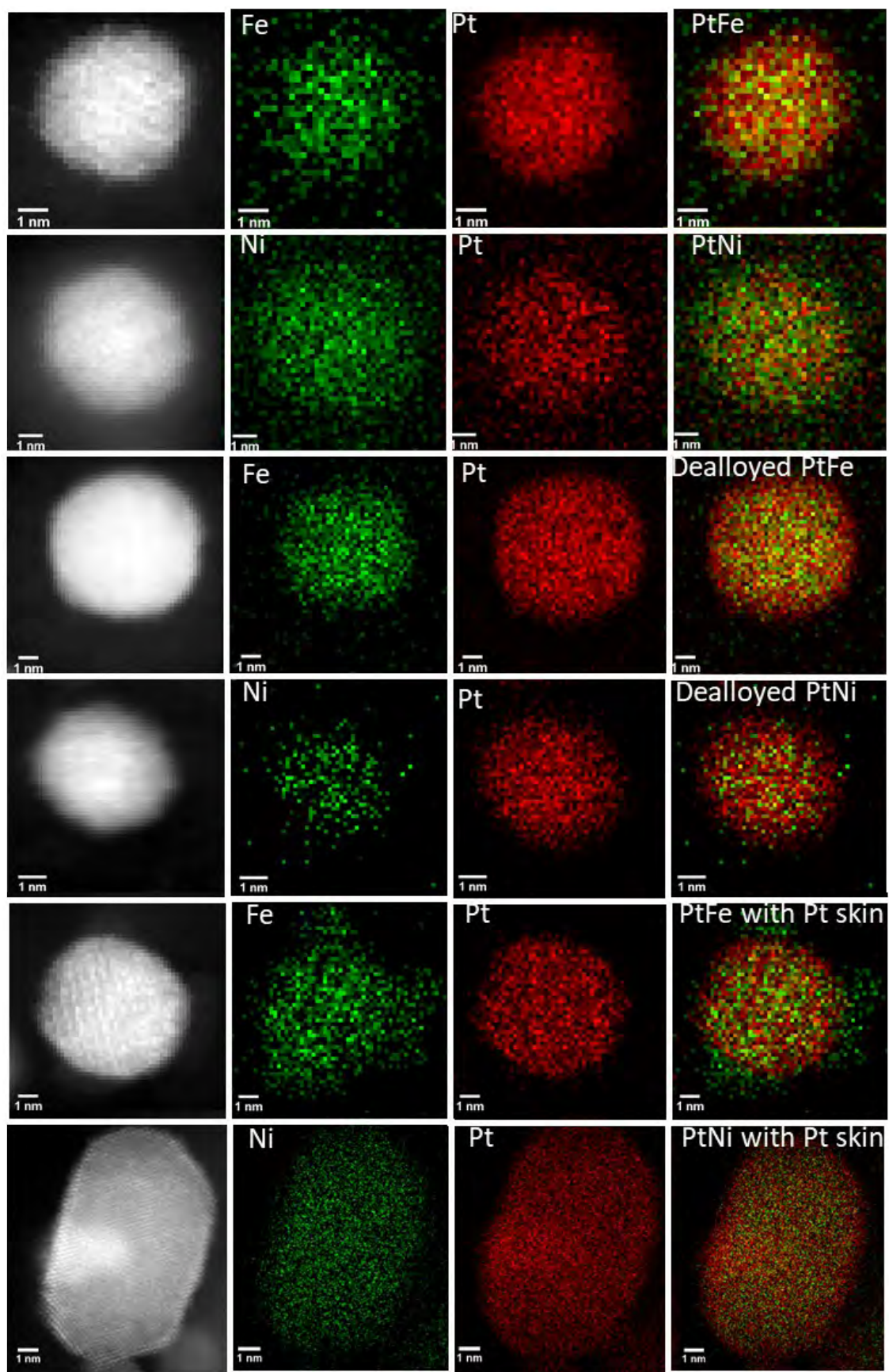


Fig. S2 EDS mapping images of PtM bimetallic samples.

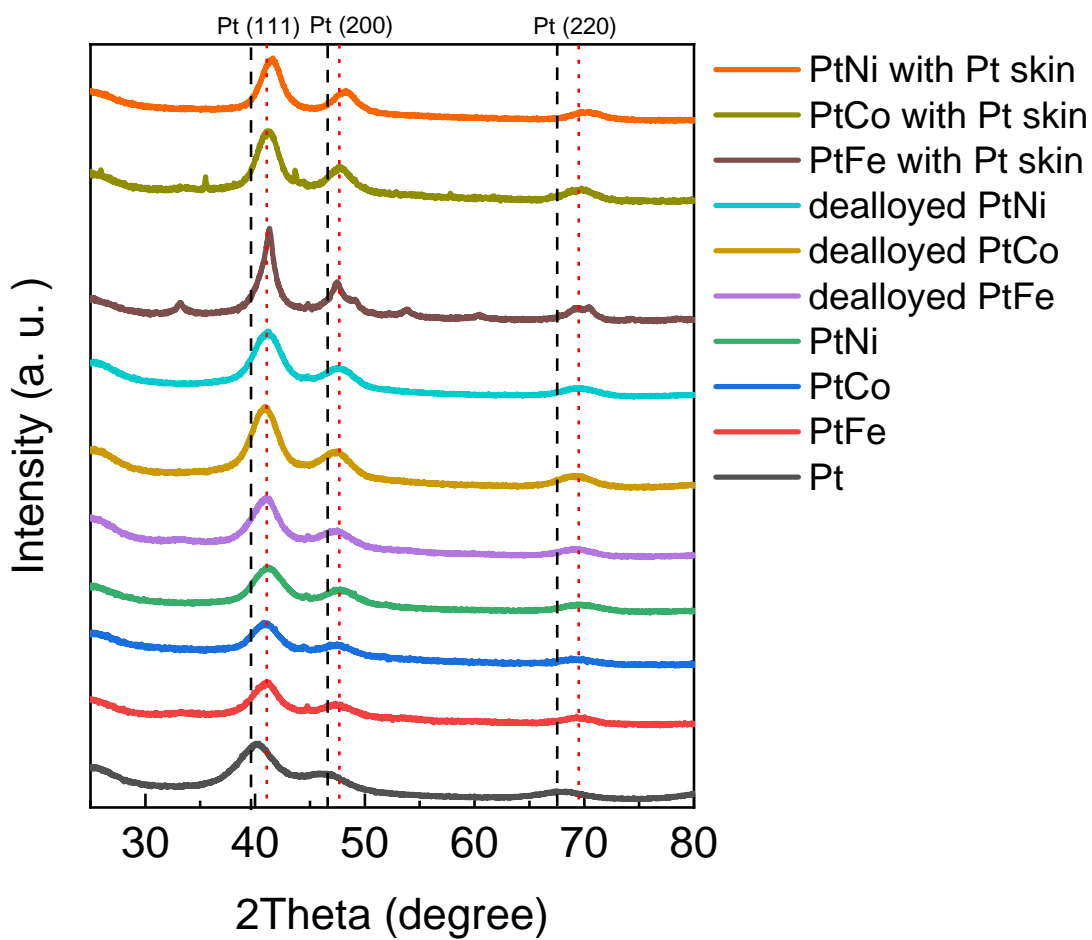


Fig. S3 XRD spectra of the Pt-based samples.

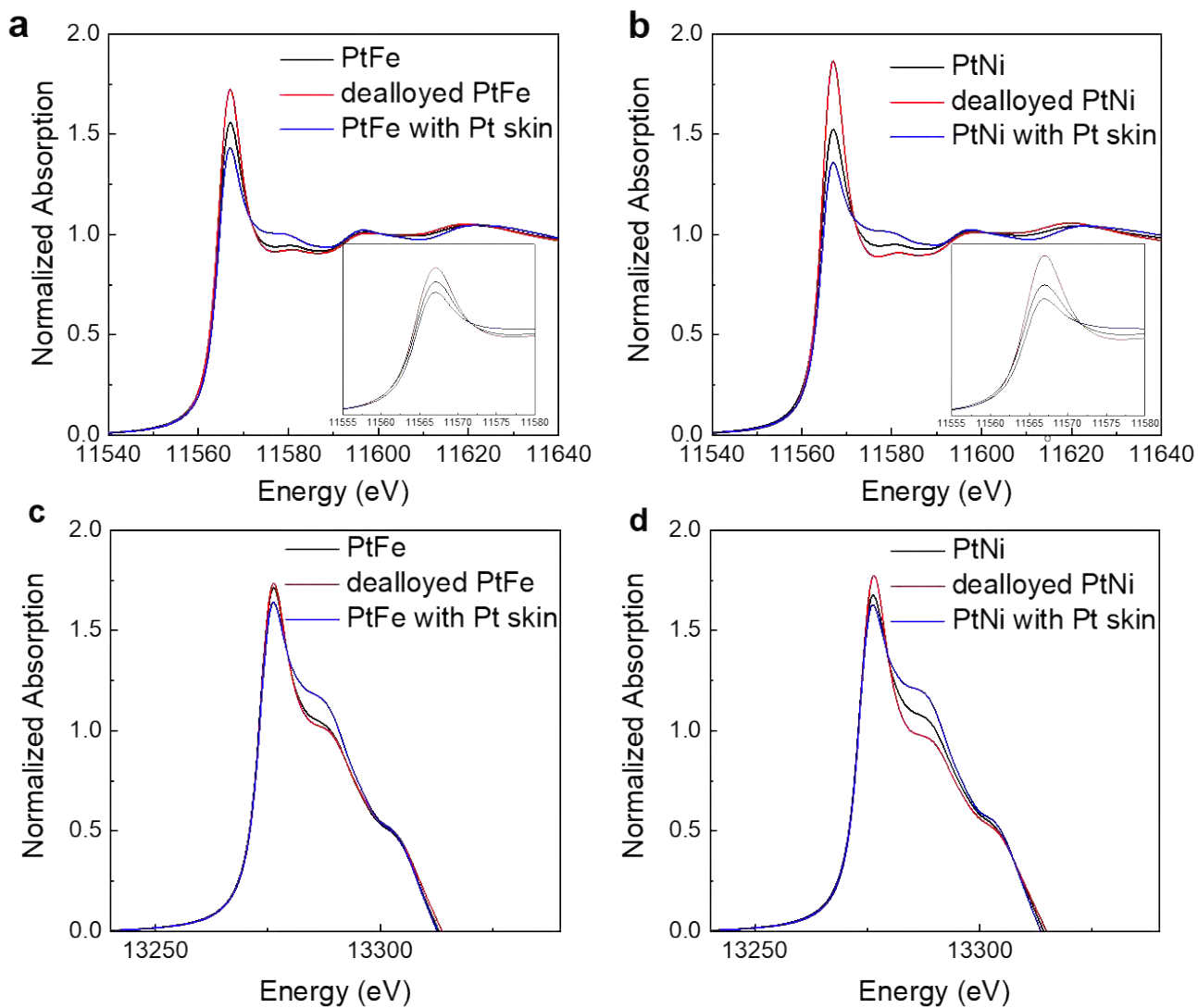


Fig. S4 Pt L_{III}-edge XANES spectra of (a) Fe (b) Ni samples. Pt L_{II}-edge XANES spectra of (c) Fe (d) Ni samples.

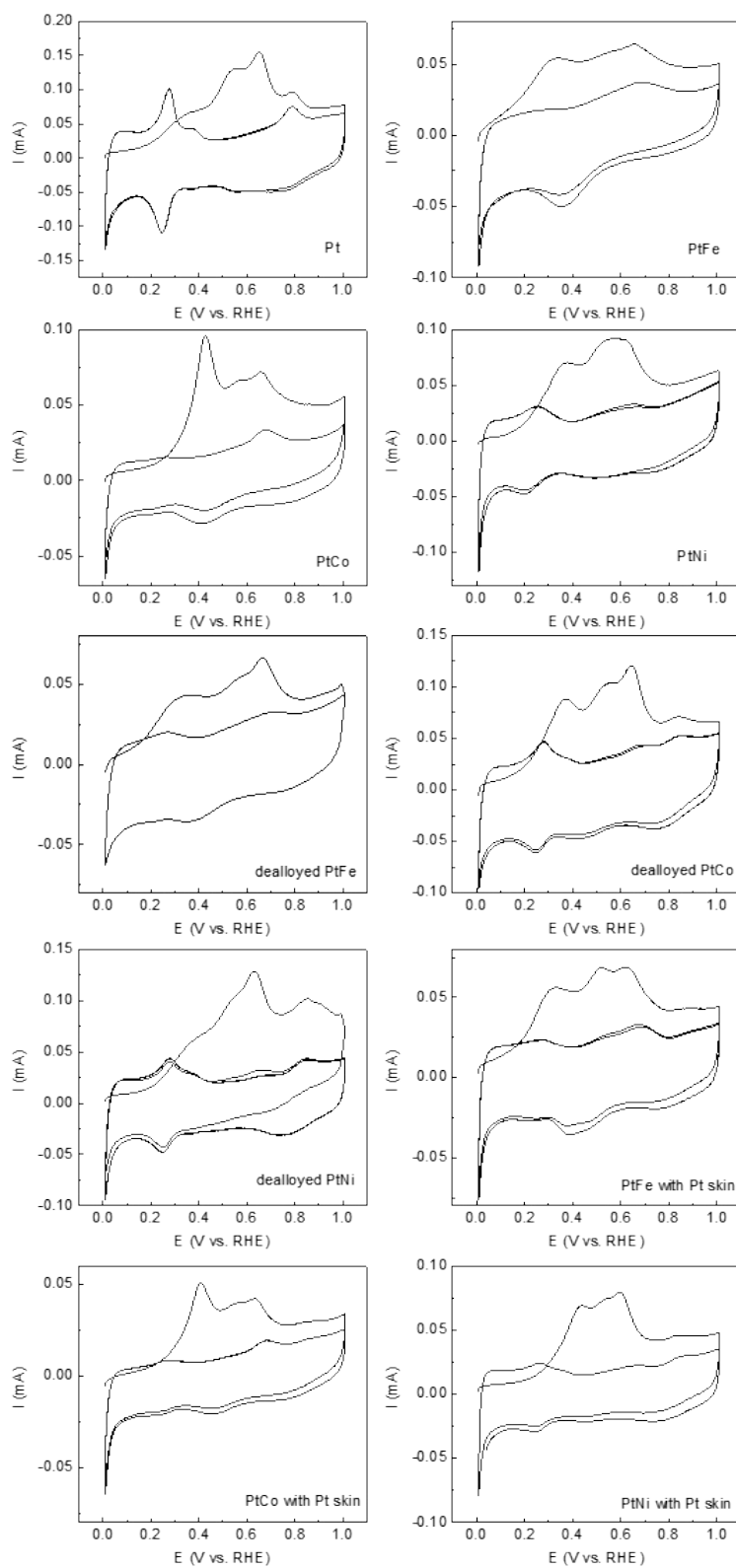


Fig S5 CO stripping of PtM samples in 1M KOH. The CO was fully pre-adsorbed on the electrocatalysts by immersing the electrode in 1 M KOH saturated with CO under potential control of 0.06 V (vs. RHE) for 20 minutes.

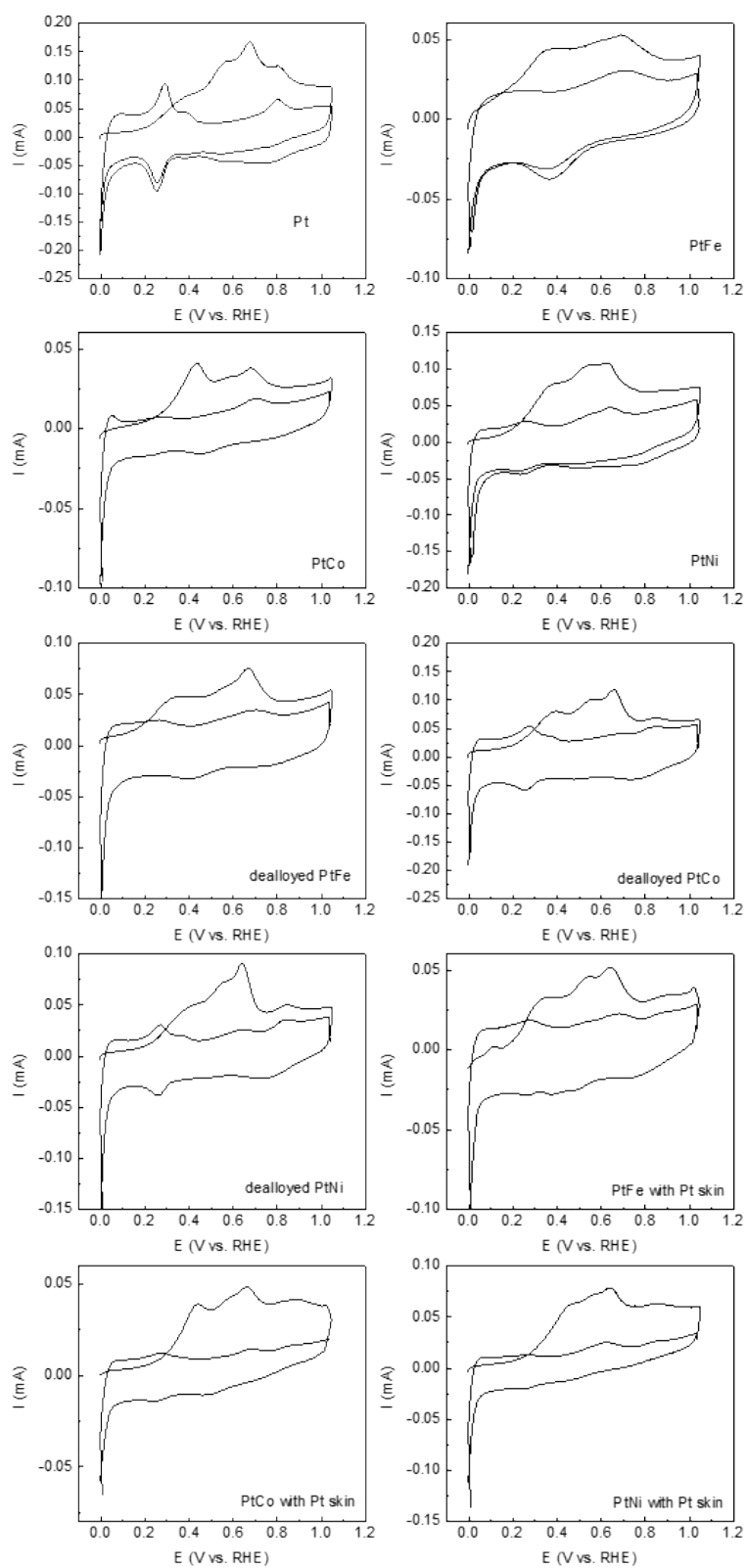


Fig S6 CO stripping of PtM samples in 0.5 M KOH. The CO was fully pre-adsorbed on the electrocatalysts by immersing the electrode in 0.5 M KOH saturated with CO under potential control of 0.06 V (vs. RHE) for 20 minutes.

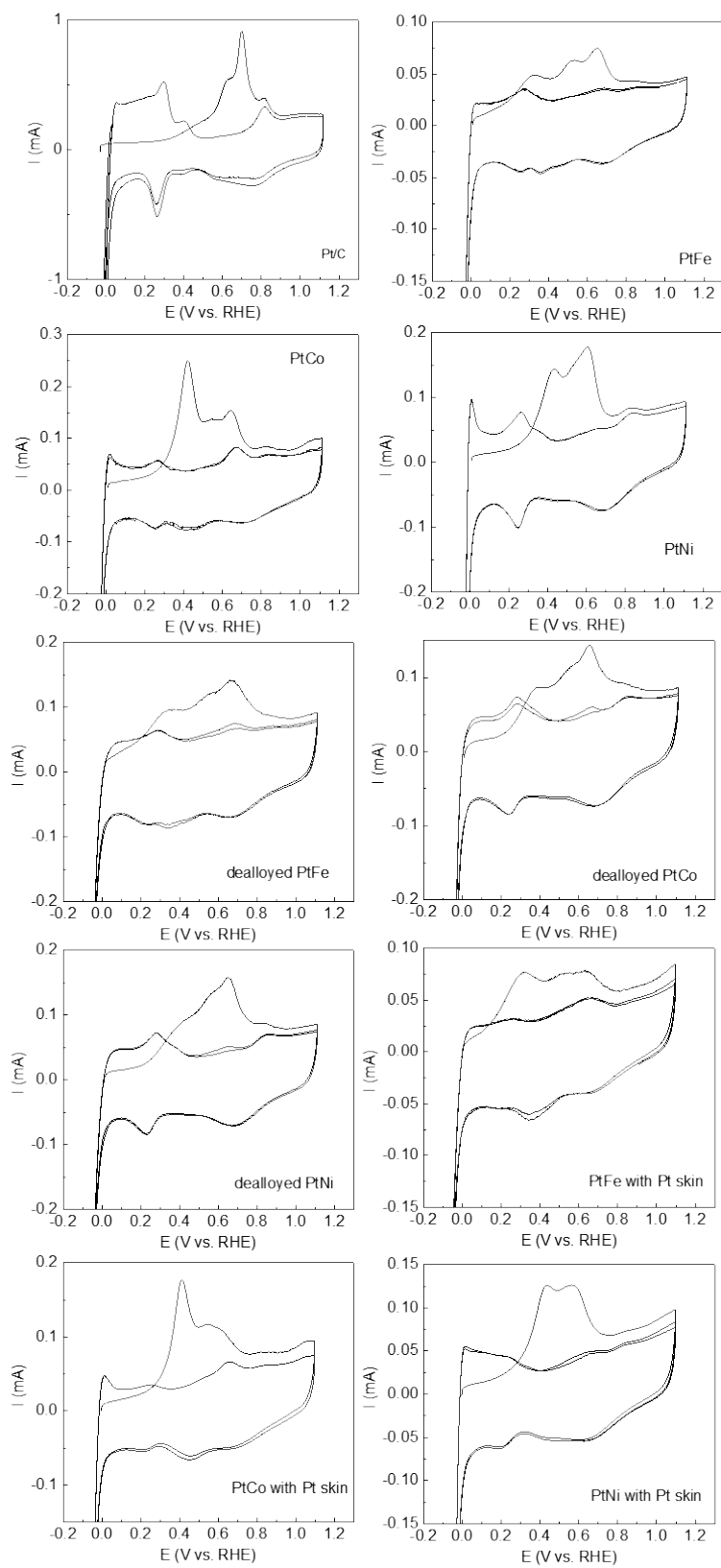


Fig. S7 CO stripping investigation on various electrocatalysts in 0.1 M KOH. The CO was fully pre-adsorbed on the electrocatalysts by immersing the electrode in 0.1 M KOH saturated with CO under potential control of 0.06 V (vs. RHE) for 20 minutes.

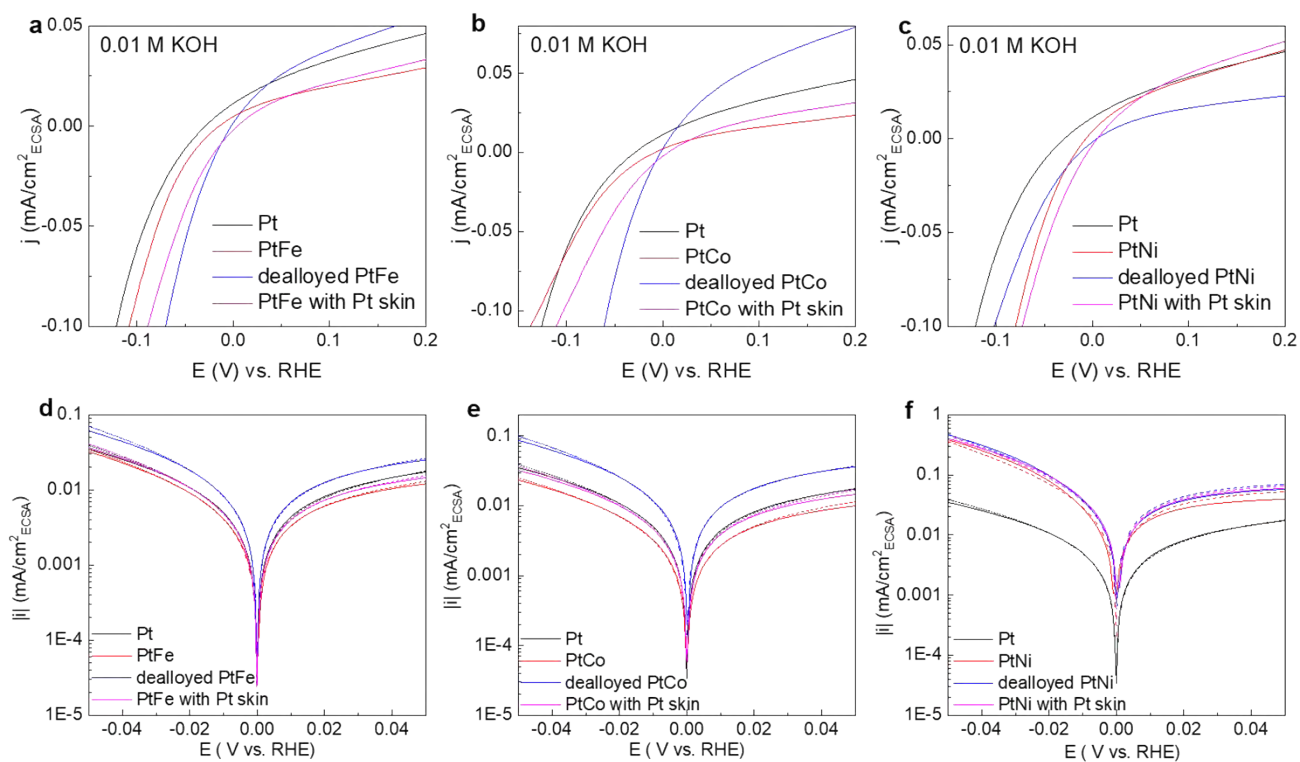


Fig. S8 HER polarization curves of (a) PtFe-containing samples and (b) PtCo-containing samples and (c) PtNi-containing samples in 0.01 M KOH solution with their corresponding Tafel plots (d-f). The dotted lines indicate Butler-Volmer fitting results.

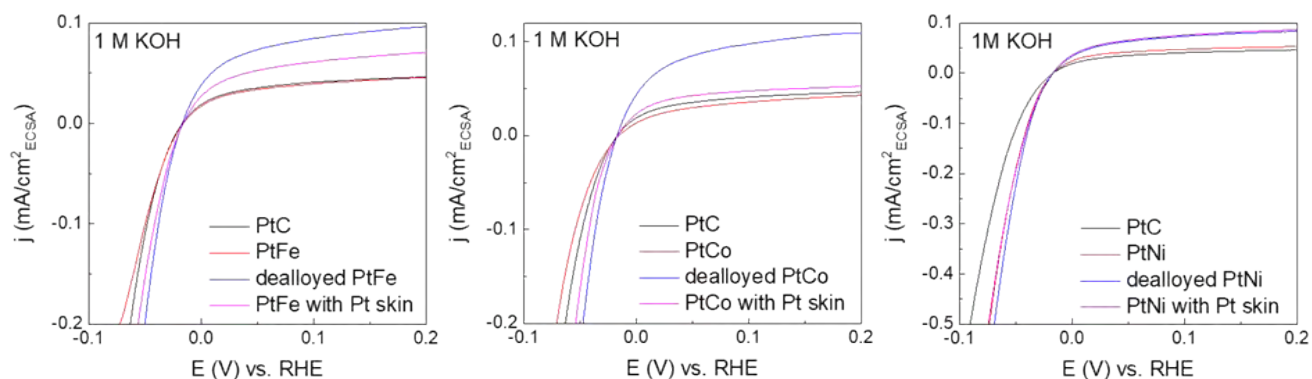


Fig. S9 HER polarization curves of (a) PtFe-containing samples and (b) PtCo-containing samples and (c) PtNi-containing samples in 1 M KOH solution.

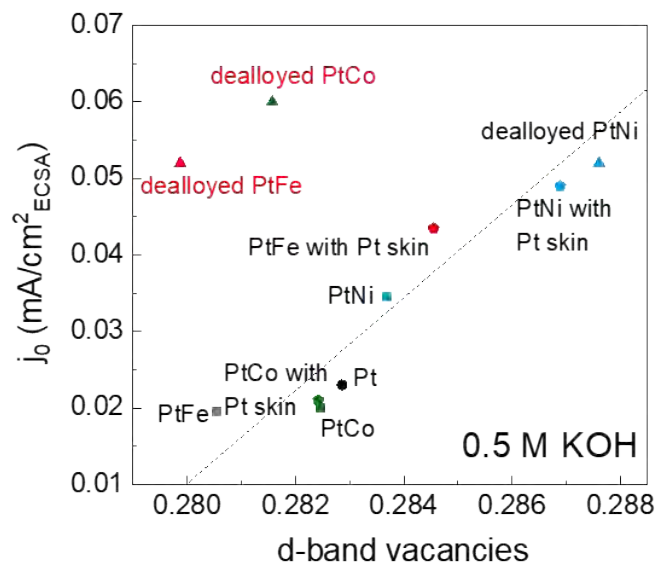


Fig S10 The experimentally acquired relationship between the d-band vacancies and j_0 for a series of Pt based materials in 0.5M KOH.

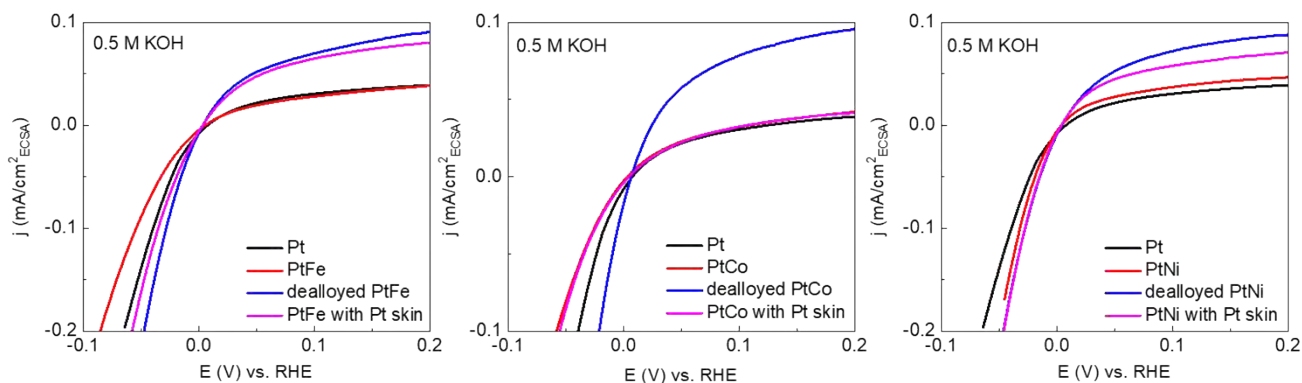


Fig S11 HER activity of PtM samples in 0.5 M KOH

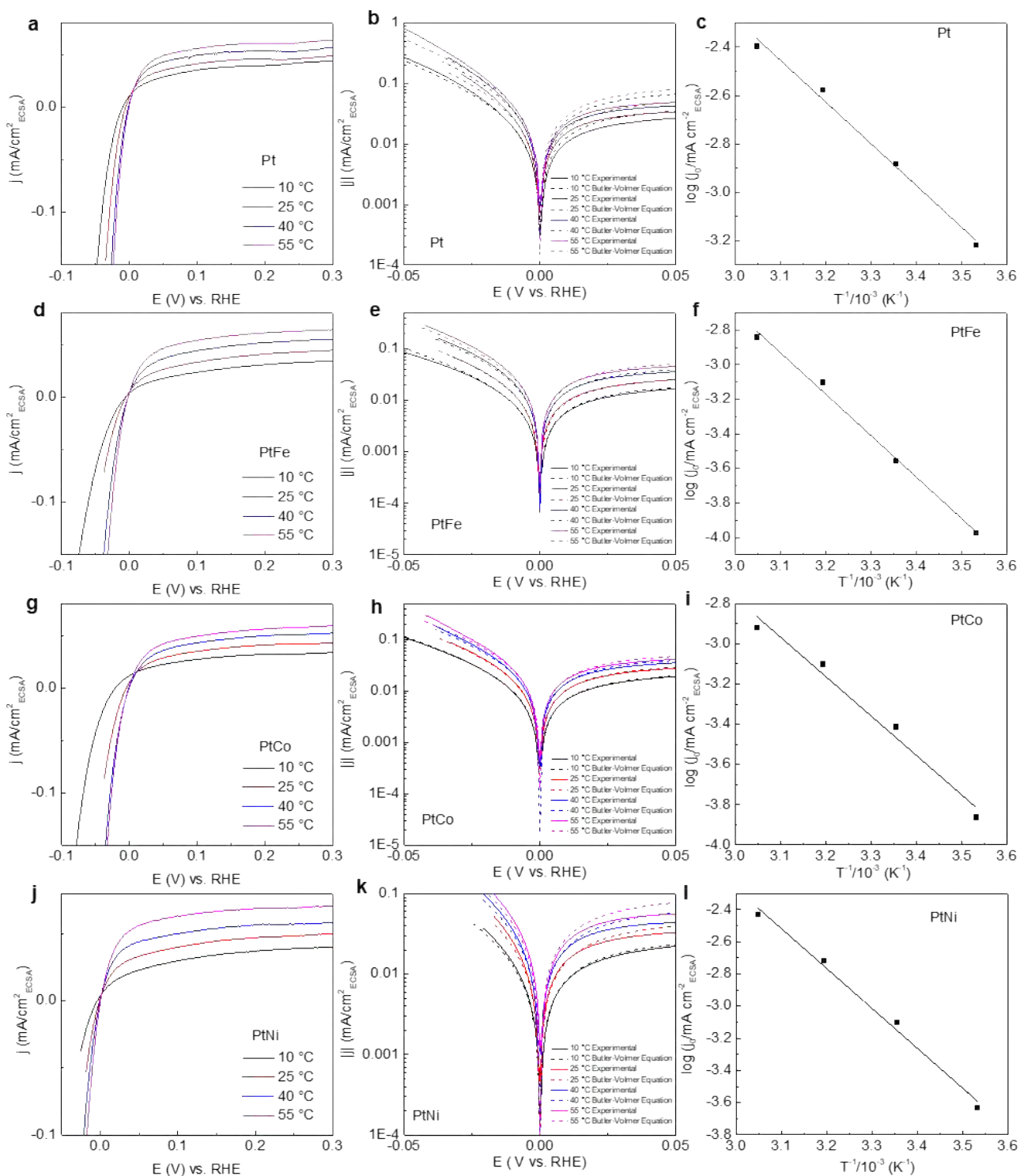


Fig. S12 (a), (d), (g), (j) HER polarization curves of the Pt and Pt alloy samples and their corresponding experimental Tafel plots (b), (e), (h), (k). The dotted lines indicate Butler-Volmer fitting results. (c), (f), (i), (l) the relationship between the reaction temperature and j_0 of the corresponding alloy electrocatalysts. All the tests were carried out in 1 M KOH solution.

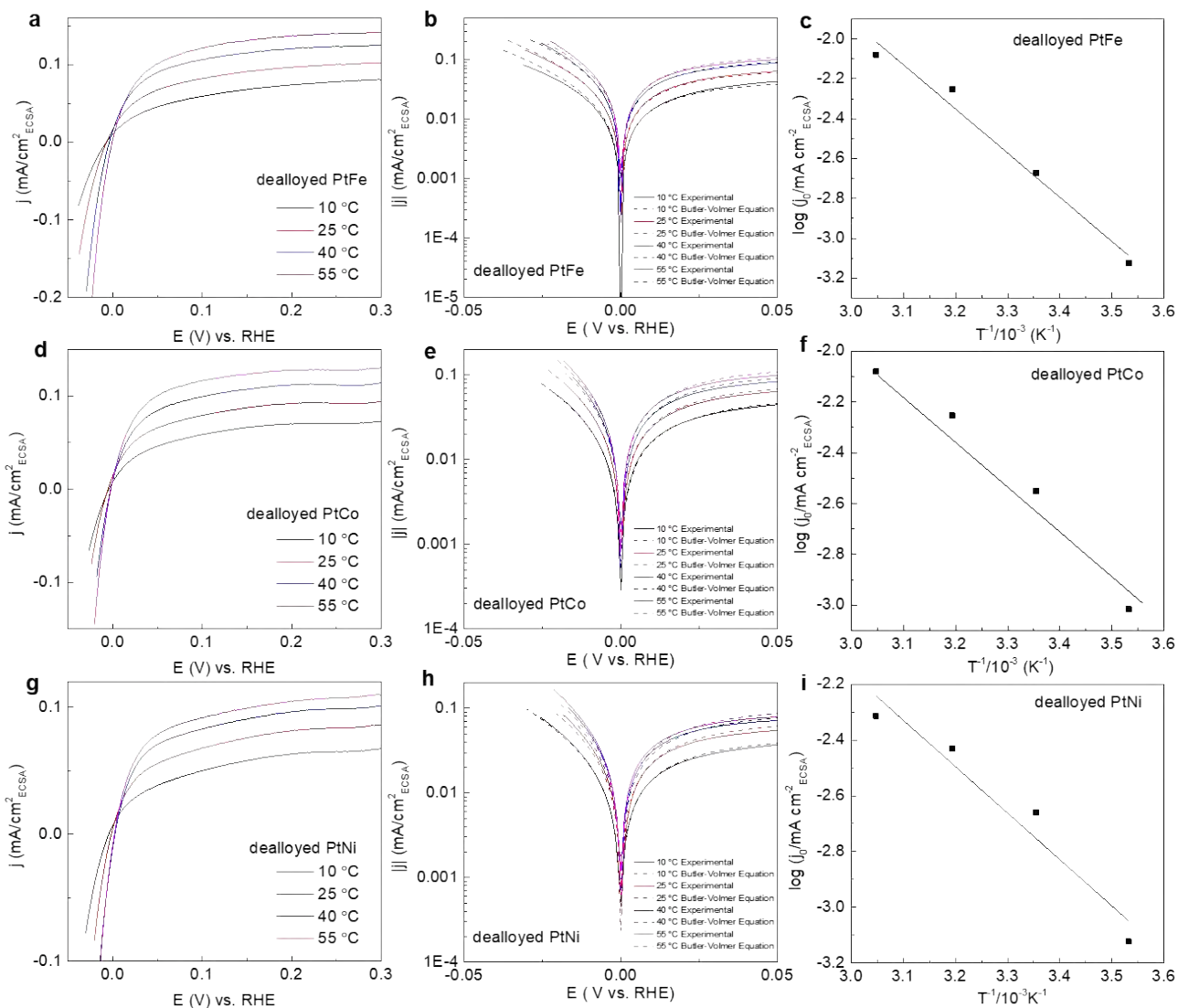


Fig. S13 (a), (d), (g) HER polarization curves of the Pt dealloyed samples and their corresponding experimental Tafel plots (b), (e), (h). The dotted lines indicate Butler-Volmer fitting results. (c), (f), (i) the relationship between the reaction temperature and j_0 of the corresponding dealloyed electrocatalysts. All the tests were carried out in 1 M KOH solution.

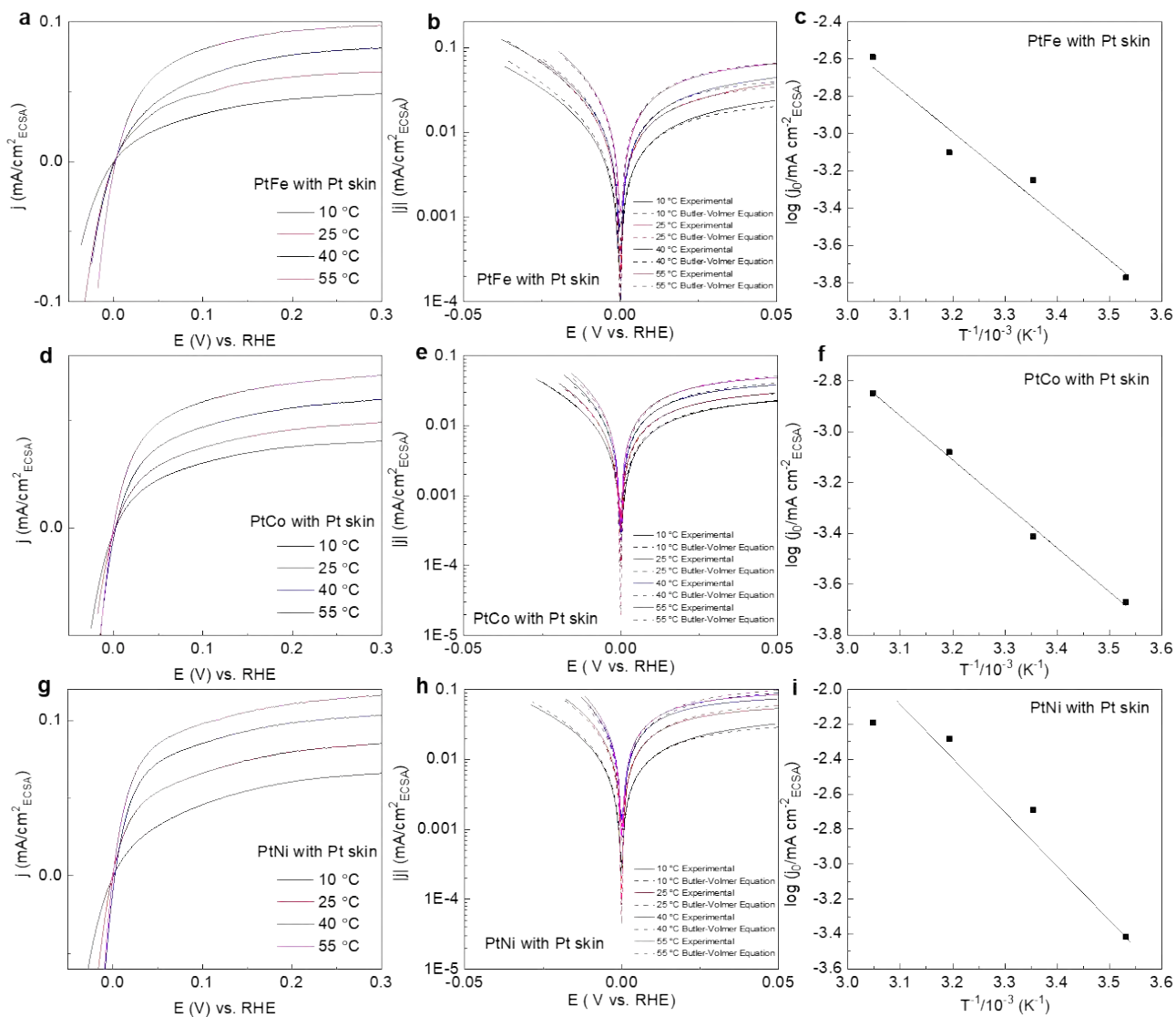


Fig. S14 (a), (d), (g) HER polarization curves of the samples with Pt skin and their corresponding experimental Tafel plots (b), (e), (h). The dotted lines indicate Butler-Volmer fitting results. (c), (f), (i) the relationship between the reaction temperature and j_0 of the corresponding Pt skinned electrocatalysts. All the tests were carried out in 1 M KOH solution.

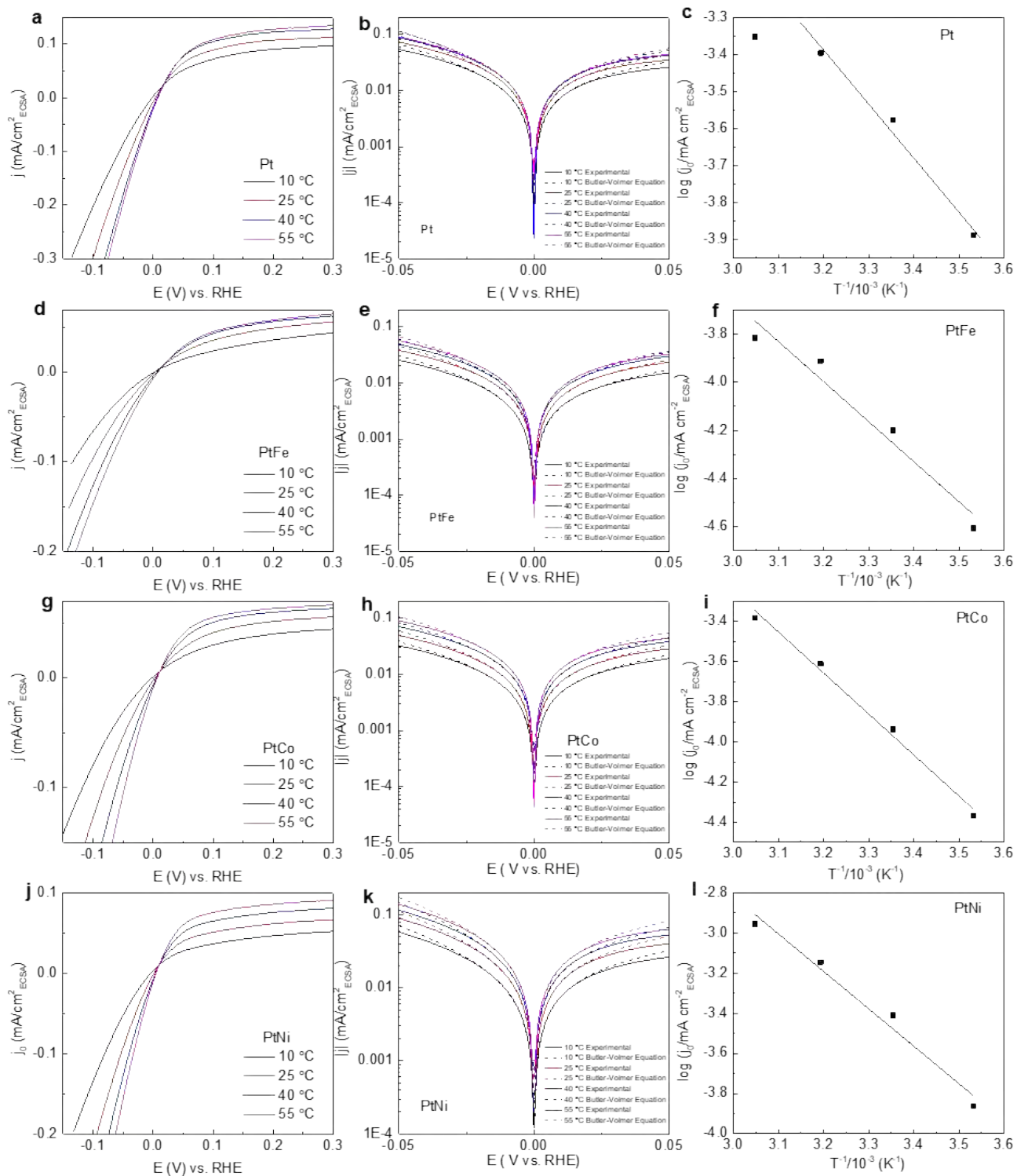


Fig. S15 (a), (d), (g), (j) HER polarization curves of the Pt and Pt alloy samples and their corresponding experimental Tafel plots (b), (e), (h), (k). The dotted lines indicate Butler-Volmer fitting results. (c), (f), (i), (l) the relationship between the reaction temperature and j_0 of the corresponding alloy electrocatalysts. All the tests were carried out in 0.1 M KOH solution.

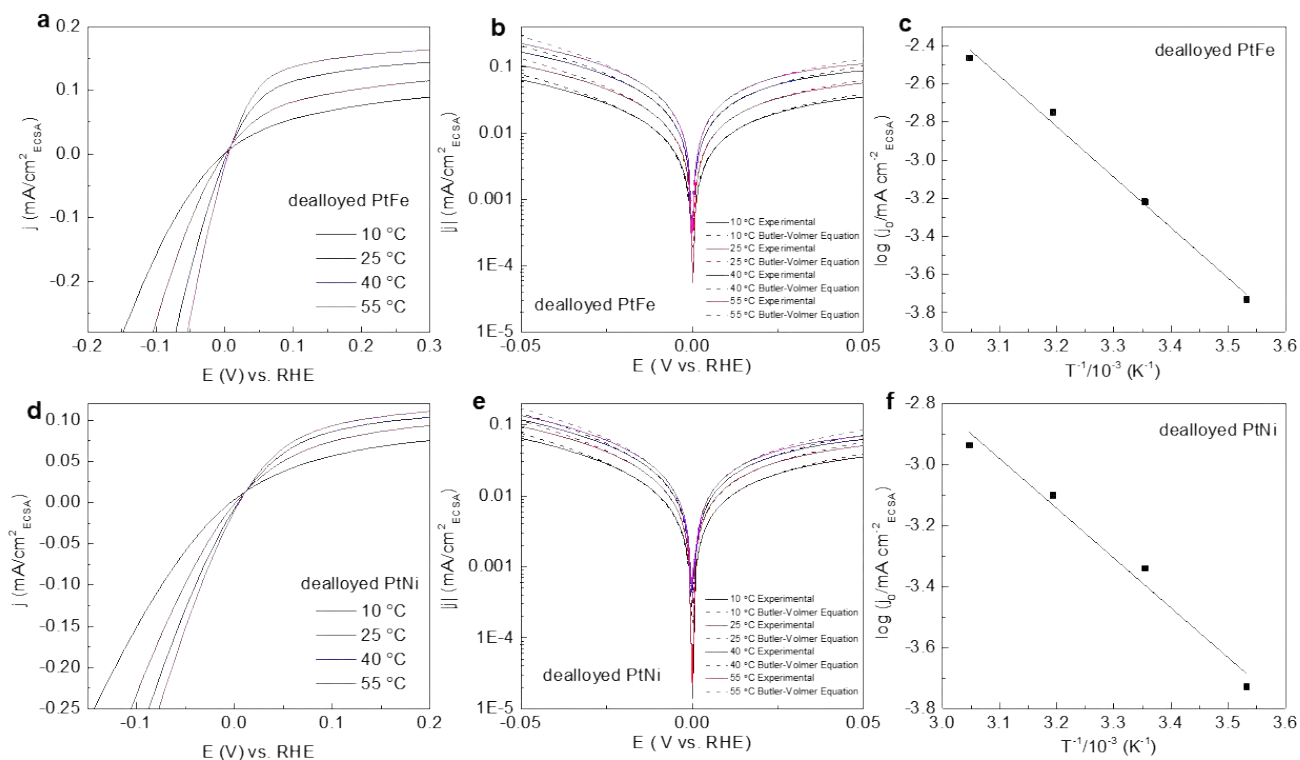


Fig. S16 (a), (d) HER polarization curves of the Pt dealloyed samples and their corresponding experimental Tafel plots (b), (e). The dotted lines indicate Butler-Volmer fitting results. (c), (f) the relationship between the reaction temperature and j_0 of the corresponding dealloyed electrocatalysts. All the tests were carried out in 0.1 M KOH solution.

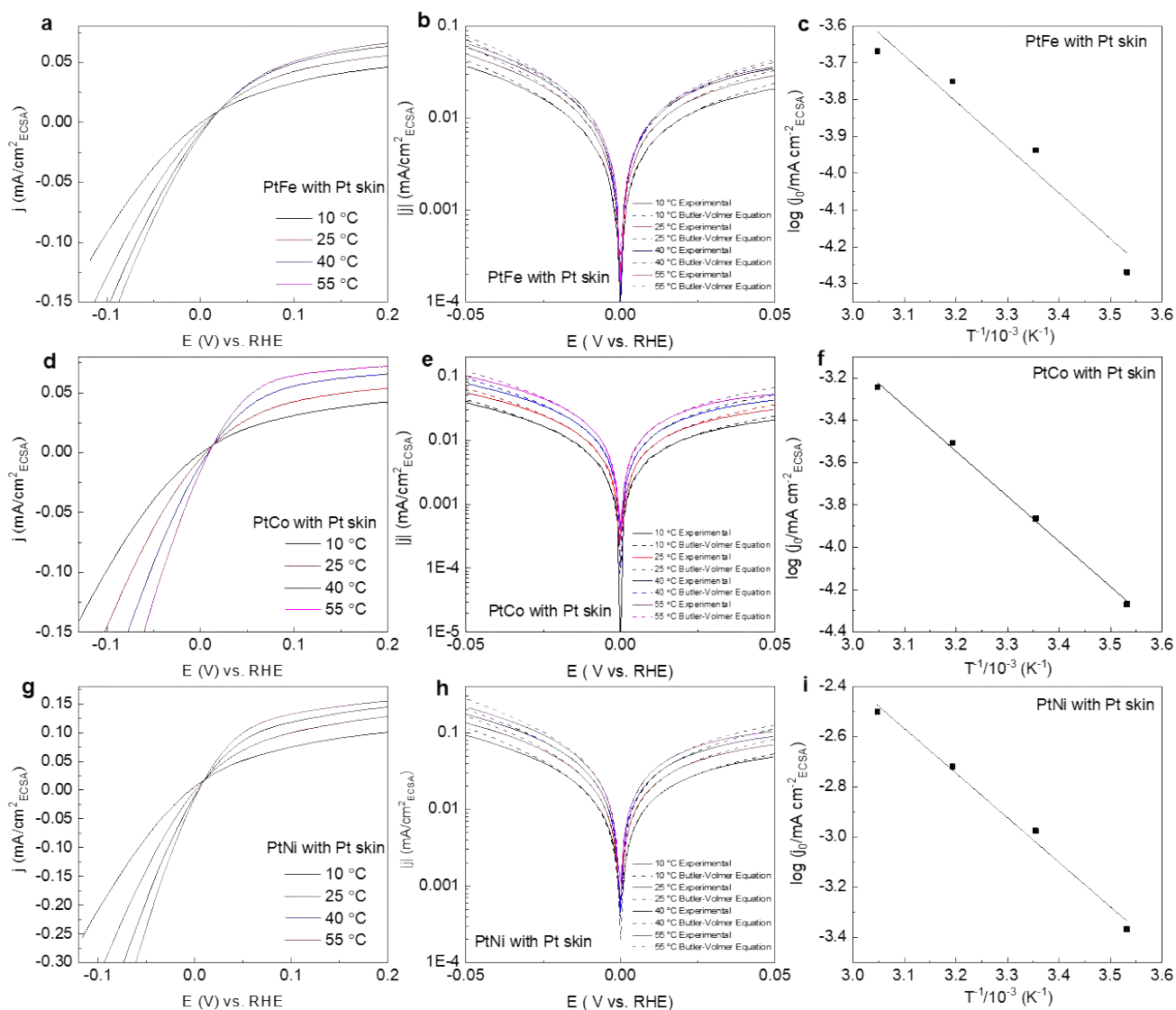


Fig. S17 (a), (d), (g) HER polarization curves of the samples with Pt skin and their corresponding experimental Tafel plots (b), (e), (h). The dotted lines indicate Butler-Volmer fitting results. (c), (f), (i) the relationship between the reaction temperature and j_0 of the corresponding Pt skinned electrocatalysts. All the tests were carried out in 0.1 M KOH solution.

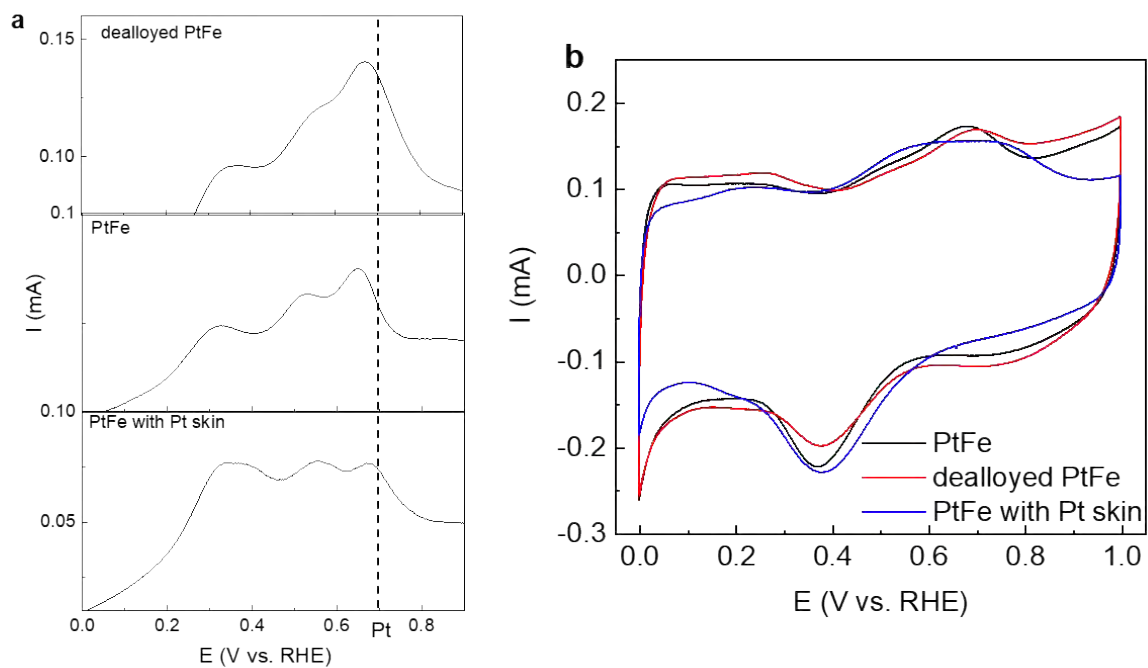


Fig. S18 (a) CO stripping of PtFe-containing bimetallic samples in 0.1 M KOH solution, (b) CVs of PtFe-containing bimetallic samples in 0.1 M KOH.

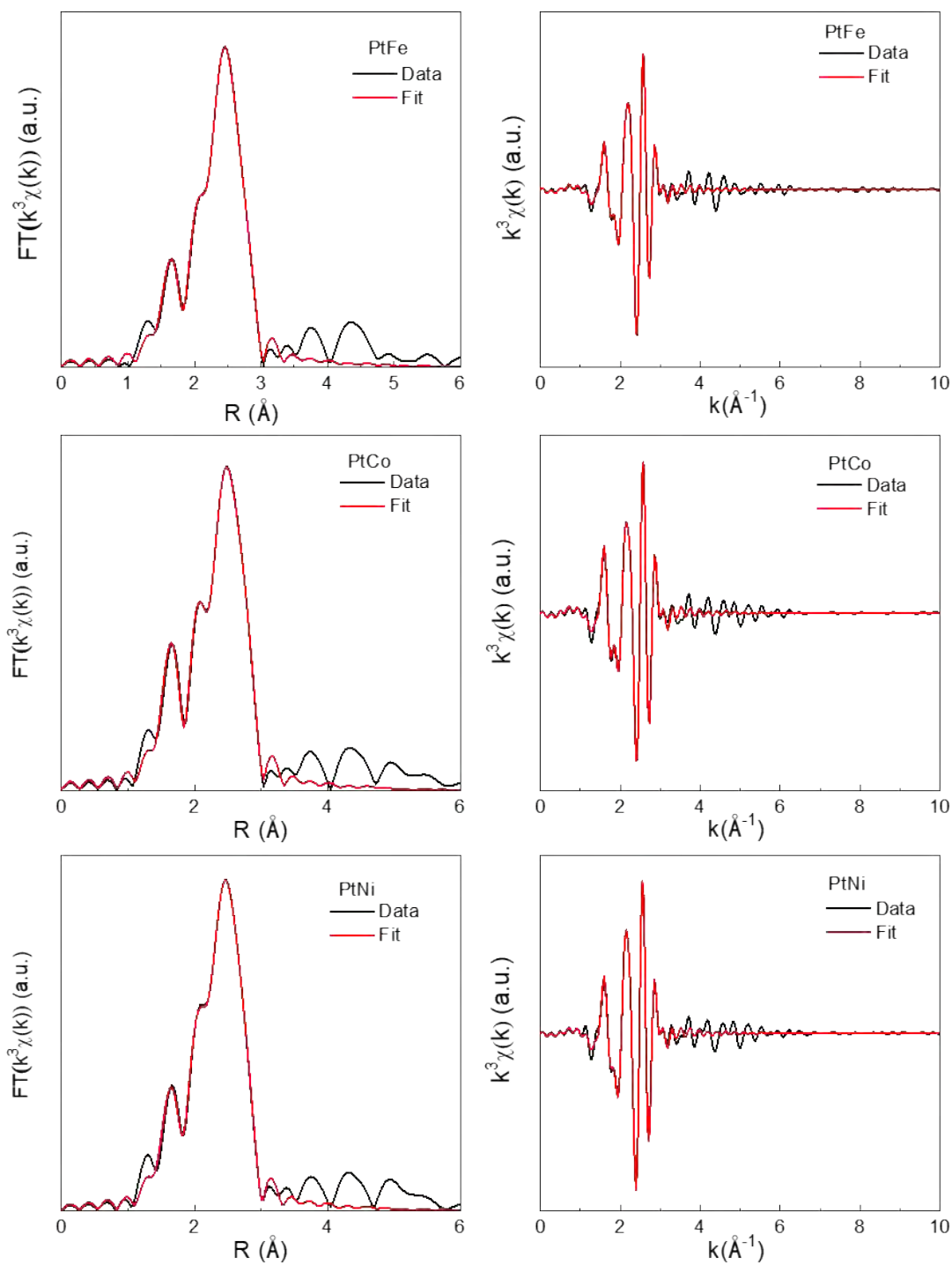


Fig. S19 Fitted EXAFS spectra of the Pt alloy samples. Left: Forward Fourier transform of the EXAFS after correction for phase shifts. Right: Fits in K -space for the Pt alloy samples.

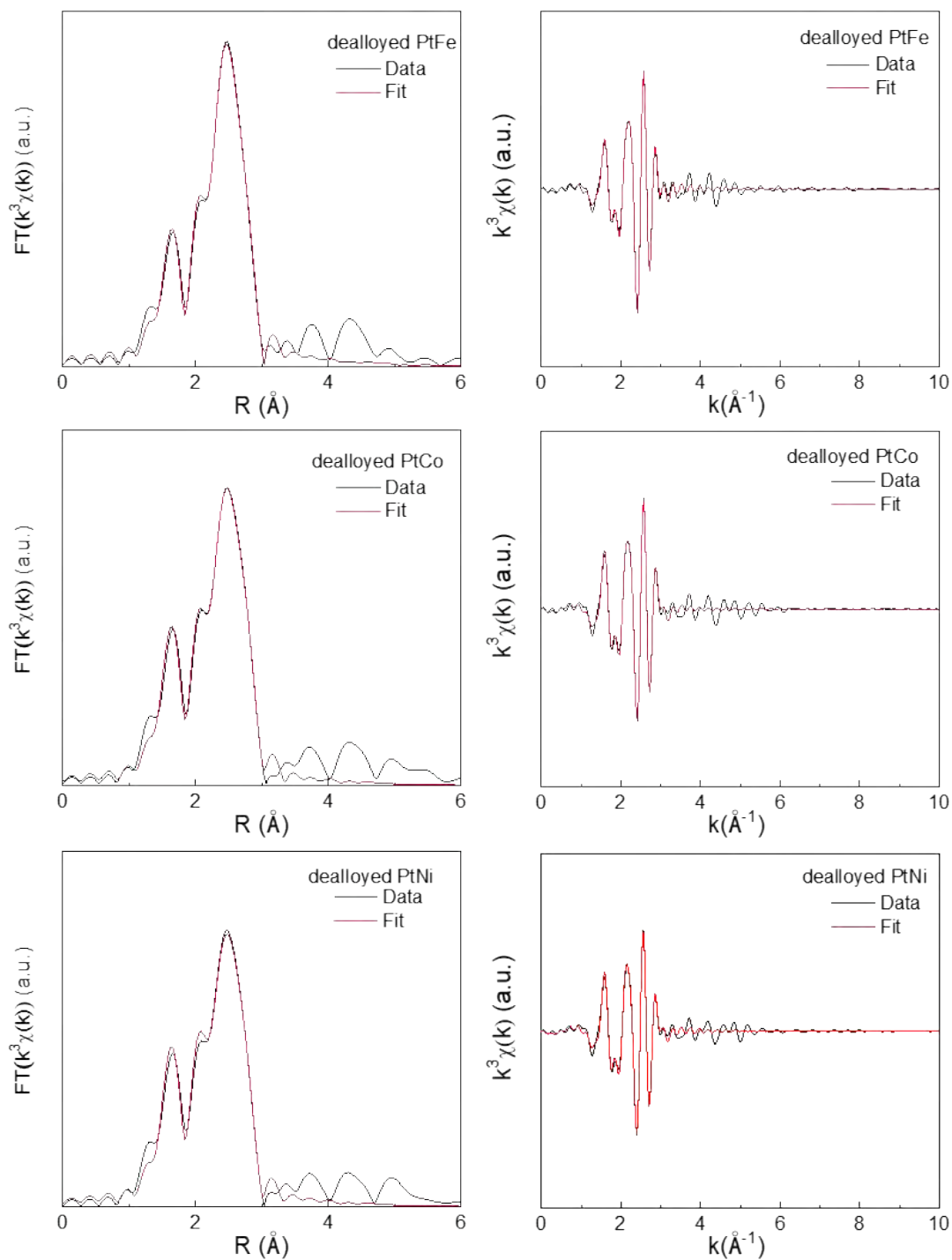


Fig. S20 Fitted EXAFS spectra of the Pt dealloyed samples. Left: Forward Fourier transform of the EXAFS after correction for phase shifts. Right: Fits in k -space for the Pt alloy samples.

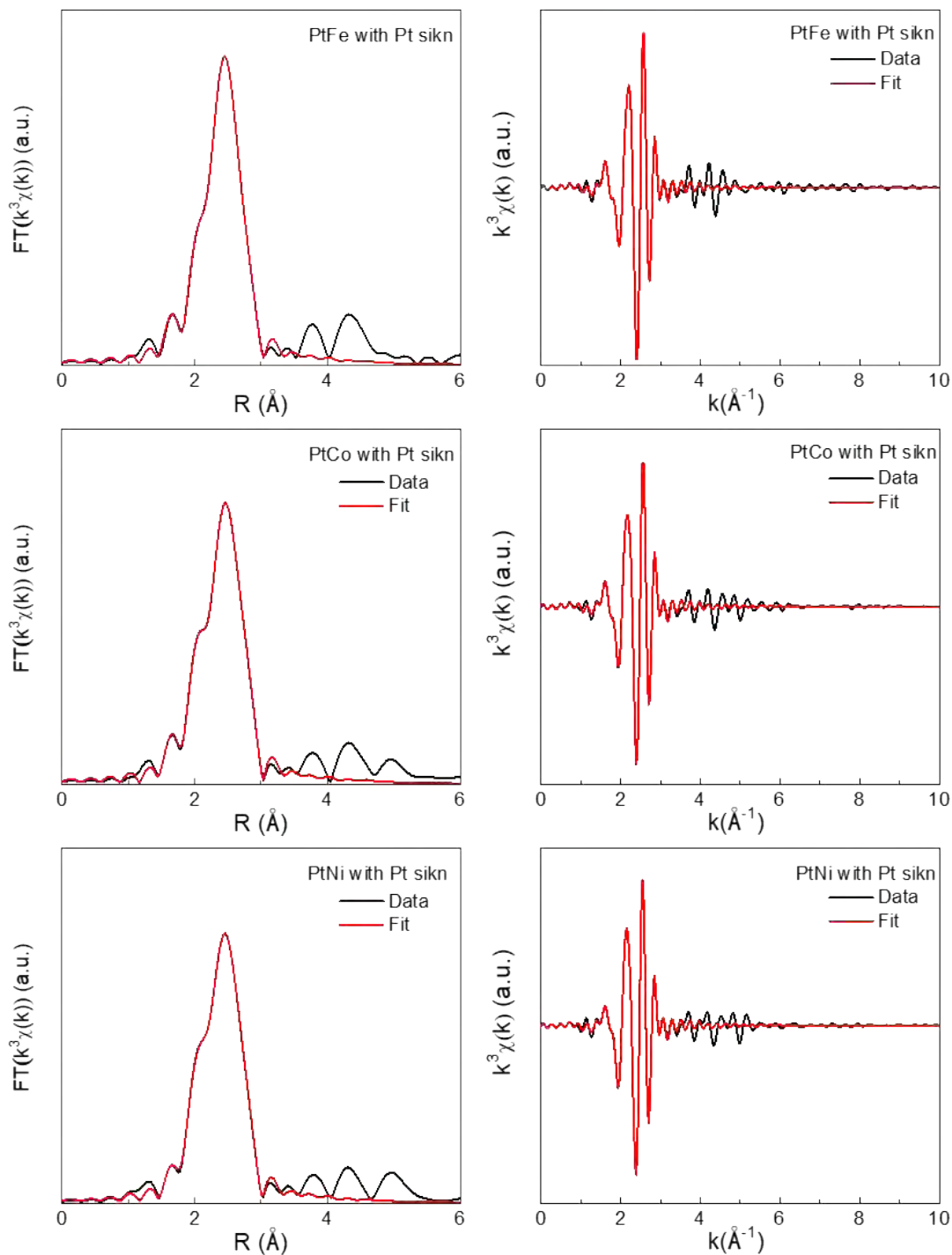


Fig. S21 Fitted EXAFS spectra of the samples with Pt skin. Left: Forward Fourier transform of the EXAFS after correction for phase shifts. Right: Fits in K-space for the Pt alloy samples.

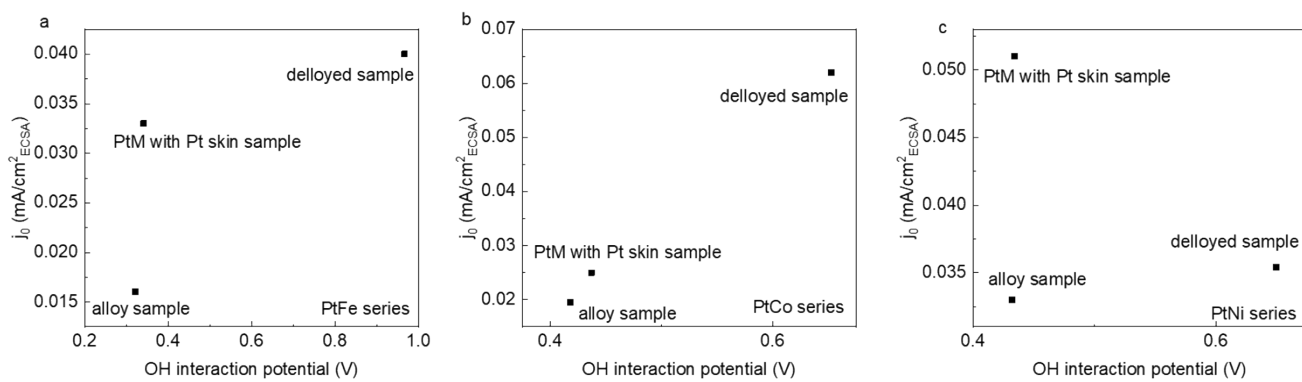


Fig S22 The relationship between the OH interaction ability and the HER activity of the catalysts in 0.1 M KOH, (a) PtFe, (b) PtCo and (c) PtNi series. No obvious relationship between the two parameters can be found.

Table S1. The d-band vacancies of the Pt-based bimetallic samples.

	Pt	PtFe	PtCo	PtNi	dealloyed PtFe
d-band vacancies	0.28286	0.28054	0.28242	0.28369	0.27987
	dealloyed PtCo	dealloyed PtNi	PtFe with Pt skin	PtCo with Pt skin	PtNi with Pt skin
d-band vacancies	0.28157	0.28761	0.28455	0.28246	0.28689

Table S2. ECSAs of the Pt based samples.

	PtC	PtFe	PtCo	PtNi	dealloyed PtFe
ECSA ($\text{m}^2/\text{g}_{\text{metal}}$)	92	87	90	82	45
	dealloyed PtCo	dealloyed PtNi	PtFe with Pt skin	PtCo with Pt skin	PtNi with Pt skin
ECSA ($\text{m}^2/\text{g}_{\text{metal}}$)	43	50	58	82	52

Table S3. EXAFS fitting results for the Pt-based bimetallic samples.

Coordination shell	EXAFS parameter	Fe			Co			Ni		
		Alloy	Dealloy	Pt skin	Alloy	Dealloy	Pt skin	Alloy	Dealloy	Pt skin
R factor		0.0019	0.0026	0.002	0.0031	0.004	0.0038	0.0009	0.001	0.0009
Pt-Pt	R (Å)	2.70(8)	2.70(6)	2.71(1)	2.70(4)	2.70(7)	2.70(2)	2.69(5)	2.69(6)	2.69(5)
	CN	6.24(8)	6.90(6)	8.02(3)	8.02(7)	9.22(0)	9.75(7)	7.97(8)	8.10(5)	7.60(4)
	$\Delta\sigma^2$	0.0075	0.00667	0.0061	0.00788	0.00806	0.0068	0.00806	0.00796	0.00601
	ΔE_0 (eV)	4.091	4.528	4.616	3.898	3.424	4.888	3.998	3.61	5.113
Pt-M	R (Å)	2.66(9)	2.67(2)	2.66(7)	2.65(7)	2.66(4)	2.64(4)	2.64(0)	2.65(3)	2.62(2)
	CN	2.39(3)	2.65(9)	5.12(2)	2.20(6)	2.34(9)	5.04(7)	2.75(2)	2.42(9)	4.69(0)
	$\Delta\sigma^2$	0.00774	0.00743	0.00688	0.00913	0.00862	0.00874	0.00912	0.00889	0.00744
	ΔE_0 (eV)	8.371	8.055	7.082	9.926	9.387	7.276	9.997	9.687	7.014
Pt-O	R (Å)	2.00(4)	2.00(2)	2.01(6)	2.00(2)	2.00(4)	1.96(6)	1.99(7)	2.00(1)	\
	CN	1.25(2)	2.06(5)	0.42(6)	1.36(0)	2.23(2)	0.82(1)	1.17(9)	2.27(2)	\
	$\Delta\sigma^2$	0.0068	0.00568	0.00304	0.00318	0.00463	0.00134	0.00383	0.00485	\
	ΔE_0 (eV)	9.395	9.629	9.192	9.946	9.734	2.601	7.714	9.877	\

Chapter 5 : Strain Effect in Bimetallic Electrocatalysts on the Hydrogen Evolution Reaction

5.1 Introduction

Bimetal materials are one of the most efficient catalysts toward some key but kinetically sluggish electrocatalytic reactions such as oxygen reduction reaction, CO₂ reduction reaction and hydrogen evolution reaction (HER), etc. However, the co-existence of geometric and electronic effects in this kind of materials has interactive influence toward their overall catalytic activities. Therefore, finding the reactivity origin of the bimetal materials is very challenging for designing active ones. Here by using two kinds of well-defined Ru-Pt nanostructures, i.e., core-shell and conventional alloy, as model catalysts, we can isolate the geometric and electronic effects and link each of them to the fundamental reaction intermediate adsorption strength during HER process. For the first time, we found that the strain effect plays a more dominant role for the activity enhancement of HER, therefore providing an important strategy for the future composition/structure design of more bimetal catalysts. The highlights of this work include:

- A new face-centred-cubic Ru core @ Pt shell structure with a highly compressively strained Pt interface was well-characterized by both atomic-level imaging and molecular dynamics simulation.
- The geometric and electronic effects of this model catalysts was isolated by using experimentally X-ray absorption spectroscopy and theoretically simulation.
- The unique strained nanostructure leads optimal adsorption/desorption of both hydrogen and hydroxyl reactive species during the reaction.
- The Ru@Pt core-shell sample with geometric effect only even showed much higher activity compared to conventional RuPt alloys with both geometric and electronic effects and single Pt.

5.2 Strain Effect in Bimetallic Electrocatalysts on the Hydrogen Evolution Reaction

This chapter is included as it appears as a journal paper published by Xuesi Wang, Yihan Xhu, Anthony Vasileff, Yan Jiao, Shuangming Chen, Li Song, Bin Zhang, Yao Zheng and Shi-Zhang Qiao: Strain Effect in Bimetallic Electrocatalysts on the Hydrogen Evolution Reaction, *ACS Energy Letter*, 2018, 3, 1198-1204

Statement of Authorship

Title of Paper	Strain Effect in Bimetallic Electrocatalysts in the Hydrogen Evolution Reaction
Publication Status	<input checked="" type="checkbox"/> Published <input type="checkbox"/> Accepted for Publication <input type="checkbox"/> Submitted for Publication <input type="checkbox"/> Unpublished and Unsubmitted work written in manuscript style
Publication Details	Wang, X.; Zhu, Y.; Vasileff, A.; Jiao, Y.; Chen, S.; Song, L.; Zheng, B.; Zheng, Y.; Qiao, S.-Z. Strain Effect in Bimetallic Electrocatalysts in the Hydrogen Evolution Reaction. ACS Energy Letters 2018, 3, 1198-1204.

Principal Author

Name of Principal Author (Candidate)	Xuesi Wang		
Contribution to the Paper	The principal author accomplished all the chemical and electrochemical experiments and wrote the paper.		
Overall percentage (%)	70%		
Certification:	This paper reports on original research I conducted during the period of my Higher Degree by Research candidature and is not subject to any obligations or contractual agreements with a third party that would constrain its inclusion in this thesis. I am the primary author of this paper.		
Signature		Date	1 July 2019

Co-Author Contributions

By signing the Statement of Authorship, each author certifies that:

- the candidate's stated contribution to the publication is accurate (as detailed above);
- permission is granted for the candidate to include the publication in the thesis; and
- the sum of all co-author contributions is equal to 100% less the candidate's stated contribution.

Name of Co-Author	Yihan Zhu		
Contribution to the Paper	This author had accomplished all the TEM relevant characterization in this paper.		
Signature		Date	1 July 2019

Name of Co-Author	Anthony Vasileff		
Contribution to the Paper	This author contributed to paper editing process.		
Signature		Date	1 July 2019

Name of Co-Author	Yan Jiao		
Contribution to the Paper	This author contributed to data analysing process.		
Signature		Date	1 July 2019

Name of Co-Author	Shuangming Chen		
Contribution to the Paper	This author contributed to data analysing process.		
Signature	<i>Shuangming Chen</i>	Date	1 July 2019

Name of Co-Author	Li Song		
Contribution to the Paper	This author contributed to data analysing process.		
Signature		Date	1 July 2019

Name of Co-Author	Bin Zheng		
Contribution to the Paper	This author contributed to data analysing process.		
Signature		Date	1 July 2019

Name of Co-Author	Yao Zheng		
Contribution to the Paper	This author contributed in providing funding and supervising the project.		
Signature		Date	1 July 2019

Name of Co-Author	Shi-Zhang Qiao		
Contribution to the Paper	This author contributed in providing funding and supervising the project.		
Signature		Date	1 July 2019

Please cut and paste additional co-author panels here as required.

Strain Effect in Bimetallic Electrocatalysts in the Hydrogen Evolution Reaction

Xuesi Wang,^{†,‡} Yihan Zhu,^{‡,‡} Anthony Vasileff,[†] Yan Jiao,[†] Shuangming Chen,[§] Li Song,[§] Bin Zheng,^{||} Yao Zheng,^{*,†} and Shi-Zhang Qiao^{*,†}

[†]School of Chemical Engineering, The University of Adelaide, Adelaide, SA 5005, Australia

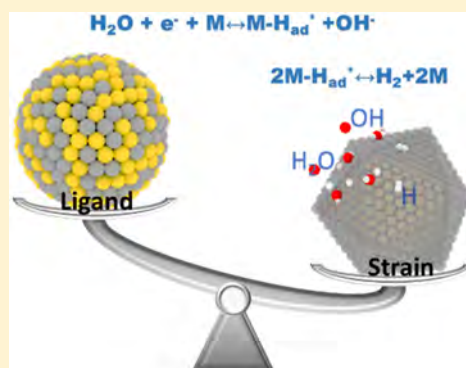
[‡]Department of Chemical Engineering, Zhejiang University of Technology, Hangzhou 310014, China

[§]National Synchrotron Radiation Laboratory, University of Science and Technology of China, Hefei 230029, China

^{||}School of Materials Science and Engineering, Xi'an University of Science and Technology, Xi'an 710054, China

Supporting Information

ABSTRACT: Unravelling the electrocatalytic activity origins of bimetallic nanomaterials is of great importance, yet fundamentally challenging. One of the main reasons for this is that the interactive contributions from geometric and electronic effects to enhancements in reaction activity are difficult to distinguish from one another. Here, on well-defined Ru–Pt core–shell (Ru@Pt) and homogeneous alloy (RuPt) model electrocatalysts, we are able to isolate these two effects. Furthermore, we observe the dominant role of strain in the intrinsic activity of the alkaline hydrogen evolution reaction. In the Ru@Pt icosahedral nanostructure, the highly strained Pt shells effectively accommodate the interfacial lattice mismatch from a face-centered cubic structured Ru core. This unique property leads to a weak binding of hydrogen and optimal interaction with hydroxyl species during the reaction, thus leading to an enhanced apparent activity of Ru@Pt.



Platinum (Pt)-based materials have shown unique and incomparable catalytic activities for a range of electrocatalytic processes such as the oxygen reduction reaction and hydrogen evolution reaction (HER) in acidic conditions.^{1–5} However, Pt is inefficient in some critical renewable energy-related processes, such as the HER in alkaline environments, which is the half-reaction in promising photoelectrocatalytic water-splitting technologies.^{6–8} The kinetics of alkaline HER on Pt are usually several orders of magnitude lower than that in acidic environments.^{9–11} In this regard, Pt-based alloys (e.g., Ni–Pt and Ru–Pt) have been developed to enhance the alkaline HER activity of Pt by introducing a secondary active site for synergistic catalysis.^{12–14} However, it is hard to identify the origin of the activity enhancement in these materials as both chemical composition (ligands) and physical structure (strain) effects always contribute interactively.^{13,15} As a result, tailoring alloys with precise control of these features is key to identifying the relationship between their physicochemical properties and catalytic performances for future rational electrocatalyst design.

In a bimetallic system, the ligand effect occurs when electrons transfer between two different atom groups and cause changes in the electronic band structures. The strain effect arises when the surface atom geometry is compressed or expanded. Theoretically, both of these effects can independently change the adsorbed states of reactive intermediates in the

reaction, thus affecting the overall activity of bimetallic electrocatalysts.^{16–18} Nevertheless, in practice, the strain and ligand effects work interactively in a certain bimetallic electrocatalyst, and this combination can have either a positive or negative influence on its catalytic activity.^{19–24} As a result, the coexistence of these two effects obscures the origin of the overall activity for these materials, especially for reactions involving several different reactive species. More importantly, a comprehensive understanding of the reaction mechanisms on most bimetallic systems is still lacking.

The HER in alkaline solutions ($2\text{H}_2\text{O} + 2\text{e}^- \rightarrow \text{H}_2 + 2\text{OH}^-$) is an ideal model reaction for investigating the above issue as it involves complex reactive species. The reaction pathway can be described as an initial water dissociation process (Volmer step: $\text{H}_2\text{O} + \text{e}^- \leftrightarrow \text{H}_{\text{ad}} + \text{OH}^-$), which produces reactive hydrogen (H_{ad}), followed by either the Heyrovsky ($\text{H}_2\text{O} + \text{H}_{\text{ad}} + \text{e}^- \leftrightarrow \text{H}_2 + \text{OH}^-$) or Tafel ($2\text{H}_{\text{ad}} \leftrightarrow \text{H}_2$) step to generate molecular hydrogen product.²⁵ Clearly, the alkaline HER activity is strongly affected by the binding ability of the electrocatalyst surface with H and/or OH species.^{26–28} To fully understand the nature of alkaline HER catalysis on bimetallic electrocatalysts, it is important to construct direct relationships

Received: March 21, 2018

Accepted: April 27, 2018

Published: April 27, 2018

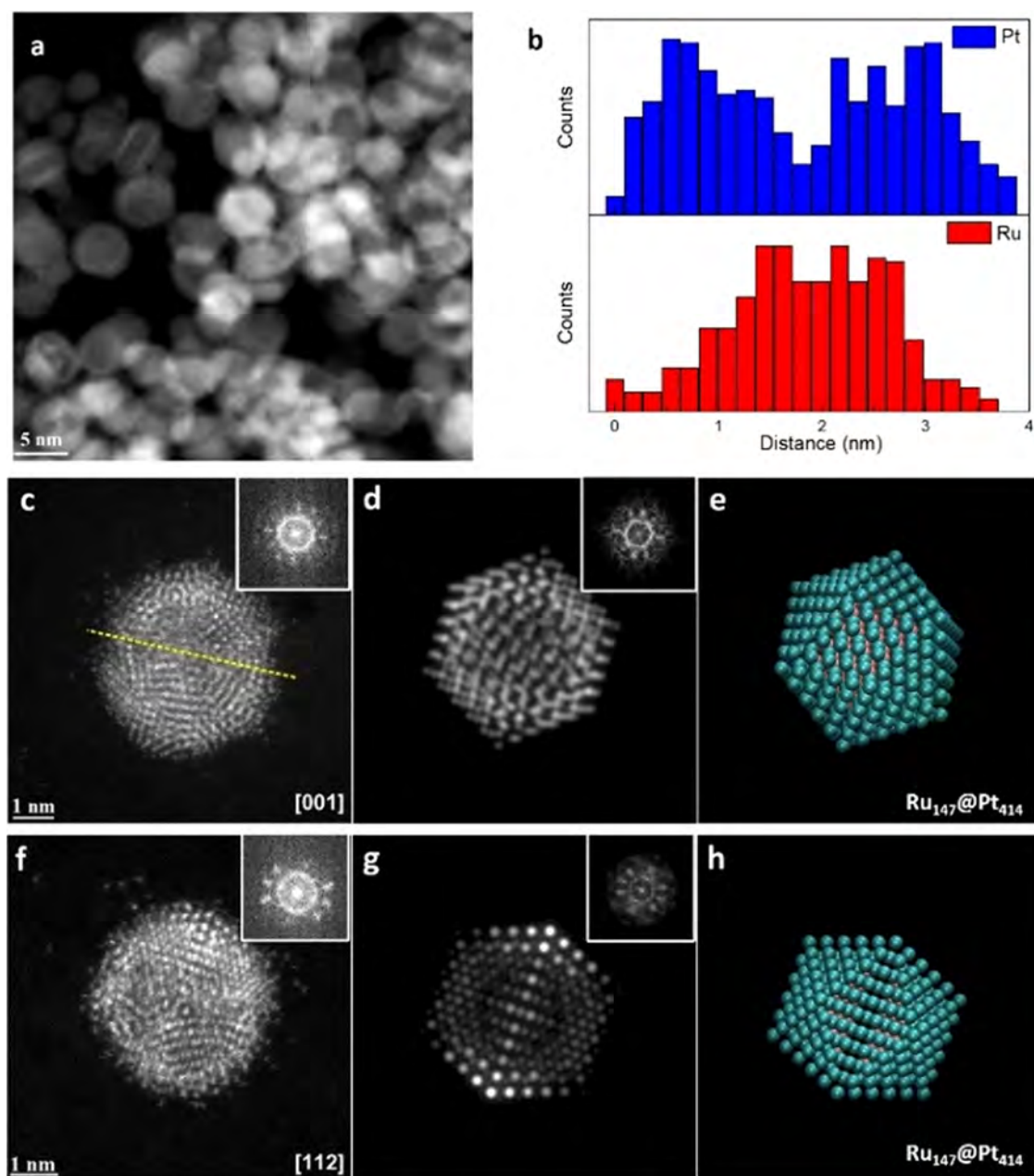


Figure 1. (a) HRSTEM image of Ru@Pt nanoparticles. (b) EDX line profiles of Pt L-edge and Ru K-edge signals from the yellow dashed line in panel c. Experimental (c, f) and simulated (d, g) HRSTEM images of individual Ru@Pt nanoparticles along [001] and [112] axes. Insets are corresponding diffractograms. (e, h) The corresponding Ru₁₄₇@Pt₄₁₄ model structure of nanoparticles. In panel e, the particle is slightly off-axis (5.8°). The Pt and Ru atoms are depicted as cyan and brown spheres, respectively.

between the electrocatalyst's strain/ligand effect and its binding ability toward each reactive species. Therefore, developing well-defined electrocatalysts with isolated strain or ligand effects is key to revealing their activity origins.

Herein, we used a pair of well-characterized Ru–Pt model electrocatalysts with identical ligand effect but different surface geometries to uncover the mechanism responsible for their HER activity enhancement in alkaline conditions. With a highly compressive strained surface, the Ru@Pt core–shell nanostructure exhibited much higher activity than the conventional strain-free RuPt alloy. When compared to acidic HER, the strain-induced enhancement on HER activity is more prominent in alkaline solutions. Electrochemical characterizations indicated that the compressive strain on the Ru@Pt led

to better interaction toward both H reactive intermediates and OH spectator species, in turn promoting the overall HER activity. Therefore, we suggest that the surface strain of bimetallic electrocatalysts is a more dominant factor compared to the ligand effect for alkaline HER activity. Core–shell nanostructure exhibited much higher activity than the conventional strain-free RuPt alloy. When compared to acidic HER, the strain-induced enhancement on HER activity is more prominent in alkaline solutions. Electrochemical characterizations indicated that the compressive strain on the Ru@Pt led to better interaction toward both H reactive intermediates and OH spectator species, in turn promoting the overall HER activity. Therefore, we suggest that the surface strain of

bimetallic electrocatalysts is a more dominant factor compared to the ligand effect for alkaline HER activity.

The Ru@Pt nanoparticles with Ru core and Pt shell were synthesized by the thermal reduction of corresponding metal salts. The Ru cores were fabricated first in ethylene glycol, followed by coating with Pt shells by the reduction of a Pt chloride precursor (see experimental details in the [Supporting Information](#)).²⁹ The high-angle annular dark-field scanning transmission electron microscopy (HAADF-STEM) images illustrate the morphologies of the nanoparticles at low magnification, which had an average size of 4 nm ([Figure 1a](#)). The difference in contrast between the core and shell regions can be assigned to a Ru@Pt core-shell structure with an approximately 2 nm Ru core and 1 nm thick Pt shell, which was further confirmed by the energy dispersive X-ray (EDX) line profile in [Figure 1b](#). Further EDX mapping of the Pt M-edge and Ru L-edge shows a distinct boundary between the Pt shell and Ru core, with only a trace Ru signal detected in the Pt layer ([Figure S2b–d](#)). This indicates that only very few Ru atoms exist on the Pt surface. The atomic-resolution HAADF-STEM images of a randomly chosen individual nanoparticle indicated a multiply twinned structure ([Figures 1c,f](#) and [S1](#)), and the contrast closely resembles the simulated images from a Ru₁₄₇@Pt₄₁₄ icosahedron model structure projected along the [001] and [112] directions, respectively ([Figure 1d,e,g,h](#)). Additional HAADF-STEM images show that that nanoparticles have homogeneous structure and are uniform ([Figure S1](#)). In addition, the simulated fast Fourier transform (FFT) results of different orientations match well with their corresponding experimental ones (insets of [Figure 1c,d,f,g](#)). All of the above observations unambiguously show that the synthesized Ru–Pt bimetallic nanoparticles exhibit a Ru@Pt icosahedral core-shell structure, where the Pt shell grows epitaxially on the anomalous face-centered cubic (fcc) structured Ru core. Notably, Ru is well-known to be stable with a hexagonal close-packed (hcp) structure, while our previous work reported a crossover between hcp and fcc structures in Ru nanoparticles upon the metal–substrate interactions.³⁰ It is thus speculated that the formation of the fcc structured Ru core may result from the Pt/Ru interfacial interactions, which also introduces compressive strain in the Pt shell to accommodate the interfacial lattice mismatch. Because of the small thickness of the Pt shell, such strain would have a more pronounced effect on the outmost surface structure of the icosahedral nanoparticle. In contrast, the homogeneous RuPt alloy nanoparticles have perfect fcc crystalline structure and have strain-free surfaces ([Figure S2](#)). Unlike the Ru@Pt nanoparticles where Ru and Pt are segregated at different regions, PtRu alloy has a random occupation of Pt and Ru in the structure which greatly minimizes the strain. This is unambiguously proven by a geometric phase analysis (GPA) conducted on an individual PtRu alloy nanoparticle, as shown in [Figure S3](#), where rather small and uniform strain fluctuations throughout the whole particle can be observed for different strain components. Such distinction can also be observed from the X-ray powder diffraction (XRD) spectra of the two bimetal structures ([Figure S4](#)). As shown in [Figure S4](#), the materials are highly consistent with reported Ru fcc and Pt fcc structures (JCPDS No. 88-2333 and JCPDS No. 04-0802, respectively). Noticeably, the peaks for Ru@Pt are broader compared to that of the RuPt alloy. This broadening is most likely due to the highly strained Pt shells of the Ru@Pt nanoparticles.

These strain-induced structure variations in the Ru@Pt core-shell structure was then modeled by energetically minimizing and equilibrating a Ru₁₄₇@Pt₄₁₄ icosahedron model using molecular dynamics (MD) (see the [Supporting Information](#)). It is clear from the calculated radial distribution function (RDF) that the Ru core remains ordered and unstrained, exhibiting sharp RDF peaks, while the Pt shell and Pt–Ru interfacial regions are highly strained, exhibiting very broad peaks ([Figure 2a](#)). The weak first-shell RDF peak in

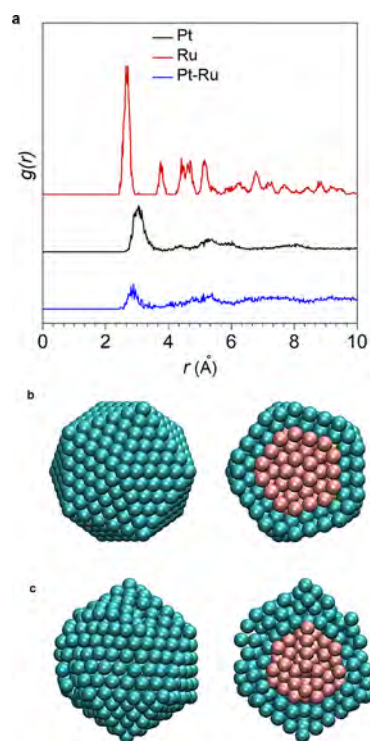


Figure 2. (a) Calculated RDF of Pt, Ru, and Pt–Ru atoms from the equilibrated Ru₁₄₇@Pt₄₁₄ model structure. Atomic structure models of (b) ideal and (c) equilibrated Ru₁₄₇@Pt₄₁₄ icosahedron.

the Pt shell corresponds to a relatively low average coordination number, arising from the formation of loosely bonded Pt sites on the surface and near-surface regions ([Figure 2b,c](#)), which are consistent with the experimental imaging results ([Figure 1c,f](#)).

The local lattice strain variations in the two different bimetallic nanostructures were also experimentally probed by extended X-ray absorption fine structure (EXAFS) spectroscopy. As shown in [Figure 3a](#), standard Pt foil has been used as a strain-free Pt control sample. When compared to Pt foil, the Pt–Pt peak of the RuPt alloy shows little shift, indicating a similar Pt–Pt atomic distance between materials. In comparison, the Ru@Pt sample has a very broad Pt–Pt peak, and both Pt–Ru and Pt–Pt peaks show negative shifts by 0.04 and 0.09 Å, respectively, compared to peaks of the RuPt alloy and standard Pt foil. This further supports the presence of a large compressive strain (~3% compared to RuPt alloy and Pt foil) in the Pt shells of the Ru@Pt nanoparticles as proposed on the basis of atomic-resolution imaging. Moreover, X-ray absorption near edge structure (XANES) spectroscopy was used to precisely study the electronic charge transfer induced by the modified ligand environment around the surface ([Figure 3b](#)). At the Pt L_{III}-edge, the white line (WL) of Ru@Pt nanoparticles has little shift compared to the RuPt alloy and

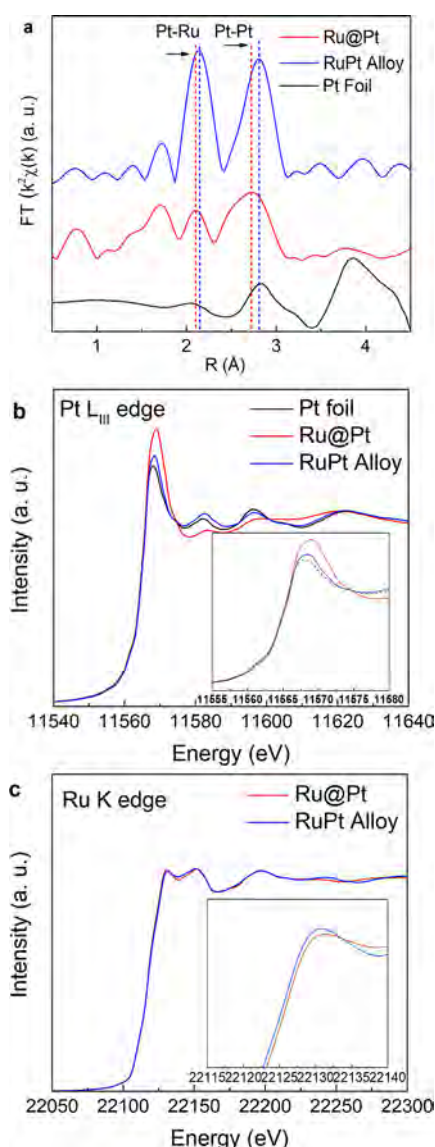


Figure 3. (a) Pt L_{III}-edge R-space EXAFS spectra of standard Pt foil, Ru@Pt, and RuPt alloy. (b) Pt L_{III}-edge and (c) Ru K-edge XANES spectra of Ru@Pt and RuPt alloy. The insets show the enlarged spectra at the Pt L_{III}-edge and Ru K-edge WL, respectively.

Pt foil, demonstrating that the three Pt-based materials had identical electron density. Also, at the Ru K-edge, there was a ~ 0.2 eV WL shift between the two bimetallic nanostructures, which may have been induced by the special electronic structure of the Ru fcc core structure in the core–shell sample compared to the conventional Ru hcp structure in the alloy sample (Figure 3c). Additionally, we observed an enhanced WL intensity of Pt L_{III}-edge for the Ru@Pt compared with the other two samples, which can be directly related to a higher unoccupied density of 5d states probably originating from the highly strained and loosely bonded Pt surface.³ Therefore, it is reasonable to assume that the ligand effect is negligible in this structure and that strain provides the dominant effect on the surface active sites.

To isolate the impact of strain effects toward H and/or OH adsorption in the alkaline HER process, a series of cyclic voltammograms (CVs) were recorded for three Pt-based electrocatalysts under both acid and alkaline environments. The bimetallic nanoparticles were loaded on carbon at a mass

fraction comparable to that of the commercial Pt/C ($\sim 20\%$; Figure S5). Notably, these samples showed very different underpotential-deposited hydrogen (H_{UPD}) adsorption–desorption behaviors, and such differences were more obvious in alkaline conditions (Figures 4a and S6). It is known that the

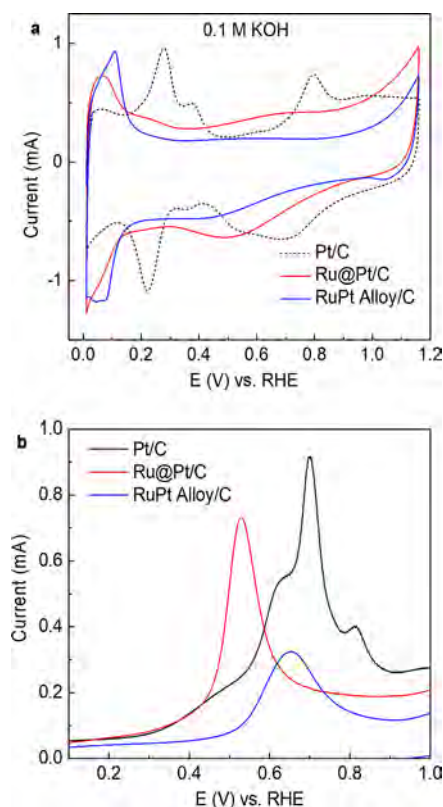


Figure 4. (a) CVs of various electrocatalysts in 0.1 M KOH showing the H_{UPD} adsorption–desorption peaks. (b) CO stripping curves of various electrocatalysts in 0.1 M KOH.

position of the H_{UPD} peaks are directly related to the hydrogen binding energy (HBE) of the catalytically active sites.³¹ For Pt-based materials, which always possess relatively strong hydrogen adsorption, a lower H_{UPD} peak potential indicates a weaker hydrogen binding. This generally facilitates H_2 product desorption, leading to an enhanced overall HER activity. At the same time, some studies have claimed that besides the reactive H_{ad} , the OH spectator is also considered to be a very important species for the HER in alkaline environments.^{32–34} Therefore, the OH adsorption–desorption behavior on these electrocatalysts was qualitatively studied by carbon monoxide (CO) stripping tests, where the electrocatalyst providing neither too weak nor too strong OH interaction will lead to an optimal CO electro-oxidation potential.^{35,36} As shown in Figure 4b, the CO oxidation potential of the three electrocatalysts downshifts as follows: Pt/C > RuPt alloy/C > Ru@Pt/C, demonstrating that the OH interaction with the electrocatalysts increases in the order of Pt/C < RuPt alloy/C < Ru@Pt/C. It is widely known that the favorable OH adsorption ability of Ru is considered to be the main reason for the significant HER performance of RuPt alloys in alkaline environments. Notably, in our study, the highly strained Pt shell in the Ru@Pt nanostructures exhibits even better interaction with OH intermediates than the RuPt alloy/C, achieving the lowest overpotential for CO oxidation.

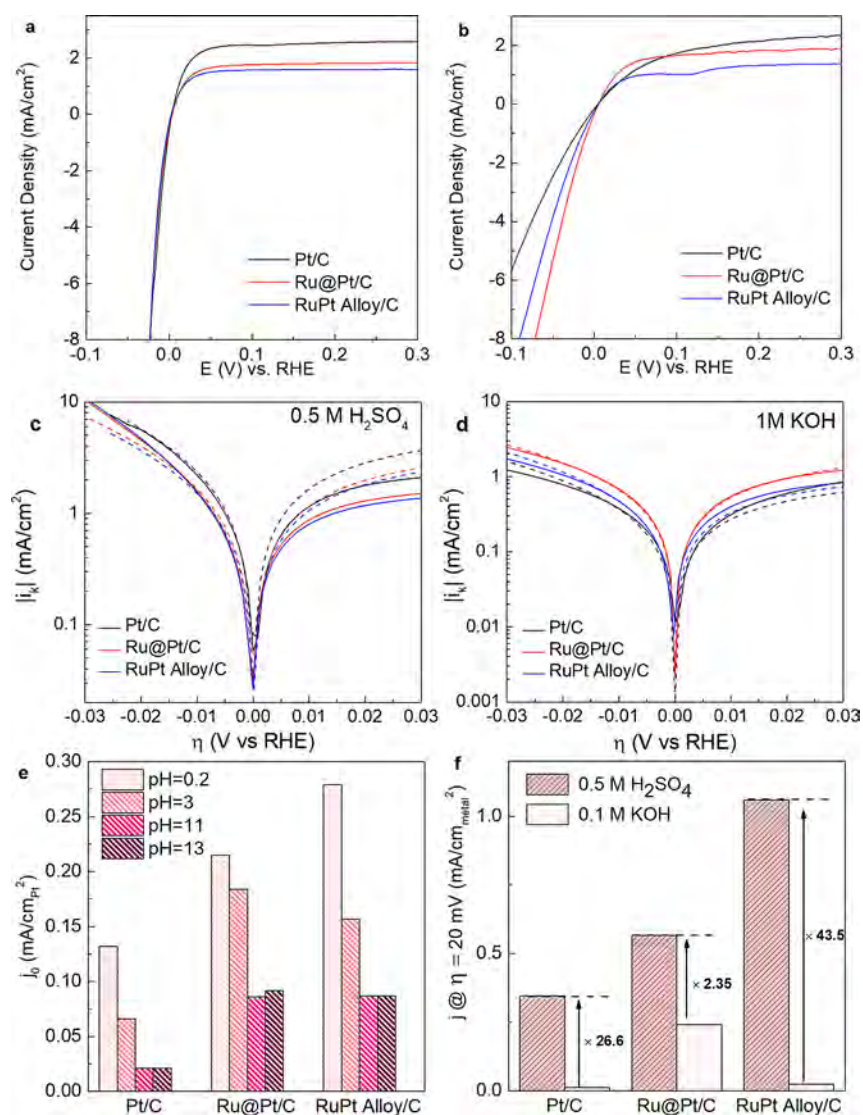


Figure 5. (a, b) IR-corrected HER polarization curves and (c, d) corresponding Tafel plots of various electrocatalysts in H₂-saturated electrolytes. The dotted lines indicate Butler–Volmer fitting. (e) Comparison of the ECSA-normalized current density of various electrocatalysts at different pH values. (f) Comparison of the ECSA-normalized current density of various electrocatalysts at an overpotential of 20 mV. The numbers indicate the scalar difference in current density between acidic and alkaline conditions.

Regarding apparent HER activity, in 0.5 M H₂SO₄, the polarization curves of the three electrocatalysts are very similar. However, in 0.1 M KOH, the activity clearly increases in the order Pt/C < RuPt alloy/C < Ru@Pt/C (Figure 5a,b). To further compare the HER kinetics of the different materials, the exchange current densities (j_0) and Tafel plots were obtained by fitting the calculated kinetic current (i_k) into the Butler–Volmer equation (see the detailed method in the Supporting Information). In 0.5 M H₂SO₄ conditions (Figure 5c), the Tafel slopes of the three electrocatalysts are very similar (around 30 mV/dec), indicating the rate-determining step (rds) is either the Heyrovsky step or the Tafel step. In contrast, there is a greater difference among the Tafel slopes of the three electrocatalysts in 0.1 M KOH conditions (Figure 5d), which are between 100 and 116 mV/dec, indicating that the water dissociation-related Volmer step is the rds for these electrocatalysts in alkaline conditions.

Furthermore, we measured the electrochemical surface area (ECSA)-normalized j_0 of the three electrocatalysts in various electrolytes with a wide range of pH values (Figures 5e and

S7–S12). As expected, the values of j_0 on all electrocatalysts decreased with an increase in pH. For example, when the pH increased from 0.2 to 3, the j_0 of Pt/C and RuPt alloy/C decreased by about half, while on Ru@Pt/C it decreased by 14.3%. Additionally, the j_0 changed very little when the pH increased from 11 to 13, consistent with previous reports on pure Pt electrocatalysts.³⁷ It is known that the HBE of Pt active sites increases (more positive) with decreasing H⁺ concentration in solution.³⁸ For Ru@Pt, the compressive lattice strain and loosely bonded Pt surface led to a relatively weaker hydrogen-binding strength compared to the RuPt alloy and pure Pt.³ Therefore, it is likely that its overall activity is comparatively less influenced by a decreased concentration of hydrogen species. Additionally, as indicated by the Tafel slopes, the water dissociation process becomes critical for the reaction kinetics of all three electrocatalysts in alkaline conditions. Despite the direct assistance of exposed Ru, which has a very low water dissociation barrier, the HER kinetics of the RuPt alloy is still lower than that of Ru@Pt with only Pt being exposed (Figure 5e). Therefore, we conclude that the

enhancement to alkaline HER activity is due to the compressive strain on the Pt surface rather than Ru. Noticeably, the stability test indicates that the performance of Ru@Pt is more stable than that of the alloy structure (Figure S13). This proves that the activity enhancement introduced by compressive strain of the Ru@Pt structure could be applied in long-term reactions.

Additionally, such strain-induced activity improvement on Ru@Pt/C in alkaline electrolyte is more significant under an applied overpotential (e.g., 20 mV) than that at the equilibrium potential. For example, the apparent HER current density gap between acidic and alkaline conditions for Ru@Pt/C is much smaller than those on the other strain-free Pt-based samples (Figure 5f). It should be noted that at such conditions, the overpotential-deposited H (H_{OPD}) becomes the dominant adsorbate in the HER pathway, which was proven to be closely related to the H_{UPD} species and to be more dependent on the electrocatalyst surface geometry.^{39,40} This indicates that strategies involving surface strain engineering should have significant influence toward both H_{UPD} and H_{OPD} sorption, and also toward reactive OH species. The cumulative effects of this should likely lead to improvements in the apparent alkaline HER activity.

In conclusion, by using the well-characterized Ru@Pt core-shell and homogeneous RuPt alloy model electrocatalysts, we evaluated the origin of the alkaline HER activity enhancement on bimetallic materials. With high compressive strain, the Ru@Pt has optimized adsorption-desorption energetics toward H intermediates and OH spectator species compared to an analogous RuPt alloy electrocatalyst with identical ligand effect but without strain. This highly strained structure was found to have significantly better HER activity in alkaline conditions. We also provided strong evidence that in alkaline conditions, strain in bimetallic electrocatalysts plays a more dominant role in the HER kinetics compared to the ligand effect. Such a strategy may direct the future design of more bimetallic electrocatalysts for other multistep reactions with complex reactive species (e.g., H and OH), such as the CO_2 reduction and N_2 reduction reactions.

■ ASSOCIATED CONTENT

Supporting Information

The Supporting Information is available free of charge on the ACS Publications website at DOI: 10.1021/acsenergylett.8b00454.

Experimental section of electrochemical tests, parameterized potentials and molecular dynamics simulation of the samples, TEM images, thermogravimetric analysis, and electrocatalytic data (PDF)

■ AUTHOR INFORMATION

Corresponding Authors

*E-mail: s.qiao@adelaide.edu.au.

*E-mail: yao.zheng01@adelaide.edu.

ORCID

Xuesi Wang: 0000-0002-2477-8111

Yan Jiao: 0000-0003-1329-4290

Li Song: 0000-0003-0585-8519

Bin Zheng: 0000-0002-5062-5637

Yao Zheng: 0000-0002-2411-8041

Shi-Zhang Qiao: 0000-0002-4568-8422

Author Contributions

[†]X.W. and Y.Z. contributed equally to this work.

Notes

The authors declare no competing financial interest.

■ ACKNOWLEDGMENTS

We gratefully acknowledge the Shanghai Synchrotron Radiation Facility for X-ray absorption spectroscopy characterizations. Y. Z. and S. -Z. Q. acknowledge financial support from the Australian Research Council through Discovery and Linkage Project programs (DP160104866, DP170104464, LP160100927, DE160101163, and FL170100154). Y. Z. acknowledges financial support from the Thousand Talents Program for Distinguished Young Scholars, National Natural Science Foundation of China (51701181) and the Zhejiang Provincial Natural Science Foundation of China (LR18B030003).

■ REFERENCES

- (1) Marković, N.; Schmidt, T.; Stamenković, V.; Ross, P. Oxygen Reduction Reaction on Pt and Pt Bimetallic Surfaces: A Selective Review. *Fuel Cells* **2001**, *1*, 105–116.
- (2) Yu, W.; Porosoff, M. D.; Chen, J. G. Review of Pt-Based Bimetallic Catalysis: From Model Surfaces to Supported Catalysts. *Chem. Rev.* **2012**, *112*, 5780–817.
- (3) Cheng, N.; Stambula, S.; Wang, D.; Banis, M. N.; Liu, J.; Riese, A.; Xiao, B.; Li, R.; Sham, T. K.; Liu, L. M.; et al. Platinum Single-Atom and Cluster Catalysis of the Hydrogen Evolution Reaction. *Nat. Commun.* **2016**, *7*, 13638.
- (4) Bing, Y.; Liu, H.; Zhang, L.; Ghosh, D.; Zhang, J. Nanostructured Pt-Alloy Electrocatalysts for PEM Fuel Cell Oxygen Reduction Reaction. *Chem. Soc. Rev.* **2010**, *39*, 2184–2202.
- (5) Bockris, J.; Ammar, I.; Huq, A. The Mechanism of the Hydrogen Evolution Reaction on Platinum, Silver and Tungsten Surfaces in Acid Solutions. *J. Phys. Chem.* **1957**, *61*, 879–886.
- (6) Walter, M. G.; Warren, E. L.; McKone, J. R.; Boettcher, S. W.; Mi, Q.; Santori, E. A.; Lewis, N. S. Solar Water Splitting Cells. *Chem. Rev.* **2010**, *110*, 6446–6473.
- (7) Cook, T. R.; Dogutan, D. K.; Reece, S. Y.; Surendranath, Y.; Teets, T. S.; Nocera, D. G. Solar Energy Supply and Storage for the Legacy and Nonlegacy Worlds. *Chem. Rev.* **2010**, *110*, 6474–6502.
- (8) Miller, E. Photoelectrochemical Water Splitting. *Energy Environ. Sci.* **2015**, *8*, 2809–2810.
- (9) Durst, J.; Siebel, A.; Simon, C.; Hasché, F.; Herranz, J.; Gasteiger, H. A. New Insights into the Electrochemical Hydrogen Oxidation and Evolution Reaction Mechanism. *Energy Environ. Sci.* **2014**, *7*, 2255–2260.
- (10) Sheng, W.; Gasteiger, H. A.; Shao-Horn, Y. Hydrogen Oxidation and Evolution Reaction Kinetics on Platinum: Acid vs Alkaline Electrolytes. *J. Electrochem. Soc.* **2010**, *157*, B1529–B1536.
- (11) Markovića, N. M.; Sarraf, S. T.; Gasteiger, H. A.; Ross, P. N. Hydrogen Electrochemistry on Platinum Low-Index Single-Crystal Surfaces in Alkaline Solution. *J. Chem. Soc., Faraday Trans.* **1996**, *92*, 3719–3725.
- (12) Scofield, M. E.; Zhou, Y.; Yue, S.; Wang, L.; Su, D.; Tong, X.; Vukmirovic, M. B.; Adzic, R. R.; Wong, S. S. Role of Chemical Composition in the Enhanced Catalytic Activity of Pt-Based Alloyed Ultrathin Nanowires for the Hydrogen Oxidation Reaction Under Alkaline Conditions. *ACS Catal.* **2016**, *6*, 3895–3908.
- (13) Wang, Y.; Wang, G.; Li, G.; Huang, B.; Pan, J.; Liu, Q.; Han, J.; Xiao, L.; Lu, J.; Zhuang, L. Pt–Ru Catalyzed Hydrogen Oxidation in Alkaline Media: Oxophilic Effect or Electronic Effect? *Energy Environ. Sci.* **2015**, *8*, 177–181.
- (14) Strmcnik, D.; Uchimura, M.; Wang, C.; Subbaraman, R.; Danilovic, N.; van der Vliet, D.; Paulikas, A. P.; Stamenkovic, V. R.; Markovic, N. M. Improving the Hydrogen Oxidation Reaction Rate by Promotion of Hydroxyl Adsorption. *Nat. Chem.* **2013**, *5*, 300–306.

- (15) Ledezma-Yanez, I.; Wallace, W. D. Z.; Sebastián-Pascual, P.; Climent, V.; Feliu, J. M.; Koper, M. T. M. Interfacial Water Reorganization as a pH-Dependent Descriptor of the Hydrogen Evolution Rate on Platinum Electrodes. *Nat. Energy* **2017**, *2*, 17031.
- (16) Kitchin, J. R.; Norskov, J. K.; Barteau, M. A.; Chen, J. G. Role of Strain and Ligand Effects in the Modification of the Electronic and Chemical Properties of Bimetallic Surfaces. *Phys. Rev. Lett.* **2004**, *93*, 156801.
- (17) Luo, M.; Guo, S. J. Strain-Controlled Electrocatalysis on Multimetallic Nanomaterials. *Nat. Rev. Mater.* **2017**, *2*, 17059.
- (18) Suo, Y.; Zhuang, L.; Lu, J. First-Principles Considerations in the Design of Pd-Alloy Catalysts for Oxygen Reduction. *Angew. Chem., Int. Ed.* **2007**, *46*, 2862–2864.
- (19) Chen, M.; Kumar, D.; Yi, C.-W.; Goodman, D. W. The Promotional Effect of Gold in Catalysis by Palladium-Gold. *Science* **2005**, *310*, 291–293.
- (20) Rodriguez, J. A.; Goodman, D. W. The Nature of the Metal-Metal Bond in Bimetallic Surfaces. *Science* **1992**, *257*, 897–903.
- (21) Wang, H.; Xu, S.; Tsai, C.; Li, Y.; Liu, C.; Zhao, J.; Liu, Y.; Yuan, H.; Abild-Pedersen, F.; Prinz, F. B.; et al. Direct and Continuous Strain Control of Catalysts with Tunable Battery Electrode Materials. *Science* **2016**, *354*, 1031–1036.
- (22) Strasser, P.; Koh, S.; Anniyev, T.; Greeley, J.; More, K.; Yu, C.; Liu, Z.; Kaya, S.; Nordlund, D.; Ogasawara, H.; et al. Lattice-Strain Control of the Activity in Dealloyed Core-Shell Fuel Cell Catalysts. *Nat. Chem.* **2010**, *2*, 454–460.
- (23) Wang, X.; Choi, S. I.; Roling, L. T.; Luo, M.; Ma, C.; Zhang, L.; Chi, M.; Liu, J.; Xie, Z.; Herron, J. A.; et al. Palladium-Platinum Core-Shell Icosahedra with Substantially Enhanced Activity and Durability Towards Oxygen Reduction. *Nat. Commun.* **2015**, *6*, 7594.
- (24) Gorin, D. J.; Sherry, B. D.; Toste, F. D. Ligand Effects in Homogeneous Au Catalysis. *Chem. Rev.* **2008**, *108*, 3351–3378.
- (25) Stamenkovic, V. R.; Strmcnik, D.; Lopes, P. P.; Markovic, N. M. Energy and Fuels from Electrochemical Interfaces. *Nat. Mater.* **2017**, *16*, 57–69.
- (26) Clark, E. L.; Hahn, C.; Jaramillo, T. F.; Bell, A. T. Electrochemical CO₂ Reduction over Compressively Strained CuAg Surface Alloys with Enhanced Multi-Carbon Oxygenate Selectivity. *J. Am. Chem. Soc.* **2017**, *139*, 15848–15857.
- (27) Liu, F.; Wu, C.; Yang, S. Strain and Ligand Effects on CO₂ Reduction Reactions over Cu–Metal Heterostructure Catalysts. *J. Phys. Chem. C* **2017**, *121*, 22139–22146.
- (28) Mahmood, J.; Li, F.; Jung, S. M.; Okyay, M. S.; Ahmad, I.; Kim, S. J.; Park, N.; Jeong, H. Y.; Baek, J. B. An Efficient and pH-Universal Ruthenium-Based Catalyst for the Hydrogen Evolution Reaction. *Nat. Nanotechnol.* **2017**, *12*, 441–446.
- (29) Alayoglu, S.; Nilekar, A. U.; Mavrikakis, M.; Eichhorn, B. Ru-Pt Core-Shell Nanoparticles for Preferential Oxidation of Carbon Monoxide in Hydrogen. *Nat. Mater.* **2008**, *7*, 333–338.
- (30) Zheng, Y.; Jiao, Y.; Zhu, Y.; Li, L. H.; Han, Y.; Chen, Y.; Jaroniec, M.; Qiao, S. Z. High Electrocatalytic Hydrogen Evolution Activity of an Anomalous Ruthenium Catalyst. *J. Am. Chem. Soc.* **2016**, *138*, 16174–16181.
- (31) Sheng, W.; Myint, M.; Chen, J. G.; Yan, Y. Correlating the Hydrogen Evolution Reaction Activity in Alkaline Electrolytes with the Hydrogen Binding Energy on Monometallic Surfaces. *Energy Environ. Sci.* **2013**, *6*, 1509–1512.
- (32) Zheng, Y.; Jiao, Y.; Vasileff, A.; Qiao, S. Z. Hydrogen Evolution Reaction in Alkaline Solution: From Theory, Single Crystal Models, to Practical Electrocatalysts. *Angew. Chem., Int. Ed.* **2017**, DOI: 10.1002/anie.201710556.
- (33) Subbaraman, R.; Tripkovic, D.; Strmcnik, D.; Chang, K.-C.; Uchimura, M.; Paulikas, A. P.; Stamenkovic, V.; Markovic, N. M. Enhancing Hydrogen Evolution Activity in Water Splitting by Tailoring Li⁺-Ni(OH)₂-Pt Interfaces. *Science* **2011**, *334*, 1256–1260.
- (34) Li, J.; Ghoshal, S.; Bates, M. K.; Miller, T. E.; Davies, V.; Stavitski, E.; Attenkofer, K.; Mukerjee, S.; Ma, Z. F.; Jia, Q. Experimental Proof of the Bifunctional Mechanism for the Hydrogen Oxidation in Alkaline Media. *Angew. Chem., Int. Ed.* **2017**, *56*, 15594–15598.
- (35) Subbaraman, R.; Tripkovic, D.; Chang, K.-C.; Strmcnik, D.; Paulikas, A. P.; Hirunsit, P.; Chan, M.; Greeley, J.; Stamenkovic, V.; Markovic, N. M. Trends in Activity for the Water Electrolyser Reactions on 3d M (Ni, Co, Fe, Mn) Hydr (oxy) oxide Catalysts. *Nat. Mater.* **2012**, *11*, 550.
- (36) Ochal, P.; Gomez de la Fuente, J. L.; Tsyppkin, M.; Seland, F.; Sunde, S.; Muthuswamy, N.; Rønning, M.; Chen, D.; Garcia, S.; Alayoglu, S.; et al. CO Stripping as an Electrochemical Tool for Characterization of Ru@Pt Core-Shell Catalysts. *J. Electroanal. Chem.* **2011**, *655*, 140–146.
- (37) Sheng, W.; Zhuang, Z.; Gao, M.; Zheng, J.; Chen, J. G.; Yan, Y. Correlating Hydrogen Oxidation and Evolution Activity on Platinum at Different pH with Measured Hydrogen Binding Energy. *Nat. Commun.* **2015**, *6*, 5848.
- (38) Zheng, J.; Sheng, W.; Zhuang, Z.; Xu, B.; Yan, Y. Universal Dependence of Hydrogen Oxidation and Evolution Reaction Activity of Platinum-Group Metals on pH and Hydrogen Binding Energy. *Sci. Adv.* **2016**, *2*, e1501602.
- (39) Barber, J.; Morin, S.; Conway, B. Specificity of the Kinetics of H₂ Evolution to the Structure of Single-Crystal Pt Surfaces, and the Relation Between OPD and UPD H. *J. Electroanal. Chem.* **1998**, *446*, 125–138.
- (40) Conway, B.; Barber, J.; Morin, S. Comparative Evaluation of Surface Structure Specificity of Kinetics of UPD and OPD of H at Single-Crystal Pt Electrodes. *Electrochim. Acta* **1998**, *44*, 1109–1125.

Supporting Information

Strain Effect in Bimetallic Electrocatalysts on the Hydrogen Evolution Reaction

Xuesi Wang,^{a†} Yihan Zhu,^{b†} Anthony Vasileff,^a Yan Jiao,^a Shuangming Chen,^c Li Song,^c Bin Zheng,^d Yao Zheng*^a and Shi-Zhang Qiao*^a

^a School of Chemical Engineering, The University of Adelaide, Adelaide SA 5005, Australia

^b Department of Chemical Engineering, Zhejiang University of Technology, Hangzhou 310014, China

^c National Synchrotron Radiation Laboratory, University of Science and Technology of China, Hefei 230029, China

^d School of Materials Science and Engineering, Xi'an University of Science and Technology, Xi'an 710054, China

* E-mail: s.qiao@adelaide.edu.au
yao.zheng01@adelaide.edu.au

† These authors contributed equally to this work.

I. Experimental Section

Chemical and materials

Commercialized Pt/C and carbon black (CB) were purchased from FuelCellStore without further treatment. All the other chemicals used in the experiments were purchased from Sigma-Aldrich Co. LLC.

Synthesis of the Ru@Pt nanoparticles

55 mg of polyvinylpyrrolidone (PVP, average mol wt 40,000) was first dissolved in 40 mL glycol in a 100 mL flask. 80 mg Ruthenium(III) acetylacetonate ($\text{Ru}(\text{acac})_3$) was added into the flask and the mixture was heated to 200 °C for 3 hours with constant stirring. Afterward, the suspension was cooled to room temperature and 54 mg platinum(II) chloride (PtCl_2) was added into the flask followed by another slow heating process to 200 °C. The suspension was then kept at 200 °C for 1.5 hours before cooled to room temperature.

Synthesis of RuPt alloy nanoparticles

51 mg tricarbonyldichlororuthenium(II) dimer $[\text{Ru}(\text{CO})_3\text{Cl}_2]_2$ and 79 mg platinum(II) acetylacetonate ($\text{Pt}(\text{acac})_2$) were added into 40 mL PVP solution under vigorous stirring. The mixture was heated to 200 °C and kept for 1.5 hours before cooled to room temperature. Both Ru@Pt and RuPt alloy nanoparticles were dialyzed in water for a week before further applications.

Preparation of electrocatalyst

First, 1 g CB was dispersed in 50 mL nitric acid (HNO_3) under ultrasound. The suspension was then heated for 12 hours in an 80 °C oil bath with reflux. The as prepared CB was then washed in water for multiple times until neutralized and freeze-dried before being used. Then, the acidic treated CB was added into a homogeneous water suspension with acetic acid (50 % volume ratio) and heated to 60 °C. Nanoparticles was then added into the suspension under stirring and the mixture was heated overnight before cooled to room temperature. The electrocatalyst was then washed until neutralized and freeze dried before collected. Finally, the dried product was heated to 250 °C first in a N_2 atmosphere for 4 hours, then in a 10 % H_2/Ar atmosphere for 3 hours. The final product had a metal loading rate at about 23.7 % (Figure S4).

Physical characterizations

Scanning transmission electron microscopy (STEM) and transmission electron microscopy (TEM) images were collected on a cubed Titan G2 80-300 Field-Emission-Gun electron microscope equipped with a Fischione model 3000 High-Angle-Annular-Dark-Field (HAADF) detector and a CEOS GmbH double-hexapole spherical-aberration corrector operating at 300 kV. HRSTEM simulations were carried out by using the qSTEM code developed by C. T. Koch (C. Koch, Ph.D.

Thesis, Arizona State University, 2002). Simulation conditions used: 300 kV; Cs = 10 μm ; Cc = 1 mm; $\Delta E = 0.7$ eV; $\Delta f = -6.1$ nm; $\alpha = 17$ mrad; inner/outer detector angle = 70/200 mrad; simulation window size (400 \times 400 pixels with 0.0075 nm point sampling). The Ru and Pt L3 edge XAFS spectra were recorded in transmission mode (Si 111) at the BL14W1 Endstation of Shanghai Synchrotron Radiation Facility (SSRF). The electron beam energy of the storage ring was 3.5 GeV with a maximum stored current of 300 mA. The data was normalized and analyzed using Athena.

Parameterize potentials for the Pt-Ru system

The Embedding-Atom method (EAM) potential,¹ as one of high-quality potential functions, was chosen to describe the Pt-Ru system here. In this potential function, the total energy of an alloy system can be expressed in the general form of

$$E_{tot} = \sum_i F_i(\rho_i(R_i)) + \sum_{i,j} \varphi(R_{ij})/2$$

where F is the embedding function, ρ defines the electron charge density and φ is the pair potential function. The indices i and j represent the embedded atom and the neighboring atom, respectively. The first term (F) is the embedding energy of i atom, reflecting the many body interactions via the atom i and its background electron charge density. The second term (φ) defines the pair interactions between atom i and j .

The EAM potential parameters were obtained by using the force-matching method² with the potfit package³⁻⁴. Target systems for fitting employed the configurations of Pt-Ru system, including clusters (Pt-Ru), face-centered-cubic crystals (Pt bulk and Pt-Ru alloy), and hcp (Ru) crystals. The cutoff radius is set to be 6.0 \AA through the entire fitting procedure. The accurate ab-initio calculations (VASP)⁵⁻⁶ were used to obtain all fitting configurations. In this method, the projector augmented wave (PAW) approach⁷⁻⁸ with the generalized gradient approximation (GGA) was chosen. The cut-off energy for the plane wave was set to 400 eV. To prevent any interaction between clusters, enough vacuum region in the x, y, and z directions was created.

Molecular dynamics (MD) simulation

The LAMMPS package⁹ was used to perform the molecular dynamics (MD) simulations. Firstly, an energy minimization based on the conjugate gradient (CG) algorithm was performed at zero temperature to guarantee the atomic positions during geometric optimization. Then, the system was thermally equilibrated at 300 K for 1 nanosecond, by using microcanonical ensemble (NVE) with a time step of 1 fs. The VMD software¹⁰ was applied to visualize the atomic structure.

Electrochemical measurements

All electrochemical measurements were conducted under identical conditions (20 $^{\circ}\text{C}$, atmospheric pressure). 2 mg electrocatalyst (20 % metal mass loading on carbon black) were homogeneously

dispersed in 1mL Nafion solution (0.05 %, water solution). 20 μ L of the electrocatalyst dispersion was then coated onto a glassy carbon rotating disk electrode (RDE, efficient surface area = 0.196 cm^2 , Pine Research Instrumentation) and dried in air.

All the electrochemical data were recorded by a CHI 760D bipotentiostat (CH Instruments, INC.). The reference electrode(RE) was an Ag/AgCl in 4 M KCl solution (0.205 V vs. reversible hydrogen electrode (RHE)). The working electrode is a glass carbon electrode with a surface area of 0.196 cm^2 . The counter electrode was a carbon rod. The electrolyte of different pH values was prepared by mixing 0.5 M H_2SO_4 or 0.1 M KOH with 0.5 M K_2SO_4 solution. The potentials reported in this work were referred to RHE through RHE calibration:

$$E_{RHE} = E_{Ag/AgCl} + 0.205 + 0.059 \times pH$$

Linear sweep voltammograms (LSVs) were carried out using an RDE at 1600 rpm under constant H_2 flow (50 mL/min) at a scan rate of 2 mV/s. All the LSV results were corrected by iR-compensation.

The electrocatalytic active surface area (ECSA) is calculated through CO stripping voltammetry tests. The CO stripping voltammetry tests were carry out with a N_2 flow (50 mL/min) being used at least 15 minutes before each test to purge the 0.5 M H_2SO_4 electrolyte. After the N_2 saturation, the working electrodes was lowered into the electrolyte for the first round of CV between -0.05 V and 1.20 V, sweeping at a scan rate of 0.01 V/s under rotation of 1600 rpm. Then the purge gas was switched to a CO (10 %) in argon gas mixture for 30 minutes, during which time a +0.06 V/RHE potential was applied on the electrode to ensure a full occupation of active sites. Another two CVs was then performed at a scan rate of 0.05 V/s. No CO oxidation could be observed in second CV, indicating a complete conversion of adsorbed CO.

The ECSA could be calculated using the function below:

$$\text{ECSA}_{(m^2/g,metal)} = \frac{Q_{CO}}{M_{metal} \times Q_{CO}^{theo}}$$

In the equation, Q_{CO} is the CO stripping charge, M_{metal} is the mass loading of the metal on the working electrode. Q_{CO}^{theo} is the theoretical value of Q_{CO} , which is 420 $\mu\text{C}/\text{cm}^2$ for a two-electron transfer of one CO molecule to a CO_2 per electrocatalyst atom. For commercial Pt/C, the underpotential deposited CO (CO_{UPD}) region is between 0.8 to 1 V vs. RHE. For Ru and Ru based nanomaterials, the CO_{UPD} region is between 0.5 to 0.8 V vs. RHE. The as calculated ECSA of Pt is 92 $\text{m}^2/\text{g}_{metal}$, within the reported range of Pt ECSA. The detailed ECSAs of Pt, Ru@Pt and RuPt alloy are as follow: Pt/C: 92 $\text{m}^2/\text{g}_{metal}$, Ru@Pt/C: 55 $\text{m}^2/\text{g}_{metal}$, RuPt alloy/C: 28 $\text{m}^2/\text{g}_{metal}$.

Exchange current density calculation

The electrocatalytic activity of HER are obtained using RDE measurement under 1600 rpm. To obtain the true kinetics of the reaction, the polarization curves are taken in H₂-saturated electrolyte. the kinetic current densities (j_k) are worked out through

$$\frac{1}{j} = \frac{1}{j_k} + \frac{1}{j_d} \#$$

where j , j_k and j_d are the measured current, kinetic current and diffusion limit current, respectively. While the HOR polarization curve is directly controlled by both kinetic and diffusion limit current, the HER current is commonly considered not limited by H⁺ transport, therefore, the diffusion current is not counted into the calculation. The j_0 of HER was obtained by fitting j_k into the Butler-Volmer equation

$$j_k = j_0 \left[\exp\left(\frac{\alpha F \eta}{RT}\right) - \exp\left(\frac{(\alpha - 1) F \eta}{RT}\right) \right] \#$$

Here α is the transfer coefficient, η is the overpotential, F is Faraday's constant, R is the universal gas constant and T is the thermodynamic temperature.

II. Supplementary Results

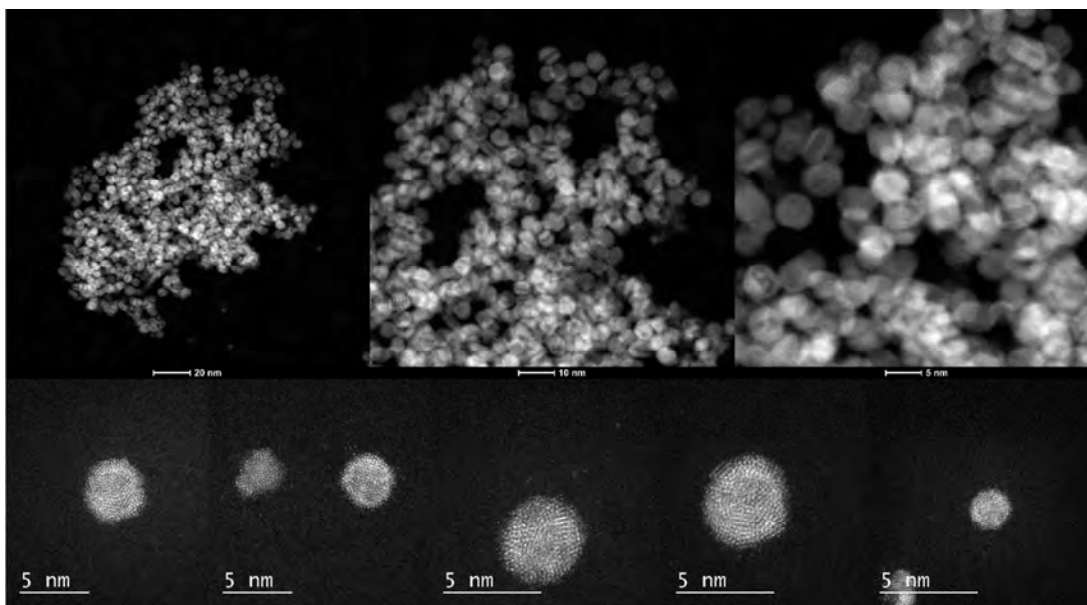


Figure S1. HRSTEM images of HAADF-STEM images of Ru@Pt nanoparticles at different scales (above) and several different individual Ru@Pt icosahedral nanoparticles from different angles (bottom).

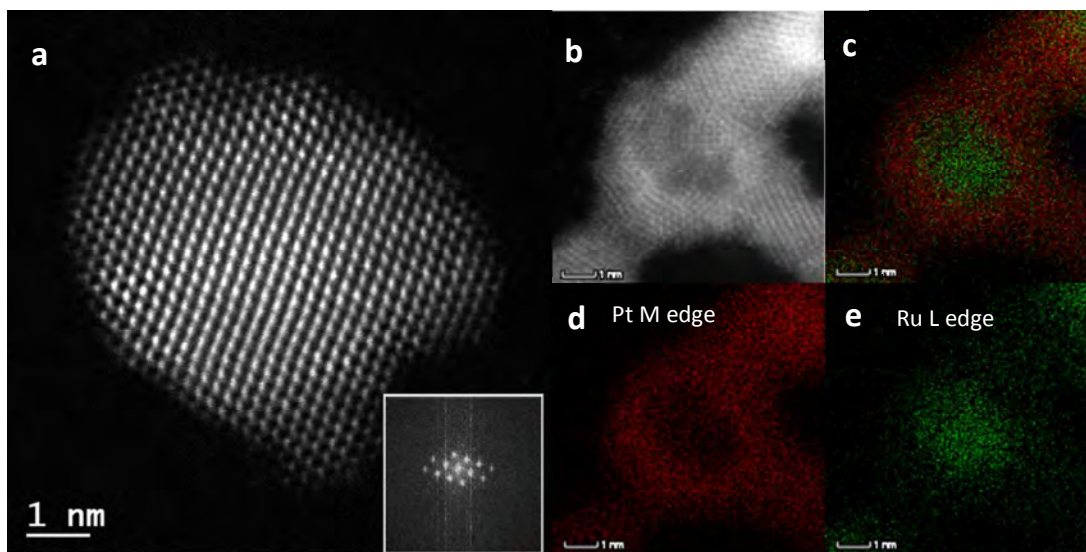


Figure. S2. (a). HRSTEM image of individual RuPt alloy nanoparticle and diffractogram (inset). (b). HAADF-STEM image of a randomly chosen Ru@Pt nanoparticle. (c)-(e). EDX mapping of: (c). combined Pt M edge and Ru L edge. (d). Pt M edge. (e). Ru L edge of a Ru@Pt nanoparticle.

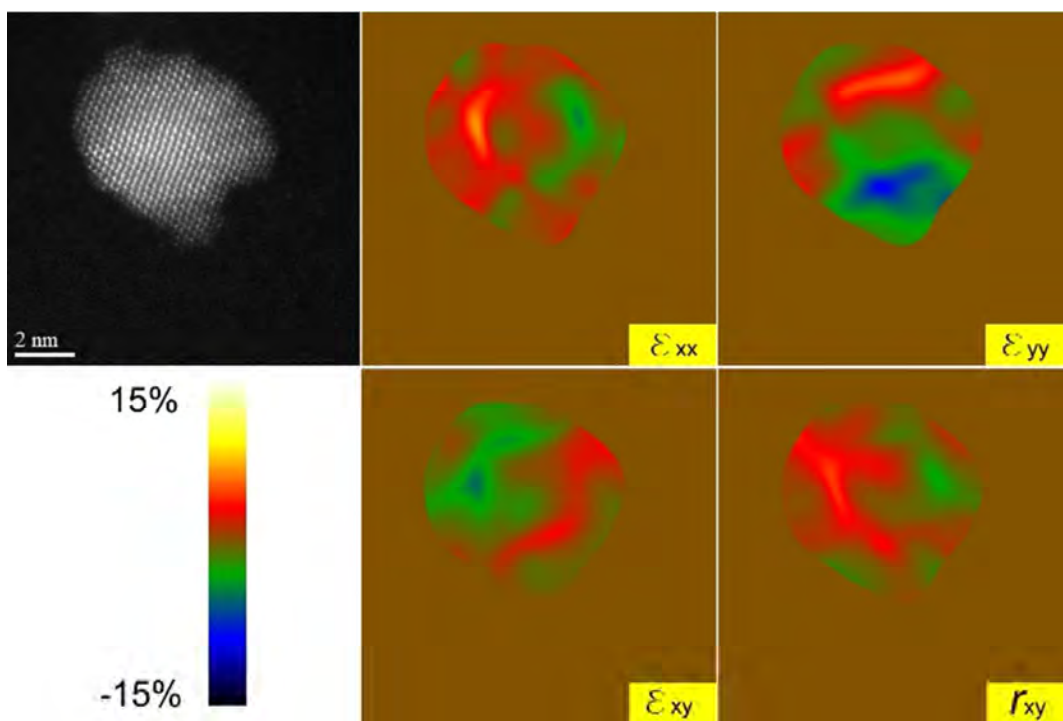


Figure S3. GPA strain analysis.

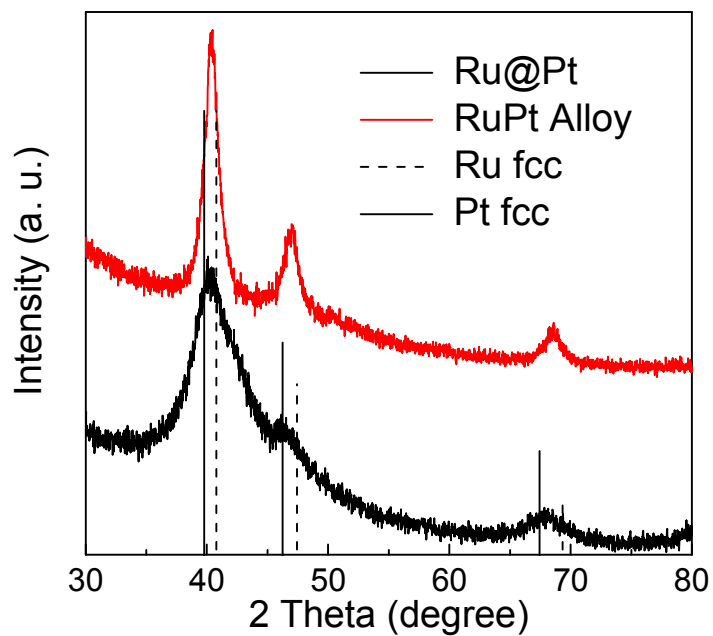


Figure. S4. XRD spectra of Ru@Pt and RuPt alloy nanoparticles. The drop lines indicate peaks for standard Ru fcc and Pt fcc structures.

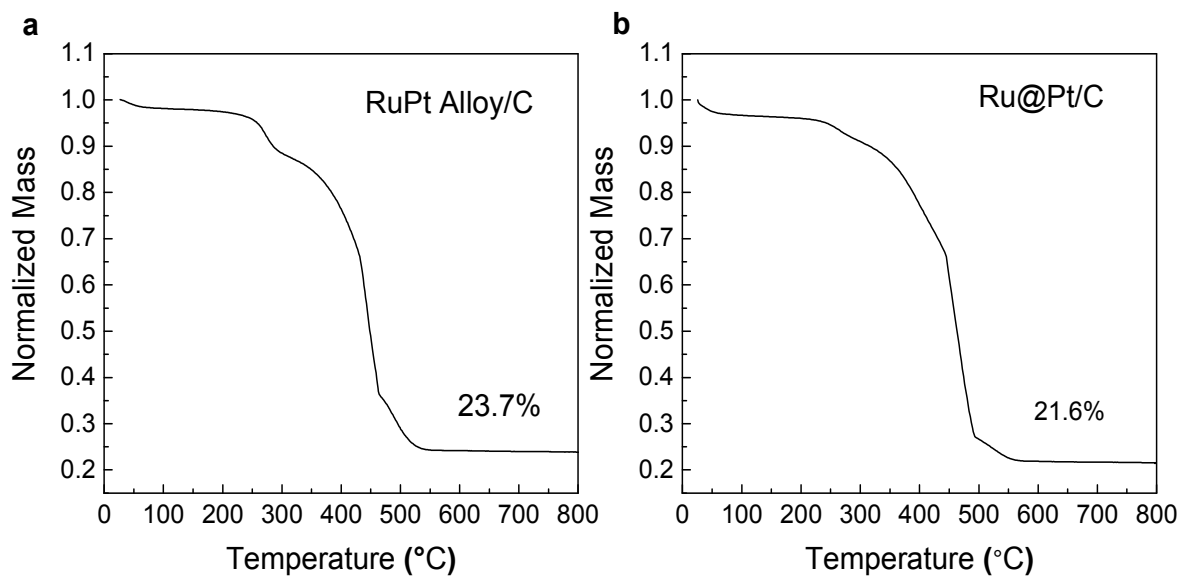


Figure. S5. Thermogravimetric analysis curve recorded in air for (a) RuPt alloy loaded on carbon. (b) Ru@Pt loaded on carbon.

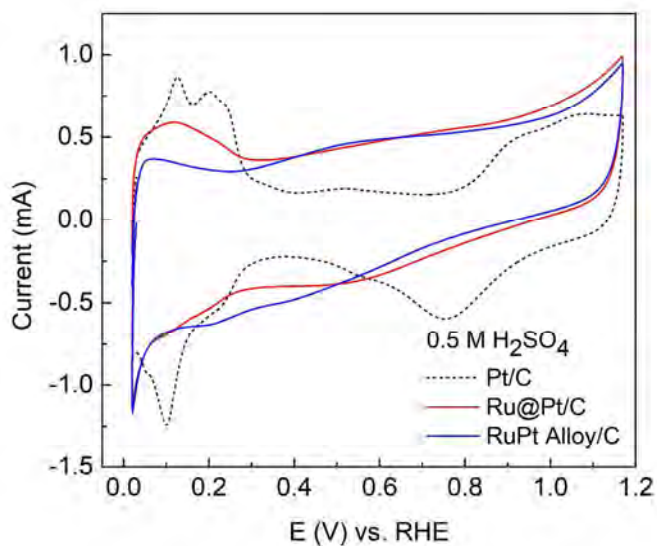


Figure. S6. Cyclic voltammograms of Pt/C (black) Ru@Pt/C (red) and RuPt alloy/C (blue) at a scan rate of 0.05 V/s in 0.5 M H₂SO₄.

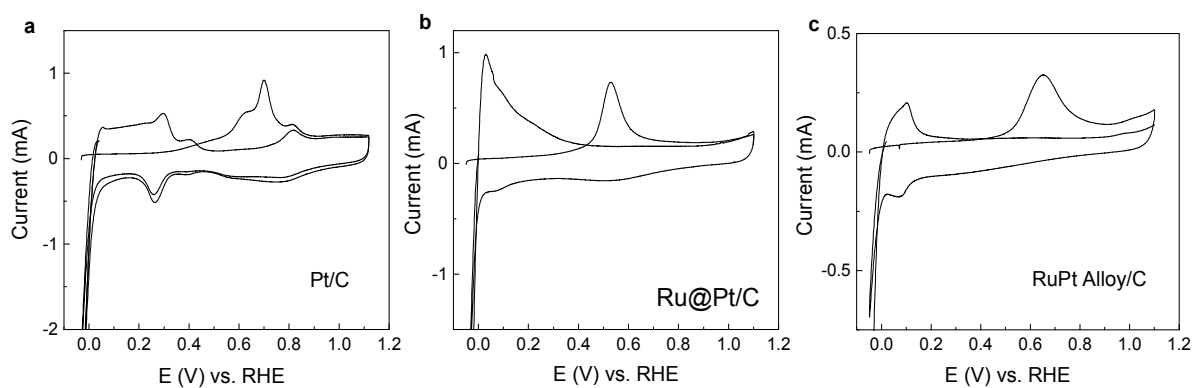


Figure. S7. (a-c). CO stripping investigation on various electrocatalysts: (a). Pt/C. (b). Ru@Pt/C. (c). RuPt alloy/C in 0.1 M KOH. The CO was fully pre-adsorbed on the electrocatalysts by immersing the electrode in 1 M KOH saturated with CO under potential control of 0.06 V (vs. RHE) for 20 minutes.

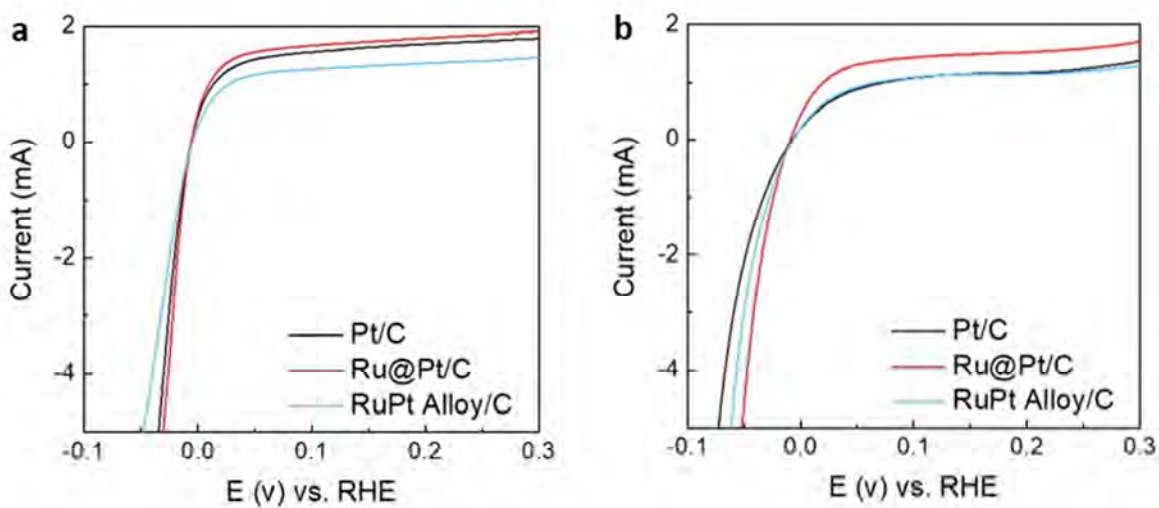


Figure. S8. HER polarization curves of various electrocatalysts in H_2 -saturated electrolyte. (a) sodium bicarbonate/sodium hydroxide buffer, pH = 11.2 (b) 1M KOH solution, pH = 13.5.

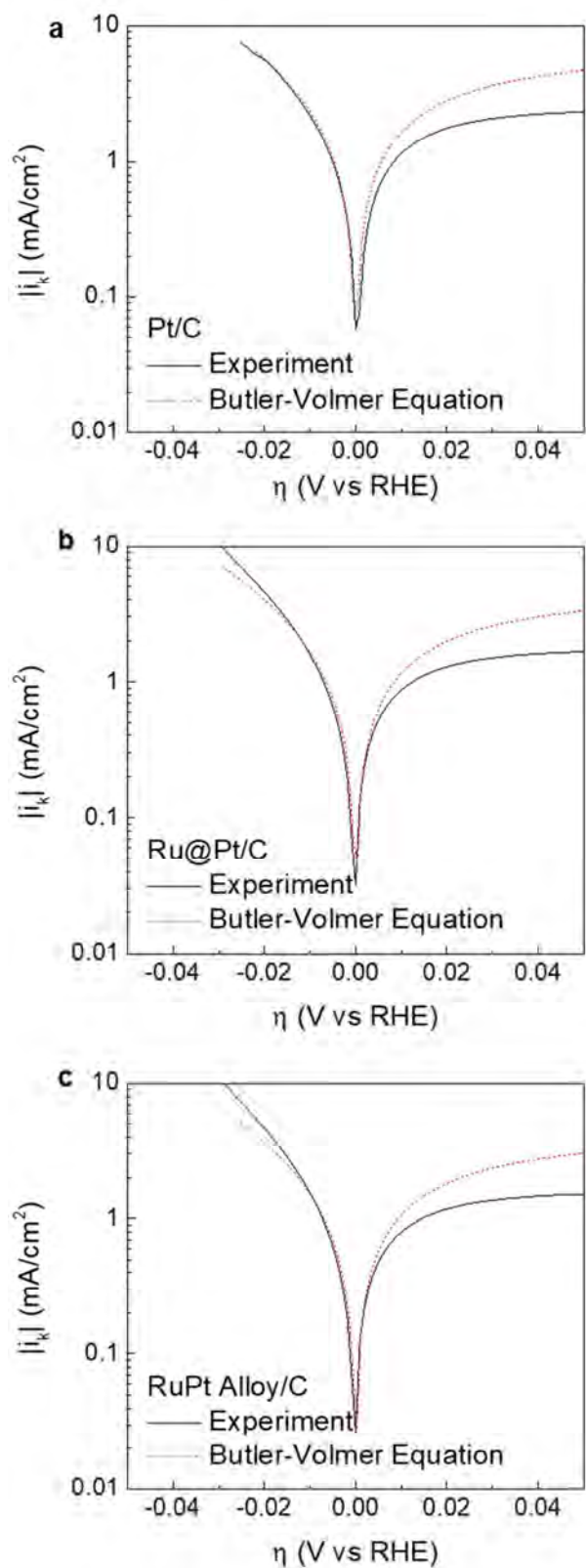


Figure. S9. From a to c: HER Tafel plots of the current density of Pt/C, Ru@Pt/C and RuPt alloy/C electrocatalysts in pH = 0.2 solution. The red line indicating Butler-Volmer fitting. The diffusion effect is not taken into count.

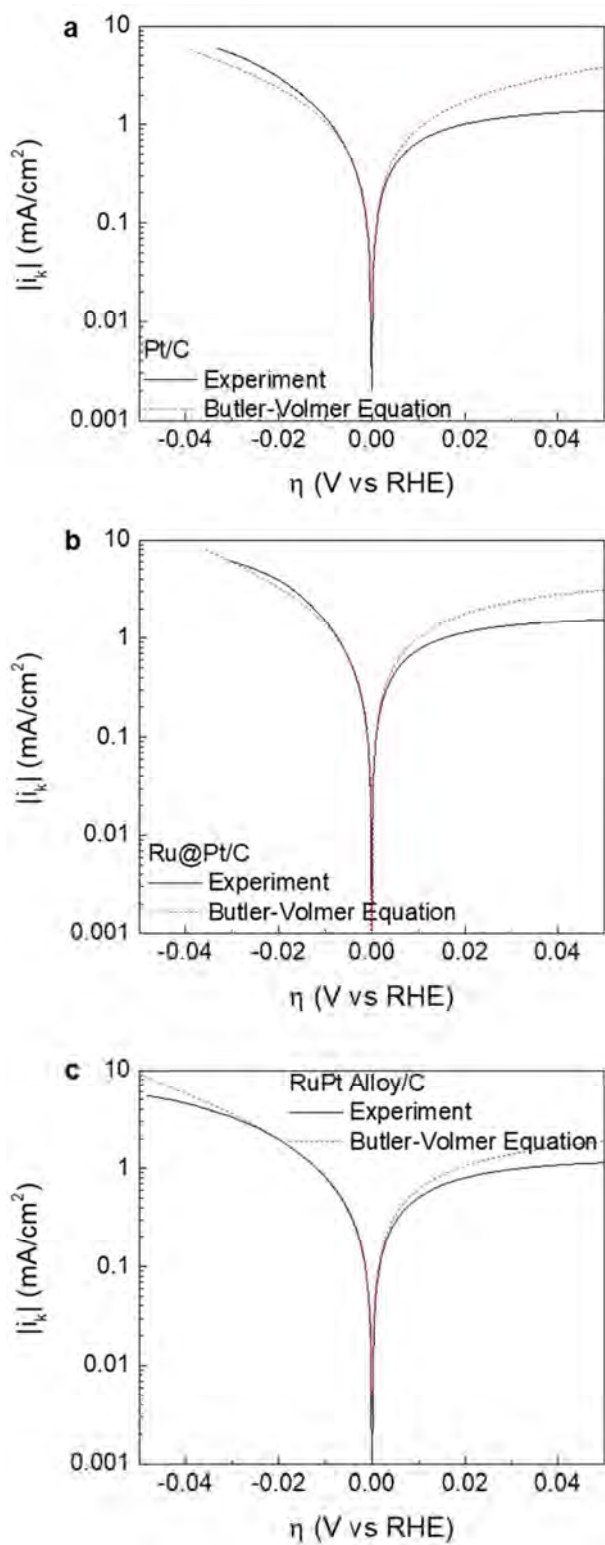


Figure. S10. From a to c: HER Tafel plots of the current density of Pt/C, Ru@Pt/C and RuPt alloy/C electrocatalysts in pH = 3 solution. The red line indicating Butler-Volmer fitting. The diffusion effect is not taken into count.

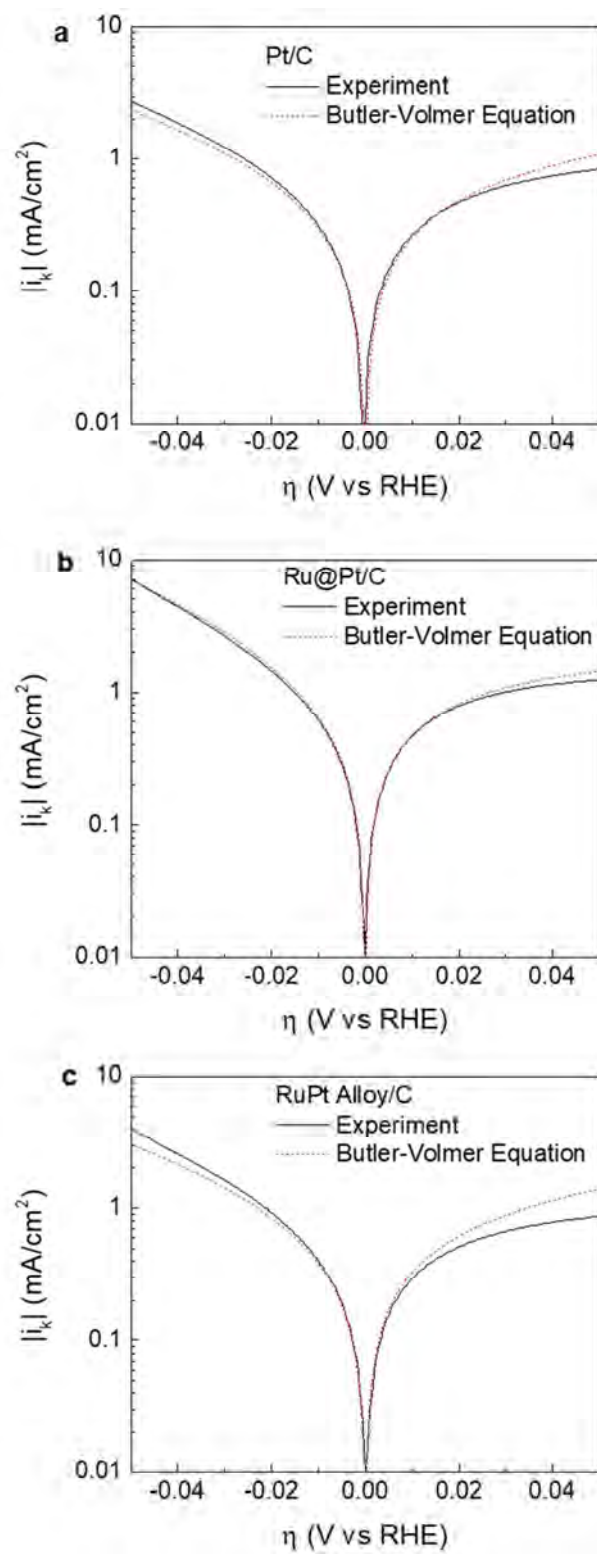


Figure. S11. From a to c: HER Tafel plots of the current density of Pt/C, Ru@Pt/C and RuPt alloy/C electrocatalysts in pH = 11 solution. The red line indicating Butler-Volmer fitting. The diffusion effect is not taken into count.

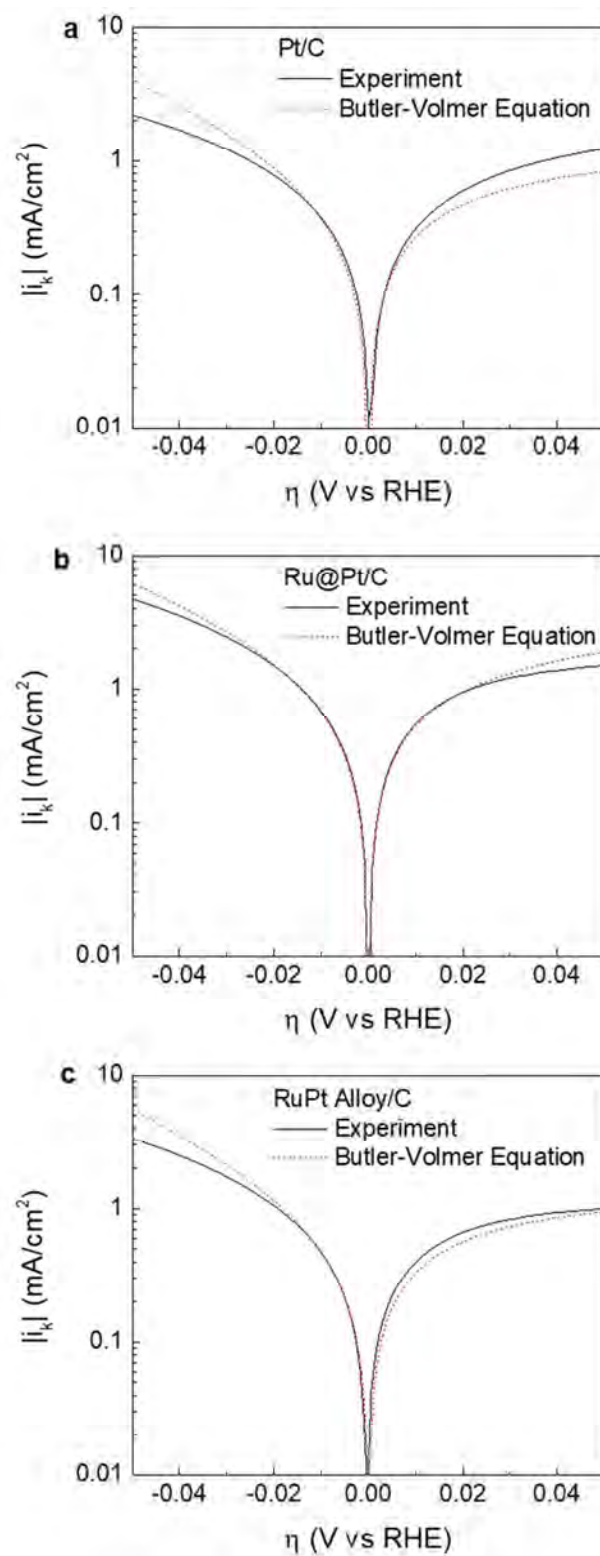


Figure. S12. From a to c: HER Tafel plots of the current density of Pt/C, Ru@Pt/C and RuPt alloy/C electrocatalysts in pH = 13 solution. The red line indicating Butler-Volmer fitting. The diffusion effect is not taken into count.

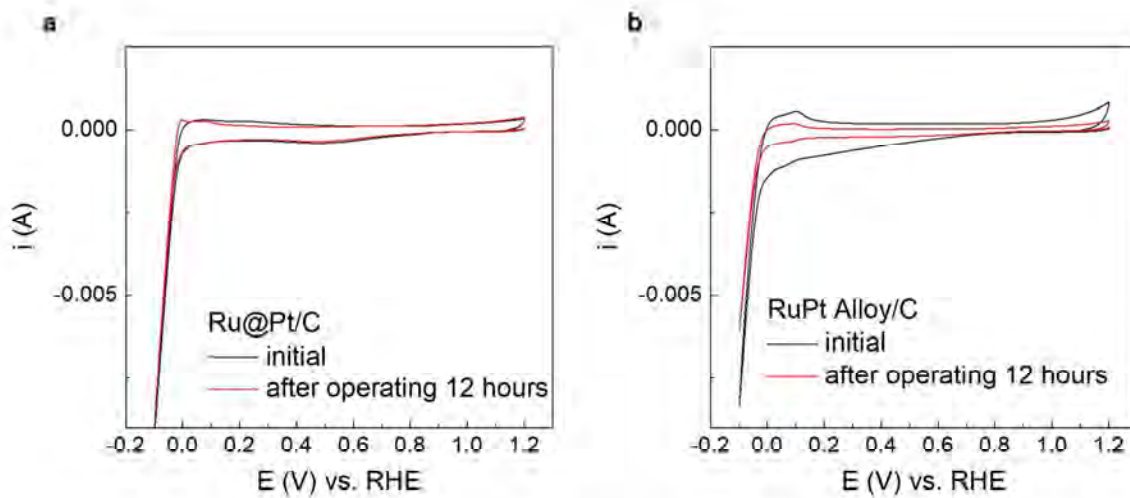


Figure. S13. Stability test of (a). Ru@Pt/C and (b). RuPt alloy/C. The CVs were taken before and after 12 hours of long term reaction.

Reference

1. Daw, M. S.; Baskes, M. I. Semiempirical, Quantum Mechanical Calculation of Hydrogen Embrittlement in Metals. *Phys. Rev. Lett.* **1983**, *50*, 1285-1288.
2. Ercolessi, F.; Adams, J. B. Interatomic Potentials from First-Principles Calculations: The Force-Matching Method. *EPL (Europhysics Letters)* **1994**, *26*, 583.
3. Brommer, P.; Gähler, F. Effective Potentials for Quasicrystals From Ab-initio Data. *Philos. Mag.* **2006**, *86*, 753-758.
4. Peter, B.; Franz, G. Potfit: Effective Potentials From Ab Initio Data. *Model. and Simul. Mater. Sci. Eng.* **2007**, *15*, 295.
5. Kresse, G.; Furthmüller, J. Efficient Iterative Schemes for Ab Initio Total-Energy Calculations Using a Plane-Wave Basis Set. *Phys. Rev. B* **1996**, *54*, 11169-11186.
6. Kresse, G.; Hafner, J. Ab Initio. *Phys. Rev. B* **1993**, *47*, 558-561.
7. Blöchl, P. E. Projector Augmented-Wave Method. *Phys. Rev. B* **1994**, *50*, 17953-17979.
8. Kresse, G.; Joubert, D. From Ultrasoft Pseudopotentials to the Projector Augmented-Wave Method. *Phys. Rev. B* **1999**, *59*, 1758-1775.
9. Plimpton, S. Fast Parallel Algorithms for Short-Range Molecular Dynamics. *J. Comput. Phys.* **1995**, *117*, 1-19.
10. Humphrey, W.; Dalke, A.; Schulten, K. VMD: Visual Molecular Dynamics. *J. Mol. Graph. Model* **1996**, *14*, 33-38.

Chapter 6 : Conclusions and perspectives

6.1 Conclusions

This thesis is devoted to deepening the insight into the reaction mechanism and the activity origin of the alkaline HER on the surface of nanostructured noble metal catalysts. The following conclusions can be drawn from the work in this thesis:

1. A distinctive alkaline HER mechanism alternative to that on bulk material has been found on nanostructured catalysts in high pH environment. In electrolyte with high $[\text{OH}^-]$ concentration, a large amount of H_3O^+ ions are generated on the surface of the nanostructured catalyst, forming an 'acid-like' environment within the electric double layer. These H_3O^+ -rich environment contributes in lowering the activation energy of the overall reaction and increase the activity of the catalyst. As a result, the nanostructured catalysts usually represent an anomalously high HER activity in electrolytes with high alkaline concentration.
2. The reaction mechanism of alkaline HER on nanostructured Pt catalysts will change with the reduction of the $[\text{OH}^-]$. In alkaline environment with $[\text{OH}^-] < 0.01 \text{ M}$, the reaction mechanism mentioned in conclusion 1 will not exist. Correspondingly, the alkaline HER activity of the catalysts will drop significantly.
3. Breaking the scaling relationship between the poorly known binding energies of H^* and OH^* was proved to be a practical designing strategy in promoting the catalytic activity of the Pt-based nanomaterials toward beyond the theoretical limitation of volcano plot. Such goal can be easily achieved via regulating the adsorption behaviors of different intermediates on dealloyed bimetallic nanoparticles. By creating oxidation site on Pt, it is possible to individually tune the H and OH adsorption affinities of the catalyst.
4. Comparing to ligand effect, the strain effect of the nanostructured Pt-based catalysts represents more dominant influence toward the alkaline HER activity. The compressive surface strain of the Ru@Pt nanoparticles can significantly alter the particles' binding energy toward H^* and OH^* intermediates and improve the HER activity of the catalyst. Such highly strained Pt can be induced to nanosized catalysts by constructing Ru@Pt core-shell structured nanoparticles with lattice mismatch between two metals.

In summary, these discoveries in alkaline HER mechanism and catalyst design can bring new understanding toward the mechanism study and the catalyst development for the reaction. Many of these insights are also applicable and may bring new inspirations to other electrocatalytic reduction reactions with multiple reactive intermediate (e. g. carbon dioxide and nitrogen reduction reaction).

6.2 Perspectives

Even considerable achievement has been accomplished in understanding and designing active catalysts for alkaline HER, much effort is still needed to get the full picture and gain control over the reaction in general.

1. While the activity of the catalysts is increasing and reaching the commercial demand, the stability of the current HER catalysts is still far beyond the need of industry. Although many kinds of cheap and abundant materials have been reported with activity very close to, or even better than that of the benchmark Pt/C in alkaline HER, the commercialization of these catalysts are restricted by their limited stability. For these cost-effective catalysts, it is urgent to significantly improve their physical/electronic structure for longer catalytic life cycle. Moreover, it is important to find what is the key aspect that determines the stability of the alkaline HER catalysts in general.
2. In-situ spectroscopy and imaging techniques, such as in-situ Raman, XAS, TEM and FTIR, should be largely induced into the study of the catalytic process. These techniques are much desired in monitoring the atomistic interaction on the surface of the catalyst during the reaction and to bring straightforward answers to the nature of the catalytic activity on different materials. Nowadays, it is still challenging to carry out in-situ characterizations due to the influence of aqueous reaction environment, extreme pH and the generation of bubbles during the reaction. More effort should be put into designing devices, instruments and general characterization methods to meet such needs.
3. In practice, the alkaline HER reaction is usually carried out under high overpotential to ensure a continuous and sufficient hydrogen production. However, the current understanding, including the computational simulations on alkaline HER mechanism, is still limited to the reaction process at around onset potential. More research work

should be done to probe into the alkaline HER reaction mechanism under high overpotential. The influence of the intrinsic electronic structure of the typical catalysts toward their activity under operating overpotential should be systematically studied.

4. Total control over the activity of the alkaline HER is specially needed in technologies such as carbon dioxide and nitrogen reduction reaction. In these reactions, methods are needed to suppress the HER activity of the certain catalysts (e. g. Cu, Au and Ag) without influencing the dissociation of water and the reduction of CO₂ or N₂.

All in all, with the fast-developing computational simulation and the more advanced in-situ characterization techniques, more challenges will be met in time and eventually, a thorough understanding and total control in alkaline HER will be achieved.

Appendix I: Publications during PhD Candidature

- [1] **Xuesi Wang**, Yihan Zhu, Anthony Vasileff, Yan Jiao, Shuangming Chen, Li Song, Bin Zheng, Yao Zheng and Shi-Zhang Qiao, Strain Effect in Bimetallic Electrocatalysts on the Hydrogen Evolution Reaction, *ACS Energy Letters*, **2018**, *3*, 1198.
- [2] **Xuesi Wang**, Anthony Vasileff, Yan Jiao, Yao Zheng* and Shi-Zhang Qiao, Electronic and Structural Engineering of Carbon-Based Metal-Free Electrocatalysts for Water Splitting, *Advanced Materials*, **2019**, *31*, 1803625.
- [3] **Xuesi Wang**, Qun He, Li Song, Mietek Jaroniec, Yao Zheng and Shi-Zhang Qiao, Breaking the volcano-plot limits for Pt-based electrocatalysts by selective tuning adsorption of multiple intermediates, *Journal of Materials Chemistry A*, **2019**, *7*, 13635.
- [4] **Xuesi Wang**, Chaochen Xu, Mietek Jaroniec, Yao Zheng and Shi-Zhang Qiao, Anomalous Hydrogen Evolution Behavior in High-pH Environment Induced by Locally Generated Hydronium Ions, *Nature Communications*, **2019**, accepted.
- [5] **Xuesi Wang**, Yao Zheng, Wenchao Sheng, Zhichuan J. Xu and Shi-Zhang Qiao, Designing Strategies for Alkaline Hydrogen Evolution Electrocatalysts, invited review to be submitted to *Materials Today*.